# Variability of the ocean circulation in the North-Atlantic in response to atmospheric weather regimes

Nicolas Barrier

présentée par

Nicolas Barrier

Préparée à l'Unité Mixte de Recherche n°6523
CNRS-IFREMER-UBO-IRD
Laboratoire de Physique des Océans

Thèse soutenue le 25 Novembre 2013
devant le jury composé de :

**Alain COLIN DE VERDIERE**
Professeur des Universités, UBO, LPO Brest / *Président*

**David MARSHALL**
Professor, University of Oxford / *Rapporteur*

**Claude FRANKIGNOUL**
Professeur des Universités, UPMC, LOCEAN Paris / *Rapporteur*

**Juliette MIGNOT**
Chargée de recherche IRD, LOCEAN Paris / *Examinatrice*

**Anne-Marie TREGUIER**
Directrice de recherche CNRS, LPO Brest / *Directrice de thèse*

**Christophe CASSOU**
Chercheur CNRS, CERFACS Toulouse / *Co-directeur de thèse*

**Julie DESHAYES**
Chercheur CNRS, LPO Brest / *Co-directrice de thèse*

# Variability of the ocean circulation in the North-Atlantic in response to atmospheric weather regimes

*The greatest good you can do for another is not just share your riches, but to reveal to him his own.*

*Le plus grand bien que vous pouvez faire aux autres n'est pas juste de partager vos richesses, mais de reveler aux autres les leurs.*

Benjamin Disraeli

# Acknowledgements

## Abstract

The aim of the PhD is to investigate the impacts of the large-scale atmospheric variability on the North-Atlantic ocean circulation. This question has already been addressed in a large number of studies, in which the atmospheric variability is decomposed into modes of variability, determined by decomposing sea-level pressure anomalies into Empirical Orthogonal Function (EOFs). These modes of variability are the North-Atlantic Oscillation (NAO), the East-Atlantic Pattern (EAP) and the Scandinavian Pattern (SCAN). EOF decomposition assumes that the modes are orthogonal and symmetric. The latter assumption, however, has been shown to be inadequate for the NAO. Hence, a different framework is used in this study to assess the atmospheric variability, the so-called weather regimes. These are large-scale, recurrent and quasi-stationary atmospheric patterns that have been shown to capture well the interannual and decadal variability of atmospheric forcing to the ocean. Furthermore, they allow to separate the spatial patterns of the positive and negative NAO phases. Hence, these weather regimes are a promising alternative to modes of variability in the study of the ocean response to atmospheric variability.

Using observations and numerical models (realistic or in idealised settings), we have shown that the Atlantic Ridge (AR), NAO$^-$ and NAO$^+$ regimes drive a fast (monthly to interannual) wind-driven response of the subtropical and subpolar gyres (topographic Sverdrup balance) and of the meridional overturning circulation (MOC, driven by Ekman transport anomalies). At decadal timescales, the subpolar gyre strengthens for persistent NAO$^+$ and Scandinavian Blocking (BLK) conditions via baroclinic adjustment to buoyancy fluxes and slackens for persistent AR conditions via baroclinic adjustment to wind-stress curl anomalies. The latter mechanism also accounts for the strengthening of the subtropical gyre for persistent NAO$^+$ conditions and its weakening for persistent AR conditions. The gyres response to persistent NAO$^-$ conditions reflects the southward shift of the gyre system (the intergyre gyre). The MOC spins-up for persistent NAO$^+$ and BLK conditions via increased deep water formation in the Labrador Sea, and conversely for the NAO$^-$ and AR regimes.

Last, heat budget calculations in the subpolar gyre and the Nordic Seas have been performed using four global ocean hindcasts. The winter averaged heat convergence in the western subpolar gyre is positively correlated with the NAO$^-$ winter occurrences, which is due to the intergyre-gyre circulation, while it is negatively correlated with AR winter occurrences, because of the wind-driven reduction of both gyres. Downward surface heat flux anomalies are negatively correlated with NAO$^+$ occurrences, and conversely for the NAO$^-$. In the Nordic Seas, they are positively correlated with BLK and to a lesser extent AR occurrences. Furthermore, we suggest that the heat content variability in the western subpolar gyre is the signature of the delayed response (6-year lag) to the time-integrated NAO$^+$ forcing, due to the combination of the immediate (0-lag) response of surface heat flux and the lagged (3 year lag) response of ocean heat convergence.

## Résumé

Le but de la thèse est d'analyser les impacts de la variabilité atmosphérique grande échelle sur la circulation océanique. Ceci a déjà fait l'objet de nombreuses publications, dans lesquelles la variabilité atmosphérique est analysée en termes de modes de variabilité, déterminés par analyse en composantes principales (EOF en anglais) des anomalies de pression de surface. Ces modes sont l'Oscillation Nord-Atlantic (NAO), le Pattern Est-Atlantique (EAP) et le Pattern Scandinave (SCAN). La décomposition en EOF implique que les modes sont orthogonaux et symétriques. Cette dernière hypothèse a été montrée comme étant invalide pour la NAO. Par conséquent, un nouveau concept est proposé dans cette étude pour estimer la variabilité atmosphérique, celui des régimes de temps. Ces derniers sont des structures spatiales de grande échelle, récurrents et quasi-stationnaires qui permettent de capturer la variabilité des forçages atmosphériques. De plus, ils permettent de séparer les patterns spatiaux des deux phases de la NAO. Ces régimes de temps sont donc une alternative prometteuse pour l'analyse de la variabilité océanique forcée par l'atmosphère.

A partir d'observation et de modèles numériques (réalistes ou idéalisés), nous avons montré que les régimes Atlantic Ridge (AR), NAO$^-$ et NAO$^+$ induisent une réponse rapide (échelles mensuelles à interannuelles) des gyres subtropical et subpolaire (via un mécanisme de Sverdrup topographique) et de la cellule de retournement (MOC, ajustement aux anomalies de transport d'Ekman). Aux échelles décennales, le gyre subpolaire s'intensifie lors de conditions NAO$^+$ et BLK persistantes via un ajustement barocline aux flux de flottabilité et s'affaiblit pour AR via un ajustement barocline aux anomalies de rotationnel de vent. Ce dernier mécanisme explique aussi l'augmentation du gyre subtropical pour une NAO$^+$ persistante et son affaiblissement pour un AR persistant. La réponse des gyres pour des conditions de NAO$^-$ persistantes est un déplacement vers le sud des gyres (l'intergyre gyre). L'intensité de la MOC est augmentée pour des conditions de NAO$^+$ et BLK persistantes, dû à l'augmentation de la formation d'eau dense en mer du Labrador, et inversement pour NAO$^-$ et AR.

Finalement, des bilans de contenu de chaleur dans la gyre subpolaire et les mers Nordiques ont été effectués dans quatre modèles océaniques globaux. Les moyennes d'hiver de convergence océanique de chaleur dans la partie ouest de la gyre subpolaire sont positivement corrélées aux occurrences d'hiver de NAO$^-$, ce qui est dû à la présence de l'intergyre, tandis que cette convergence est négativement corrélée aux occurrences d'AR, ce qui est dû à la réduction des deux gyres qui lui est associée. Les flux de chaleur vers l'océan dans la gyre subpolaire sont négativement corrélés aux occurrences d'hiver de la NAO$^+$ et inversement pour la NAO$^-$. Dans les mers Nordiques, ils sont positivement corrélés aux occurrences de BLK et, dans une moindre mesure, aux occurrences de AR. De plus, nous suggérons que la variabilité du contenu de chaleur dans la partie ouest du gyre subpolaire est la réponse décalée (lag de 6 ans) à l'intégration temporelle du forçage lié au régime NAO$^+$, due à la combinaison de la réponse en phase (0-lag) des flux de chaleur et à la réponse décalée (lag de 3 ans) de la convergence de chaleur.

# Contents

# List of abbreviations

**A**

| | |
|---|---|
| AL | Atlantic Low |
| AR | Atlantic Ridge |

**B**

| | |
|---|---|
| BLK | Scandinavian Blocking |

**E**

| | |
|---|---|
| EAP | East-Atlantic Pattern |
| EGC | East-Greenland Current |
| ENAC | Eastern North-Atlantic Current |
| EOF | Empirical Orthogonal Function |

**F**

| | |
|---|---|
| FC | Faroe Current |

**H**

| | |
|---|---|
| HR | High Resolution |

**I**

| | |
|---|---|
| IC | Irminger Current |

**L**

| | |
|---|---|
| LR | Low Resolution |
| LS | Labrador Sea |

**M**

| | |
|---|---|
| MSLP | Mean Sea-Level Pressure |

**N**

| | |
|---|---|
| NAE | North-Atlantic/Europe |
| NAO | North-Atlantic Oscillation |
| NATL | North-Atlantic |
| NIIC | North Irminger Icelandic Current |
| NWAC | Norwegian Atlantic Current |

**O**

| | |
|---|---|
| OC | Ocean heat convergence |

**P**

| | |
|---|---|
| PC | Principal Component |
| PSMSL | Permanent Service for Mean Sea-Level |
| PW | Petawatts ($10^{15}\ W$) |

**S**

| | |
|---|---|
| SBL | Scandinavian Blocking |
| SC | Shetland Current |
| SCAN | Scandinavian Pattern |
| SF | Surface flux |
| SSH | Sea-Surface Height |
| SSS | Sea-Surface Salinity |
| SST | Sea-Surface Temperature |
| SV | Sverdrup ($10^6\ kg\ m^{-3}$) |

**T**

| | |
|---|---|
| TOC | Time-integrated ocean heat convergence |
| TSF | Time-integrated surface flux |
| TW | Terawatts ($10^{12}\ W$) |

**W**

| | |
|---|---|
| WNAC | Western North-Atlantic Current |
| WR | Weather Regime |

**Z**

| | |
|---|---|
| Z500 | Geopotential height at 500 $mb$ |
| ZJ | Zetta joule ($10^{21}\ J$) |

# Introduction étendue en français

Les probables impacts sociétaux et environnementaux du changement climatique (inondations, exodes massifs, maladies) ont considérablement favorisé le développement des sciences du climat telles que la climatologie, la météorologie, la biogéochimie ou l'océanographie. Le but de la thèse est de mieux comprendre la réponse de l'océan Atlantique à la variabilité atmosphérique, pour éventuellement mieux prédire son devenir dans le contexte du changement climatique.

La source principale de chaleur de la Terre provient de l'énergie solaire. Cependant, cette énergie n'est pas répartie équitablement à l'échelle du globe: il y a un excès de chaleur aux Tropiques et un déficit de chaleur aux Pôles. Pour atteindre un climat stationnaire, il est donc nécessaire que ce déséquilibre soit comblé, ce qui est accompli par les circulations atmosphérique et océanique. La contribution de l'océan est dominante dans les Tropiques tandis que la contribution atmosphérique domine aux latitudes moyennes, bien que la contribution océanique y soit non négligeable. De plus, dans le contexte du changement climatique, la température moyenne de surface à l'échelle du globe risque d'augmenter dramatiquement de par les rejets de plus en plus importants de gaz à effet de serre. L'océan ayant une inertie thermique bien plus grande que l'atmosphère ou les continents, la plupart de cet excès de chaleur sera stocké par les océans. Cette augmentation du contenu de chaleur est responsable d'environ 30% de l'augmentation du niveau de la mer observé entre 1993 and 2007, via les effets thermostériques, tandis que 55% de cette augmentation est due à la fonte des glaciers et des calottes glaciaires (Cazenave and Llovel 2010). De par sa contribution au transport méridien de chaleur et de par sa grande capacité de stockage, l'océan est donc une composante majeure du système climatique.

Lorsque le transport méridien de chaleur par l'océan est décomposé en trois contributions, celles de l'océan Pacifique, de l'océan Indien et de l'océan Atlantique, on remarque une particularité importante de ce dernier: le transport méridien est dirigé vers le nord à toutes les latitudes, contrairement

à l'océan Pacifique, pour lequel le transport est dirigé vers le nord dans l'hémisphère nord et inversement dans l'hémisphère sud. Dans le Pacifique, le transport méridien de chaleur est principalement dû à la circulation horizontale (les gyres subtropicaux et subpolaires), tandis que dans l'Atlantique, ce transport est dû à la circulation méridienne de retournement (MOC). Cette MOC est responsable de la douceur du climat d'hiver en Europe de l'Ouest, en comparaison à celui de la côte Est du Canada.

Ce rôle important de l'océan, et plus particulièrement de l'océan Atlantique, justifie les nombreuses études qui lui ont été dédiées. Dans un effort de prédiction de son état futur, il est en effet nécessaire de comprendre son évolution passée. Cette évolution, nommée variabilité, mélange des échelles de temps et des mécanismes très différents. Par exemple, la variabilité de l'insolation solaire va moduler la variabilité de l'océan, et plus particulièrement de la température de surface, à l'échelle du jour (cycle journalier), de l'année (cycle saisonnier) et peut-être même à l'échelle de la dizaine de milliers d'années (cycles de Milankovitch). Une autre source de variabilité océanique provient des changements de conditions atmosphériques (vent, température de l'air, humidité spécifique), qui vont influencer à la fois la circulation océanique via les effets mécaniques du vent sur l'océan mais aussi les flux de flottabilité via les flux turbulents (flux sensible et latent, évaporation). Le but de la thèse est d'analyser la variabilité océanique en Atlantique-Nord forcée par l'atmosphère et d'appréhender les mécanismes associés.

Cette question a déjà été abordée dans un nombre important d'études. Cependant, de nombreuses questions nécessitent encore de l'attention. Premièrement, la plupart de ces études font appel au concept de modes de variabilité qui permet de réduire significativement le nombre de degrés de liberté de la variabilité atmosphérique. Ces modes de variabilité sont généralement déterminés par analyse en composante principale (EOF en anglais), qui permet de décomposer un champ 3d (de dimensions temps, longitude et latitude) en une série de patterns spatiaux fixes dans le temps (EOFs ou vecteurs propres), chacun associé à un indice variable dans le temps (composante principale, PC en anglais). Par construction, ces modes sont orthogonaux et symétriques. Dans un premier temps, nous allons passer en revue la littérature concernant l'impact des modes de variabilité particuliers à l'Atlantique-Nord sur la circulation océanique. Les limitations de cette décomposition vont être abordées et un concept alternatif va être proposé, celui des régimes de temps. Leur potentiel dans l'analyse de la

variabilité océanique forcée par l'atmosphère va être estimé.

Le mode de variabilité dominant en Atlantique Nord est l'Oscillation Nord-Atlantique (NAO en anglais), qui peut, au premier ordre, être interprétée comme une mesure de l'intensité des vents moyens en Atlantique Nord: une NAO positive implique un renforcement des vents et inversement pour une NAO négative. Par conséquent, le gyre subtropical en Atlantique Nord étant principalement forcée par le vent (Cabanes et al. 2006; Hong et al. 2000), les changements de NAO devraient s'accompagner de changements d'intensité du gyre subtropical, comme suggéré par Ezer (1999). Cependant, Hakkinen et al. (2011a) ont montré que les anomalies de vent associées à la NAO ne sont pas efficaces pour influencer l'intensité de la circulation horizontale. Cette dernière serait plutôt forcée par les anomalies de vent associées au deuxième mode de variabilité, l'East-Atlantic Pattern (EAP en anglais). En utilisant des observations de hauteur de mer dans le gyre subtropicale (altimétrie et données marégraphiques) ainsi que le concept des régimes de temps, nous allons déterminé quel pattern atmosphérique est effectivement dominant pour la variabilité du gyre subtropical. De plus, un modèle planétaire géostrophique nous permettra d'analyser les mécanismes en jeu. Ces résultats ont fait l'objet d'une publication dans *Climate Dynamics*.

Des analyses similaires ne peuvent pas être effectuées de manière satisfaisante sur le gyre subpolaire et la MOC à cause du manque d'observations. Une alternative aux observations est fournie par les modèles numériques de circulation générale. De nombreuses études ont fait appel à des modèles océaniques forcés par des champs atmosphériques idéalisés afin d'analyser la réponse océanique à une NAO positive persistante (Eden and Willebrand 2001,Herbaut and Houssais 2009, Lohmann et al. 2009). Ces forçages idéalisés sont généralement construits à l'aide de l'indice NAO traditionnel, soit en régressant cet indice sur les anomalies de forçages, soit en moyennant les forçages sur des années caractérisées par de fortes NAO. Nous allons dans un premier temps évaluer la robustesse de ces méthodes. Puis une méthode alternative de génération de forçages idéalisés, basée sur les régimes de temps, sera proposée et évaluée à son tour. Ensuite, ces forçages seront utilisés pour déterminer l'impact de chacun des régimes sur la circulation océanique en Atlantique Nord (gyres subtropical et subpolaire, MOC) à des échelles de temps mensuelles à décennales. Ces résultats ont fait l'objet d'une publication dans le *Journal of Physical Oceanography*.

Finalement, nous allons nous intéresser à la variabilité passée du contenu de chaleur dans le gyre

subpolaire et les Mers Nordiques. Nous allons déterminer dans quelle mesure cette variabilité peut être liée aux régimes de temps et à travers quel mécanisme (flux de chaleur à la surface, convergence de chaleur océanique). Puisque les observations profondes sont rares, elles sont insuffisantes pour reconstruire la variabilité des contenus de chaleur intégrés depuis la surface jusqu'au fond. Cependant, ces observations seront utilisées pour valider les contenus de chaleur obtenus à l'aide de quatre modèles océaniques globaux. La considération de plusieurs modèles permet d'estimer la robustesse des résultats vis-à-vis des incertitudes des modèles, qui peuvent être liées au choix des forçages atmosphériques, de la résolution (horizontale ou verticale) et des paramétrisations.

# Chapter 1

# Introduction

## Contents

Climate change studies have increasingly become one of the major scientific challenges because of its possible important societal and environmental impacts: floods, sea-level rise or temperature extremes that are likely to favour diseases and to reduce crop yields (McMichael et al. 2006). As a consequence, climatology, meteorology, biogeochemistry and oceanography have considerably developed in the recent decades.

Understanding the response of the North Atlantic Ocean to atmospheric variability, as observed during the last 50 years, is the overall objective of this PhD. This understanding is important to improve our understanding and hence forecasting of climate change.

## 1.1   The role of the ocean in the climate system

The major source of energy for the Earth is the solar energy. This energy, however, is not equally distributed because of the sphericity of the Earth. The global horizontal radiation with two incoming solar beams that carry the same amount of energy are illustrated in figure 1.1a. The beam that catches the Tropics is nearly orthogonal to the Earth: the illuminated surface is small hence the insolation intense. The beam that reaches the Pole catches a greater surface, inducing a weaker insolation. As the outgoing terrestrial radiation is almost the same at every latitude, there is a net surplus of heat in the tropics and a deficit of heat in the poles. To reach a stationary climate, this discrepancy
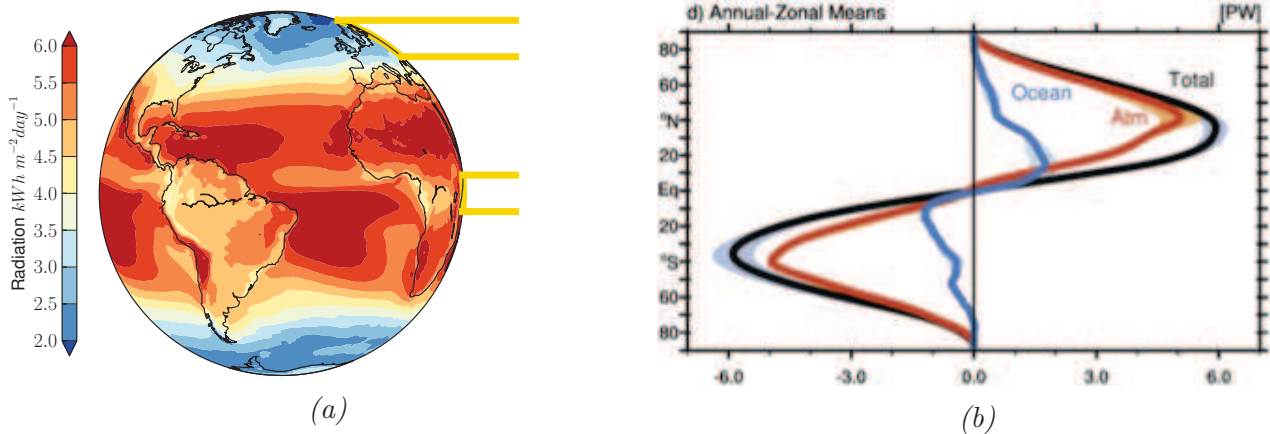
*Figure 1.1: a) Color shading: global horizontal radiation in $kWh\ m^{-2}day^{-1}$(data from `http://eosweb.larc.nasa.gov/`). The yellow lines show two sun beams that carry the same amount of energy but at different latitudes. b) Meridional heat transport partition as a function of latitude (source: Fasullo and Trenberth, 2008)*

needs to be balanced. This is achieved by the oceanic and atmospheric circulations. The partition of meridional heat transport into its atmospheric and oceanic components is shown in figure 1.1b as a function of latitude. In the tropics (10°S-10°N), meridional heat transport is dominated by the ocean while at midlatidudes, it is dominated by the atmosphere, although the oceanic contribution remains significant.

Furthermore, the ocean is essential to the climate system as it is the principal heat reservoir. In the context of climate change, the global surface temperature is expected to rise significantly because of anthropogenic greenhouse gas concentrations (Meehl et al. 2007). As the ocean is much effective than the atmosphere (approximately 1000 times) or than land (approximately $100$[1] times) to store heat, this excess of heat will mostly be stored by the ocean. This increase in global ocean heat content (figure 1.2) has been shown to be responsible for some 30% of the global upward sea-level trend between 1993 and 2007 (Cazenave and Llovel 2010) via thermosteric effect (Cabanes et al. 2001; Willis et al. 2004; Antonov et al. 2005), while 55% of this trend result from the melting of mountain glaciers and ice sheets (Cazenave and Llovel 2010).

The partition of oceanic meridional heat transport (blue curve in figure 1.1b) into the contributions of the Pacific Ocean, of the Indian Ocean and of the Atlantic Ocean (figure 1.3) reveals strong differences. In the Pacific Ocean, the heat transport is northward in the northern hemisphere and southward in the southern hemisphere. This transport is mainly due to the horizontal circulation

---

[1]source: `http://oceanworld.tamu.edu/resources/ocng_textbook/chapter05/chapter05_01.htm`
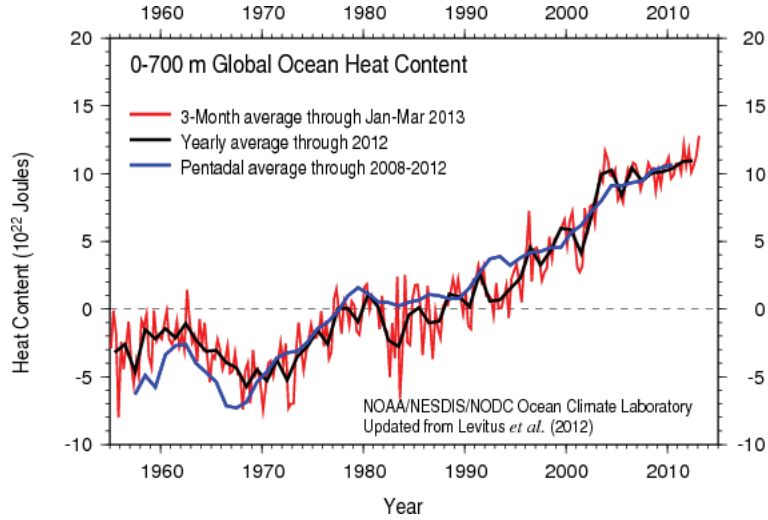
*Figure 1.2: Global average of heat content over $0 - 700\ m$. Source:*
$http: // www. nodc. noaa. gov/ OC5/ 3M\_HEAT\_CONTENT/$

(gyre), which is approximated by the barotropic streamfunction $\psi_{baro}$

$$\psi_{baro}(x,y) = \int_{x_E}^{x} \int_{-H}^{0} v(x',y,z)\ dx'\ dz \tag{1.1}$$

where $v$ is the meridional velocity, $(x,y,z)$ are longitude, latitude and depth, $H$ is the bottom depth and $x_E$ the eastward limit of the domain.

On the contrary, the Atlantic Ocean shows a northward heat transport at each latitude. This particularity of the Atlantic Ocean is due to the presence of a deep-reaching overturning circulation, described as the Atlantic Meridional Overturning Circulation (AMOC). The AMOC transports near-surface warm water to the North pole and deep cold water to the southern hemisphere. The strength of the AMOC is assessed by the overturning streamfunction $\psi_{over}$:

$$\psi_{over}(y,z) = \int_{x_E}^{x_O} \int_{-H}^{z} v(x,y,z')\ dx\ dz' \tag{1.2}$$

with the same notations than in equation 1.1 and $x_O$ the western limit of the basin.

In the present-day climate, the localisation of this overturning circulation in the Atlantic is due to higher densities in the North-Atlantic than in the North-Pacific (figure 1.4). The mechanism behind the AMOC can be summarised as follows. The Gulf-Stream/North-Atlantic Current system carries warm and salty water northward. This water is cooled and salinised by contact with the atmosphere (via sensible and latent heat exchanges and evaporation), hence gets denser. When this water is
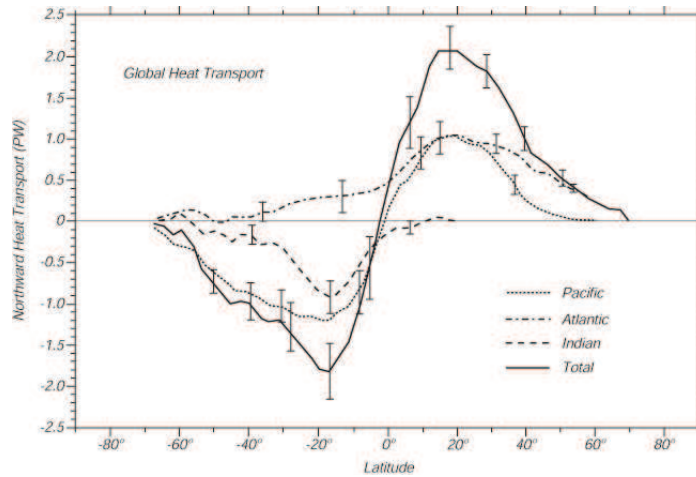
*Figure 1.3: Ocean heat transport decomposed into the contributions of the Pacific, Atlantic and Indian Oceans. Source: Houghton et al. 1996 with data of Trenberth and Solomon, 1994*

dense enough, it sinks and forms the North-Atlantic Deep Water that feeds the lower limb of the AMOC. The presence of the AMOC is of major importance for the climate in western Europe as it is responsible for the mild winters in Western Europe, in contrast to the cold winters of Canadian west coast. In the context of climate change, a stronger hydrological cycle and an increase in Greenland ice melting would lead to fresher/lighter waters in the North-Alantic and in turn to a weaker or even a shut-down of the AMOC, although there is a strong dispersion among the climate change projections (Meehl et al. 2007).
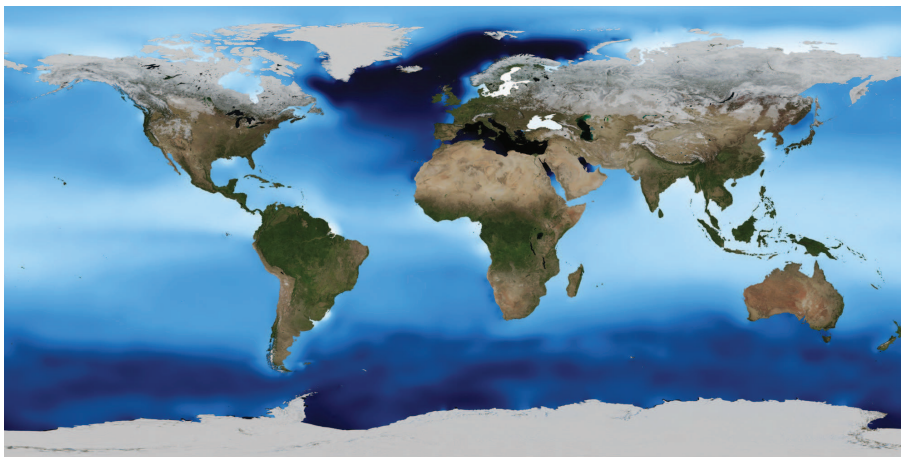


*Figure 1.4: Sea-surface density (kg $m^{-3}$). Deep blue characterises density greater than 1017 $kgm^{-3}$. Source: NASA/Goddard Space Flight Center Scientific Visualisation Studio, with data from the World Ocean Atlas 2005 (Locarnini et al., 2006).*

This central role of the North-Atlantic Ocean in the climate system motivates the efforts of the oceanographers to understand the past evolution of the ocean circulation, to potentially predict its

future state in the context of climate change. This past evolution, which is named variability, occurs at different timescales. If one considers a continuous time series of observed sea-surface temperature that extends as far as the ocean's origins[1]. Its evolution over time would be governed by:

$$\frac{\partial T}{\partial t} + \nabla.(T\mathbf{U}) = Q_{net} = Q_{rad} + Q_{tur} \tag{1.3}$$

where $\nabla$ is the nabla operator, $T$ is the temperature, $\mathbf{U}$ is the velocity vector. $Q_{net}$ is the net downward surface heat flux, which can be decomposed into a radiative (shortwave and longwave, $Q_{rad}$) and a turbulent (latent and sensible, $Q_{tur}$) component. A spectral analysis of the temperature time series would first probably reveal variabilities related to changes in $Q_{rad}$:

- A variability with a period of 1 day, which would reflect the diurnal cycle (temperatures are warmer at noon than at midnight).

- Variabilities with a period of 1 year, which would reflect the seasonal cycle (temperatures are warmer in summer than in winter).

- We also could observe variabilities with periods of approximately 21700 and 41700 years, which would reflect the modulations of solar insolation by the Earth's orbital parameters (the Milankovitch cycles, Foucault 2009).

We would also observe variabilities with periods ranging from monthly to centennial. These variabilities would be due to the turbulent surface fluxes $Q_{turb}$, but also to the advection term $\nabla.(T\mathbf{U})$. Part of the variability of the advection term is caused by the intrinsic variability of the ocean, due to the presence of mesoscale and submesoscale structures such as eddies (Penduff et al. 2011). But the main contributor to the variability of $Q_{turb}$ and $\nabla.(T\mathbf{U})$ originates from the atmosphere because:

  i) the turbulent heat fluxes strongly depend on the atmospheric state (especially the wind speed, the temperature contrast between the atmosphere and the ocean and the specific humidity)

  ii) the wind-stress, through frictional effects at the sea surface, drives the ocean circulation.

---

[1]Such a time series is unfortunately imaginary.

Hence, at interannual and centennial timescales, the variability of atmospheric forcings is a major driver of oceanic variability.

## 1.2 Atmospheric forcing of the North-Atlantic Ocean
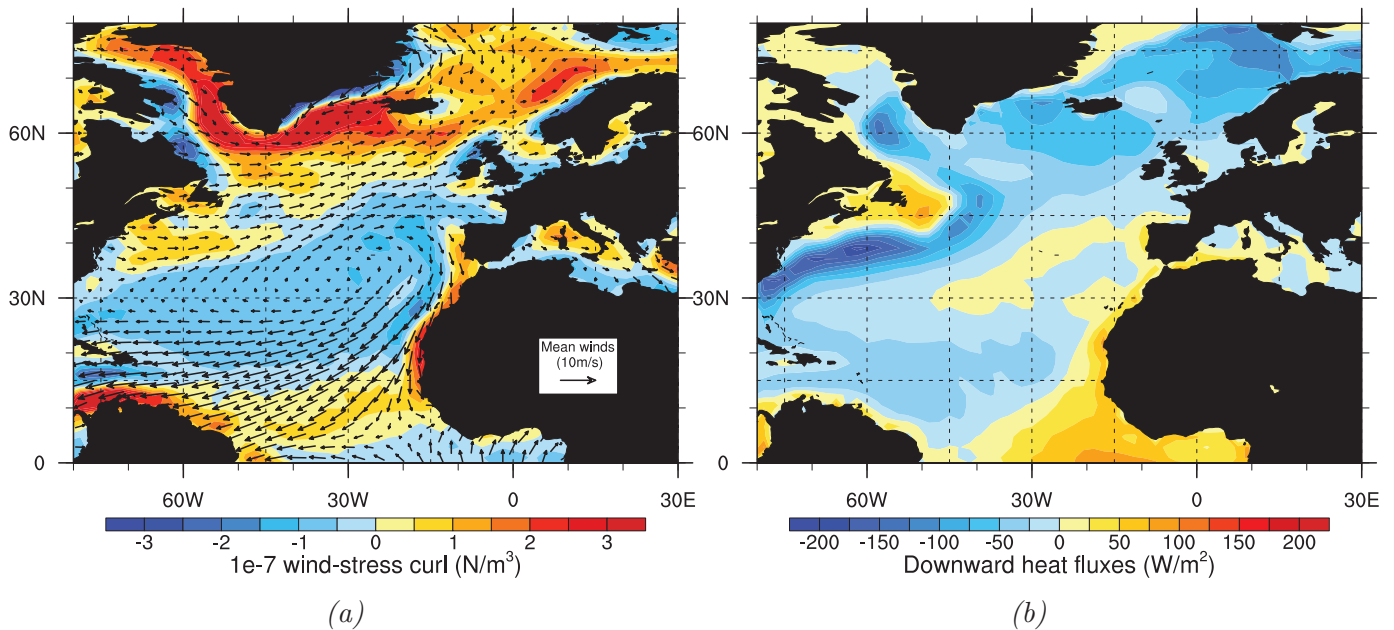


*Figure 1.5: Atmospheric forcing fields averaged from* 1948 *to* 2007*. a) Wind (black arrows) and wind-stress curl (color shading). b) Downward heat fluxes (sum of latent, sensible, shortwave and longwave). Negative values indicate a heat loss of the ocean. Data source: NCEP/NCAR reanalysis (Kalnay et al., 1996)*

From the equator to 30°N, trade winds blow south-westward, while north of 30°N the midlatitude westerlies blow north-eastward (figure 1.5a). In the subtropics, the wind-stress curl is negative and is associated with Ekman pumping and anticyclonic ocean circulation (the subtropical gyre). At midlatitudes, the wind-stress curl is positive and is associated with Ekman suction and cyclonic ocean circulation (the subpolar gyre).

In the North-Atlantic, heat fluxes are primarily directed from the ocean to the atmosphere. Hence, on average, the atmosphere is warmed by the ocean (figure 1.5b). The strongest anomalies are found in the Gulf Stream region, which is a key region for the storm cyclogenesis in winter (Brayshaw et al. 2011). Strong anomalies are also observed in the Western Labrador Sea and in the Nordic Seas, where deep water is formed by deep convection and feeds the lower limb of the AMOC.

# 1.3 Aims of the PhD

Changes in atmospheric forcings (meridional shifts of the winds, changes in the intensity of surface forcings, etc) strongly impact the variability of the ocean circulation in the North-Atlantic, as already addressed in a large number of studies. However, many questions still deserve attention. The aim of the PhD is to address some of these questions.

The first one is related to the concept of modes of variability, often used to analyse the changes in ocean circulation induced by the changes in atmospheric forcings. What are their limitations? Are the so-called weather regimes an interesting alternative? What are their added values compared to the modes of variability? These questions are addressed in chapter 2.

The dominant mode of variability in the North-Atlantic/Europe domain is the North-Atlantic Oscillation (NAO), which, to first order, measures the intensity of the mean winds in the North-Atlantic (figure 1.5a). Accordingly, the NAO is expected to influence the strength of the subtropical gyre, as suggested by Ezer (1999). However, Hakkinen et al. (2011a) suggest that the second mode of variability, the East-Atlantic Pattern, is more effective to imprint changes in the strength of the gyres. Which mode of variability is dominant for the variability of the subtropical gyre in the 1949-1998 period? Through which mechanism? These questions are addressed in chapter 3.

The atmosphere is also expected to impact the circulations of the subpolar gyre and of the meridional overturning, observations of which are sparse and do not cover a long time-period. An alternative to observations is provided by the ocean general circulation models. In the literature, the response of the ocean circulation to persistent positive NAO has been thoroughly investigated using ocean general circulation models. Using the weather regime framework, these studies are revisited. What are the impacts, at monthly to decadal timescales, of the weather regimes on the modelled ocean circulation in the North-Atlantic? Does the NAO asymmetry matter when investigating the ocean response to $NAO^-$ and $NAO^+$? These questions are addressed in chapter 4.

Finally, a major clue for climate change is to investigate heat content changes over the last decades in the North Atlantic Ocean. To what extent are fluctuations in the atmospheric weather regimes responsible for changes in heat content within the subpolar gyre and the Nordic Seas? Through which mechanism: changes in surface heat fluxes and/or changes in ocean heat convergence? Observations of the ocean circulation are insufficient to reconstruct changes in heat advection hence storage, but

allow to validate model results. Because of the uncertainty inherent to each ocean simulation, it is important to estimate how much these results depend on the model setting (atmospheric forcing fields, ocean resolution, model parameters). Hence these questions are addressed by inter-comparing four different ocean hindcasts.

To summarise, the guideline of the PhD is to analyse the impacts of the atmosphere on the North-Atlantic Ocean (horizontal and overturning circulations, heat content) by using the weather regime framework, which allows to circumvent the limitations of the traditionally used modes of variability, as discussed in the following section.

# Chapter 2

# Atmospheric modes of variability and weather regimes

## Contents

## 2.1 Introduction

To investigate how the atmospheric variability influences the ocean, one must take into account the $3D$ nature (time, longitude, latitude) of each atmospheric variable that may impact the ocean circulation, e.g. winds, air-temperature, specific humidity and precipitation. A way to overcome such a difficult task is generally achieved by reducing the spatio-temporal variability of the atmosphere into a finite number of spatial patterns, and to determine the time-varying indices that are associated with these patterns. In this section, we review two main concepts: the "modes of variability" and the weather regimes.

As a preliminary step, the importance of the winter season for atmospheric variability is discussed. The standard deviations of daily zonal and meridional wind anomalies[1] for the whole year, for winter (December to March, hereafter DJFM) and for summer (June to September, hereafter JJAS) are compared in figure 2.1. Although the patterns are very similar among the seasons, the standard deviations are much larger in winter than in summer. Hence, it is in winter that the atmosphere is the most likely to imprint its signature on the oceanic variability. This will be shown when investigating the impact of atmospheric variability on subtropical sea-surface height anomalies (chapter 3). As a consequence, only the winter season is considered hereafter when discussing atmospheric variability.
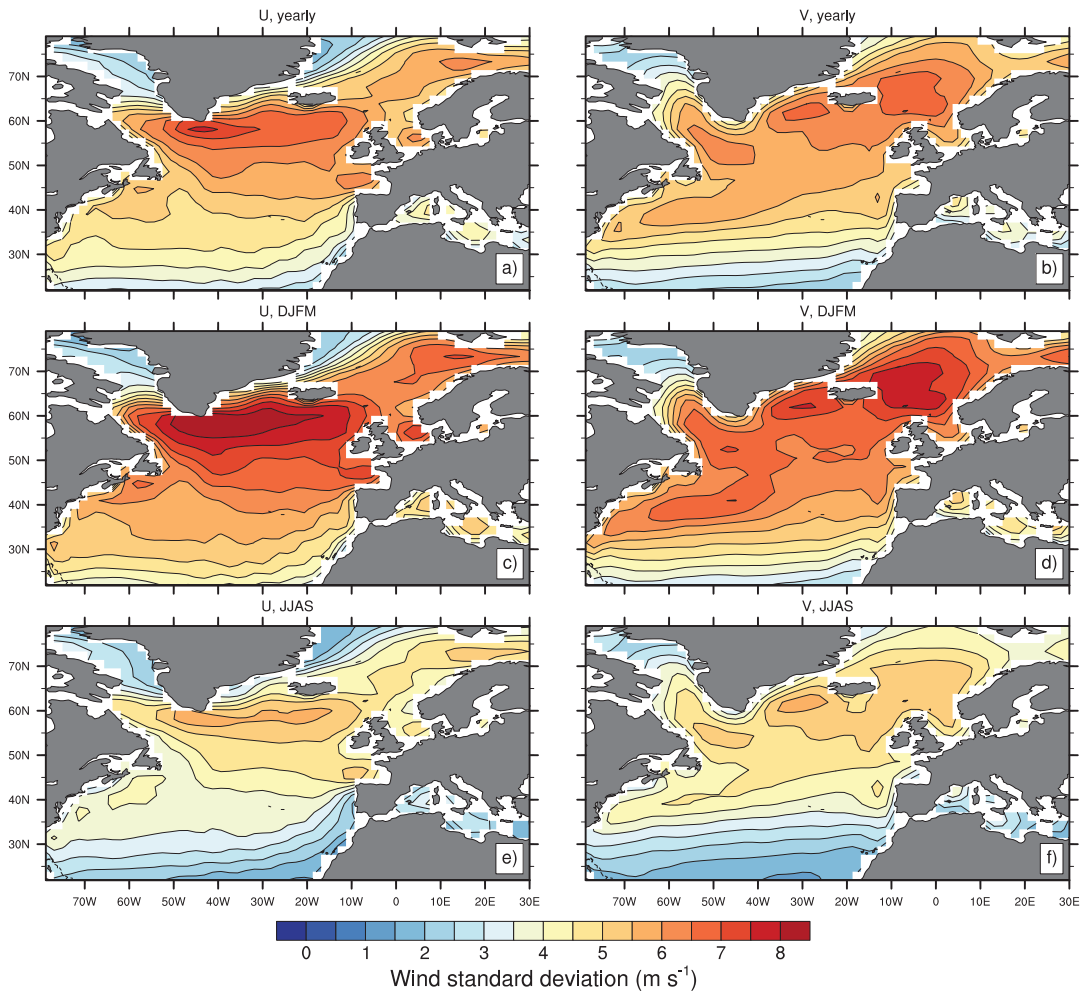


*Figure 2.1: Daily variance of zonal and meridional components. a) and b): for the whole year. b) and c) for DJFM days d) and e) for JJAS days*

---

[1]Computed by removing a smoothed seasonal cycle with two harmonics retained

## 2.2 Winter modes of variability

The simple idea behind the concept of modes of variability is to reduce the $3D$ nature of the atmosphere into a fixed number of spatial patterns, to which are associated a time series (Barnston and Livezey 1987; Grossmann and Klotzbach 2009). In this section, the three main modes of variability in the North-Atlantic/Europe domain, the North-Atlantic Oscillation (NAO), the East-Atlantic Pattern (EAP) and the Scandinavian Pattern (SCAN), are introduced.

### 2.2.1 North-Atlantic Oscillation (NAO)

The NAO, described by Hurrell (1995), is the dominant mode of variability in the North-Atlantic/Europe domain, since it explains 50% of the winter averaged sea-level pressure anomalies variance. It characterises the sea-level pressure fluctuations between the two main atmospheric systems in the North-Atlantic, the Icelandic Low and the Azores High, which are reinforced during positive NAO conditions. Figure 2.2 illustrates the mean atmospheric conditions during the positive (figure 2.2a) and the negative (figure 2.2b) NAO phases. During positive NAO phase, westerlies are intensified in a northeastward trajectory, inducing warm/wet winters in northern Europe/eastern USA and cold/dry winters in Labrador, eastern Greenland and southern Europe. Positive NAO conditions are also associated with increase heat loss to the atmosphere in the subpolar gyre region. Negative NAO conditions are characterised by weakened westerlies with more zonal trajectories, inducing climate conditions opposite to those associated with the NAO$^+$ (figure 2.2b)

The temporal variability of the NAO is given by the NAO index, which can be computed different ways. Historically, the NAO index has been computed as the normalised sea level pressure difference between Lisbon (Portugal) and Stykkisholmur/Reykjavik (Iceland). This station-based NAO index extends as far back as 1864. Another way to compute the NAO index is to decompose the 3D sea-level pressure anomalies over the North-Atlantic domain into Empirical Orthogonal Function (hereafter, EOF). The NAO sea-level pressure anomaly pattern is given by the first EOF and the NAO index is defined as the associated normalised principal component (PC). This method has been increasingly used thanks to the development of global atmospheric reanalyses.

Approximately 4,800 articles are returned by a search of the topic "North-Atlantic Oscillation" (source: Web of Knowledge). Among them, there are a large number of studies concerning the
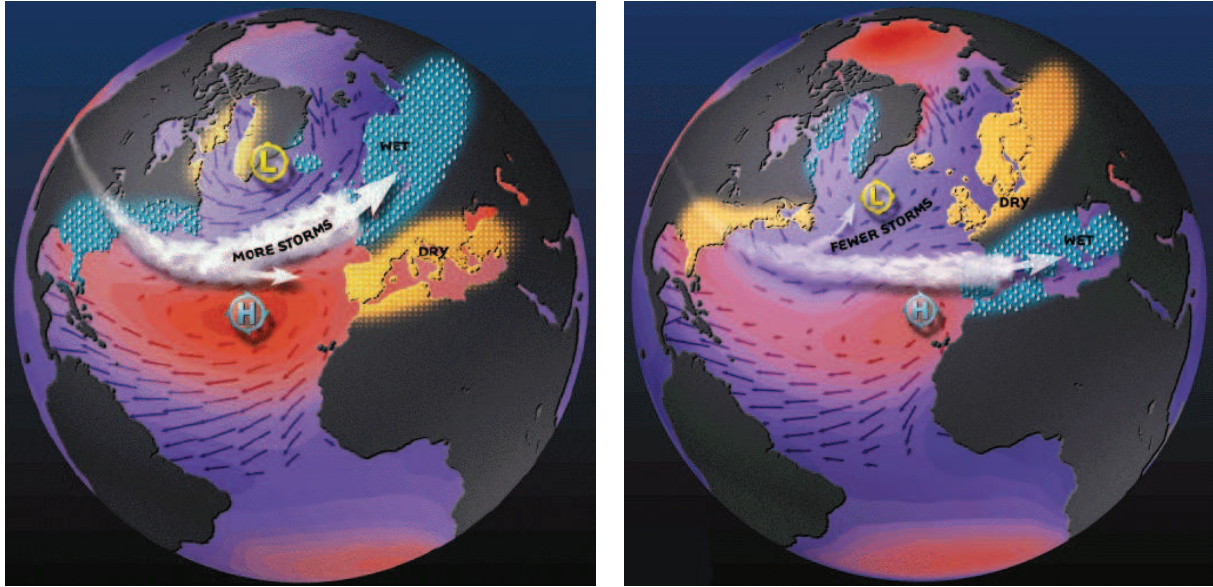
(a) *Schematic for NAO+ phase*          (b) *Schematic for NAO- phase*

*Figure 2.2: Schematic for positive and negative NAO phases. Source:*
`http://www.ldeo.columbia.edu/res/pi/NAO/`

impacts of the NAO on the ocean circulation. For example Curry and McCartney (2001), Marshall et al. (2001), Eden and Willebrand (2001), Bellucci and Richards (2006), Deshayes and Frankignoul (2008), Bellucci et al. (2008), Herbaut and Houssais (2009), or Lohmann et al. (2009) all investigate the impacts of the NAO on the gyre and overturning circulations in the North-Atlantic on interannual to decadal time scales.

The general agreement among these studies is that the response of the ocean to the NAO depends on the timescales of interest. At monthly to interannual timescales, the NAO impacts the ocean circulation via wind-driven mechanisms. Positive NAO conditions (i.e. enhanced and northward shifted westerlies) give rise to an anticyclonic gyre circulation anomaly located at the boundary between the subtropical and subpolar gyres (the intergyre-gyre, Marshall et al. 2001). This pattern is the signature of the linear (Sverdrup-like) response of the gyres to the NAO-driven meridional shifts of the wind-stress curl (Eden and Willebrand 2001). At these timescales, the AMOC shows top-to-bottom negative anomalies north of 45°N, and positive anomalies to the south, which are the signature of Ekman induced surface flow compensated at depth by a return flow.

On longer (decadal) timescales, the subtropical and subpolar gyres intensify in response to positive NAO conditions. The adjustment of the subtropical gyre is driven by the baroclinic adjustment to anomalous wind-stress curl, while the subpolar gyre adjusts via baroclinic adjustment to changes in

heat fluxes (Eden and Willebrand, 2001). At these timescales, the AMOC response to positive NAO is a large scale strengthening of the circulation, which mostly occurs through enhanced convection and deep water formation, in the Labrador Sea especially.

### 2.2.2   East-Atlantic Pattern (EAP)

The EAP, introduced by Barnston and Livezey (1987), is the second mode of variability in the North-Atlantic Ocean (15% of winter averaged sea-level pressure anomalies variance explained). It is characterised by anticyclonic sea-level pressure anomalies centered at near 55°N, 25°W. Positive EAP conditions are associated with warm air-temperature anomalies in the subpolar gyre, cold anomalies and reduced precipitations in western Europe.

The literature concerning the EAP is far from being as abundant as for the NAO: only 44 articles are returned by a search of the topic "East-Atlantic Pattern" (source: Web of Knowledge). However, recent studies suggest that despite the small fraction of the atmospheric variability that is explained by the EAP, the latter is rather effective in forcing the gyre circulation. Hakkinen et al. (2011a) suggest, using observations, that to understand the variability of the gyres, one must consider the second EOF of wind-stress curl anomalies (related to the EAP) rather than the first one (related to the NAO). Indeed, this second EOF projects fairly well onto the mean position of the gyres and is accordingly rather effective in impacting their variability (hence the name of this EOF, "gyre-mode"). Positive EAP conditions are associated with a reduced gyre-mode and a reduced gyre circulation. Langehaug et al. (2012), using the control[1] experiment of the Bergen Climate Model, came to a similar conclusion.

Msadek and Frankignoul (2009) and Ruprich-Robert and Cassou (2013), using a control[1] simulation of the IPSL-CM4 and CNRM-CM5 climate models respectively, suggest that the AMOC multidecadal variability is closely related to the EAP. In their model, positive EAP induces a reduction in the salt advection by the North-Atlantic Current that reduces deep convection in the Nordic Seas and in turn the strength of the AMOC.

---

[1]No external forcing (i.e. greenhouse gaz emission or solar forcing)

## 2.2.3 Scandinavian Pattern (SCAN)

SCAN is the third mode of atmospheric variability in the North-Atlantic domain (approximately 12% of winter averaged sea-level pressure anomalies variance explained). Its positive phase is characterised by anticyclonic conditions over Europe that prevent the westerlies to penetrate inland, hence leading to warm air-temperature anomalies in Europe. The number of articles in which the topic contains the words "Scandinavian Pattern" is comparable with that of the EAP (37, source: Web of Knowledge).

The impacts of the SCAN on the ocean circulation have mainly been assessed using coupled climate models. Medhaug et al. (2011) suggest that it impacts the AMOC trough meridional heat transport: positive SCAN conditions induce a weaker gradient of sea-surface height across the Greenland-Scotland-Ridge, which leads to a barotropic adjustment of the circulation and to a decrease in poleward heat transport across the ridge. This decrease in poleward heat transport influences the AMOC directly, through water mass transformation in the Nordic Seas (4 years after a change in the SCAN index) and remotely, through reduced freshwater discharge by the sea-ice melting. The resulting salinisation will favour deep convection in the Nordic Seas and the Labrador Sea, which both will lead to an increase in the strength of the AMOC (approximately 7 years after a change in the SCAN index, see figure 14 of Medhaug et al. 2011).

## 2.2.4 Limitations of the modes of variability

The decomposition of sea-level pressure anomalies into EOFs, which allow to determine the spatial patterns and time indices of the NAO (first EOF), the EAP (second EOF) and of the SCAN (third EOF), relies on strong assumptions. First, by construction, EOF analysis assumes that the modes are orthogonal. The implications of such an assumption are illustrated by considering the following 3D vector:

$$F(x, y, t) = V_1(t) \times F_1(x, y) + V_2(t) \times F_2(x, y)$$

where $F_1/F_2$ are spatial patterns that represent $2D$ Gaussian distributions (figures 2.3a and b) and $V_1/V_2$ are their standardised time variations (figure 2.3c), obtained via random drafts following a Gaussian distribution (mean=0, standard deviation=1). By construction, the spatial patterns are monopolar and, at each grid point, $F$ has a 0-mean.

The first EOF of $F$ shows a monopolar pattern that resembles to $F_1$ (figure 2.3d). The second EOF, on the other hand, shows a dipolar pattern, with positive anomalies near the center that are reminiscent of $F_2$, and negative anomalies elsewhere. Hence, it fails to fully capture the monopolar spatial pattern of $F_2$. This peculiar behaviour of EOF decomposition, due to the orthogonality constraint, has been discussed in Richman (1986). One way to overcome this constraint is to rotate the EOFs, as initially introduced by Richman (1986).
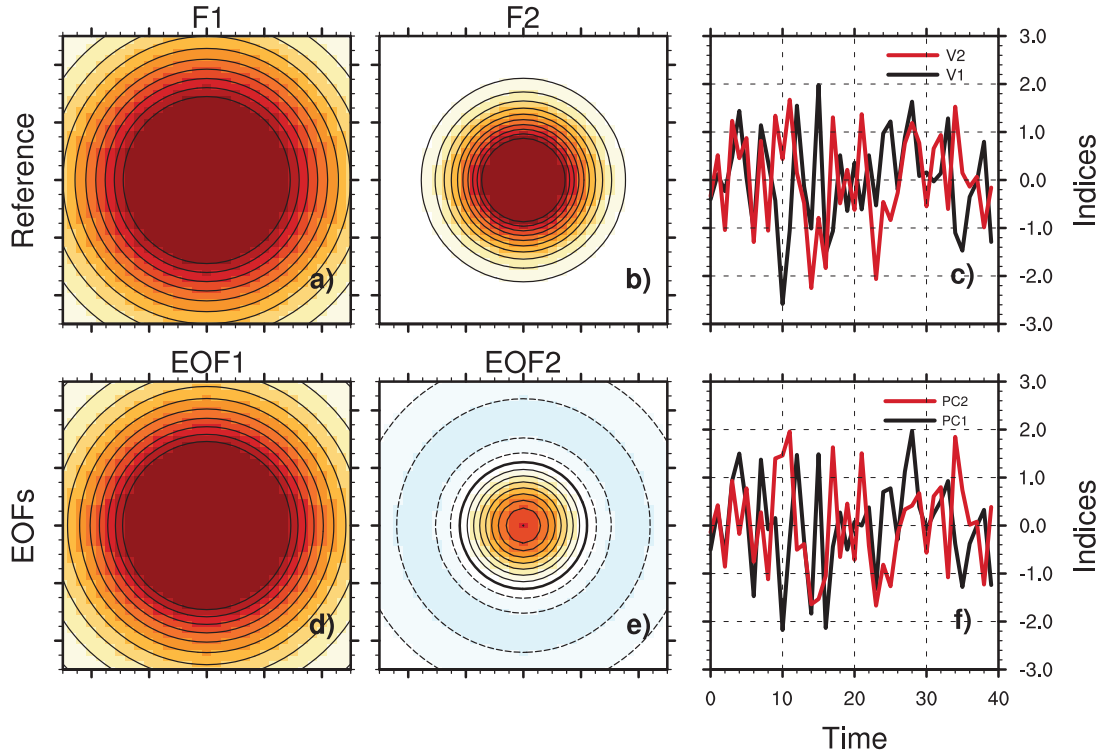


*Figure 2.3: Top panels: the two spatial patterns (a and b) and their associated time-series (c) used to construct the idealised 3D vector $F$. Bottom panels: the spatial patterns of the first two EOFs of F (d and e) and their associated principal components (f).*

A greater limitation is that EOF decomposition assumes that the two phases of the modes are symmetric. Indeed, the spatio-temporal variability of the mode is obtained by multiplying the time-varying index, with negative and positive values since time indices are most often centered on a 0-mean, by a fixed spatial pattern. The latter assumption has been shown to be partially inadequate for the NAO (Cassou et al. 2004), where the deeper Icelandic Low/stronger Azores High are northeastward shifted in NAO$^+$ compared to NAO$^-$. To overcome this issue, an "augmented" NAO index has been proposed by Wang et al. (2012), in which the angle between the two centers of actions is used in addition to the classical NAO index, indicative of the strength of the anomalies.

However, such an index is hard to use in order to analyse the impacts of the NAO on the ocean circulation.

## 2.3 Winter weather regimes

Weather regimes are known since 1950 (Rex, 1950), when empirical atmospheric observations revealed that large-scale anomaly patterns recurrently occur in the North-Atlantic domain. The weather regimes can be simply described as recurrent (i.e. that occur repeatedly), quasi-stationary (i.e. with a life-span of a few days) and large-scale atmospheric patterns (Vautard and Legras 1988; Vautard 1990). They have often been used in atmospheric studies: some 450 articles contain the words "weather regime(s)" in the topic (source: Web of Knowledge). Among them, one can cite Mallet et al. (2013), Robertson and Ghil (1999), Yiou and Nogaj (2004), Plaut and Simonnet (2001).

The weather regimes have, to our knowledge, not yet been used to assess the influence of large-scale atmospheric variability on the ocean circulation. However, Cassou et al. (2011); Minvielle et al. (2011) have shown that they are effective in capturing the interannual to decadal variability of the surface forcings to the ocean, hence are a promising tool to address this question.

### 2.3.1 Decomposition

In this study, sea-level pressure anomalies have been decomposed into weather regimes using the $k$-mean algorithm of Michelangi et al. (1995), which agglomerates days that share some ressemblance. This method assumes that the number of regimes, $k$, is a priori known, which is a rather strong assumption. The common value in winter is 4, which is consistent with other methods of decomposition (Vautard and Legras 1988; Vautard 1990) and which has been validated by significance tests (Michelangi et al. 1995). Hence, four winter weather regimes are considered in the following.

The classification algorithm has been applied on winter daily sea-level pressure anomalies, extracted from the NCEP/NCAR reanalysis (Kalnay et al. 1996). Anomalies are computed by removing a smoothed seasonal cycle (two harmonics retained). Contrary to Cassou et al. (2011), who used geopotential height at 500 $mb$, sea-level pressure anomalies are used in this study because, at large-scale, the wind is in geostrophic balance and follows the contours of sea-level pressure. However,

we have verified that using geopotential height instead of sea-level pressure leads to similar weather regimes.

## 2.3.2 Regime statistics

The output of the classification algorithm is schematised in figure 2.4 for one regime: a value of 1 means that the regime is excited and that the other regimes are not (value of 0). From this array of boolean, one can determine the regime statistics that will be used in the next chapters.

|  | December | January | February | March |
|---|---|---|---|---|
| Year 1 | 0011100000011100 | 0000111000000000 | 1111111001110000 | 1111100001111000 |
| Year 2 | 1111000001111000 | 0000000111000000 | 0000001110000000 | 0111110000000000 |

*Figure 2.4: Outputs of the classification algorithm schematized for one regime. Values of 1 indicate that the regime is excited and that the other regimes are not (values of 0). Colors represents months.*

**Cendroids and composites**

Centroids refer to the spatial patterns of the weather regimes. They are computed by averaging the field used in the classification (in this study, winter daily sea-level pressure anomalies) over all the days in which the regime is excited (values of 1 in figure 2.4). Surface forcing composites are determined in the same way.

**Occurrences**

*Monthly occurrences* are defined as the number of days within a month during which the regime is excited. They are computed by summing the values within each frame of figure 2.4. In this example, the monthly occurrences for the first year are 6, 3, 11 and 10 in December, January, February and March, respectively.

   *Winter occurrences* refer to the number of winter (DJFM) days during which the regime is excited. They are computed by summing the values of table 2.4 over each line. In our example, the winter occurrence during the first year is 30.

33

**Intra- and inter-regime distance**

Let $D$ be a day belonging to regime R1. The *intra-regime* distance $d_{intra}$ is defined as the euclidian distance between the daily map of sea-level pressure anomalies of $D$, which we call $M_D(x, y)$, and the centroid of R1, which we call $C_{R1}(x, y)$:

$$d_{intra} = \sum_x \sum_y [M_D - C_{R1}]^2$$

The *inter-regime* distances are the euclidian distances between $M_D(x, y)$ and the centroids of the other three regimes. Another similarity criterion is given by the spatial correlation between $M_d$ and $C_{R1}$. However, the euclidian criteria is used here since it better captures the variability of surface forcing (Marie Minvielle, personal communication).

## 2.3.3 Regime description

In this section, the winter weather regimes used in this study and their associated forcing anomalies are described. The dataset used in this section is the NCEP/NCAR reanalysis (Kalnay et al. 1996) in the period starting in $1957 - 12 - 01$ and ending in $2010 - 03 - 31$. Figure 2.5 shows the centroids of the 4 winter weather regimes as well as the corresponding winter occurrences

The first regime is known as the Atlantic-Ridge (AR). It is characterised by anticyclonic anomalies off Europe. The second regime is known as the Blocking regime (BLK) and is characterised by anticyclonic anomalies in Northern Europe and cyclonic anomalies centered in Southern Greenland. The NAO$^-$ regime is characterised by positive sea-level pressure anomalies centered in Greenland and negative anomalies in the south, while the NAO$^+$ regime is characterised by negative anomalies eastward of Iceland and positive anomalies in the south. In the literature, NAO$^+$ and NAO$^-$ are often described as the *Zonal regime* and the *Greenland Anticyclone* regime, respectively (Vautard, 1990).

The winter occurrences (right column in figure 2.5) show a mixture of interannual and decadal variability. The decadal variability is however more important for the two NAO regimes, with greater NAO$^-$ winter occurrences in the first half and weaker ones in the second half, and conversely for the NAO$^+$. In the 1958-2010 period, the regime that occurs the most is the NAO$^+$ (27.75%), followed
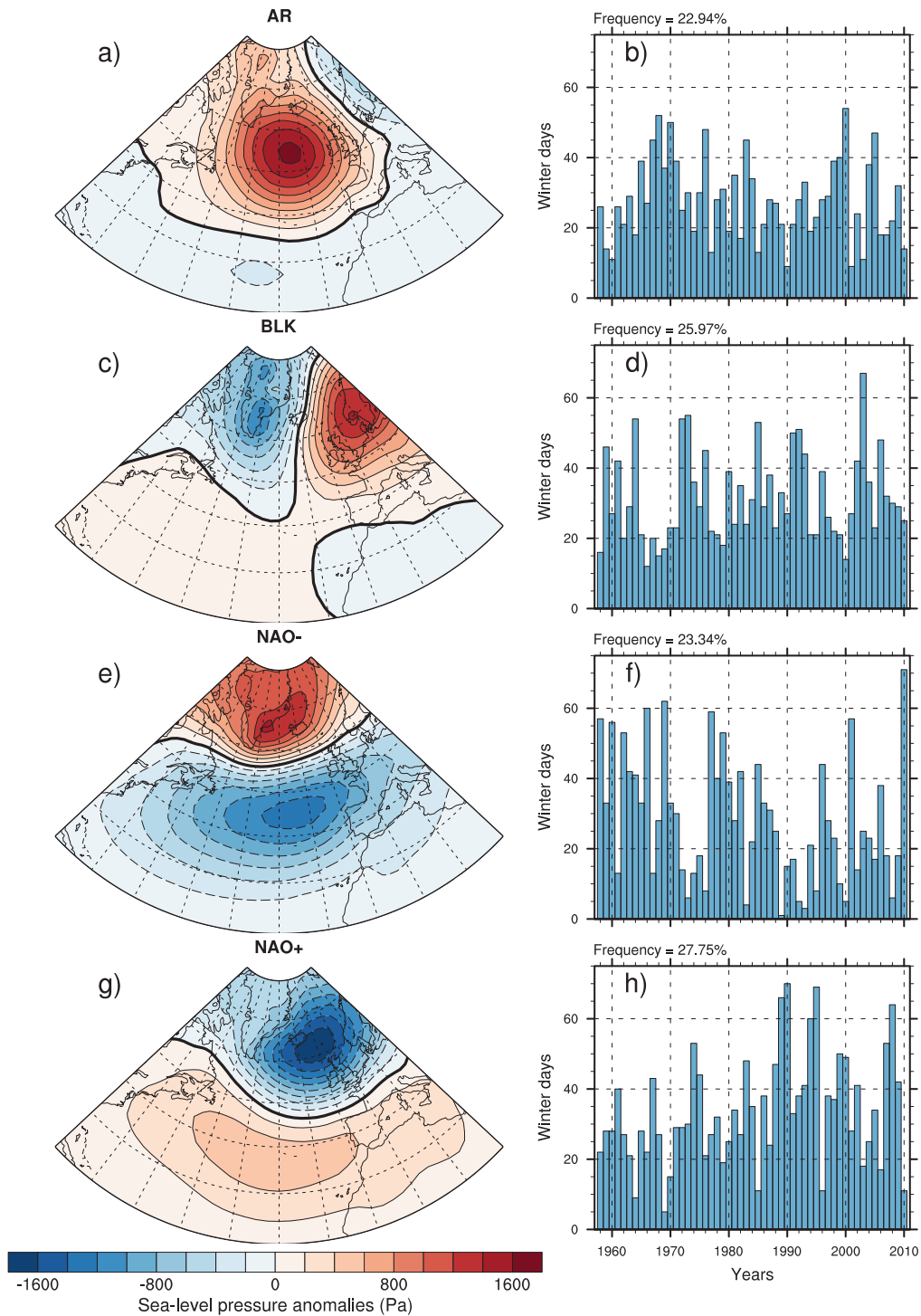
Figure 2.5: Centroids (left panel) and winter occurrences (right panel) obtained by the classification into four regimes. The total frequency of occurrence is indicated at the top of the time series.

by the BLK (25.97%), the NAO⁻ (23.34%) and finally the AR (22.94%).

The asymmetry of the NAO is clear in figure 2.5 and is further confirmed by the comparison between Hurrell's NAO index[1] and the winter occurrences of the NAO⁺ and NAO⁻ regimes (figure

[1]http://climatedataguide.ucar.edu/sites/default/files/cas_data_files/asphilli/nao_pc_djfm_1.txt

2.6). A stronger correlation is obtained between the NAO index and the NAO$^-$ occurrences ($-0.92$), while the correlation with the NAO$^+$ occurrences is slightly weaker (0.78), hence suggesting that the spatial pattern of the NAO mode projects fairly well onto the spatial pattern of the NAO$^-$ regime.
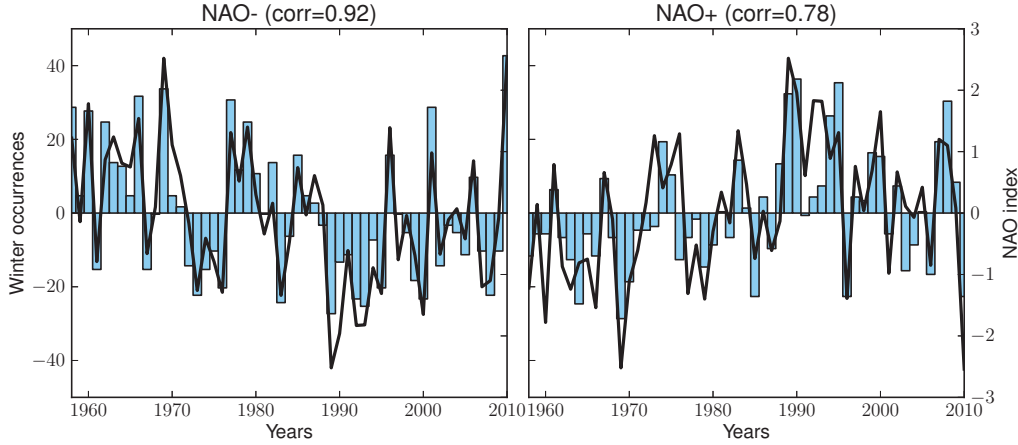


*Figure 2.6: Comparison between Hurrell's NAO index (black lines) and the anomalies of winter occurrences of the NAO$^+$ and NAO$^-$ regimes (vertical blue bars). Correlations between the time series are indicated.*

The weather regimes are associated with wind and air-temperature anomalies (figure 2.7). Wind-anomalies usually follow the contours of MSLP anomalies described in figure 2.5, since at large-scale the wind is in geostrophic balance. Hence, AR is characterised by anticyclonic wind anomalies off Europe, while BLK is characterised by a northward shift of the winds near 20°W, caused by the anticyclone centered in Europe that prevents the westerlies from penetrating inland. To first order, the NAO$^+$ pattern shows a strengthening of the mean winds (figure 1.5a), while the NAO$^-$ pattern shows a weakening of those winds. Regarding air-temperature, AR is characterised by warm anomalies in the subpolar gyre and negative anomalies in the Nordic Seas. BLK is characterised by cold anomalies in the Labrador Sea region, probably caused by the advection of cold air originating from northern Canada, and by warm anomalies in the Nordic Seas. For the two NAO related regimes, air-temperature anomalies show the well known tripole pattern (Cayan 1992b). NAO$^+$ pattern shows a warming in the Labrador Sea and a cooling at midlatitudes and in the Nordic Seas. To first order, the opposite anomalies are obtained for the NAO$^-$. However, as will be shown in 4, the NAO asymmetry is essential to fully understand the ocean response to changes in the NAO.

Delecluse (2011) compares the centroids and the winter occurrences of the four regimes using different atmospheric reanalysis (figure 2.8). The differences are very small and fall within the range
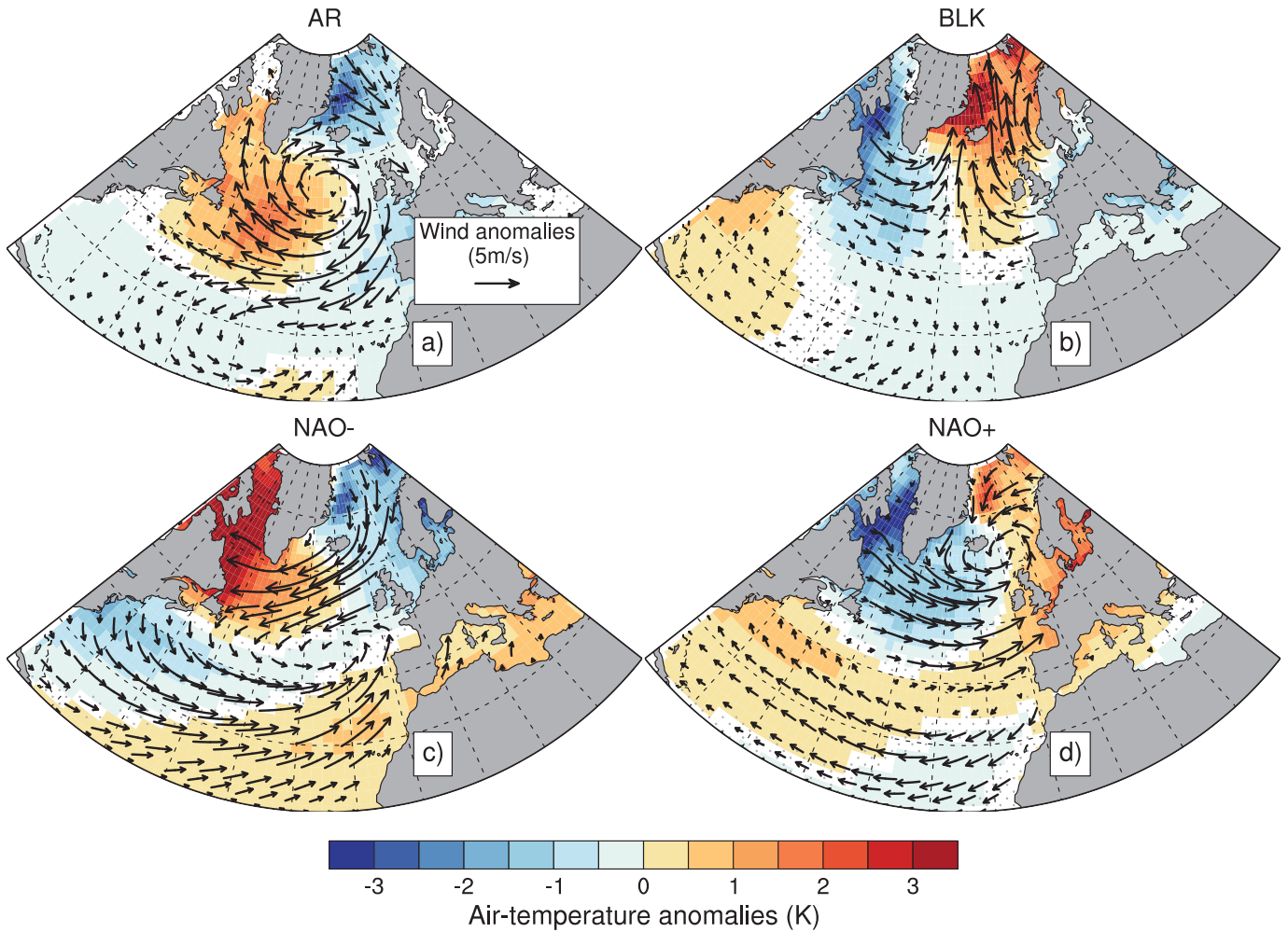
*Figure 2.7: Daily composites of surface wind (black arrows) and air-temperature (color shading) anomalies for the four weather regimes. Non-significant data are omitted. Significativity was computed from a Student test with a 95% confidence interval.*

of uncertainty of the method. Furthermore, figure 2.8 highlights the robustness against time of the weather regime decomposition and also the interannual and decadal variability of the winter occurrences. As already discussed, the decadal variability is more important for the NAO$^-$ and the NAO$^+$ regimes than for the other two regimes.
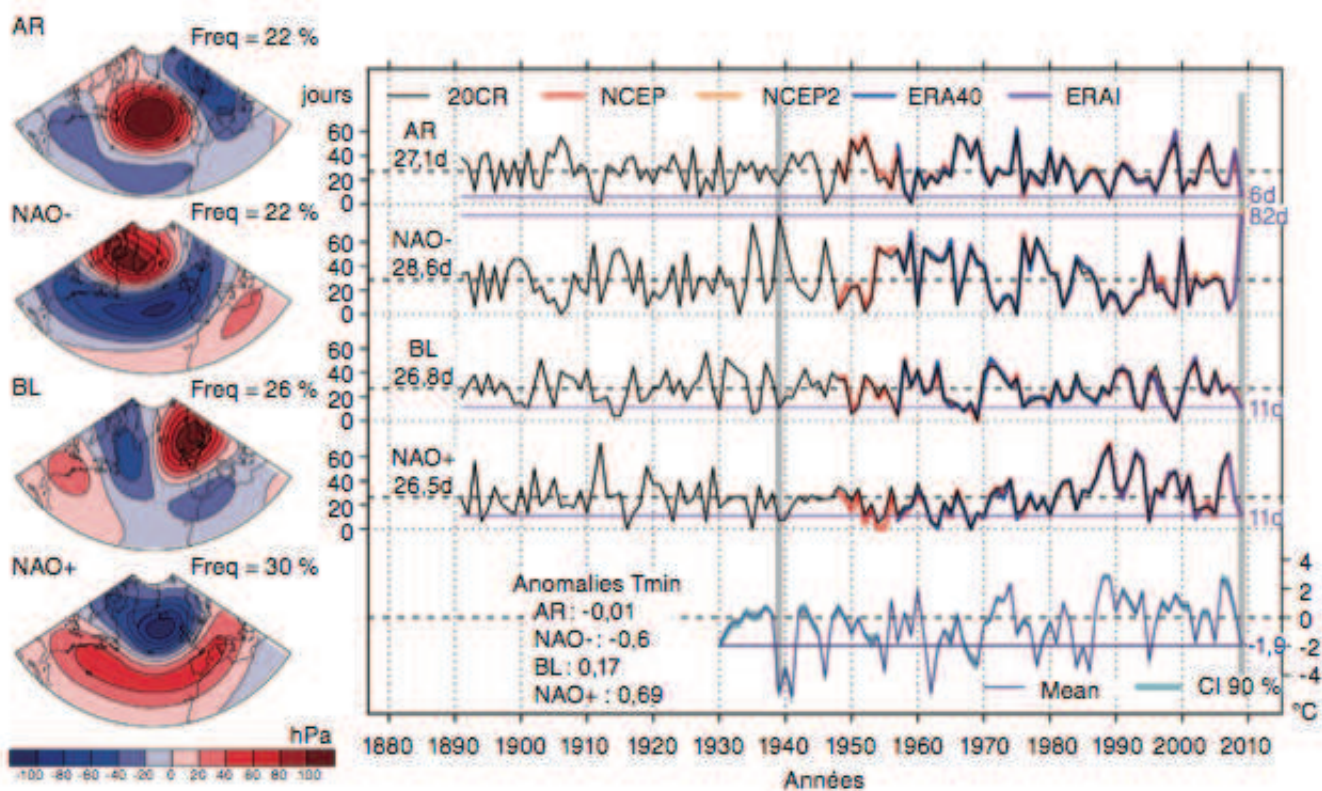
Figure 2.8: *Centroids and winter occurrences for winter (DJF) weather regimes computed from geopotential height at 500 m. The occurrences are shown for the different reanalysis used in the calculation. Source: Delecluse (2011).*

## 2.4 Linkages between weather regimes and surface forcings

The skill of the weather regimes to capture the variability of surface forcings has been investigated in Minvielle (2009); Cassou et al. (2011); Minvielle et al. (2011). Their main results are summarised in this section.

They have used multiple linear regression analysis between winter averaged forcings (zonal and meridional winds, air-temperature anomalies) and the winter occurrences of weather regimes to assess the latter's skills in capturing the interannual variability of surface forcings (figure 2.9). The reconstructed zonal wind (figure 2.9a) shows maximum correlations at the latitudes of the NAO wind composites (figure 2.7), while the meridional wind (figure 2.9b) shows maximum correlation in the northeastern Atlantic, which can be attributed to BLK and AR. Maximum correlations between observed and reconstructed air-temperature (figure 2.9c) are obtained in the Labrador Sea and the Irminger Sea.



*(a) Zonal wind*     *(b) Meridional wind*     *(c) Air-temperature*
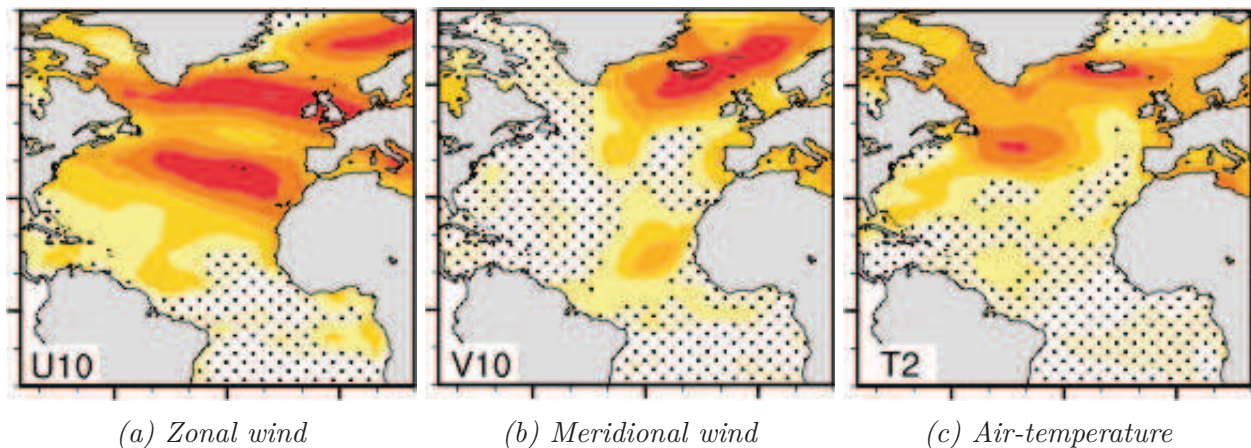
*Figure 2.9: Interannual linear correlations between winter averaged observed forcings and reconstructed forcings via multiple linear regression with the weather regimes winter occurrences. Contour interval: 0.1 (red indicates correlations of 0.7). Source: Cassou et al. (2011)*

Cassou et al. (2011) also suggest that the intra-regime distance defines the signs of the anomalies (for instance strengthened westerlies and air-temperature tripole for NAO$^+$), while the three inter-regime distances control their intensities, as schematised in figure 2.10. For the two days (yellow and red crosses), the sign of the anomalies and the intra-regime distances (pink arrows) are the same. However, the intensity of the anomalies and the inter-regime distances are different. The day represented by the red cross has the strongest anomalies and has the greatest inter-regime distance. This property will be used in chapter 4.
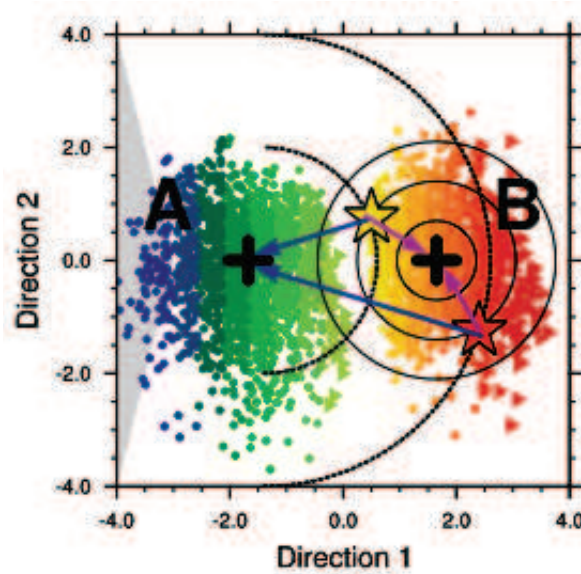
*Figure 2.10: Schematic diagram of inter and intra regime distance influence on surface variable anomalies. Crosses represent two different days. Black crosses represent two regime centroids. Pink arrows represent intra regime distances and blue arrows inter regime distances. Coloured points represent anomalies (red=warm, blue=cold for instance). Source: Cassou et al. (2011).*

## 2.5    Conclusion

In this chapter, we have introduced the concept of modes of variability, which has often been used by the oceanographers as a proxy of atmospheric variability. The three main modes of variability in the North-Atlantic/Europe domain are the North-Atlantic Oscillation (NAO), the East-Atlantic Pattern (EAP) and the Scandinavian Blocking (SCAN). Historically, the oceanic variability has been mainly linked to the NAO variations. However, recent studies have emphasised the importance of the two other modes.

The decomposition into modes of variability assume that these modes are orthogonal and symmetric. However, the latter assumption has been shown to be inappropriate for the NAO. As an alternative, the use of the weather regime framework to assess the atmospheric variability has been proposed. These regimes fairly well capture the variability of surface forcings, which make of them interesting candidates to assess the impacts of atmospheric variability on the ocean circulations.

The philosophy behind the modes of variability is different from the philosophy behind the weather regimes, as schematised in figure 2.11 for the NAO. The variability of the NAO mode can be viewed as the oscillation[1], over time, between two states (figure 2.11a), while the two NAO regimes can be

---

[1]This term is however misleading since one would expect oscillatory temporal variations, which are far from obvious

*(a) Mode of variability*   *(b) Weather regime*
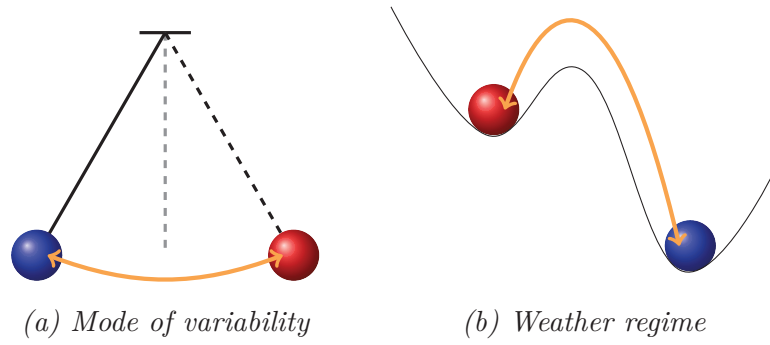
*Figure 2.11: Schematic of the two visions of the NAO described in this chapter. Positive NAO is represented by a red marble, negative NAO is represented by a blue marble. Orange arrows represent changes from one phase to another.*

viewed as two distinct steady states 2.11b).

The potential in using the weather regimes to analyse and understand the ocean response to atmospheric forcing is promoted in the next chapters.

# Chapter 3

# Impact of North-Atlantic Weather Regimes on subtropical sea-surface height

## Contents

## 3.1 Introduction

The variations in the strength of the subtropical gyre have often been analysed using sea-level anomalies. Among the numerous studies in that regard, one can cite Sturges and Hong (1995), Sturges et al. (1998), Ezer (1999), Hong et al. (2000) or Cabanes et al. (2006). All these studies agree to say that the major forcing component of subtropical sea-level anomalies is open ocean wind-stress curl, via Sverdrup transport and westward propagation of planetary waves.

The NAO (section 2.2.1) can be viewed, to first order, as a measure of the strength of the mean winds in the North-Atlantic. Hence, negative NAO conditions (i.e. reduced westerlies and Trade winds) could be expected to slacken the subtropical gyre, as suggested by Ezer (1999) to explain the weakening that occurred in the 70s. However, Hakkinen et al. (2011a,b) suggest that the wind-stress curl anomalies associated with the NAO are not effective in modulating the strength of the horizontal circulation, contrary to the wind-stress curl anomalies associated with the EAP (section 2.2.2).

The aim of the present chapter is to determine which large-scale atmospheric pattern effectively impacts the interannual variability of the subtropical gyre by using sea-surface height observations and a theoretical model.

## 3.2   Bermuda tide-gauge data

Monthly and yearly tide gauge data at Bermuda are provided by the "Permanent Service for Mean Sea Level" (PSMSL[1]). There are, however, two main limitations in using the yearly PSMSL time-series in our study:

- Weather regimes are computed from DJFM sea-level pressure anomalies, while PSMSL yearly averages are computed between January and December. To be consistent with weather regime calculations, the continuity of winter months must be preserved.

- In PSMSL, yearly data are computed as the average of monthly data. Hence, when monthly data are missing, the yearly data are also missing, giving a discontinuous yearly time-series between 1949 to 1998.

Hence, a yearly time-series that overcome these issues has been constructed using the raw monthly PSMSL data (figure 3.1).
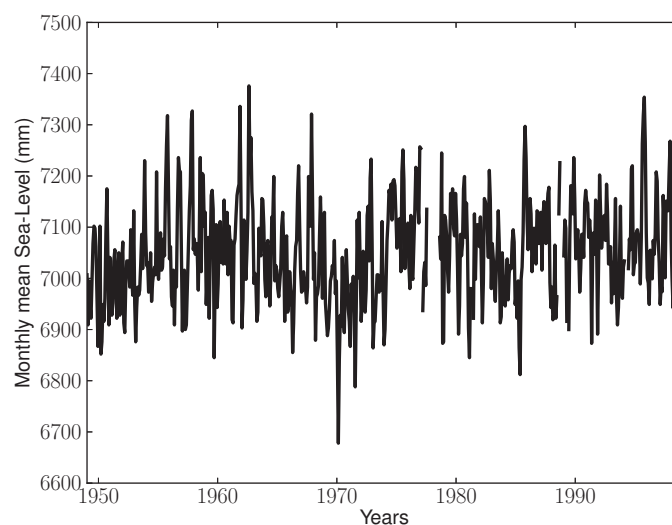


*Figure 3.1: Raw PSMSL time series, station St Georges/Esso Pier.*

---

[1]http://www.psmsl.org/

## 3.2.1 Inverse barometer effect

As the scope of this study is to investigate the impacts of WRs on the strength of the subtropical gyre (assessed through Bermuda sea-level anomalies), the direct effect of sea-level pressure anomalies on sea-surface height, the so-called inverse barometer effect, must be corrected. This is achieved by removing the "inverse barometer correction" IBC, defined as:

$$IBC = -\frac{-P'}{\rho_0 \; g} \; , \; P' = P - P_{ref} \tag{3.1}$$

with $P$ the sea-level pressure at Bermuda and $P_{ref}$ a reference pressure. In this study, $P_{ref}$ is the sea-level pressure at Bermuda averaged over 1949-1998. As Bermuda Island is far from the main atmospheric systems, the impacts of the inverse barometer effect on the sea-level are weak (cf. table 3.1)

|      | Min    | Max   | Stddev |
|------|--------|-------|--------|
| SSH  | -373.1 | 342.9 | 100.5  |
| IBC  | -91.2  | 93.2  | 23.9   |

*Table 3.1: Minimum, maximum and standard deviations of the raw monthly bermuda time-series and of the IBC. Units=mm*

## 3.2.2 Removing of a long-term trend

Figure 3.2 shows the $IBC$-corrected time-series and the long-term trend ($1.2 \; mm.year^{-1}$) estimated from non-missing monthly data. The trend compares well with the estimates of Bindoff et al. (2007) and is likely the signature of thermosteric sea-level rise (Antonov et al. 2005). This trend has been removed.

## 3.2.3 Computation of yearly time-series

The next step is to determine a yearly time-series from these pre-processed monthly data. To do so, a mean seasonal cycle is first computed using the non-missing monthly data and is removed from the records.

These monthly sea-surface height anomalies are then averaged from December to November to keep the continuity of winter months. This reconstructed time-series is correlated at 0.96 with the
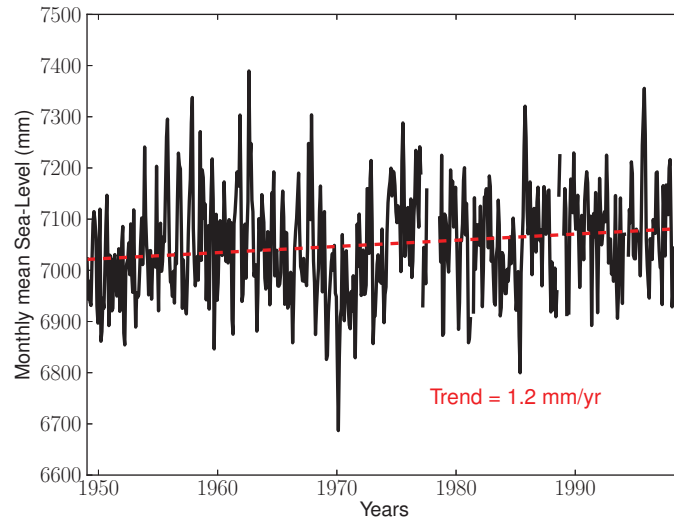
*Figure 3.2: IBC-corrected time-series (black lines) and long-term trend (dashed red line), the coefficient of which is indicated.*

yearly time-series of PSMSL, validating the reconstruction method (figure 3.3).
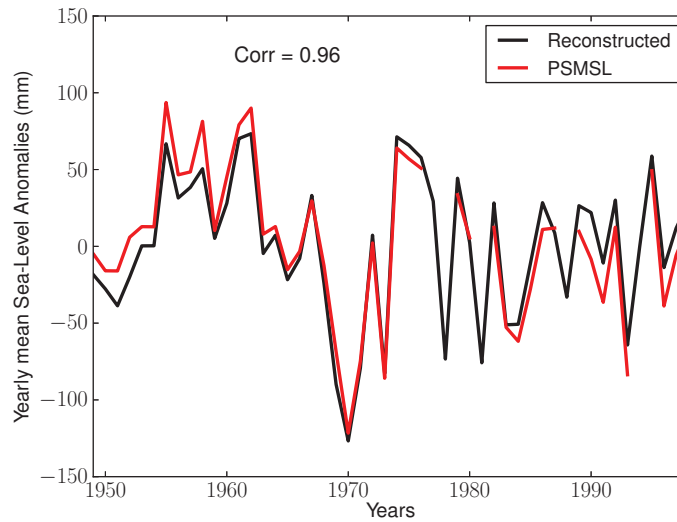


*Figure 3.3: PSMSL (red) and reconstructed (black) yearly time-series. The correlation coefficient between the two time-series is indicated.*

46

## 3.3 Article

In Barrier et al. (2012), published in *Climate Dynamics*, the linkages between the strength of the subtropical gyre and the WRs are analysed. This is achieved by using correlation analysis between the December-to-November averages of sea-surface height observations in the subtropical gyre and the winter regime occurrences. The observation datasets are the Bermuda yearly time series described in the above and the "Maps of Absolute Dynamic Topography" (MADT) issued from the AVISO[1] dataset. The analysis is completed by using the planetary geostrophic model of Cabanes et al. (2006), which allows the understanding of the mechanisms involved in the variations of subtropical sea-surface height anomalies.

---

[1] `http://www.aviso.oceanobs.com/en/`

# Impact of the winter North-Atlantic weather regimes on subtropical sea-surface height variability

Nicolas Barrier · Anne-Marie Treguier ·
Christophe Cassou · Julie Deshayes

**Abstract** Interannual variability of subtropical sea-surface-height (SSH) anomalies, estimated by satellite and tide-gauge data, is investigated in relation to wintertime daily North-Atlantic weather regimes. Sea-level anomalies can be viewed as proxies for the subtropical gyre intensity because of the intrinsic baroclinic structure of the circulation. Our results show that the strongest correlation between SSH and weather regimes is found with the so-called Atlantic-Ridge (AR) while no significant values are obtained for the other regimes, including those related to the North Atlantic Oscillation (NAO), known as the primary actor of the Atlantic dynamics. Wintertime AR events are characterized by anticyclonic wind anomalies off Europe leading to a northward shift of the climatological wind-stress curl. The latter affects subtropical SSH annual variability by altered Sverdrup balance and ocean Rossby wave dynamics propagating westward from the African coast towards the Caribbean. The use of a simple linear planetary geostrophic model allows to quantify those effects and confirms the primary importance of the winter season to explain the largest part of SSH interannual variability in the Atlantic subtropical gyre. Our results open new perspectives in the comprehension of North-Atlantic Ocean variability emphasizing the role of AR as a driver of interannual variability at least of comparable importance to NAO.

N. Barrier (✉) · A.-M. Treguier · J. Deshayes
Laboratoire de Physique des oceans, CNRS-Ifremer-UBO-IRD,
UMR 6523, Brest, France
e-mail: Nicolas.Barrier@ifremer.fr

C. Cassou
CNRS Cerfacs, Toulouse, France

## 1 Introduction

In the context of climate change, the detection of multi-decadal trends and their potential attribution to human influence is a major challenge. A special attention is devoted to sea-surface height (SSH) that integrates the forcings, whatever their origins (natural such as volcanic/tropospheric aerosols and solar fluctuations, or anthropogenic such as sulfates and greenhouse gazes emission, etc.), over long periods of time. Its recent accelerating rise is expected to have regionally potential disastrous impacts. Observed SSH variability from seasonal to decadal timescales can be considered as a superimposition of a global upward trend in response to external forcings and a signal associated with intrinsic or natural variability of the climate system. The latter is due to the coupling between components of very different time-scale and spatial-scale characteristics of variability and to the presence of nonlinear processes. Its variance is presently one order of magnitude larger than the externally-forced component and it is thus necessary to quantify and understand the mechanisms of that natural variability to be able to remove it from the observed records and assess long-term trends. In the North-Atlantic, ocean variability mostly comes from changes in wind and buoyancy forcings related to large-scale modes of atmospheric variability. From daily to decadal timescales, the North-Atlantic Oscillation (NAO) is the dominant pattern in the Northern Atlantic/Europe domain. As a matter of fact, many studies were devoted to investigate the impacts of NAO on ocean circulation, especially on SSH and meridional heat transport (MHT) anomalies. MHT anomalies influence basin-scale SSH in turn, via heat content changes (Hakkinen 1999; Esselborn and Eden 2001). We briefly review, below, a selection that is relevant for our study.

Ezer (1999) uses sensitivity experiments of an ocean model to surface forcings to investigate the variability of the subtropical gyre. His results suggest that changes in wind-patterns in the northeastern Atlantic, that he attributes to NAO, cause negative surface elevation. The proposed mechanism is the westward propagation of long Rossby waves, consistently with Cabanes et al. (2006) and references therein. Hakkinen (1999) argues from a forced ocean model that the NAO is the dominant forcing of MHT via altered surface forcings (wind-stress and heat fluxes). The author states that MHT immediate response to changes in NAO occurs via anomalous Ekman transport, while the low-frequency response mainly occurs via the integration of NAO-induced heat fluxes in the subpolar gyre and the southward export of Labrador Sea Water, that causes MHT anomalies to propagate from 45°N to 25°N within one year. Both Eden and Willebrand (2001) and Gulev et al. (2003) show an immediate MHT response likely driven by NAO-related wind anomalies. However, their numerical experiments show a delayed ocean response of different nature. While in Eden and Willebrand (2001) the lagged baroclinic response is mainly wind-driven, Gulev et al. (2003) argue that it is due to buoyancy forcings and Labrador Sea Water formation in the subpolar gyre. Esselborn and Eden (2001) investigate, from satellite data and forced ocean model, basin-scale SSH interannual variability in relation with the NAO. They argue that the immediate response to a switch from a positive to a negative NAO phase induces a dipole pattern, with negative anomalies in the subpolar gyre and positive anomalies in the subtropical gyre. They propose that NAO-related changes in wind-stress curl leads to ocean circulation anomalies that induce anomalous advection of temperature (term $\overline{u'\overline{T}}$). This leads to anomalous heat convergence/divergence that in turn induces this SSH dipole pattern. The impacts of NAO on subpolar and subtropical gyres have also been investigated from observations. Curry and McCartney (2001) use observed potential energy anomalies (PEA), that can be reflected in SSH anomalies, to estimate the impact of NAO on both gyres. They argue that NAO-induced PEA in the subtropical gyre are dominated by vertical displacements of the pycnocline, driven by open-ocean wind-stress forcings integrated westward (see also Sturges and Hong 1995; Sturges et al. 1998; Hong et al. 2000). But changes in the Eighteen Degree Water property (Joyce et al. 2000) and changes in the deep ocean (due to altered import of Labrador Sea Water, Curry et al. 1998) can also impact this NAO-induced PEA in the subtropical gyre. In the subpolar region, PEA come primarily from changes in local heat fluxes but also from changes in the rates at which the water is imported and exported from the interior basin.

As described above, the NAO is an essential driver of both immediate and delayed oceanic variability (see also Lohmann et al. 2009). However, recent work of Hakkinen et al. (2011a, b) suggests that one has to go beyond the sole NAO contribution to understand the observed changes. In particular, the NAO fails to explain the warming and salinization of the early 2000s in the North-Eastern Atlantic. They argue that the latter could be due to the decadal fluctuations of winter blocking conditions, assessed in their study from the NOAA-20CR reanalysis (Compo et al. 2011) through traditional atmospheric metrics based on daily variance of mean sea-level pressure (MSLP) anomalies. The blocking associated space-time structure of wind-anomalies, the so-called "gyre-mode" (Hakkinen et al. 2011a), is related to the second mode of variability in the North-Atlantic atmospheric circulation, the so-called East-Atlantic Pattern (EAP, Barnston and Livezey 1987). When EAP dominates atmospheric variability, the subtropical gyre expands northward and the subpolar gyre shrinks; this facilitates the invasion of warm, salty subtropical water into the eastern subpolar gyre.

The relative importance of NAO versus EAP atmospheric patterns in forcing ocean circulation thus still appears to be an open question according to the literature. The major goal of this study is to determine which large-scale atmospheric circulation is responsible for the interannual SSH variability in the North Atlantic subtropical gyre estimated from satellite and tide-gauge data. The atmospheric anomalous circulation is assessed here through the weather regime (WR) circulation paradigm, preferred to classical modes of variability. WRs have been thoroughly studied in the literature (Vautard 1990; Michelangi et al. 1995, among others) and shown to be very efficient at capturing the interannual variability of the surface ocean forcings in the North Atlantic (Cassou et al. 2011). A second objective is to clarify which mechanisms drive the ocean response to changes in atmospheric conditions described by the WRs. The paper is organized as follows. Section 2 describes the data and the methodology used in this study. Section 3 describes the observed winter North Atlantic WR; a comparison between EOF and WR circulation patterns is provided. Section 4 depicts the relationship between WR occurrences and observed subtropical SSH anomalies. Section 5, based on a simple linear planetary geostrophic model, investigates the physical mechanism at work. Conclusions are given in Sect. 6.

## 2 Data and methodology

### 2.1 Subtropical sea-level

Subtropical sea-level anomalies are extracted from two different datasets. We first use AVISO Maps of Absolute

Dynamic Topography (MADT, Ducet et al. 2000), available from October, 1992 to March, 2010. MADT maps are first regridded at a coarser resolution (1°, similarly to Cabanes et al. 2006). As winter weather regimes occurrences are determined over winter, yearly averaged MADT anomalies are computed from December to November in order to keep the continuity of winter months. As the dataset is not complete in 1992 and 2010, those years are discarded. Additionally, a subtropical MADT time-series is computed by the averaging of MADT anomalies over the box (64°W–73°W, 24°N–30°N), which encompasses the subtropical gyre core without being influenced by the Gulf-Stream.

As the AVISO yearly time series spans a very short time-period (17 years), it is completed by a longer record. We use tide-gauge data at Bermuda, located in the subtropical gyre. Data were obtained from the Permanent Service for Mean Sea Level (PSMSL, http://www.psmsl.org/), station Esso Pier/St Georges (32.367°N, 64.700°W), between the period 1949–1998. To recover the missing values in the PSMSL annual time series, due to some missing data in the monthly records, we proceed as follows. The inverted barometer correction, following Ponte (2006), is first applied to non-missing data of the raw PSMSL monthly time-series. A linear trend of 1.2 mm/year, which is comparable with the existing literature (e.g. Bindoff et al. 2007), is removed from this monthly time series and anomalies are calculated by subtracting the mean seasonal cycle. Values are finally yearly averaged according to the same December-November average convention. We verify that our yearly index, which spans 50 years, is correlated at 0.98 to the one given by PSMSL (not shown).

## 2.2 Classification into weather regimes

The WR framework, based on daily circulation changes, accounts for the existence of preferred large-scale spatial states of the extratropical atmosphere set by the stationary waves (Molteni et al. 1990). The WR framework differs from fixed station indices such as the traditional NAO index (Hurrell 1995), polluted by circulations that are unrelated to the latitudinal alternation of the mean westerly flow that defines the NAO itself (e.g Hurrell and VanLoon 1997). It also differs from the traditional decomposition in modes of variability based for instance on EOF or Singular Value Decomposition that make symmetry assumptions for spatial fluctuations. Additionally, the WR paradigm also accounts for time-scale interaction: weather changes are interpreted as transitions between WR while climate variability is understood in terms of time-integration of daily WR occurrences and internal characteristics (strength for instance) over the time-scale of interest. This temporal integration property is promising for ocean variability

studies (Minvielle et al. 2011), the ocean being often viewed as the integrator of atmospheric noise (Frankignoul et al. 1997).

To decompose atmospheric variability into WRs, we proceed as follows. NCEP-NCAR (Kalnay et al. 1996) daily maps of mean sea-level pressure (MSLP) anomalies are computed inside the North-Atlantic domain (20°N–80°N, 80°W–30°E) by removing a smoothed seasonal cycle (two harmonics retained). Winter (December–January–February–March, hereafter DJFM) days are selected and MSLP anomalies are normalized by the cosine of the latitude. The classification is done in EOF space in order to reduce the degrees of freedom and thus facilitate the calculation. 20 EOFs, which explain 98.9 % of the total variance, are retained. It should be noted that contrary to Ayrault et al. (1995) or Smyth et al. (1999), no filtering is applied to our data. This allows us to keep the synoptic-scale variability (2–6 days), the slow-synoptic processes (6–11 days) and the low frequency variability (11–30 days) described in Gulev et al. (2002). Part of the ultra-high frequency variability (UHFV, 6 h to 2 days) is lost by the daily averaging. Even if the variance associated with UHFV is small, associated small scale events can lead to significant winds, which will thus not be considered here.

While there are many classification techniques (mixture model clustering: Smyth et al. 1999; non-linear equilibration: Vautard and Legras 1988; Vautard 1990), we use the k-mean algorithm described in Michelangi et al. (1995) and Cassou (2008), which relies on the recurrence property of the weather regimes. The aim of the method is to agglomerate days that share some resemblance (Euclidian criteria). It assumes that the number of clusters, $k$, is known. The algorithm, described in Michelangi et al. (1995), is as follows. $k$ days are randomly chosen among all the dataset and their anomalous circulations define the $k$ centroids $C_k$ (initial seeds). Then, the method attributes to each day $x$ the cluster that minimizes the Euclidian distance between $x$ and $C_k$, that we call $d(x, C_k)$. This initial partition, that we call $P_k^0$, is used to re-compute the centroids by averaging all the days that belong to the same regime. We call these new centroids $C_k^0$. The aggregation is iteratively repeated until the sum of variances within clusters of the $n$th iteration, defined as:

$$W(P^n) = \sum_{k=1}^{N} \sum_{x \in C_k^n} d^2(x, C_k^n) \tag{1}$$

reaches a local minimum. As this method strongly depends on the initialization of the algorithm, the entire process is repeated 50 times in order to get as many partitions. The one that minimizes the ratio of the sum of variances within clusters, $W(P)$, on the sum of variances outside clusters, $J(P)$, defined as:

$$J(P) = \sum_{k=1}^{N} \sum_{x \notin C_k} d^2(x, C_k) \qquad (2)$$

is selected. Finally, daily occurrences are summed over DJFM days from 1949 to 2010 to obtain a time-series of yearly occurrences for each regime.

One limitation of the $k$-mean algorithm is the assumption that the number of regimes is a priori known. However, Michelangi et al. (1995) determined that the number of clusters that allows classificability and reproducibility is 4, which is the value determined from other methods (Vautard 1990). In the following, we thus retain 4 winter weather regimes. A second limit, as mentioned in Smyth et al. (1999), is that this algorithm is inadequate if there is strong overlapping in the spatial patterns of the regimes. Finally, most studies that deal with weather regimes use geopotential height to compute weather regimes (Vautard 1990; Michelangi et al. 1995; Smyth et al. 1999; Cassou et al. 2011). We preferred to use MSLP, similarly with Santos et al. (2005), as MSLP can easily be related to surface winds. We checked that comparable centroids and yearly occurrences are obtained using anomalies of geopotential height at 500 hPa (not shown).

## 3 North-Atlantic Weather regimes

The four winter weather regimes that we obtain are depicted in Fig. 1 (left panels): the Atlantic Ridge (AR) characterized by an anticyclonic anomaly off Europe, the Scandinavian-Blocking (BLK) dominated by a meridional pressure dipole, north of 40°N, with an anticyclonic anomaly over northern Europe and a cyclonic circulation between Greenland and Iceland, and the Greenland Anti-cyclone and Zonal regimes linked to the negative and positive phases of the NAO, respectively. NAO− is characterized by a positive anomaly north of 50°N centered around Greenland and aligned at 30°W with a negative pressure anomaly south of 50°N. NAO+ is dominated by negative anomalies between Iceland and the North Sea while positive anomalies prevail south of 50°N. As shown in Fig. 1 (right panels, blue bars), winter occurrences time series highlight a strong interannual to decadal variability with neither pronounced nor significant trends.

Weather regimes have been shown to impact the "storm track" position. Ayrault et al. (1995) used the 2–6 days variance of geopotential height at 500 hPa ($Z_{500}$) as a proxy for the eastern position of the jet. The author states that NAO+ and NAO− are more likely to affect northern and southern Europe, respectively, while blocking regimes are likely to impact North-Eastern America. Rudeva and Gulev (2011), using clustering techniques on cyclone

**Fig. 1** (*Left*) Centroids of daily sea-level pressure anomalies for the four weather regimes (*colors*, contour interval: 200 Pa) and EOF-derived modes of variability computed from DJFM averaged sea-level pressure anomalies (*black* contours, contour interval: 50 Pa). The variance explained by each EOF is indicated between *parenthesis*. (*Right*) Number of days per winter of WR winter occurrences (*bars*) and corresponding principal components (PC) from EOF (see text for details). The correlations between the occurrences and the PCs are indicated. For *panel* **c**, the NAO$_{EOF}$ pattern and associated PC are multiplied by −1 so that they share the same sign as the NAO− regime

observations, suggest that cyclones formed in the Gulf-Stream region under NAO+/NAO− conditions are likely to end-up in the northeastern/eastern Central Atlantic, respectively. On the other hand, cyclones generated under AR conditions will decay in the Labrador-Sea while cyclones formed under blocking regimes will decay in the southeastern Atlantic. We performed a similar diagnosis as Ayrault et al. (1995) to determine the position of the eastern part of the jet within our four regimes. We use NCEP/NCAR (Kalnay et al. 1996) 2–6 days $Z_{500}$ anomalies and computed the standard deviation within each cluster (Fig. 2, color shading) and compare it with the climatological one (Fig. 2, black contours). For AR, one can see that the climatological core of variability, localized off northeastern America, is tilted toward the Labrador-Sea, consistently with Gulev et al. (2002). There is also a core of high standard deviation located in the Irminger Sea. In BLK, we notice that the variability is higher in the northeastern America, while there seems to be a north-eastern tilt of the eastern part of the jet, probably due to the long-lasting anticyclone off Europe (Fig. 1). The standard deviation in NAO− seems weaker and more zonal, while in NAO+ it has a greater zonal extension. This seemingly implies more cyclones in northeastern Atlantic, consistent with Rudeva and Gulev (2011).

As described above, the WR paradigm differs from the traditional decomposition in modes of variability, which, by construction, makes symmetry assumptions. Figure 1 (left panels) contrasts the MSLP patterns obtained from winter WR decomposition (color shading) to those of the corresponding modes of variability (black contours). The latter are obtained from EOF decomposition performed on DJFM averages of MSLP anomalies over the same North-Atlantic domain than the WR. From Fig. 1, we can infer that AR is the positive phase of the EAP (Barnston and Livezey 1987, 2nd EOF of MSLP) and BLK is the positive phase of the so-called Scandinavian (SCAN) pattern (3rd EOF of MSLP). Finally, NAO− and NAO+ project respectively on the positive and negative phases of the NAO (1st EOF of MSLP). From Fig. 1, it is worth noticing that the spatial symmetry assumption is not valid for the NAO. Indeed, the spatial pattern of NAO$_{EOF}$ is closer to NAO−$_{WR}$ than to

**(a)** AR, EAP (14.6%)

**(b)** BLK, SCAN (12.7%)

**(c)** NAO-, NAO (49.7%)

**(d)** NAO+, NAO (49.7%)

Sea-level pressure anomalies (Pa)

**(e)** Correlation = 0.75

**(f)** Correlation = 0.42

**(g)** Correlation = 0.89

**(h)** Correlation = 0.67

Number of days per winter

Principal component
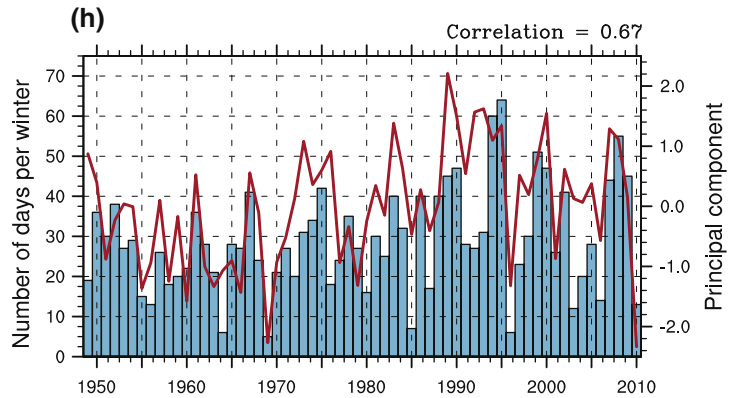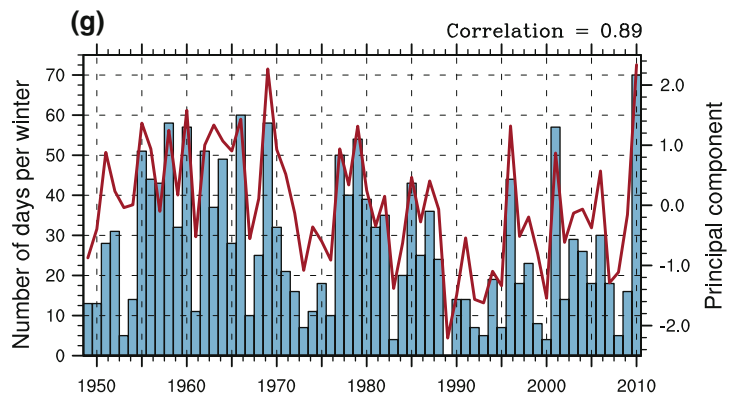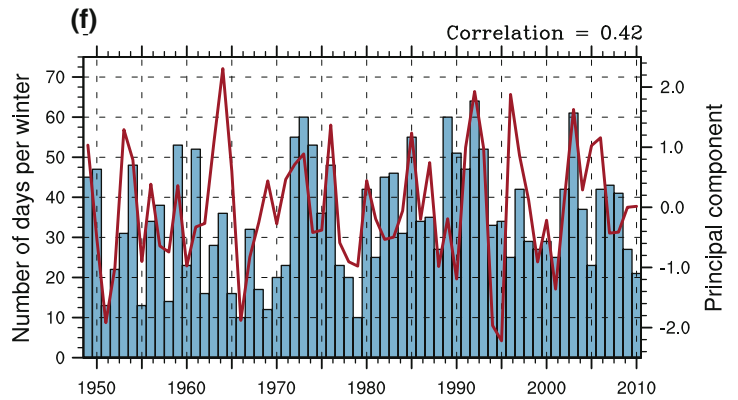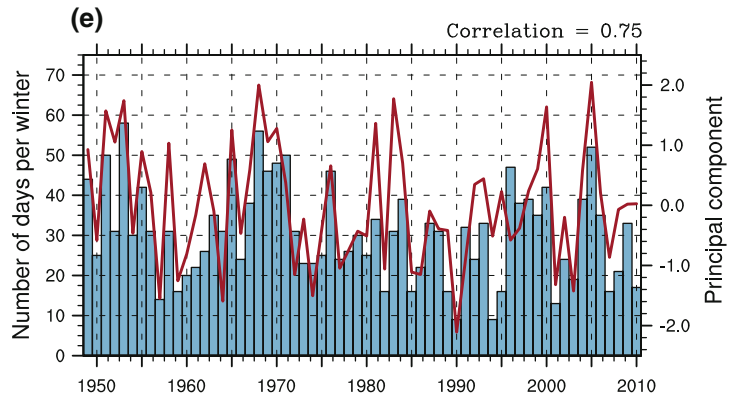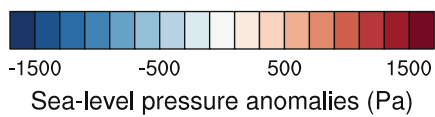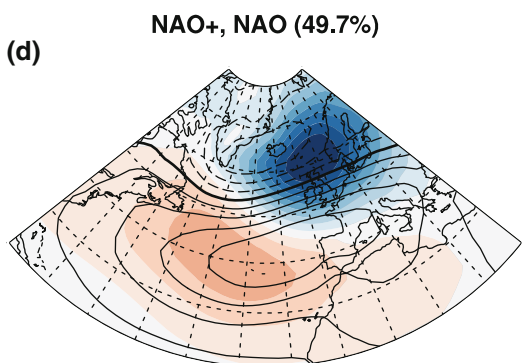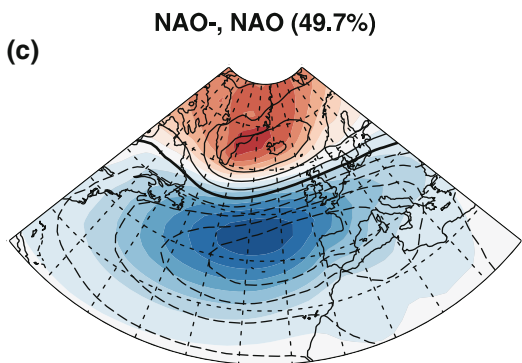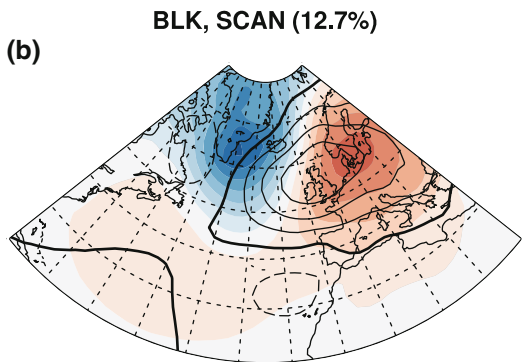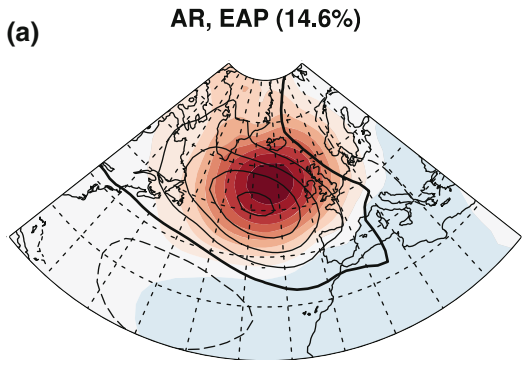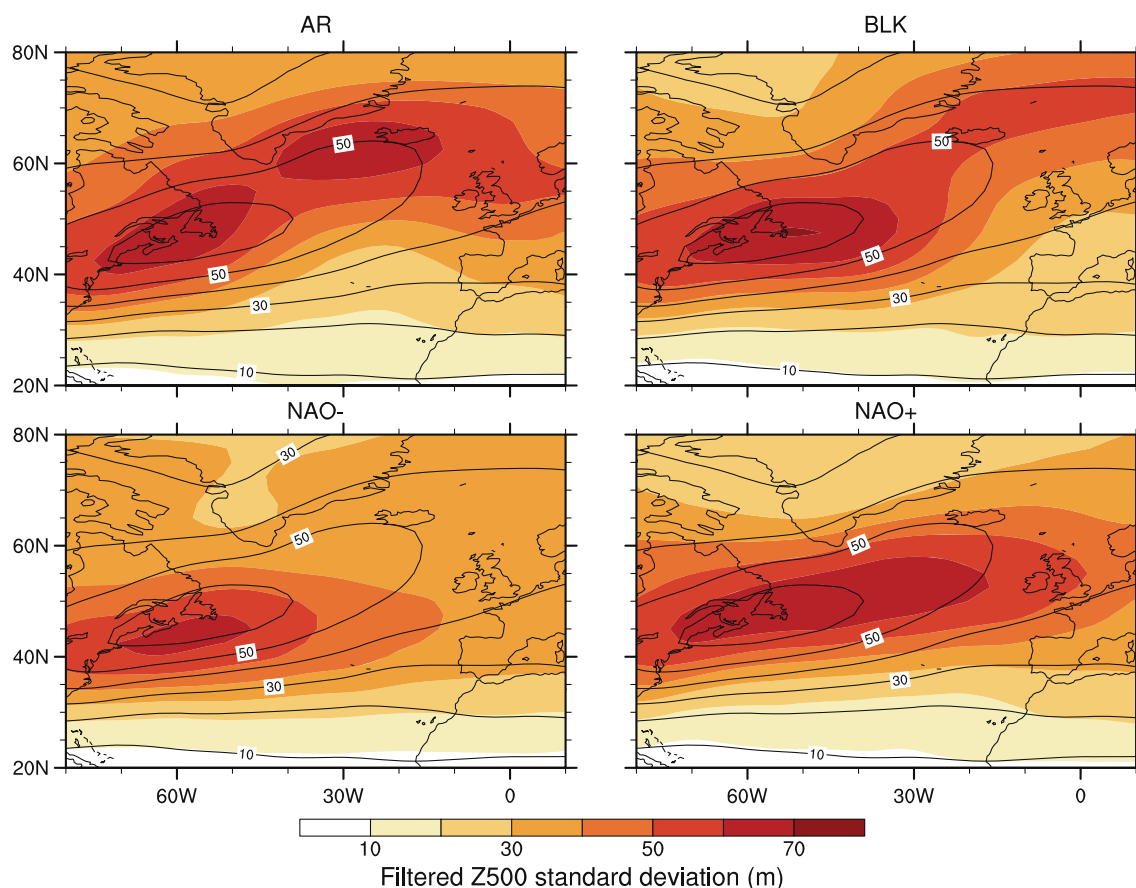
**Fig. 2** Daily DJFM standard deviation of filtered (2–6 days) $Z_{500}$ anomalies (*black contours* climatological, *color shading* within each weather regime)

NAO+$_{WR}$ obtained from classification: the NAO+$_{WR}$ northernmost negative anomaly is shifted eastward and the southernmost positive anomaly is tilted southeastward. Such a difference is associated with the intrinsic dynamics of the upper-level tropospheric jet and is inherent to the two states of its latitudinal position (Cassou et al. 2004).

Consistently, the correlation between NAO$_{EOF}$ index (Fig. 1, red line, defined as the 1st normalized principal component of MSLP anomalies) and NAO+$_{WR}$ occurrences is 0.67 while the correlation between NAO$_{EOF}$ index and NAO−$_{WR}$ occurrences is higher and reach −0.89. Regarding AR$_{WR}$ regime, there is a good correspondance with the EAP$_{EOF}$ pattern, although the maximum positive anomaly is shifted northeastward in AR$_{WR}$ compared to EAP$_{EOF}$; as expected, the two time-series are well correlated (R = 0.75). The SCAN pattern is somehow different from BLK and the two time series are less correlated. A possible cause for this discrepancy is the orthogonality constraint of the EOF decomposition and also the fact that "inverse blocking" events do not exist in nature as opposed to SCAN−$_{EOF}$ (by construction).

To summarize, the consideration of winter WR rather than the consideration of classical EOF modes of variability allows to take into account the NAO spatial asymmetry and the sole existence of blocking states without any constraint of orthogonality, which could lead to unrealistic spatial patterns. As a consequence the atmospheric variability in this study is only assessed through the WR paradigm.

## 4 Subtropical sea-level response to weather regimes

The impact of wintertime WRs on sea-level anomalies can occur via mechanisms of different nature. At seasonal and interannual timescales, the so-called inverted barometer effect links SSH variations in ocean basins to the variation of surface atmospheric pressure (Ponte 2006; Tsimplis and Shaw 2008; Woodworth et al. 2010, and references therein). This effect is not considered here as inverted barometer corrections have been applied to the sea-level observations.

Weather regimes are associated with wind-anomalies (consistent with MSLP patterns, Fig. 3, black arrows) and air-temperature anomalies (not shown), that are traditionnaly assessed by daily composites. AR is dominated by a
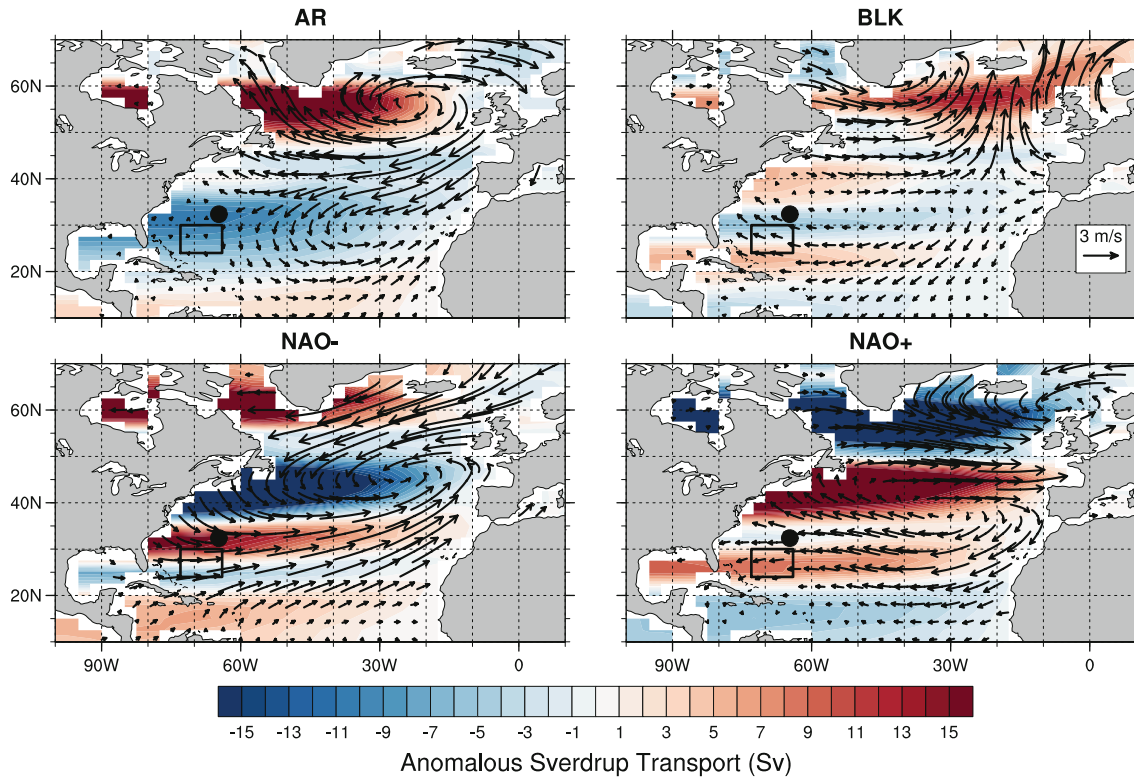
**Fig. 3** Daily composites of winter wind-field anomalies (*arrows*, reference = 3 m.s$^{-1}$) and corresponding anomalous Sverdrup transport (*colors*, contour interval = 1 Sv). The *black point* shows the location of the Esso-Pier (Bermuda) station and the *black rectangle* our subtropical *box* used in the correlation (see text and Table 1)

strong anticyclonic anomaly off Europe and by a surface warming centered at the intergyre region and extending in the northwestern subpolar gyre. BLK depicts anticyclonic anomalous circulation centered on Europe that prevents the mean midlatitude Westerlies to penetrate inland. Temperatures are colder off Newfoundland while warmer conditions occur in the GIN seas due to the low-level advection of warm air from the South. NAO− (resp. NAO+) is characterized by a reduction (resp. strengthening) and southward (northward) shift of the mean midlatitude Westerlies and the subtropical Trade winds that imprint a tripolar temperature pattern in latitude (Cayan 1992), with a warming (resp. cooling) in the Labrador Sea/subtropics and a cooling (resp. warming) in the GIN seas and the midlatitudes.

Those wind and air-temperature anomalies can lead to subtropical SSH response via either halosteric/thermosteric effects or the dynamical adjustment to the wind-stress forcing. The first mechanism corresponds to the thermal/haline dilatation of the ocean water column induced by temperature changes (Tsimplis et al. 2006) or changes in the global freshwater budget (e.g. icecaps melting, Stammer et al. 2011). Those changes can be induced either by changes in heat/freshwater fluxes from the atmosphere to the ocean or by anomalous tracer advection. The second

mechanism, associated with the long-term changes of open ocean wind-stress curl, induces both a barotropic (Sverdrup-like dynamics) and a baroclinic (westward propagation of Rossby waves) ocean response (Sturges and Hong 1995; Sturges et al. 1998; Ezer 1999; Hong et al. 2000; Cabanes et al. 2006). It is shown that such a mechanism can explain locally as much as 40% of the decadal variance in the Atlantic subtropical gyre (Cabanes et al. 2006) and is likely to be the dominant one. Our working hypothesis will thus be that subtropical SSH response to WRs is driven by open ocean wind-stress curl.

As a first step to characterize the ocean response to winter WR wind circulations, we compute the corresponding Sverdrup transport anomalies composites $\widetilde{\psi_{Sv}}$ (Fig. 3, color shading) as:

$$\widetilde{\psi_{Sv}}(x, y) = \frac{1}{\rho_0 \beta} \int\limits_{x_E}^{x} curl_z(\widetilde{\tau}(x', y)) dx' \tag{3}$$

where $\rho_0 = 1{,}030$ kg m$^{-3}$ is the reference density of seawater, $\beta$ the meridional gradient of the Coriolis parameter, $\widetilde{\tau}$ the wind stress anomalies associated with WRs (Fig. 3, black arrows) and $x_E$ the position of the Eastern boundary. These anomalies can be related to the mean pattern of the subpolar and subtropical gyres shown in Fig. 4.

**Mean MADT (cm) and zero wind-stress curl**



(a)

**AR composites of MADT Anomalies (cm)**



(b)
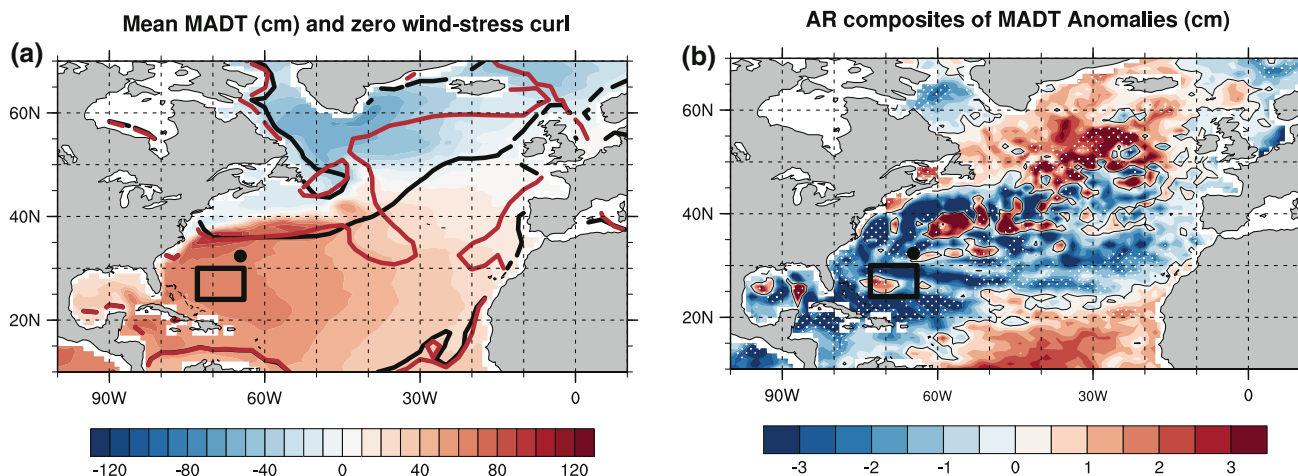
**Fig. 4** (*Left*) Mean map of absolute dynamic topography (*colors*). Climatological (*black* contours) and AR composite (*red* contours) zero wind-stress curl. (*Right*) Map of absolute dynamic topography

(MADT) anomalies composite for extreme Atlantic Ridge events (zero contours are depicted in *black*). Significant values, based on *t* statistics at the 80 % level of confidence, are *white dotted*

AR is characterized by strong positive anomalies in the Labrador Sea associated with anomalous southerly winds that contrast with slackened westerlies at midlatitudes (between 20°N and 40°N). BLK anomalies are very weak, except for positive anomalies south of Iceland. NAO− is characterized by positive anomalies in the northern boundary of the Labrador Sea and Irminger Sea and at 30°N, and negative anomalies between 40°N and 50°N in the intergyre region. NAO+ is characterized by opposite anomalies although shifted southward compared to NAO− in agreement with the spatial asymmetry of the two NAO phases captured through WR. For AR, note that the Sverdrup transport anomalies project very well onto the mean position of the gyres (Fig. 4a); hence AR is expected to play a central role in the subtropical gyre variability consistently with Hakkinen et al. (2011a) "gyre-mode" (their Fig. 3a).

To further estimate the possible roles of WR in forcing the North Atlantic subtropical SSH variability, we calculate the correlations between WR winter occurrences and the annual subtropical SSH anomaly index (after removing a linear trend). A correlation of −0.34 is obtained with AR yearly occurrences over 1993–2009, significant at the 80 % level (Table 1). The confidence interval is computed by a Student test, in which the degree of freedom is multiplied by a correction factor depending on the 1 year-lag autocorrelation of each time series (Bretherton et al. 1999, their equation 31). No correlations are found for neither NAO+ or NAO− while a positive correlation of 0.36 is found with BLK.

As documented earlier, AR regime is characterized by a persistent anticyclonic anomaly off Europe (Fig. 3) that displaces the climatological zero-wind-stress curl northward (Fig. 4, left panel, red contours). Considering simple

Sverdrup balance, this causes a decrease of subtropical SSH as confirmed in Fig. 4 (right panel) from MADT composites. The latter are computed for extreme AR years, defined as winters for which the seasonal occurrences are greater than one standard deviation. When AR winter events are frequent, a large scale negative anomaly encompasses the subtropical gyre, consistently with the correlation previously discussed. The subpolar gyre is also characterized by positive anomalies that are stronger in its eastern part and indicate a weakening of circulation there. All together, this is consistent with the anomalous Sverdrup contribution from WR wind characteristics as discussed above.

The results presented so far suggest the importance of AR for subtropical SSH interannual variability. However, those could be criticized because of the shortness of the AVISO time series. In order to corroborate our findings, we have used observations from tide-gauge at Bermuda (located in the subtropical gyre, Fig. 3, black point) to compute similar correlations, but over a much longer period of time (50 vs. 17 years for AVISO). Maximum correlation at −0.39, significant at the 95 % level, is found again for AR (Table 1) and consistently with AVISO, no significant correlations are found for NAO+ and NAO−. The correlation for BLK observed in the AVISO dataset no longer stands (0.17, not significant at the 95 % level) and could therefore be attributed to the shortness of the data or to some non stationarity of the ocean-atmosphere relationship yet to be investigated.

The correlations previously described simply give the information that subtropical SSH and AR occurrences significantly covary in time over 1948-1998. No information on the amplitude of the AR-induced SSH anomalies nor on the stationarity of the relationship has been provided

**Table 1** List of correlations cited in the text

| Time series | Period | Confidence interval (%) | Correlation |
|---|---|---|---|
| AR winter occurrences versus subtropical AVISO MADT | 1993–2009 | 80 | −0.34 |
| AR winter occurrences versus observed Bermuda SSH | 1949–1998 | 95 | −0.39 |
| AR-induced SSH versus observed Bermuda SSH | 1949–1998 | 95 | 0.39 |
| PG model versus observed Bermuda SSH | 1954–1998 | 95 | 0.53 |
| AR winter occurrences versus PG model | 1954–2006 | 95 | −0.53 |

"AR-induced SSH" refers to the regressed reconstructed series (solid line in Fig. 5) and "PG model" refers to the linear solution calculated from daily wind fields (dashed line in Fig. 5 and black line in Fig. 6)

so far. The temporal evolution of the AR-induced signal of Bermuda SSH is now reconstructed (Fig. 5, solid line) by linearly regressing the normalized AR occurrences onto the Bermuda SSH index (light grey bars). The regression coefficient estimated over 1948–1998 equals −17.5 mm per standard deviation of winter AR occurrences. Dark grey bars from 2003 onwards are independent data taken from the tide-gauge data but past the missing gap (see PSMSL website). The latter can be used as cross-validation to assess the skill of the method. The reconstructed signal does capture a large part of the decadal variability up to the mid-70s in agreement with the strong dominance of AR over those decades. While interannual fluctuations in the 80s and early 90s are reproduced to some extent, the late 70s SSH significant rise is completely missed. A possible cause is that the late 70s decade is characterized by strong NAO− events between 1977 and 1980 (Fig. 1) preceded by years of strong BLK. Both have a local imprint around Bermuda (not shown) and may be lowering the impact of AR, that is less frequent in that period. Note that the variance of the reconstructed time series is weaker than the observed one as expected by construction using regression models (von Storch 1999).

## 5 Mechanisms of interannual subtropical SSH variability in response to WR

As stated earlier, we propose that subtropical SSH response to WRs is driven by open ocean wind-stress curl. This working hypothesis discards the thermosteric/halosteric effects caused by atmospheric heat/freshwater fluxes and by tracer advection. The correlations discussed in the above seem to indicate that the AR anticyclonic circulation, which tilts the wind-stress curl northward, causes a decrease in SSH yearly anomalies.

In order to test our hypothesis, we have computed the wind-driven barotropic $\eta_p$ and baroclinic $\eta_c$ components of sea-level from observed daily wind stress curl following Cabanes et al. (2006) linear planetary geostrophic model (their equations 11 and 20):
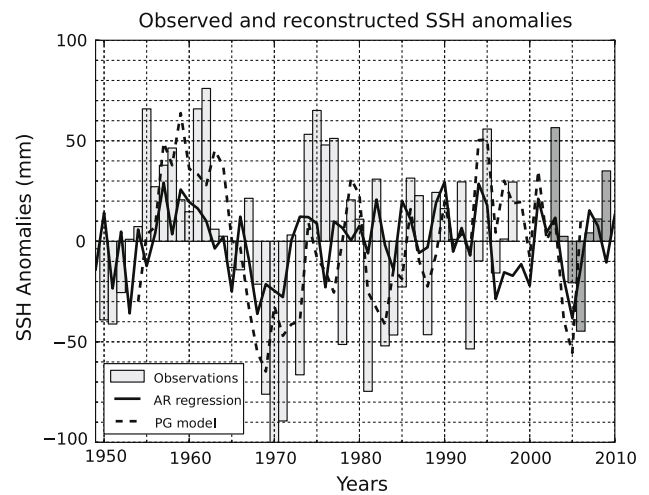


**Fig. 5** Observed time-series of Bermuda Sea-Surface Height anomalies (in mm, *light grey bars* are the tide-gauge observations used in the regression while *dark gray bars* are independent tide-gauge observations), regressed SSH onto AR occurrences (*solid line*) and the planetary geostrophic model of sea-level (*dashed line*)

$$\eta_p(x, y, t) = \int_{xe}^{x} \frac{f^2}{H\beta g} curl\left(\frac{\tau}{\rho_0 f}\right) \tag{4}$$

$$\eta_c(x, y, t) = -C_{rn}^{-1} \int_{x}^{x_e} \left[A_n curl\left(\frac{\tau}{\rho_0 f}\right)\right](x', y, t - t_{x'})dx' \tag{5}$$

where $t_{x'} = (x - x_{x'})/C_{rn}$ is the propagation time of the wave generated by local atmospheric forcing east of longitude $x$, $C_{rn} = -\beta/\lambda_n^2$ is the wave propagation speed of the $n$th baroclinic mode (which eigenvalue is $\lambda_n$) and $A_n$ the wind-stress curl projection on this mode. The derivation of those two equations, described in Cabanes et al. (2006), relies on planetary geostrophic (PG) dynamics, neglects bottom topography, advection by the mean currents and assumes a rigid lid. The wind-stress forcing is implemented as a body force in the mixed layer of constant depth (100 m). The values of C are computed by inversion of the eigenvalue problem:

$$\partial_z\left(\frac{f^2}{N^2}\partial_z F\right) + \lambda^2 F = 0 \qquad (6)$$

where $F(z)$ is the vertical baroclinic structure, $\lambda$ the corresponding eigenvalue and $N^2$ the Brunt-Vaisala frequency (computed from *World Ocean Atlas 2005* climatology of Locarnini et al. 2006; Antonov et al. 2006, following the procedure of Chelton et al. 1998). Equation 6 is verified by an infinity of orthogonal vertical modes but, consistently with Cabanes et al. (2006), the first baroclinic mode is found to be dominant in the subtropical area. We consistently discard the higher-ranked modes in our study. The values of $C$ and $A$ are longitude dependent but, similarly to Cabanes et al. (2006), we have used their zonal means. The computation has been performed at (33.3°N–78.8°W) with $C$ and $A$ are equal to $-0.025$ m.s$^{-1}$ and $11.10^{-4}$ respectively. We have chosen daily wind fields instead of monthly fields because the latter give too weak an amplitude of SSH (Cécile Cabanes, personal communication) and also to better account for the intrinsic properties and advantages of the WR as above-described. NCEP/NCAR daily wind fields are available from 1948 to 2006. The first five years of the PG sea-level anomalies are discarded as part of the spin-up.

Total (ie. barotropic+baroclinic) contribution of wind-stress curl to sea-level anomalies is depicted in Fig. 5 (dashed line) and a significant correlation of 0.53 is found with observations (Table 1). Note that the amplitude of the barotropic component is approximately 3 times smaller than the baroclinic one (not shown). This is consistent with the results of Hong et al. (2000) who argue that, to first order, Bermuda sea-level can be approximated by the first baroclinic mode. Interestingly, when the regression (solid black line) has some skill to reproduce observed SSH variability, so does the PG SSH anomalies. This tends to confirm that AR impact on Bermuda SSH is very likely due to the strong anticyclone off Europe, which tilts the wind-stress curl northward, and brings some confidence in our physical interpretation of the observations. Especially, the dramatic drop of 1970 is well captured by the regression and the PG model. This is consistent with Ezer (1999) who argues that the 1970 drop is due to changes in open-ocean wind-stress curl. However, Ezer (1999) attributes it to changes in NAO while we attribute it to changes in AR regime.

So far, correlations have been computed using the occurrences of wintertime WRs, considering the higher variance and mean values of the atmospheric forcing with respect to the other seasons (Minvielle et al. 2011). Using the planetary geostrophic model, we will verify that summer atmospheric dynamics play indeed a lesser role in the total interannual changes. We run two additional sensitivity experiments in which the PG model is either forced with

vairable DJFM winds or forced with variable JJAS winds. Results shown in Fig. 6 confirm that the variance of the interannual time-series is indeed mostly due to DJFM winds. The sole exception where the two seasons contributions are comparable is in the 1960s and the mid-2000s. Spring and Fall months (ie October–November and April–May) are treated as intermediate months dominated by either summer and winter dynamics (Minvielle et al. 2011); they are therefore not considered here.

In the results above-described, we have used spatial uniform wave propagation speed and wind-stress curl projection on the first baroclinic mode. We have run additional sensitivity experiments in which $C$ is set at the minimum or at the maximum value at the Bermuda latitude. We found that changes in $C$ have a non-negligible impact on interannual variability given by the PG model. The time-series are indeed time shifted by one year compared to the original one. Note that the choice of the mean value ($-0.025$ m.s$^{-1}$) appears to be the best as it maximizes the correlation between the reconstructed series and the observations (not shown). Changes in $A$ have no effect, as $A$ appears in Eq. 5 as a multiplying factor.

## 6 Discussion and conclusion

Since atmospheric modes of variability have been described in the literature (e.g. Barnston and Livezey 1987), many studies investigated the ocean response to those modes of variability, focussing essentially on the impact of the NAO on the circulation and hydrography in the North Atlantic. However, recent studies highlighted the role of the East-Atlantic Pattern (EAP). Msadek and Frankignoul (2009) suggest that multidecadal variability of Atlantic
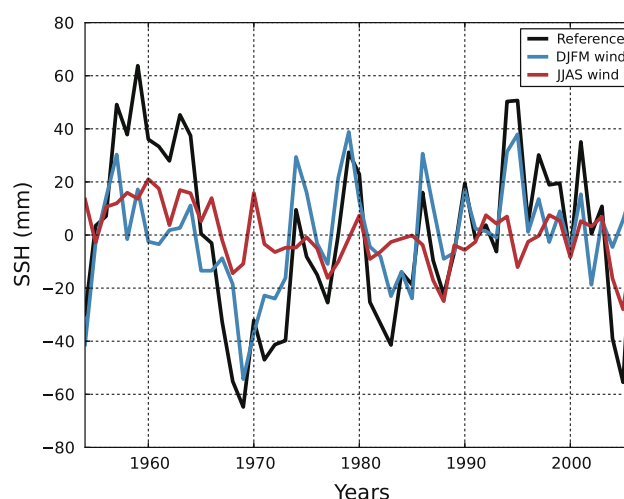
**Fig. 6** Planetary geostrophic model forced by observed wind (*black*) and sensitivity experiments with variable DJFM wind only (*blue*) and variable JJAS wind only (*red*)

Meridional Overturning Circulation (AMOC) is closely related to EAP, while Langehaug et al. (2012) suggest that subpolar gyre strength is significantly correlated with the EAP. Hence the EAP is at least as important as the NAO in driving variability in the North Atlantic. Nevertheless, these two studies rely on the analysis of coupled climate models that have important biases in the convection sites.

The present study is a step toward the investigation of such a relationship in observations, with a special focus laid on subtropical gyre variability. The question we address is which large-scale atmospheric pattern influences subtropical gyre variability, and through which mechanism. We use the weather regime (WR) paradigm to describe the wintertime North-Atlantic atmospheric variability and investigate its impact on subtropical SSH interannual-to-decadal variability. WR, treated as populations of days sharing common large-scale atmospheric circulation anomalies, are different from classical modes of variability (estimated for instance through EOF), because they have no orthogonality constraint and account for potential spatial asymmetries of the patterns. This is especially true for NAO+ and NAO− events and may be of central importance, as processes driving the variability of the mixed layer (turbulent and latent heat fluxes for example) are nonlinear (Cassou et al. 2011). WRs have been shown to be efficient in capturing surface forcing variability from daily-to-interannual timescales (Cassou et al. 2011).

Over the longest time period of available record over Bermuda (tide-gauge data in the Bermuda available from 1948 to 1998), we find that AR is the dominant atmospheric weather regime driving SSH variability in the subtropical gyre. Sverdrup transport anomalies related to AR conditions (wind-stress curl changes off Europe) show positive anomalies north of 50°N and negative anomalies south of it. The dipole projects very well on the mean position of the gyres and is thus very efficient in forcing the large-scale mean circulation. The sole barely significant relationship between SSH in Bermuda and the NAO could be obtained in the framework of our study when the period is restricted to 1958–1998. This suggests that the connection between the two, if any, is not stationary, or at least not overly dominant contrary to what has been suggested in previous studies. Over a limited period of time, independent satellite observations from 1993 onwards confirm that years with frequent AR conditions in winter lead to negative SSH anomalies that encompass the full subtropical gyre, Bermuda included, suggesting a weakening of subtropical gyre strength.

We used a simple planetary geostrophic model (PG) to explore the physical mechanisms linking wind-stress curl associated with daily wintertime WR and SSH interannual variability in Bermuda. The reconstructed signal using both the barotropic (Sverdrup like) and baroclinic (westward propagation of planetary waves) model components, which covary in phase, is highly correlated to observations suggesting that the largest part of the variability in Bermuda SSH is wind-driven. Sensitivity experiments confirm that most of the interannual signal is due to winter wind conditions integrated over time while summer wind anomalies have a second-order contribution to the yearly signal.

AR is closely related to the "gyre mode" defined in Hakkinen et al. (2011a, b) that is linked to the second EOF mode of wind-stress curl explaining part of warm and saline intrusion from the subtropical gyre into the subpolar ocean. AR also corresponds to the positive phase of the EAP and we verify that our results are robust when using EAP time series instead of AR occurrences (correlation of −0.34 between the EAP index and Bermuda SSH anomalies instead of −0.39 for AR). Consistently with Hakkinen et al. (2011a, b) our finding highlights the primarily importance of the atmospheric patterns of variability other than the NAO to understand the North Atlantic ocean dynamics.

Our study mainly focused on the immediate (0-year lag) response of subtropical SSH to changes in winter-weather regime occurrences. However, Curry and McCartney (2001) suggest that remote mechanisms, such as Eighteen Degree Water formation, Gulf-Stream intertial recirculation and deep-density structure, influence subtropical gyre variability. While remote (both in time and space) influence of NAO on ocean circulation has been thoroughly studied (Eden and Willebrand 2001; Deshayes and Frankignoul 2008), our results demonstrate that the possible influence of other modes of variability needs to be considered.

# References

Antonov J, Locarnini R, Boyer T, Mishonov A, Garcia H (2006) World Ocean Atlas 2005, vol 2: salinity. NOAA Atlas NESDIS 62

Ayrault F, Lalaurette F, Joly A, Loo C (1995) North-Atlantic ultra-high frequency variability: an introductory survey. Tellus Ser A Dyn Meteorol Oceanogr 47(5, Part1):671–696

Barnston A, Livezey R (1987) Classification, seasonality and persistence of low-frequency atmospheric circulation patterns. Mon Weather Rev 115(6):1083–1126

Bindoff N, Willebrand J, Artale V, Cazenave A, Gregory J, Gulev S, Hanawa K, Qur CL, Levitus S, Nojiri Y, Shum C, Talley L, Unnikrishnan A (2007) Observations: oceanic climate change and sea level. Climate change 2007: the physical science basis contribution of working Group I to the fourth assessment report of the intergovernmental panel on climate change

Bretherton C, Widmann M, Dymnikov V, Wallace J, Blade I (1999) The effective number of spatial degrees of freedom of a time-varying field. J Clim 12(7):1990–2009

Cabanes C, Huck T, De Verdiere AC (2006) Contributions of wind forcing and surface heating to interannual sea level variations in the Atlantic Ocean. J Phys Oceanogr 36(9):1739–1750

Cassou C (2008) Intraseasonal interaction between the Madden-Julian Oscillation and the North Atlantic Oscillation. Nature 455(7212):523–527

Cassou C, Terray L, Hurrell J, Deser C (2004) North Atlantic winter climate regimes: spatial asymmetry, stationarity with time, and oceanic forcing. J Clim 17(5):1055–1068

Cassou C, Minvielle M, Terray L, Perigaud C (2011) A statistical-dynamical scheme for reconstructing ocean forcing in the Atlantic. Part I: weather regimes as predictors for ocean surface variables. Clim Dyn 36(1–2):19–39

Cayan D (1992) Latent and sensible heat-fluxes anomalies over the Northern Oceans—driving the sea-surface temperature. J Clim 5(4):354–369

Chelton D, DeSzoeke R, Schlax M, El Naggar K, Siwertz N (1998) Geographical variability of the first baroclinic Rossby radius of deformation. J Phys Oceanogr 28(3):433–460

Compo GP, Whitaker JS, Sardeshmukh PD, Matsui N, Allan RJ, Yin X, Gleason BE Jr, Vose RS, Rutledge G, Bessemoulin P, Broennimann S, Brunet M, Crouthamel RI, Grant AN, Groisman PY, Jones PD, Kruk MC, Kruger AC, Marshall GJ, Maugeri M, Mok HY, Nordli O, Ross TF, Trigo RM, Wang XL, Woodruff SD, Worley SJ (2011) The twentieth century reanalysis project. Q J R Meteorol Soc 137(654, Part a):1–28

Curry R, McCartney M (2001) Ocean gyre circulation changes associated with the North Atlantic Oscillation. J Phys Oceanogr 31(12):3374–3400

Curry R, McCartney M, Joyce T (1998) Oceanic transport of subpolar climate signals to mid-depth subtropical waters. Nature 391(6667):575–577

Deshayes J, Frankignoul C (2008) Simulated variability of the circulation in the North Atlantic from 1953 to 2003. J Clim 21(19):4919–4933

Ducet N, Le Traon P, Reverdin G (2000) Global high-resolution mapping of ocean circulation from TOPEX/Poseidon and ERS-1 and -2. J Geophys Res Oceans 105(C8):19,477–19,498

Eden C, Willebrand J (2001) Mechanism of interannual to decadal variability of the North Atlantic circulation. J Clim 14(10):2266–2280

Esselborn S, Eden C (2001) Sea surface height changes in the North Atlantic Ocean related to the North Atlantic Oscillation. Geophys Res Lett 28(18):3473–3476

Ezer T (1999) Decadal variabilities of the upper layers of the subtropical North Atlantic: an ocean model study. J Phys Oceanogr 29(12):3111–3124

Frankignoul C, Muller P, Zorita E (1997) A simple model of the decadal response of the ocean to stochastic wind forcing. J Phys Oceanogr 27(8):1533–1546

Gulev S, Jung T, Ruprecht E (2002) Climatology and interannual variability in the intensity of synoptic-scale processes in the North Atlantic from the NCEP-NCAR reanalysis data. J Clim 15(8):809–828

Gulev S, Barnier B, Knochel H, Molines J, Cottet M (2003) Water mass transformation in the North Atlantic and its impact on the meridional circulation: Insights from an ocean model forced by NCEP-NCAR reanalysis surface fluxes. J Clim 16(19):3085–3110

Hakkinen S (1999) Variability of the simulated meridional heat transport in the North Atlantic for the period 1951–1993. J Geophys Res Oceans 104(C5):10,991–11,007

Hakkinen S, Rhines PB, Worthen DL (2011a) Atmospheric blocking and Atlantic multidecadal ocean variability. Science 334(6056):655–659

Hakkinen S, Rhines PB, Worthen DL (2011b) Warm and saline events embedded in the meridional circulation of the northern North Atlantic. J Geophys Res 116:1–13

Hong B, Sturges W, Clarke A (2000) Sea level on the US East Coast: decadal variability caused by open ocean wind-curl forcing. J Phys Oceanogr 30(8):2088–2098

Hurrell J (1995) Decadal trends in the oscillation—regional temperatures and precipitations. Science 269(5224):676–679

Hurrell J, VanLoon H (1997) Decadal variations in climate associated with the north Atlantic oscillation. Clim Change 36(3–4):301–326

Joyce T, Deser C, Spall M (2000) The relation between decadal variability of subtropical mode water and the North Atlantic Oscillation. J Clim 13(14):2550–2569

Kalnay E, Kanamitsu M, Kistler R, Collins W, Deaven D, Gandin L, Iredell M, Saha S, White G, Woollen J, Zhu Y, Chelliah M, Ebisuzaki W, Higgins W, Janowiak J, Mo K, Ropelewski C, Wang J, Leetmaa A, Reynolds R, Jenne R, Joseph D (1996) The NCEP/NCAR 40-year reanalysis project. Bull Am Meteorol Soc 77(3):437–471

Langehaug HR, Medhaug I, Eldevik T, Ottera OH (2012) Arctic/Atlantic exchanges via the subpolar gyre. J Clim 25(7):2421–2439

Locarnini R, Mishonov AV, Antonov J, Boyer T, Garcia H (2006) World Ocean Atlas 2005, vol 1: temperature. NOAA Atlas NESDIS 61

Lohmann K, Drange H, Bentsen M (2009) Response of the North Atlantic subpolar gyre to persistent North Atlantic oscillation like forcing. Clim Dyn 32(2–3):273–285

Michelangi P, Vautard R, Legras B (1995) Weather regimes—recurrence and quasi-stationarity. J Atmos Sci 52(8):1237–1256

Minvielle M, Cassou C, Bourdalle-Badie R, Terray L, Najac J (2011) A statistical-dynamical scheme for reconstructing ocean forcing in the Atlantic. Part II: methodology, validation and application to high-resolution ocean models. Clim Dyn 36(3–4):401–417

Molteni F, Tibaldi S, Palmer T (1990) Regimes in the wintertime circulation over northren extratropics. 1. Observational evidence. Q J R Meteorol Soc 116(491, Part a):31–67

Msadek R, Frankignoul C (2009) Atlantic multidecadal oceanic variability and its influence on the atmosphere in a climate model. Clim Dyn 33(1):45–62

Ponte R (2006) Low-frequency sea level variability and the inverted barometer effect. J Atmos Ocean Technol 23(4):619–629

Rudeva I, Gulev SK (2011) Composite analysis of North Atlantic extratropical cyclones in NCEP-NCAR reanalysis data. Mon Weather Rev 139(5):1419–1446

Santos J, Corte-Real J, Leite S (2005) Weather regimes and their connection to the winter rainfall in Portugal. Int J Climatol 25(1):33–50

Smyth P, Ide K, Ghil M (1999) Multiple regimes in Northern Hemisphere height fields via mixture model clustering. J Atmos Sci 56(21):3704–3723

Stammer D, Agarwal N, Herrmann P, Koehl A, Mechoso CR (2011) Response of a coupled ocean-atmosphere model to Greenland ice melting. Surv Geophys 32(4–5, SI):621–642

Sturges W, Hong B (1995) Wind forcing of the Atlantic Thermocline along 32 degrees N at low frequencies. J Phys Oceanogr 25(7):1706–1715

Sturges W, Hong B, Clarke A (1998) Decadal wind forcing of the North Atlantic subtropical gyre. J Phys Oceanogr 28(4):659–668

Tsimplis M, Shaw A, Flather R, Woolf D (2006) The influence of the North Atlantic Oscillation on the sea-level around the northern European coasts reconsidered: the thermosteric effects. Philos Trans R Soc A Math Phys Eng Sci 364(1841):845–856

Tsimplis MN, Shaw AGP (2008) The forcing of mean sea level variability around Europe. Global Planet Change 63(2–3, SI):196–202

Vautard R (1990) Multiple weather regimes over the North-Atlantic. Analysis of precursors and successors. Mon Weather Rev 118(10):2056–2081

Vautard R, Legras B (1988) On the source of midlatitude low-frequency variability. Part 2: non-linear equilibration of Weather Regimes. J Atmos Sci 45(20):2845–2867

von Storch H (1999) On the use of "inflation" in statistical downscaling. J Clim 12(12):3505–3506

Woodworth P, Pouvreau N, Woeppelmann G (2010) The gyre-scale circulation of the North Atlantic and sea level at Brest. Ocean Sci 6(1):185–190

## 3.4 Conclusion and discussions

The impacts of the weather regimes on the interannual variability of the subtropical gyre have been analysed in this chapter. This has been done using observations of sea-surface height anomalies in the subtropical gyre and a planetary geostrophic model.

The major findings of this chapter are:

- The major driver of sea-surface height anomalies in the subtropical gyre is open ocean wind-stress curl through Sverdrup dynamics and westward propagation of planetary waves. These results are consistent with Sturges and Hong (1995); Sturges et al. (1998); Ezer (1999); Hong et al. (2000); Cabanes et al. (2006) among others.

- The large scale atmospheric pattern that is the most effective to influence the variability of the subtropical gyre is AR, consistently with the gyre-mode of Hakkinen et al. (2011a). Although the NAO can be viewed as a proxy of wind intensity, the associated wind-stress curl anomalies are not effective in modulating the strength of the subtropical gyre.

- Sensitivity experiments suggest that most of the wind-driven interannual variability of the subtropical gyre originates from the winter season. This validates the sole consideration of the winter regimes, as discussed in section 2.1.

There are, however, some limitations in our study. Our results are chiefly grounded on correlations. The correlation of 0.39, obtained with AR, is significant but remains weak: the associated explained variance is $0.39^2 \approx 15\%$, which can be considered as negligible. Furthermore, significant correlations do not necessarily imply causal relationship, since the variations of two correlated time-series might just be driven by a common cause[1].

Second, the emphasis was on the 0-lag response of the subtropical gyre, since correlations at higher lags were not significant. Accordingly, the correlation between the AR winter occurrences and the strength of the subtropical gyre can be interpreted as the fast (within a year) response of the gyre to changes in AR conditions. It does not bring any insights into the slow (within decades) adjustment of the subtropical gyre to changes in weather regime conditions.

---

[1] A good example is provided by Messerli (2012), whose results have been thoroughly criticised by the scientific community, who suggest a misinterpretation of the correlations (e.g. Maurage et al. 2013; Winters and Roberts 2012)

Third, the variability of the sole subtropical gyre has been analysed since tide-gauge data at Bermuda spans a sufficiently long time-period to make robust enough statistical analysis. Observations of the subpolar gyre are too sparse to make a similar analysis. To overcome these issues, a full scale laboratory, provided by a realistic general circulation model, is used in the next chapter to:

- Analyse the impacts of the weather regimes on the subpolar gyre and on the Atlantic Meridional Overturning Circulation.

- Differentiate the fast (monthly to interannual time scales) and the slow (decadal timescales) changes in the ocean circulation that are induced by changes in weather regime frequency of occurrences.

- Understand the mechanisms involved by performing sensitivity experiments.

# Chapter 4

# Impact of North-Atlantic Weather Regimes on the ocean circulation

## Contents

## 4.1 Introduction

Many authors used ocean general circulation models to investigate the impacts of persistent positive NAO (the mode of variability, $NAO_M$ hereafter) on the ocean circulation (e.g. Eden and Willebrand 2001, Herbaut and Houssais 2009, Lohmann et al. 2009 among others). This is achieved by forcing the model with idealised $NAO_M$-like forcings. However, as discussed in chapters 2.1 and 3, the other modes of variability, such as the East-Atlantic Pattern or the Scandinavian Pattern (EAP and SCAN, respectively), might significantly contribute to the variability of the ocean circulation. To our knowledge, no studies aimed at investigating the ocean response to persistent EAP or SCAN conditions. Using the weather regime framework, this is the aim of the present chapter.

In the aforementioned studies, two methods are generally used to construct $NAO_M$-like forcings:

- The first one consists in linearly regressing the monthly $NAO_M$ index onto monthly forcing fields (wind-stress and heat fluxes), as done in Visbeck et al. (1998) and Herbaut and Houssais

(2009).

- The second method consists in averaging the monthly forcing fields over "strongly" positive $NAO_M$ years, as done in Lohmann et al. (2009) or Zhu and Demirov (2011).

These methods, however, might not be appropriate as a year of strongly positive $NAO_M$ index does not necessarily imply a year with numerous $NAO^+$ days (the weather regime, $NAO_R{}^+$ hereafter), as illustrated in figure 4.1.
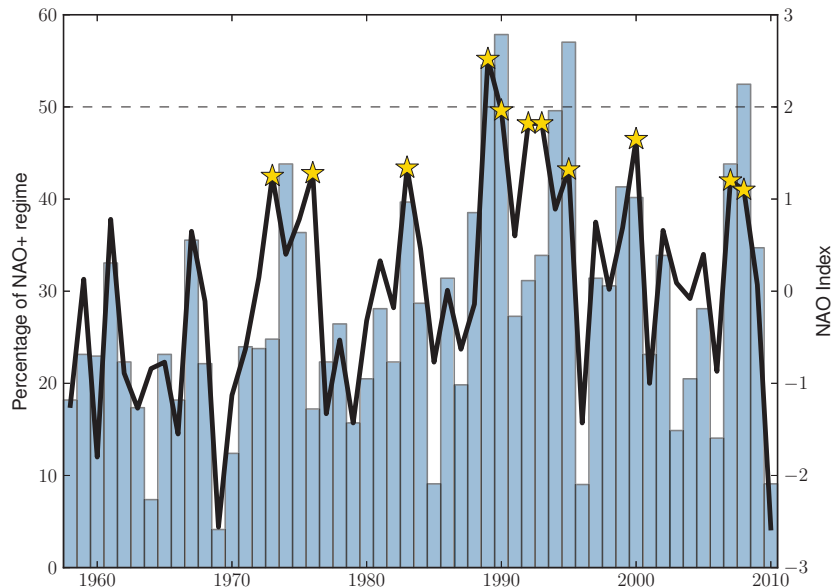


*Figure 4.1: Hurrell's winter $NAO_M$ index (black line) and percentage of winter days belonging to $NAO_R{}^+$ (blue histograms). Yellow stars indicate years with a $NAO_M$ index greater than unity.*

Among the winters with a $NAO_M$ index stronger than unity, only four winters are actually dominated by $NAO_R{}^+$ (occurrences greater than 50%): 1989, 1990, 1995 and 2008. Years 1992 and 1993, on the other hand, are dominated by the BLK regime. Hence, the strongly positive $NAO_M$ index is mainly due to the weak number of $NAO^-{}_R$ days during these years. As a consequence, the use of the $NAO_M$ index may not be the best choice for estimating the sensitivity of the ocean circulation to specific atmospheric conditions.

The aim of the present chapter is to propose an alternative method of generation of idealised forcings in order to analyse the response of the ocean circulation at monthly to decadal timescales.

## 4.2   Idealized forcing construction

The method used in the generation of the idealised forcings consists in making random drafts of days that belong to one particular regime. The way these random drafts are made is addressed in this section.

### 4.2.1   Statistics of the intra and inter regime distances

As discussed in section 2.4, the weather regimes are very effective in capturing the variability of surface forcings. Especially, the intra and inter-regime distances (defined in section 2.3.2) have been shown to respectively define the sign and the strength of the anomalies (Cassou et al. 2011, see also section 2.4).

Hence, to capture the statistics of the forcings associated with the weather regimes, one has to capture the statistics of intra and inter regime distances. The intra-regime distances are characterised by lower means (expected by the definition of inter regime distances) and lower standard deviations (figure 4.2), and conversely for inter-regime distances.
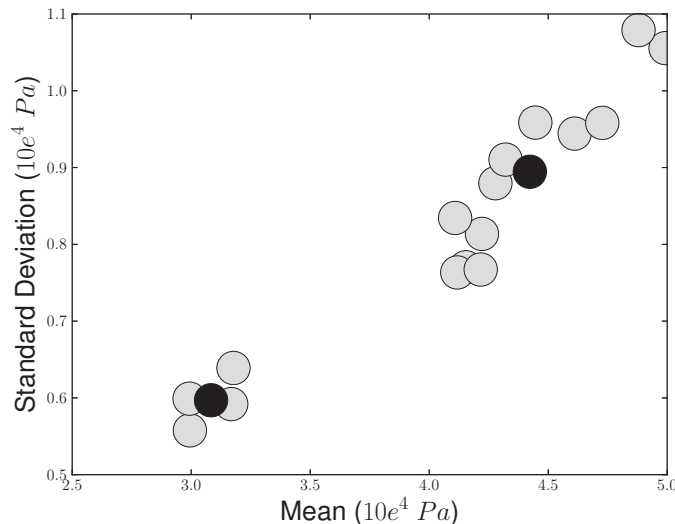


*Figure 4.2: Standard deviations as a function of the means for the 16 intra and inter-regime distances. Black points represent the averages over the 4 intra-regime distances (lower left) and over the 12 inter-regime distances (upper right).*

The Probability Density Functions (PDFs) of intra and inter-regime distances apparently follow Gaussian distributions (figure 4.3), given by:

$$f(x, \mu, \sigma^2) = \frac{1}{\sigma\sqrt{2\pi}} e^{-\frac{1}{2}\left(\frac{x-\mu}{\sigma}\right)^2}$$

with $\mu = 310\ hPa$[1], $\sigma_D = 60\ hPa$ for the intra-regime distances and $\mu = 442\ hPa$, $\sigma_D = 89\ hPa$ for the inter-regime distances (these parameters correspond to the black points in figure 4.2). These properties are used to make the random drafts of weather regime events.
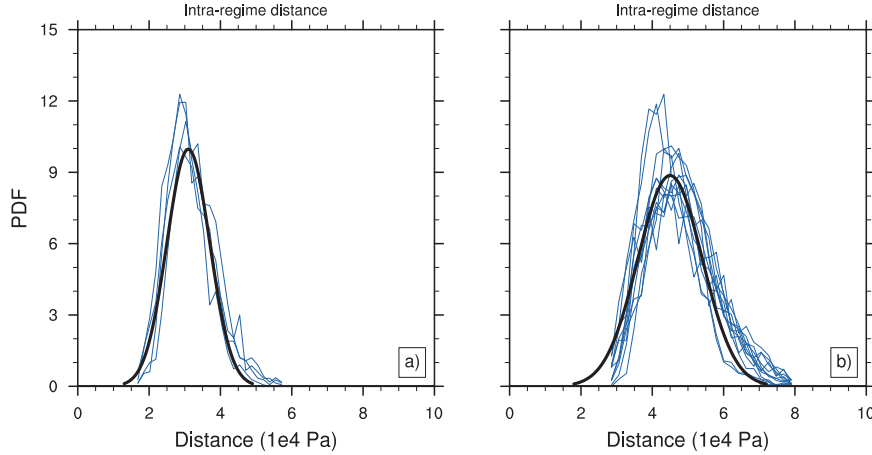


*Figure 4.3: Probability density function of intra-regime (a) and inter-regime (b) distances. Black solid lines: Gaussian distributions (see text for details).*

## 4.2.2   Random draft of regime events

In this subsection, the algorithm used to make the random drafts is described, by taking as an example the construction of $NAO^+{}_R$ like forcings. As a first step, four random drafts are made:

- One random draft of intra-regime distance (i.e. distance to $NAO^+{}_R$), following the Gaussian distribution of figure 4.3a.

- Three random drafts of inter-regime distances (i.e. distances to $NAO^-{}_R$, AR and BLK), following the Gaussian distribution of figure 4.3b.

We call this random distance vector $R$, which has four dimensions. $R$ is then compared to the *observed* distance vector, $O$, which has $nt \times 4$ dimensions (with $nt$ the number of winter days in the study period). The day for which $O$ is the closest to $R$ (Euclidian criteria) is selected. If this selected day does not belong to the right regime, or if the regime event to which this day belongs is

---

[1] $1\ hPa = 10^2\ Pa$

shorter than 3 days, another random draft is performed. If these two conditions are respected, then the entire event is selected and the time counter is incremented, as summarised in figure 4.4.
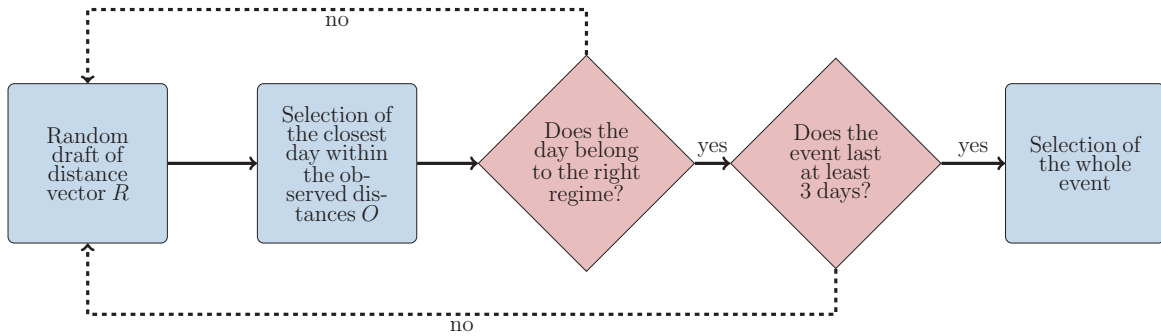


*Figure 4.4: Summary of the construction algorithm.*

## 4.3 Article

In Barrier et al. (2013), in press in the *Journal of Physical Oceanography*, the impacts of the weather regimes on the horizontal gyres (subtropical and subpolar) and on the overturning circulation are analysed using an ocean only model. A realistic historical simulation is used to analyse the fast (monthly to interannual timescales) adjustment of the ocean circulation in the North-Atlantic to changes in weather regime conditions.

The new method of generation of idealised forcings, which is described in section 4.2, is then used to force the model in order to assess the transient response (within decades) of the ocean circulation to persistent regime conditions and to understand the associated mechanisms.

# Response of North-Atlantic Ocean circulation to atmospheric weather regimes

NICOLAS BARRIER [*]

*Laboratoire de Physique des oceans, CNRS-Ifremer-UBO-IRD, Brest, France*

CHRISTOPHE CASSOU

*CNRS Cerfacs, Toulouse, France*

JULIE DESHAYES AND ANNE-MARIE TREGUIER

*Laboratoire de Physique des oceans, CNRS-Ifremer-UBO-IRD, Brest, France*

_____

[*]*Corresponding author address:* Nicolas Barrier, LPO Ifremer, Pointe du Diable, 29280 Plouzane, France.

E-mail: Nicolas.Barrier@ifremer.fr

ABSTRACT

A new framework is proposed for investigating the atmospheric forcing of North-Atlantic ocean circulation. Instead of using classical modes of variability, such as the North-Atlantic Oscillation (NAO) or the East-Atlantic Pattern, we here use the weather regimes paradigm. Using this framework we avoid problems associated with the assumptions of orthogonality and symmetry that are particular to modal analysis and known to be unsuitable for the NAO.

Using ocean-only historical and sensitivity experiments, we investigate the impacts of the four winter weather regimes on horizontal and overturning circulations. Our results suggest that the Atlantic Ridge (AR), NAO$^-$ and NAO$^+$ regimes induce a fast (monthly to interannual timescales) adjustment of the gyres via topographic Sverdrup dynamics and of the meridional overturning circulation via anomalous Ekman transport. The wind anomalies associated with the Scandinavian Blocking regime (SBL) are ineffective in driving a fast wind-driven oceanic adjustment.

We also estimate the response of both gyre and overturning circulations to persistent regime conditions. AR causes a strong, wind-driven reduction in the strengths of the subtropical and subpolar gyres, while NAO$^+$ causes a strengthening of the subtropical gyre via wind-stress curl anomalies and of the subpolar gyre via heat flux anomalies. NAO$^-$ induces a southward shift of the gyres due to the southward displacement of the wind-stress curl. The SBL regime is found to impact the subpolar gyre only via anomalous heat fluxes. The overturning circulation is shown to spin-up following persistent SBL and NAO$^+$ and to spin-down following persistent AR and NAO$^-$ conditions. These responses are driven by changes in deep water formation in the Labrador Sea.

1

# 1. Introduction

A large part of the atmospheric variability in the North-Atlantic/Europe (NAE) domain is controlled by the North-Atlantic Oscillation (NAO, Hurrell 1995). The NAO is traditionally defined either as an index (normalized pressure difference between the Azores High and the Icelandic Low atmospheric pressure centers) or by the first Empirical Orthogonal Function (EOF) of the mean sea-level pressure (MSLP) or geopotential height anomalies over the North-Atlantic domain. MSLP fluctuations between the Azores High and the Icelandic Low are accompanied by changes in midlatitude westerlies and trade winds that are strengthened during positive NAO conditions, and conversely during negative NAO. These changes have been shown to strongly impact the ocean circulation in the North Atlantic.

Several modeling and observational studies suggest that the oceanic response to NAO fluctuations depends on the timescales. At monthly to interannual timescales, the ocean primarily responds to related changes in wind intensity and position. Positive NAO phases generate anticyclonic gyre circulation anomalies situated at the boundary between the subtropical and subpolar gyres (hereafter the "intergyre gyre" following Marshall et al. 2001). Concurrently, the NAO alters the Meridional Overturning Circulation (MOC) creating a dipolar anomaly pattern with a weakening north of 40°N and a strengthening to the south. This dipole is generated by anomalous Ekman transport (Eden and Willebrand 2001; Bellucci et al. 2008): strengthened westerlies generate southward Ekman transport anomalies along the 40-60°N latitudinal band while strengthened trade winds generate northward Ekman transport anomalies, causing convergence at 40°N and a subsequent dipole.

At decadal timescales, positive NAO conditions leads to an intensification of both subtropical and subpolar gyres via baroclinic adjustment (Eden and Willebrand 2001; Lohmann et al. 2009; Zhu and Demirov 2011), while the MOC undergoes basin-wide strengthening driven by increased heat loss in the Labrador Sea and subsequent changes in deep convection (Eden and Willebrand 2001; Curry and McCartney 2001; Lohmann et al. 2009).

While the impact of the NAO on ocean circulation has been widely studied, only a few

2

studies have investigated the impacts of the other modes of atmospheric variability, such as the East-Atlantic Pattern (EAP) or the Scandinavian pattern (SCAN), descriptions of which can be found in Barnston and Livezey (1987). Msadek and Frankignoul (2009) and Ruprich-Robert and Cassou (2013), using a control simulation of the IPSL-CM4 and CNRM-CM5 climate models respectively, suggest that the MOC multidecadal variability could be closely related to the EAP. In their models, the EAP induces anomalous advection of salinity that impacts deep convection in the Nordic Seas, driving MOC changes in turn. Medhaug et al. (2011) found that in the Bergen climate model control simulation, convection in the Labrador Sea accounts for one-third of North-Atlantic Deep Water transport while the remaining two-thirds originate from the Greenland-Scotland-Ridge overflows. They argue that convection in the Labrador Sea is correlated with the NAO, while water mass exchange across the Greenland-Scotland-Ridge is correlated with the SCAN index. Using the same experiment, Langehaug et al. (2012) suggest that the strength of the subpolar gyre is significantly correlated with the EAP index. Altogether, these findings suggest that the EAP and the SCAN might be as important as the NAO in forcing the ocean circulation in the North-Atlantic from seasonal to decadal timescales. However, these studies rely on coupled climate models that undergo many biases (mean position of the NAC, unrealistic deep convection). It is therefore of interest to perform sensitivity experiments using forced ocean models, since they better reproduce the ocean variability as compared to coupled climate models, although they are limited by the absence of coupling at the air-sea interface (Griffies et al. 2009).

The important role of the EAP on the horizontal circulation has been confirmed in recent observational studies. Hakkinen et al. (2011a,b) suggest that the NAO alone is not enough to gain an understanding of the observed warming and salinization in the Eastern subpolar gyre in the mid 1990s. They attribute the latter to decadal fluctuations in the occurrence of winter blocking conditions, assessed through traditional atmospheric metrics based on daily variance of MSLP anomalies (Scherrer et al. 2006). The space-time structure of wind-anomalies associated with blocking, which Hakkinen et al. (2011a) introduce as the gyre-

mode, in fact projects very well onto the EAP: when the EAP is positive, the subpolar gyre weakens and shrinks; despite slackened circulation, this facilitates the northward penetration of warm, salty subtropical water into the eastern subpolar gyre (Hátún et al. 2005).

The aforementioned studies typically diagnosed the atmospheric variability by decomposing it into modes of variability, using methods such as EOF. These methods have some limitations, insofar as they assume orthogonality and spatial symmetry of the modes. The latter assumption has been shown to be partially inadequate for the NAO (Cassou et al. 2004), where the deeper Icelandic Low/stronger Azores High are northeastward shifted in NAO$^+$ compared to NAO$^-$. Additionally, EOF decomposition assumes that both phases of the modes exist in nature, which may not be the case for the SCAN pattern that is linked to blocking conditions controlled by nonlinear eddy-mean flow interactions. These limitations of EOF-derived modes of variability can potentially lead to misinterpretation of atmospheric variability and, as a consequence, of the associated ocean response. To avoid those constraints, the so-called Weather Regimes (WR) paradigm is an alternative method. The regimes are large-scale, recurrent and quasi-stationary atmospheric patterns computed from daily atmospheric circulation anomalies (e.g. Vautard 1990). Within this framework, Cassou et al. (2004) document the spatial asymmetry of the NAO dynamics and better isolate the blocking conditions characterized by high pressure anomalies over Scandinavia and low pressure anomalies over the Labrador Sea. They found four typical regimes in winter named NAO$^+$, NAO$^-$, SBL for Scandinavian Blocking (as used in Vautard 1990) and AR for Atlantic Ridge. AR is characterized by anticyclonic sea-level pressure anomalies in the North-Atlantic, while SBL is characterized by anticyclonic conditions over Europe and cyclonic conditions over Greenland. In a previous study, we have used the WR decomposition to investigate the impacts of the related atmospheric forcing on the variability of the subtropical gyre intensity based on observed sea-surface height anomalies (Barrier et al. 2012). There we suggested that the two NAO related regimes have very little impact on the subtropical gyre strength as compared to AR (which can be viewed as a positive EAP phase),

whose associated wind-stress curl anomalies induce barotropic (Sverdrup like) and baroclinic (westward propagation of planetary waves) sea-level anomalies.

The findings of Barrier et al. (2012) are consistent with the results of Hakkinen et al. (2011a), though it should be noted that the methods of Barrier et al. (2012) were restricted to an analysis of the subtropical gyre response to atmospheric variability at 0 year lag only. The aim of the present study is to extend the analysis of Barrier et al. (2012) by investigating the response of the horizontal and overturning components of the circulation to the four NAE WR using a forced realistic ocean model. The questions we address are i) what are the impacts of each WR on both the horizontal and overturning circulations as a function of timescale? ii) what are the physical mechanisms involved? To address these questions, North-Atlantic Ocean horizontal and meridional circulation anomalies in a historical ocean simulation (forced with interannualy varying atmosphere) are investigated in response to variability of the WR regimes. Sensitivity experiments, in which the model is forced with heat and momentum fluxes that correspond to a given WR, are then performed to isolate the role of the WR regimes on ocean circulation.

The paper is organized as follows. Section 2 describes the North-Atlantic WR paradigm. Section 3 describes the numerical model and the atmospheric forcings used in this study. Section 4 investigates the variability of the historical experiment in relation to observed WR changes. Section 5 describes the sensitivity experiment and addresses the impact of each WR taken separately on ocean circulation. The discussion and conclusions are provided in sections 6 and 7, respectively.

# 2. North-Atlantic weather regimes

Spatial and temporal characteristics of the NAE WRs as well as their statistical and physical properties have been described in detail in Cassou et al. (2011) and Barrier et al. (2012). In this study we use the same approach as in Barrier et al. (2012), limiting our

analyses to the winter season (ie. December-January-February-March, hereafter DJFM). However, the time period over which WRs are determined from NCEP reanalysis (Kalnay et al. 1996) starts in 1957-12-01 here instead of 1948-12-01 as in Barrier et al. (2012). This choice has been made because we here also use forcing datasets spanning the ERA40 period (1958-2002). The four regimes considered in this study are the Atlantic Ridge (AR), which is characterized by anticyclonic anomalies in the center of the subpolar gyre, the Scandinavian Blocking regime (SBL), characterized by a anticyclonic anomalies over Europe and cyclonic anomalies over Greenland and the two NAO phases (NAO$^-$ and NAO$^+$ for the negative and positive phases, respectively). In this paper, we only discuss the wind-stress curl, Ekman transport and air-temperature anomalies associated with the weather regimes, since we expect them to play the major roles in driving ocean circulation. The reader is referred to Cassou et al. (2011) for a complete description of the WR related surface ocean variables.

Anomalous daily maps of meridional wind, zonal wind and air temperature anomalies from NCEP are computed by removing a smoothed seasonal cycle (two harmonics retained). Anomalous Ekman transport and wind-stress curl anomalies, averaged over the days attributed to each WR, are shown in Fig. 1. AR is characterized by negative (anticyclonic) wind-stress curl anomalies north of 40°N and positive (cyclonic) anomalies to the south. Ekman transport anomalies are northward from 30°N to 50°N and southward in the Irminger and Norwegian seas, leading to transport convergence at the center of the AR anticyclone. SBL is characterized by weaker anomalies, except along the East-Greenland Current location where anomalies are positive. Regarding NAO$^-$ curl anomalies, strong zonal positive anomalies between 30°N and 55°N dominate, while strong negative anomalies prevail to the north of 60°N and expand from the Eastern side of the Labrador Sea to the Norwegian sea, encompassing the Irminger basin. The NAO$^-$ Ekman transport anomalies diverge near 45°N. Curl anomalies for NAO$^+$ are very different from those of NAO$^-$. With NAO$^+$, the positive anomalies in the North-Eastern subpolar gyre are tilted south-eastward and almost vanish in the Labrador Sea. The Ekman transport anomalies for NAO$^+$ converge around

162  40°N. AR, NAO$^-$ and NAO$^+$ are marked with strong and zonally extended anomalies and

163  are thus expected to have a significant wind-driven impact on both horizontal and meridional

164  ocean circulations.

165  Fig. 2 shows the daily air-temperature anomaly composites associated with the weather

166  regimes. In the Labrador Sea, colder than average temperatures occur for SBL and NAO$^+$,

167  while the anomalies are positive for NAO$^-$. For AR, positive anomalies are located in

168  the center of the subpolar gyre. These temperature anomalies can be viewed as a proxy

169  for anomalous downward (i.e. into the ocean) heat fluxes. As convection and deep water

170  formation in the Labrador Sea are primarily driven by anomalous heat fluxes (Straneo 2006),

171  buoyancy driven variability of ocean circulation in the North-Atlantic is likely to be impacted

172  by the WRs.

# 3. Experimental set-up and mean state

174  In this study, we use the regional North-Atlantic configuration of the NEMO model to

175  assess the variability of the ocean circulation driven by the NAE WRs. In this section

176  we describe the different model experiments, which are summarized in Table 1. A complete

177  description of the model can be found in Appendix A. The model is initialized from Levitus et

178  al. (1998) climatology and spun-up from rest using DFS4.3 (Brodeau et al. 2010) interannual

179  forcing over the period from 1958 to 2002. The reference experiment (hereafter REF) is run

180  with identical forcing, starting from the end of the 45 year spin-up. Fig. 3a shows the mean

181  barotropic streamfunction of REF. Subtropical and subpolar gyre intensities each reach

182  about 35 Sv, which compares well with other z-level OGCM of similar resolution (Eden and

183  Willebrand 2001). The Labrador Current transport is 32 Sv, which is within the range of

184  observations (Pickart and Spall 2007). However, the Deep Western Boundary Current is

185  only 7 Sv, slightly weak compared to the observational estimate of 12.4 Sv (Pickart and

186  Spall, 2007); a possible cause is the under-representation of the Greenland-Scotland-Ridge

Overflows, which contribute to its intensity (Dickson and Brown 1994). The Gulf-Stream separates too far south and the North-Atlantic Current (NAC) is too zonal, which are well known biases of coarse resolution models (e.g. Smith et al. 2000; Treguier et al. 2005). The variability of the gyre transport compares well with other studies. The upward trend in subpolar gyre intensity from 1980 to 1995 (Treguier et al. 2005) and its decline from 1995 to 2000 (Hakkinen and Rhines 2004) are accurately reproduced. Variability in the subtropical gyre is additionally found to compare well with observations. For example, model sea-level anomalies at Bermuda correlate with the tide-gauge data of the Permanent Service for Mean Sea Level (used in Barrier et al. 2012) at 0.63. The mean MOC for REF is shown in Fig. 3b. Its maximum, located at near 26°N and at a depth of 1000 m, is approximately 17 Sv. The North-Atlantic Deep Water cell is slightly deeper and stronger than that reported by Biastoch et al. (2008). This is due to our different choice of forcing dataset, as shown by an unpublished comparison of two global ORCA05 simulations run with these different atmospheric forcings (J.M. Molines, personal communication). The time series of maximum overturning at 46°N compares well with the results of Biastoch et al. (2008) and Boening et al. (2006), obtained from a higher resolution model.

Wind and buoyancy forcing are connected through the turbulent flux of heat and evaporation, which depend on the surface wind-speed (Large and Yeager 2004). To isolate the mechanical influence of interannually varying wind-stress (i.e. via the momentum equation) from their influence on turbulent fluxes, a "wind-only" model configuration is constructed as follows. Smoothed daily climatologies (two harmonics retained) of air-temperature, specific humidity and wind speed are computed using the 6-hourly forcing fields issued from DFS4.3. These climatologies are read and used by the model to compute the turbulent fluxes of evaporation and heat, while the wind-stress is computed in the same way as in REF (i.e. using the 6 hourly wind fields issued from DFS4.3). The wind-only reference experiment (hereafter, WREF) is integrated from the end of the respective wind-only spin-up run. The mean state in WREF compares well with REF, although the MOC and subpolar gyre are

8

weaker in WREF, the latter particularly so in the Labrador Sea. Our methodology matches that of Biastoch et al. (2008), who use a global configuration of NEMO run at the same resolution. Their results suggest that the variability of the MOC can be interpreted as the linear sum of wind-driven interannual variability and buoyancy driven decadal variability.

We have also built a barotropic configuration of the regional model that uses a single vertical level and that is only forced by the winds. In this configuration, salinity and temperature are constant in time and uniform in space (horizontally and vertically). Hence, the "Joint Effect of Baroclinicity and Relief" (JEBAR) term is neglected. The wind-stress has been computed assuming a constant drag coefficient of $1.5 \ 10^{-3}$. This simple configuration permits to reproduce the linear dynamics of ocean circulation, namely the Sverdrup balance as will be shown shortly.

# 4. Oceanic fast response to recurrent winter weather regime conditions

In this section, the immediate response of the ocean to recurrent weather regime conditions throughout a monthly timescales is analyzed as follows. AR monthly occurrences are computed as the number of days, in each DJFM months over the period 1958-2002, that belong to AR. The months that are characterized by extreme AR conditions (in a temporal sense), defined as the months for which the monthly occurrences exceed the mean by 1.5 standard deviations, are sought for. Monthly anomalies of barotropic and overturning streamfunctions issued from REF (computed by removing the seasonal cycle) are then averaged over these extreme AR months, hence giving a picture of monthly circulation anomalies associated with AR (Fig. 4a and 4b). This methodology is then repeated for the other three regimes. The monthly composites of modeled wind-stress curl anomalies, computed using this method, compare well with the daily composites of Fig. 1 (not shown), hence validating this methodology.

9

The extreme AR events are characterized by anomalies that project well on the mean position of the gyres with a polarity that implies a weakening of the horizontal circulation (Fig. 4a). For extreme NAO$^-$ conditions (Fig. 4e), negative anomalies are centered at near 45°N, while south of 30°N anomalies are positive. Extreme NAO$^+$ conditions show slightly weaker anomalies of opposite polarity with respect to NAO$^-$ events and centered at near 40°N (Fig. 4g). This is 5° further south of the NAO$^-$ anomalies due to a southward shift of the wind-stress curl anomalies (figure 1). Both NAO composites share the same splitting of the altered circulation into two branches, one recirculating southeastward and the other one shifting northward towards the center of the subpolar gyre, even though these anomalies are reduced in NAO$^+$. The two NAO patterns are consistent with the intergyre-gyre pattern (Marshall et al. 2001) and can be interpreted as the signature of meridional shifts of the gyres due to NAO-induced north-south shifts of the position of wind-stress curl. One can notice in Fig. 4 the strong control of topography on the shape of the barotropic streamfunction anomalies, especially in the vicinity of the Mid-Atlantic Ridge.

These results are likely due to topographic Sverdrup balance (Koblinsky 1990; Vivier et al. 1999), consistent with Eden and Willebrand (2001). To investigate this hypothesis additional numerical experiments have been performed using the barotropic configuration of the model. The model is separately forced with constant wind anomaly composites that correspond to each WR (excluding SBL which induces no significant ocean response, Fig. 4b). Two simulations have been run for 4 years, when the equilibrium is reached: one in which the model bathymetry is the same as in REF, and a second one in which the bathymetry is flat (3000 m everywhere except on land). The results are shown in Fig. 5 averaged over the last year of integration. With the REF bathymetry, the barotropic configuration reproduces very well the patterns of Fig. 4. With the idealized bathymetry, stronger and more zonally-elongated circulations are obtained (Fig. 5b, 5e, 5h), which are consistent with classical Sverdrup theory (Fig 5c, 5f, 5i) and thereby confirm that the gyre anomalies of Fig. 4 are due to topographic Sverdrup balance, in agreement with Eden and Willebrand (2001).

10

However, the "instantaneous oceanic barotropic response" of Eden and Willebrand (2001) (their figure 8a) does not seem to be as constrained by the topography as indicated by the patterns in Fig. 4. This difference arises from the different timescales of interest. While we discuss monthly anomalies, Eden and Willebrand (2001) discuss yearly anomalies. We have thus computed the correlations at 0 lag between the yearly gyre anomalies (computed as the average from December to November to keep the continuity of winter months) and the winter sum of daily WR occurrences (hereafter, winter occurrences). Each time-series has been detrended prior to calculating the correlations. We notice a clear correspondence between the monthly gyre composites and the correlation patterns (Fig. 6), confirming that the signature of the barotropic, wind-driven response of ocean circulation to WRs occurs within a year. However, the influence of topography is no longer obvious in the yearly correlations, indicating that the barotropic mode has been modified by the baroclinic ones (Anderson and Killworth 1977).

We now analyze the overturning streamfunction anomaly composites for extreme WR occurrences (Fig. 4b, 4d, 4f and 4h). While no significant responses are again found for SBL, significant anomalies extend from the surface to the bottom for the remaining three WRs. The AR composite shows a tripolar pattern, with positive anomalies between $30°N$ and $55°N$ and negative anomalies elsewhere. The $NAO^-$ composite shows a dipolar pattern with positive anomalies north of $45°N$ and negative anomalies in the south. The $NAO^+$ composite is comparable to the $NAO^-$ pattern, but opposite in sign and southward shifted. The anomalies are, in each case, located between the latitudes of convergence/divergence of Ekman transport anomalies (dashed lines in Fig. 4) and are thus the signature of a near-surface flow driven by Ekman transport anomalies, compensated by a depth-independent flow (Jayne and Marotzke 2001; Köhl and Stammer 2008). Hence, these patterns reflect changes in volume transport rather than changes in water mass transformation. Comparable patterns are obtained from correlations between yearly MOC anomalies and the winter occurrences, except north of $45°N$ where the significant correlations are restricted to the surface and at

11

depth, which we fail to explain.

# 5. Transient ocean response to winter regime conditions

In the previous section we have shown that the fast response of ocean horizontal/meridional circulation to WRs is mostly driven by linear dynamics (Sverdrup and Ekman). How does the ocean adjust to persistent weather regime conditions on decadal timescales? This question has been addressed many times for the NAO using numerical experiments with idealized forcings that represent either strongly positive or strongly negative NAO conditions (e.g. Eden and Willebrand 2001; Lohmann et al. 2009; Zhu and Demirov 2011). To reconstruct such forcing conditions, the usual method is to add the observed daily variability of the forcing to idealized (NAO-like) monthly forcing, which can either be the composite monthly anomalies computed over years of strong NAO conditions (Lohmann et al. 2009; Zhu and Demirov 2011) or the regression of monthly anomalies onto the monthly NAO index (Visbeck et al. 1998; Eden and Willebrand 2001). A major drawback of these methods is that the NAO index is polluted by i) large-scale anomalous circulations that may not be representative of the NAO meridional see-saw pressure pattern, and ii) synoptic storms that pass either over Iceland or the Azores. This thereby gives artificial weight to one of the NAO fixed points. Put differently, in the context of the WR paradigm, a year of positive NAO index may include a significant number of days that belong to the three other weather regimes. To illustrate this, table 2 provides the winter occurrences of each regime during the years usually employed in the NAO$^+$ composite calculation (Lohmann et al. 2009; Zhu and Demirov 2011). During these 7 years, only three of them (1989, 1990 and 1995) are dominated by the NAO$^+$. For example, year 1992 is dominated by SBL and has only 31% of NAO$^+$ days. The traditional NAO index is thus strongly positive in 1992 because NAO$^-$ episodes almost never occurred during that winter. Hence, we suggest that the use of monthly indexes may not be the best

12

choice for estimating the sensitivity of ocean circulation to specific atmospheric conditions.

As an alternative, we propose a new method based on WRs that constructs idealized surface forcings that we believe better capture the true nature of the NAE atmospheric circulation and their impacts upon the ocean. This method is significantly different from those described above as it is done on daily criteria instead of monthly means, as detailed below for the NAO$^+$. Idealized forcings are generated using only the winter months (December to March). As an example we here describe the construction of the December 1st forcings. One NAO$^+$ event is randomly selected from the 1958-2002 pool of WR NAO$^+$ days. This selected NAO$^+$ event may correspond, for instance, to the one that occurred on Jan. 24th 1989 that lasted 4 days. The anomalous surface forcing fields (computed as done in section 2) of this 4 day period are then added to the Dec.1st-Dec.4th daily climatology. The same methodology is repeated for Dec. 5th. Let us say that a strong NAO$^+$ event lasting 13 days is now randomly selected. The 13-day sequence is used to construct forcings from Dec. 5th to Dec. 18th by adding the anomalous NAO$^+$ conditions to the daily climatology. This process is continued up until March 31st. The same procedure is then repeated to construct 45 NAO$^+$ winters that are then used to force the model.

This technique allows us to better isolate the atmospheric circulation of interest and enables us to better retain the statistical characteristics of the circulation. It is important to note that NAO$^+$ conditions refer to a range of NAO$^+$ events of different strength, duration and spatial characteristics. These statistics can be assessed by the so-called distance to the WRs centroids, which we use to verify that our method allows us to accurately sample both the distribution of distances that correspond to NAO$^+$ conditions and also the variety of duration of the NAO$^+$ events. Accordingly, we reproduce fairly well the forcing statistics of the NAO$^+$ events, as shown in Appendix B. The same technique is applied to construct forcing fields for all four regimes. Note that only winter days are rebuilt while DFS4.3 is still used for the other seasons. Moreover, we have chosen to use climatologies for radiative fluxes, snow and precipitation in the idealized forcing datasets that have been applied in the

13

sensitivity experiments. We have verified that this choice has no effect on gyre or overturning circulation variability by running an additional experiment that is identical to REF except that it uses climatological snow, precipitation and radiative fluxes (not shown).

A set of 4 experiments has been performed (one for each regime) in which the model was integrated with the idealized forcings for 45 years, initiated following the same spin-up as for REF. These experiments will henceforth be referred to as AR, SBL, NAO$^-$ and NAO$^+$. Another set of 4 idealized experiments have also been performed to isolate the influence of the wind-forcing. These experiments, referred to as WAR, WSBL, WNAO$^-$ and WNAO$^+$, have been integrated starting from the WREF spin-up and forced using only the wind component of each WR. The numerical experiments are summarized in table 1.

## a. Gyre circulation

The difference between the barotropic streamfunction averaged over the last ten years of the WR sensitivity experiments and the reference barotropic streamfunction (averaged over the full 45 years of the REF experiment, see Fig. 3a) is displayed in Fig. 7. AR and NAO$^+$ (Fig. 7a and 7d) exhibit anomalies that project well onto the mean circulation and thus depict a change in the intensity of the circulation (about 15 Sv). The circulation is weaker for AR, especially on the western side of the basin, and strengthened for NAO$^+$, especially in the central part of the subtropical gyre and eastern part of the subpolar gyre. SBL anomalies (Fig. 7b) are similarly strengthened in the western part of the subpolar gyre while the subtropical gyre is not altered. NAO$^-$ anomalies (Fig. 7c) displays a tripolar anomaly pattern, consistent with a southward shift of the gyres (the intergyre-gyre, Marshall et al. 2001), and a strengthening of the circulation in the northeastern limb of the subpolar gyre, with maximum anomalies in the Labrador Sea.

Similar comparisons are performed for the wind-only experiments (Fig. 7, e to h). WR and WWR anomalies show very comparable patterns in the subtropics (south of 45°N). Accordingly, the response of the subtropical gyre to persistent WRs is interpreted to be

14

mostly driven by the baroclinic adjustment of the gyre to anomalous wind-stress curl, via the westward propagation of planetary waves (Cabanes et al. 2006; Hong et al. 2000; Barrier et al. 2012). In the subpolar gyre, the ocean response is regime-dependent. AR and WAR show very comparable anomalies, indicating that the adjustment of the subpolar gyre to persistent AR is also mostly wind-driven, although the contribution of buoyancy forcing cannot be neglected. This extends to the subpolar gyre the conclusions found in Barrier et al. (2012) for the subtropical gyre, and is consistent with the gyre-mode of Hakkinen et al. (2011a). Similar conclusions cannot be drawn for the other 3 regimes. Indeed, the strength of the subpolar gyre is barely affected in the WSBL, WNAO$^-$ and WNAO$^+$ experiments. Following Biastoch et al. (2008), who linearly decompose the circulation anomalies into wind-driven and buoyancy driven components, the difference between the WR and WWR experiments would correspond to the signal being driven by buoyancy fluxes. Accordingly, the strengthening of the subpolar gyre in SBL and NAO$^+$ and its slackening in NAO$^-$ are interpreted as being mostly driven by baroclinic adjustment to persistent heat flux anomalies. Interestingly, the WWR spatial anomalies are very similar to the correlation patterns of Fig. 6. This further confirms that these correlation patterns are a signature of the baroclinic adjustment following the perturbation by the wind-forcing.

Fig. 8 shows the time evolution of the maximum gyre transport in the four WR and WWR experiments. The subtropical gyre adjustment is achieved in 6-8 years, consistent with the timescales of baroclinic adjustment to wind-stress curl. It is worth noting that only the AR regime leads to a slackened subtropical gyre, consistent with Hakkinen et al. (2011b), while the three others tend to intensify it. Despite differences in the mean states that are controlled by the winter forcing, REF, SBL and NAO$^+$ share very similar interannual variability. This is presumably due to the fact that during SBL and NAO$^+$ days, the variance of winter wind-stress curl is weaker (not shown), hence less likely to influence the interannual variability of the subtropical gyre. As a consequence, the interannual variability of the subtropical gyre in SBL and NAO$^+$ is dominated by the atmospheric forcing of the other seasons, especially

15

spring and fall (April, May, October and November), during which both summertime and wintertime dynamics statistically occur (Cassou et al. 2011, figure 12).

The subpolar gyre adjustment is achieved in approximately 10-12 years. The longer adjustment timescale in the subpolar gyre compared to the subtropical gyre presumably reflects both (i) that the subpolar gyre is primarily driven by heat flux rather than wind stress curl anomalies (cf. Eden and Willebrand 2001; Eden and Jung 2001), and (ii) that Rossby waves speeds decrease with increasing latitude. In the NAO$^-$ and WNAO$^-$ idealized experiments the subpolar gyre has not stabilized after 45 years, presumably reflecting a positive feedback via anomalous advection of warm subtropical water in the northeastern North-Atlantic that spreads throughout the subpolar gyre and further decreases its strength (Sarafanov et al. 2008; Herbaut and Houssais 2009)

## b. *Overturning circulation*

We now consider the difference between the overturning streamfunction averaged over the last ten years of the WR experiments and the reference overturning streamfunction (the average over the 45 years of the REF experiment, see Fig. 3b). For persistent AR and NAO$^-$ conditions (Fig. 9a and 9c) the MOC experiences a large-scale weakening, while persistent SBL and NAO$^+$ conditions induce a large-scale strengthening of the MOC (Fig. 9b and 9d). The anomalies are stronger for NAO$^-$ and NAO$^+$ (4 Sv); SBL anomalies reach 3 Sv while AR ones are weaker still at 2 Sv. On top of the large-scale changes, small overturning circulation changes induced by Ekman transport anomalies are visible from 0 to approximately 500 m. In WAR, WNAO$^-$ and WNAO$^+$ (Fig. 9e, 9g, 9h), the anomalies are of the same sign but with much smaller amplitude. In WSBL, however, the anomalies have the opposite sign and are almost zero (Fig. 9f). Since these differ from the immediate MOC response to extreme WR conditions (both on monthly and yearly timescales, Figs. 4 and 6), the MOC patterns in WAR, WNAO$^-$ and WNAO$^+$ likely reflect the impact of the adiabatic (wind-driven) changes in gyre circulation. Because the MOC anomalies are much smaller in

16

the wind-only experiments (i.e. WAR vs AR, WNAO$^-$ vs NAO$^-$ and WNAO$^+$ vs NAO$^+$), the MOC adjustment to persistent WRs is clearly demonstrated to be mostly due to heat flux anomalies. Nevertheless, the fact that the structure and sign of the anomalies is similar within each pair of sensitivity experiments suggests that the adiabatic gyre adjustment contributes to the MOC adjustment. We speculate that this effect is actually dampened by the absence of interannual heat flux anomalies in the wind-only experiments since the stronger stratification of the subpolar gyre in WREF compared to REF may limit the gyres influence on MOC.

We find that the MOC anomalies for persistent regime conditions are mostly driven by changes in Labrador Sea deep convection associated with heat flux anomalies: AR and NAO$^-$ show an anomalous heat gain that reduces convection while SBL and NAO$^+$ are characterized by a strong heat loss that enhances deep convection. This is further confirmed by the mean late winter (January to March) mixed-layer depth maximum in the Labrador Sea, which is 1000 m shallower in AR and NAO$^-$ than in REF, and 1000 m deeper in NAO$^+$ and SBL than in REF (not shown). Consistent with the studies of Eden and Greatbatch (2003), Boening et al. (2006) or Biastoch et al. (2008), enhanced deep convection precedes positive MOC anomalies at latitudes north of 45°N by 0-2 years. These anomalies are then rapidly (within a year) propagated southward, presumably by fast boundary Kelvin waves, as discussed by Getzlaff et al. (2005) (and references therein).

Fig. 10 shows the temporal adjustment of the MOC diagnosed from the maximum overturning at 46°N in the WR and WWR experiments. The strengthening of the MOC during persistent SBL and NAO$^+$ is achieved within 12-15 years. In contrast to the horizontal circulation, it is worth emphasizing that MOC indices in our sensitivity experiments are much less correlated at interannual timescales. It can therefore be suggested that most of the changes in the MOC are controlled by winter conditions.

17

# 6. Discussion

In this study, we have assumed that NAE atmospheric winter dynamics can be partitioned into four WRs, a commonly accepted number based on simple statistical significance tests (Michelangi et al. 1995). The number of regimes remains subjective, however, because of the shortness of the observational datasets, the types of algorithm used for clustering, the choice of the null hypothesis used for assessing statistical robustness, etc. (Rust et al. 2010). As such, we have therefore repeated the present analyses when 5 regimes are retained instead of 4. The fifth one resembles the opposite of AR and is characterized by a cyclonic anomaly located at the same latitude as the AR anticyclone but shifted eastward; we name this regime Atlantic Low (hereafter, AL). The gyre response to persistent AL mirrors the response to persistent AR as the wind-stress curl anomalies are at the same latitude. MOC anomalies for persistent AL conditions show a pattern that ressembles the AR one, but with smaller amplitudes. This is presumably because the AL eastward shifted pattern displaces the wind and air-temperature anomalies out of the Labrador Sea, hence preventing deep water formation. As a consequence, MOC anomalies only reflect the contributions of Ekman transport anomalies and of the adiabatic spin-up of the gyres. Both AL and AR project very well onto the EAP but our results highlight that in order to understand the ocean response to atmospheric changes it is of primary importance to account for the spatial asymmetry associated with the phases of the mode.

The analyses presented here have been carried out using a coarse resolution regional model whose low computational demand allows us to perform several targeted integrations following a mechanistic approach. However, such a configuration has non-negligible drawbacks. First, the choice of closed boundaries can lead to a misrepresentation of the mean state and variability of the MOC. Its interannual variability due to exchanges with the Arctic (Jungclaus et al. 2005) and changes in the overflows from the Nordic Sea (Schweckendiek and Willebrand 2005; Danabasoglu et al. 2010) is indeed missing. To verify, however, that our regional model has some skill in reproducing the variability of the subpolar gyre and

18

overturning circulation, we have compared our results with the global, ocean only simulation of NEMO described in Treguier et al. (2007). As shown in Fig. 11, although the two model configuration have different means, the interannual variability is very similar (correlations greater than 0.9). This gives us confidence that our results are robust despite the use of a regional model. Second, our coarse resolution model does not resolve mesoscale eddies, which are parameterized following Gent and McWilliams (1990). As described in Deshayes et al. (2009), eddies play a major role for North-Atlantic Deep Water formation and so our findings might be subjected to the misrepresentation of key associated physics. Eddies establish the time-scales of integration of surface buoyancy forcing in the Labrador Sea and their inclusion in ocean models significantly improve the representation of the ocean mean state, especially the Gulf-Stream separation location and the NAC pathway (Smith et al. 2000; Treguier et al. 2005).

# 7. Conclusions

The North-Atlantic/Europe atmospheric variability is usually partitioned into modes of variability, such as the North-Atlantic Oscillation (NAO, Hurrell 1995) or the East-Atlantic Pattern (EAP, Barnston and Livezey 1987). This partition assumes that the modes are orthogonal and their phases spatially symmetric. In this study, we revisit the impact of atmospheric forcings upon the circulation of the North-Atlantic Ocean by using Weather Regimes (WR) instead of the more traditional approaches of isolating modes commonly found in the literature. WRs are defined as large-scale, recurrent and quasi-stationary atmospheric patterns. Their use enables the spatial differences between the two NAO phases to be distinguished and Scandinavian Blocking events to be isolated. Cassou et al. (2011) and Minvielle et al. (2011) have shown that WRs capture the interannual variability of the surface ocean forcing and are very useful for assessing the ocean response to atmospheric changes. As the variance of atmospheric forcings is greater in winter months (from December to March),

19

with an accordingly larger impact on ocean circulation, only winter WRs are considered in this study. The four weather regimes are the so-called Atlantic Ridge (AR), the Blocking regime (SBL) and the two NAO phases (NAO$^-$ and NAO$^+$).

We have here investigated the imprints of the WRs on the horizontal and vertical North Atlantic Ocean dynamics using a series of numerical experiments performed with a regional, coarse resolution ocean model. We have separated the fast oceanic response (with timescales of a month to a year) from the transient response (within decades) in our analysis. The former has been analyzed using statistical analyses (composites and correlations) of an historical experiment, while the latter has been analyzed using sensitivity experiments forced with idealized representations of each WR. The forcing datasets are constructed from the full distribution of observed WR events. In contrast to more traditional methods, we can verify that this novel approach captures the entire statistical distribution of the atmospheric circulation.

The fast response of the gyre circulation is found to be mostly wind-driven and to be significant for AR, NAO$^-$ and NAO$^+$ but negligible for SBL. On a monthly basis, gyre anomalies are shown to be clearly constrained by the topography and are thus likely driven by topographic Sverdrup balance, which we confirm using a barotropic configuration of the model. As time goes on, the initial barotropic mode is modified by the baroclinic modes that eventually remove the influence of the topography (Anderson and Killworth 1977). The transient response of the subtropical gyre to WRs is an intensification for NAO$^+$ but a weakening for AR, in each case adjusting over a timescale of about 6-8 years. The gyre response for persistent NAO$^-$ consists in a southward shift of the subpolar front (the intergyre-gyre, Marshall et al. 2001) due to the southward shift of wind-stress curl in NAO$^-$. No change occurs for SBL. Additional sensitivity experiments in which forcings were limited to the wind components were performed, which confirm that the changes in the subtropical gyre are primarily a response to wind forcing. At higher latitudes, weakening of the subpolar gyre is found during persistent AR conditions that is also mainly attributed to wind forcings

20

though also in part to anomalous heat fluxes. In the case of persistent SBL and NAO$^+$ conditions, the anomalous heat fluxes play a dominant role in driving changes in the subpolar gyre. Buoyancy fluxes also play a crucial role in the reduction of the circulation in the northern limb of the subpolar gyre during NAO$^-$ conditions.

The fast response of the MOC is also found to be wind-driven, simply reflecting an Ekman-induced surface flow that is compensated at depth (Jayne and Marotzke 2001). The transient response of the MOC to persistent WRs is characterized by a large-scale weakening during persistent AR and NAO$^-$ and a large-scale strengthening during persistent SBL and NAO$^+$. These signals are driven by changes in Labrador Sea Water production that are driven by heat flux anomalies associated with the WRs. When only the influence of wind-stress is considered, we obtain weak anomalies that are likely driven by the adiabatic spin-up of the gyres. However, under such conditions, greater stratification in the subpolar gyre likely reduces the gyres influence on the MOC. It then presumably leads to an underestimation of the influence of the adiabatic spin-up of the gyres on the MOC transient response.

The strong contrast between the gyre responses to persistent NAO$^-$ and NAO$^+$ conditions illustrates the usefulness of WR paradigm. Our study also highlights that atmospheric variability cannot be described solely by a single NAO index. By assuming so, one misses the important wind-driven contribution associated with AR and the buoyancy-driven contribution of SBL. Our study raises the question of whether the oceanic response to WRs is dependent on the oceanic mean state. Accordingly, sensitivity experiments are currently being carried out that use ocean states representative of the end of the 21st century when anthropogenic forcing is predicted to have substantially modified the 3-dimensional North Atlantic ocean states and surface fluxes.

21

# APPENDIX A

# **Detailed model description**

The ocean model used in this study is the Nucleus for European Modeling of the Ocean (NEMO, Madec 2008) that is coupled with the Louvain-la-Neuve Ice Model version 2 (LIM2, Fichefet and Maqueda 1997). We use a regional North-Atlantic configuration generated from the global ORCA05 version described by Biastoch et al. (2008) that is part of the model hierarchy of the Drakkar Group (http://www.drakkar-ocean.eu). The regional domain covers the North-Atlantic from 20°S to 80°N and includes the Nordic Seas and the western Mediterranean sea. This configuration has a resolution of 0.5° at the equator and is implemented on a quasi-isotropic tripolar grid that avoids a North-Pole singularity. At this resolution, mesoscale eddies are represented by an isopycnal mixing/advection parameterization following Gent and McWilliams (1990). In the vertical, 46 levels are used that decrease in resolution with depth (6 $m$ at the surface, 250 $m$ at depth). Vertical eddy viscosity and diffusivity coefficients are computed from a Turbulent Kinetic Energy (TKE) scheme as described in Blanke and Delecluse (1993). We use a filtered free-surface (Roullet and Madec 2000), a Total Variance Diminishing tracer advection scheme (Levitus et al. 2001) and an energy-enstrophy conservation scheme (Arakawa and Lamb 1981) for the momentum equation. A bilaplacian diffusion of momentum ($-7.8e^{11}$ $m^4 s^{-1}$ at the equator, decreasing with latitude proportionally to $\Delta X^3$ where $\Delta X$ is the grid cell width) is applied on geopotential levels, while laplacian lateral mixing of tracers (1000 $m^2 s^{-1}$ at the equator, decreasing with latitude proportionally to $\Delta X$) is applied along iso-neutral surfaces. The northern and southern boundaries of the North-Atlantic domain are closed, and salinity and temperature at these boundaries are restored to the vertically structured Levitus et al. (1998) climatology. A buffer zone of 14 grid points is defined at each boundary, with a linear damping time of 3

23

days at the boundary limit and of 100 days at the ocean limit.

The model is forced with the DFS4.3 atmospheric forcing of Brodeau et al. (2010), which uses 6-hourly air-temperature ($t_2$), specific humidity ($q_2$) and wind fields ($u_{10}$, $v_{10}$) corrected from ECMWF ERA40 reanalysis (1958-2002, Uppala et al. 2005). Satellite products of long-wave/shortwave radiation ($1984 - 2002$) and of monthly snow and precipitation ($1979 - 2002$) are preferentially used because of their improved quality over their equivalent in reanalysis products (Large and Yeager 2009). Prior to 1984 climatological radiative fluxes are applied and prior to 1979, climatological snow and precipitation are used.

Turbulent fluxes are estimated every 6-hours from surface atmospheric state variables and modeled sea-surface temperature (SST) using the bulk formulae described in Large et al. (1997) and Large and Yeager (2004). Modeled sea-surface salinity is restored to Levitus et al. (1998) climatology with a restoring coefficient of 166.6mm.day$^{-1}$. As DFS4.3 is based on ERA40 while we computed WRs from NCEP-NCAR reanalysis, we have checked that there are no discrepancies between the two datasets by comparing the wind-anomalies composites of both datasets, which are very similar (not shown).

# APPENDIX B

# Validation of the forcing construction

Here we describe how we verified that the idealized forcing statistics corresponding to each regime are well captured by our construction method. We have first averaged daily DJFM zonal ($u_{10}$) and meridional ($v_{10}$) wind components and air-temperature ($t_2$) anomalies over four different regions depicted in Fig. 12: midlatitude western Atlantic (MLW), midlatitude eastern Atlantic (MLE), northwestern Atlantic (NW) and northeastern Atlantic (NE). For each box we have computed the Probability Density Functions (PDF) within each regime for

24

the DFS4.3 forcing used in REF, which we compared with the PDFs of the idealized forcings computed in the same domain boxes (Fig. 12). The PDFs obtained using the DFS4.3 forcings are consistent with the wind anomalies that characterize winter WRs (Cassou et al. 2011). For instance, the reinforcement of westerlies in the NW and NE boxes associated with the $NAO^+$ regime is well captured, and conversely for $NAO^-$.

The PDFs of the idealized forcing generally compare well with the PDFs of the original forcing. This is especially true in the NE and NW boxes where the differences between the statistics of the reconstructed and original forcing are marginal. In line with the introduction, the NAO asymmetry in $u_{10}$ is striking here. Midlatitude strengthening of the westerlies seems slightly underestimated in the MLE box. For $v_{10}$, significant differences between the regimes are only found in the NW and NE boxes. Notably the northward shift of midlatitude westerlies particular to SBL conditions is well captured in the NE box. Regarding $t_2$, notable differences between the regimes are only found in the NW box, with the negative anomalies during SBL/$NAO^-$ and the positive anomalies during AR/$NAO^+$ (figure 2) that are well captured.

Fig. 13 shows the observed winter daily variance of both wind components of each regime, and the variance of the idealized forcings. The major features of daily variance can be seen to be well captured by the construction scheme. The regions of high $u_{10}$ variance in the midlatitude westerlies that are particular to AR, SBL and $NAO^+$ regimes have the correct magnitude, and the southward shifted pattern of high $NAO^-$ variability is well reproduced. In the case of $v_{10}$, which generally shows weaker variance than $u_{10}$, the patterns are also fairly well reproduced both in terms of spatial scales and amplitudes. The AR pattern of high variability at 40°N in the western part of the basin is well captured.

It should be noted that only winter forcings are constructed. The influence of summer forcing is not considered here because the variance of atmospheric forcing is strongest in winter, thereby allowing us to make a more effective and persistent imprint on large scale ocean changes. Furthermore, radiative fluxes (shortwave and longwave), precipitation and

25

640   snow are not reconstructed.

# REFERENCES

Anderson, D. L. and P. D. Killworth, 1977: Spin-up of a stratified ocean, with topography. *Deep Sea Research*, **24 (8)**, 709–732.

Arakawa, A. and V. Lamb, 1981: A potential enstrophy and energy conserving scheme for the shallow-water equations. *Monthly Weather Review*, **109 (1)**, 18–36.

Barnier, B., et al., 2006: Impact of partial steps and momentum advection schemes in a global ocean circulation model at eddy-permitting resolution. *Ocean Dynamics*, **56 (5-6)**, 543–567.

Barnston, A. and R. Livezey, 1987: Classification, seasonality and persistence of low-frequency atmospheric circulation patterns. *Monthly Weather Review*, **115 (6)**, 1083–1126.

Barrier, N., A.-M. Treguier, C. Cassou, and J. Deshayes, 2012: Impact of the winter north-atlantic weather regimes on subtropical sea-surface height variability. *Climate Dynamics*, 1–13.

Bellucci, A., S. Gualdi, E. Scoccimarro, and A. Navarra, 2008: NAO-ocean circulation interactions in a coupled general circulation model. *Climate Dynamics*, **31 (7-8)**, 759–777.

Biastoch, A., C. W. Boening, J. Getzlaff, J.-M. Molines, and G. Madec, 2008: Causes of Interannual-Decadal Variability in the Meridional Overturning Circulation of the Midlatitude North Atlantic Ocean. *Journal of Climate*, **21 (24)**, 6599–6615.

Blanke, B. and P. Delecluse, 1993: Variability of the Tropical Atlantic-Ocean simulated by a general-circulation model with 2 different mixed-layer physics. *Journal of Physical Oceanography*, **23 (7)**, 1363–1388.

27

Boening, C. W., M. Scheinert, J. Dengg, A. Biastoch, and A. Funk, 2006: Decadal variability of subpolar gyre transport and its reverberation in the North Atlantic overturning. *Geophysical Research Letters*, **33 (21)**.

Brodeau, L., B. Barnier, A.-M. Treguier, T. Penduff, and S. Gulev, 2010: An ERA40-based atmospheric forcing for global ocean circulation models. *Ocean Modelling*, **31 (3-4)**, 88–104, doi:{10.1016/j.ocemod.2009.10.005}.

Cabanes, C., T. Huck, and A. C. De Verdiere, 2006: Contributions of wind forcing and surface heating to interannual sea level variations in the Atlantic Ocean. *Journal of Physical Oceanography*, **36 (9)**, 1739–1750.

Cassou, C., M. Minvielle, L. Terray, and C. Perigaud, 2011: A statistical-dynamical scheme for reconstructing ocean forcing in the Atlantic. Part I: weather regimes as predictors for ocean surface variables. *Climate Dynamics*, **36 (1-2)**, 19–39.

Cassou, C., L. Terray, J. Hurrell, and C. Deser, 2004: North Atlantic winter climate regimes: Spatial asymmetry, stationarity with time, and oceanic forcing. *Journal of Climate*, **17 (5)**, 1055–1068.

Curry, R. and M. McCartney, 2001: Ocean gyre circulation changes associated with the North Atlantic Oscillation. *Journal of Physical Oceanography*, **31 (12)**, 3374–3400.

Danabasoglu, G., W. G. Large, and B. P. Briegleb, 2010: Climate impacts of parameterized Nordic Sea overflows. *Journal of Geophysical Research-Ocean*, **115**.

Deshayes, J., F. Straneo, and M. A. Spall, 2009: Mechanisms of variability in a convective basin. *Journal of Marine Research*, **67 (3)**, 273–303.

Dickson, R. R. and J. Brown, 1994: The production of north atlantic deep water: sources, rates, and pathways. *Journal of Geophysical Research: Oceans (1978–2012)*, **99 (C6)**, 12 319–12 341.

28

Eden, C. and R. J. Greatbatch, 2003: A damped decadal oscillation in the north atlantic climate system. *Journal of climate*, **16 (24)**, 4043–4060.

Eden, C. and T. Jung, 2001: North Atlantic interdecadal variability: Oceanic response to the North Atlantic oscillation (1865-1997). *Journal of Climate*, **14 (5)**, 676–691.

Eden, C. and J. Willebrand, 2001: Mechanism of interannual to decadal variability of the North Atlantic circulation. *Journal of Climate*, **14 (10)**, 2266–2280.

Fichefet, T. and M. Maqueda, 1997: Sensitivity of a global sea ice model to the treatment of ice thermodynamics and dynamics. *Journal of Geophysical Research-Oceans*, **102 (C6)**, 12 609–12 646.

Gent, P. and J. McWilliams, 1990: Isopycnal mixing in ocean circulation models. *Journal of Physical Oceanography*, **20 (1)**, 150–155.

Getzlaff, J., C. W. Böning, C. Eden, and A. Biastoch, 2005: Signal propagation related to the north atlantic overturning. *Geophysical research letters*, **32 (9)**.

Griffies, S. M., et al., 2009: Coordinated Ocean-ice Reference Experiments (COREs). *Ocean Modelling*, **26 (1-2)**, 1–46.

Hakkinen, S. and P. Rhines, 2004: Decline of subpolar North Atlantic circulation during the 1990s. *Science*, **304 (5670)**, 555–559.

Hakkinen, S., P. B. Rhines, and D. L. Worthen, 2011a: Atmospheric Blocking and Atlantic Multidecadal Ocean Variability. *Science*, **334 (6056)**, 655–659.

Hakkinen, S., P. B. Rhines, and D. L. Worthen, 2011b: Warm and saline events embedded in the meridional circulation of the northern North Atlantic. *Journal of Geophysical Research*, **116**.

Hátún, H., A. B. Sandø, H. Drange, B. Hansen, and H. Valdimarsson, 2005: Influence of the atlantic subpolar gyre on the thermohaline circulation. *Science*, **309 (5742)**, 1841–1844.

29

Herbaut, C. and M. Houssais, 2009: Response of the eastern North Atlantic subpolar gyre to the North Atlantic Oscillation. *Geophysical Research Letters*, **36**.

Hong, B., W. Sturges, and A. Clarke, 2000: Sea level on the US East Coast: Decadal variability caused by open ocean wind-curl forcing. *Journal of Physical Oceanogaphy*, **30 (8)**, 2088–2098.

Hurrell, J., 1995: Decadal Trends in the North-Atlantic Oscillation - Regional temperatures and precipitations. *Science*, **269 (5224)**, 676–679.

Jayne, S. R. and J. Marotzke, 2001: The dynamics of ocean heat transport variability. *Reviews of Geophysics*, **39 (3)**, 385–411.

Jungclaus, J., H. Haak, M. Latif, and U. Mikolajewicz, 2005: Arctic-North Atlantic interactions and multidecadal variability of the meridional overturning circulation. *Journal of Climate*, **18 (19)**, 4013–4031.

Kalnay, E., et al., 1996: The NCEP/NCAR 40-year reanalysis project. *Bulletin of the American Meteorological Society*, **77 (3)**, 437–471.

Koblinsky, C., 1990: THE GLOBAL DISTRIBUTION OF F/H AND THE BAROTROPIC RESPONSE OF THE OCEAN. *JOURNAL OF GEOPHYSICAL RESEARCH-OCEANS*, **95 (C3)**, 3213–3218.

Köhl, A. and D. Stammer, 2008: Variability of the meridional overturning in the north atlantic from the 50-year gecco state estimation. *Journal of Physical Oceanography*, **38 (9)**, 1913–1930.

Langehaug, H. R., I. Medhaug, T. Eldevik, and O. H. Ottera, 2012: Arctic/Atlantic Exchanges via the Subpolar Gyre. *Journal of Climate*, **25 (7)**, 2421–2439.

Large, W., G. Danabasoglu, S. Doney, and J. McWilliams, 1997: Sensitivity to surface

forcing and boundary layer mixing in a global ocean model: Annual-mean climatology. *Journal of Physical Oceanography*, **27 (11)**, 2418–2447.

Large, W. G. and S. G. Yeager, 2004: Diurnal to Decadal Global Forcing for Ocean and Sea-ice Models : The Data Sets and Flux Climatologies. Tech. rep., NCAR Technical Note: NCAR/TN-460+STR.

Large, W. G. and S. G. Yeager, 2009: The global climatology of an interannually varying air-sea flux data set. *Climate Dynamics*, **33 (2-3)**, 341–364.

Levitus, S., J. Antonov, J. Wang, T. Delworth, K. Dixon, and A. Broccoli, 2001: Anthropogenic warming of Earth's climate system. *SCIENCE*, **292 (5515)**, 267–270.

Levitus, S., T. Boyer, M. Conkright, J. O'Brien, T. Antonov, C. Stephens, S. L., J. D., and R. Gelfeld, 1998: NOAA Atlas NESDIS 18 and World Ocean Database 1998. *NOAA Atlas NESDIS 18 and World Ocean Database 1998.*

Lohmann, K., H. Drange, and M. Bentsen, 2009: Response of the North Atlantic subpolar gyre to persistent North Atlantic oscillation like forcing. *Climate Dynamics*, **32 (2-3)**, 273–285.

Madec, G., 2008: *NEMO ocean engine.*

Marshall, J., H. Johnson, and J. Goodman, 2001: A study of the interaction of the North Atlantic oscillation with ocean circulation. *Journal of Climate*, **14 (7)**, 1399–1421.

Medhaug, I., H. Langehaug, T. Eldevik, and T. Furevik, 2011: Mechanisms for multidecadal variability in a simulated Atlantic Meridional Overturning Circulation. *Climate Dynamics.*

Michelangi, P., R. Vautard, and B. Legras, 1995: Weather Regimes - Recurrence and quasi-stationarity. *Journal of Atmospheric Sciences*, **52 (8)**, 1237–1256.

Minvielle, M., C. Cassou, R. Bourdalle-Badie, L. Terray, and J. Najac, 2011: A statistical-dynamical scheme for reconstructing ocean forcing in the Atlantic. Part II: methodology,

31

validation and application to high-resolution ocean models. *Climate Dynamics*, **36 (3-4)**, 401–417.

Msadek, R. and C. Frankignoul, 2009: Atlantic multidecadal oceanic variability and its influence on the atmosphere in a climate model. *Climate Dynamics*, **33 (1)**, 45–62.

Pickart, R. S. and M. A. Spall, 2007: Impact of Labrador Sea convection on the north Atlantic meridional overturning circulation. *Journal of Physical Oceanography*, **37 (9)**, 2207–2227.

Roullet, G. and G. Madec, 2000: Salt conservation, free surface, and varying levels: a new formulation for ocean general circulation models. *Journal of Geophysical Research-Oceans*, **105 (C10)**, 23 927–23 942.

Ruprich-Robert, Y. and C. Cassou, 2013: Combined influences of seasonal east atlantic pattern and north atlantic oscillation to excite atlantic multidecadal variability in a climate model. *Climate Dynamics*, **submitted**, submitted.

Rust, H. W., M. Vrac, M. Lengaigne, and B. Sultan, 2010: Quantifying Differences in Circulation Patterns Based on Probabilistic Models: IPCC AR4 Multimodel Comparison for the North Atlantic. *JOURNAL OF CLIMATE*, **23 (24)**, 6573–6589.

Sarafanov, A., A. Falina, A. Sokov, and A. Demidov, 2008: Intense warming and salinification of intermediate waters of southern origin in the eastern subpolar North Atlantic in the 1990s to mid-2000s. *JOURNAL OF GEOPHYSICAL RESEARCH-OCEANS*, **113 (C12)**.

Scherrer, S., M. Croci-Maspoli, C. Schwierz, and C. Appenzeller, 2006: Two-dimensional indices of atmospheric blocking and their statistical relationship with winter climate patterns in the Euro-Atlantic region. *International Journal of Climatology*, **26 (2)**, 233–249, doi:{10.1002/joc.1250}.

32

Schweckendiek, U. and J. Willebrand, 2005: Mechanisms affecting the overturning response in global warming simulations. *Journal of Climate*, **18 (23)**, 4925–4936.

Smith, R., M. Maltrud, F. Bryan, and M. Hecht, 2000: Numerical simulation of the North Atlantic Ocean at 1/10 degrees. *Journal of Physical Oceanography*, **30 (7)**, 1532–1561.

Straneo, F., 2006: Heat and freshwater transport through the central Labrador Sea. *JOURNAL OF PHYSICAL OCEANOGRAPHY*, **36 (4)**, 606–628.

Treguier, A., S. Theetten, E. Chassignet, T. Penduff, R. Smith, L. Talley, J. Beismann, and C. Boning, 2005: The North Atlantic subpolar gyre in four high-resolution models. *Journal of Physical Oceanography*, **35 (5)**, 757–774.

Treguier, A. M., M. H. England, S. R. Rintoul, G. Madec, J. Le Sommer, and J. M. Molines, 2007: Southern Ocean overturning across streamlines in an eddying simulation of the Antarctic Circumpolar Current. *OCEAN SCIENCE*, **3 (4)**, 491–507.

Uppala, S., et al., 2005: The ERA-40 re-analysis. *Quaterly Journal of the Royal Meteorological Society*, **131 (612, Part b)**, 2961–3012.

Vautard, R., 1990: Multiple weather regimes over the North-Atlantic. Analysis of precursors and successors. *Monthly Weather Review*, **118 (10)**, 2056–2081.

Visbeck, M., H. Cullen, G. Krahmann, and N. Naik, 1998: An ocean model's response to North Atlantic Oscillation-like wind forcing. *Geophysical Research Letters*, **25 (24)**, 4521–4524.

Vivier, F., K. Kelly, and L. Thompson, 1999: Contributions of wind forcing, waves, and surface heating to sea surface height observations in the Pacific Ocean. *JOURNAL OF GEOPHYSICAL RESEARCH-OCEANS*, **104 (C9)**, 20 767–20 788.

Zhu, J. and E. Demirov, 2011: On the mechanism of interannual variability of the Irminger Water in the Labrador Sea. *Journal of Geophysical Research-Oceans*, **116**.

# List of Tables

34

TABLE 1. List of the numerical experiments discussed in the text. All the experiments are run for 45 years (1958-2002).

| Configuration | Forcings | Description |
|---|---|---|
| *Spinup REF* | DFS4.3 | Reference spin-up. Initialization from ocean at rest. Tracer initialization from Levitus et al. (1998) climatology |
| *REF* | Same as *Spinup REF* | Started from *Spinup REF*. |
| *WR* | Idealized winter wind, temperature and humidity. DFS4.3 in summer. Climatological radiative fluxes, precipitation and snow. | Started from *Spinup REF*. |
| *Spinup WREF* | DFS4.3 winds and climatological temperature, humidity, radiative fluxes, precipitations and snow. | Wind-only spinup. Initialization from ocean at rest. Tracer initialization from Levitus et al. (1998) climatology. |
| *WREF* | Same as *Spinup WREF* | Started from *Spinup WREF*. |
| *WWR* | Identical to *Spinup WREF*, except for the winds that are identical to *WR*) | Started from *Spinup WREF*. |

35

TABLE 2. Number of regime occurrences during the winters characterized by strongly positive EOF-derived NAO index.

| Year | AR | SBL | NAO$^-$ | NAO$^+$ | % NAO$^+$ |
|------|-----|------|---------|---------|-----------|
| 1983 | 45 | 24 | 4 | 48 | 39.7% |
| **1989** | **21** | **33** | **1** | **66** | **54.5**% |
| **1990** | **9** | **27** | **15** | **70** | **57.9**% |
| 1992 | 28 | 51 | 5 | 38 | 31.1% |
| 1994 | 19 | 21 | 21 | 60 | 49.6% |
| **1995** | **23** | **21** | **8** | **69** | **57.0**% |
| 2000 | 54 | 14 | 5 | 49 | 40.2% |

# List of Figures

37

38

FIG. 1. NCEP-NCAR composites of winter wind-stress curl (color shading) and Ekman transport (black arrows) anomalies computed from daily anomalies occurring in each WR. Significativity is assessed based on *t*-statistics at the 95% level of confidence. Non-significant Ekman transport anomalies are omitted, non-significant wind-stress curl anomalies are stippled. Dashed gray lines represent meridional Ekman transport anomalies convergence/divergence, determined from zonally averaged zonal winds.
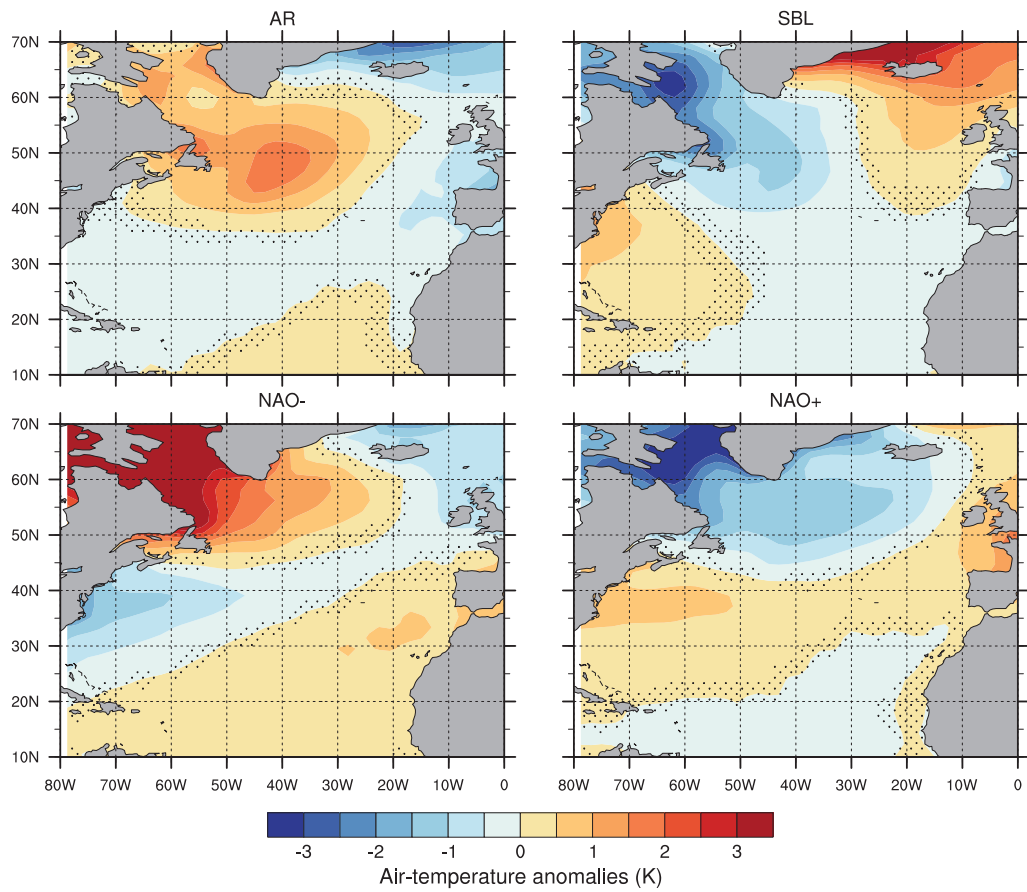
Fig. 2. Similar to figure 1 but for air-temperature anomalies.
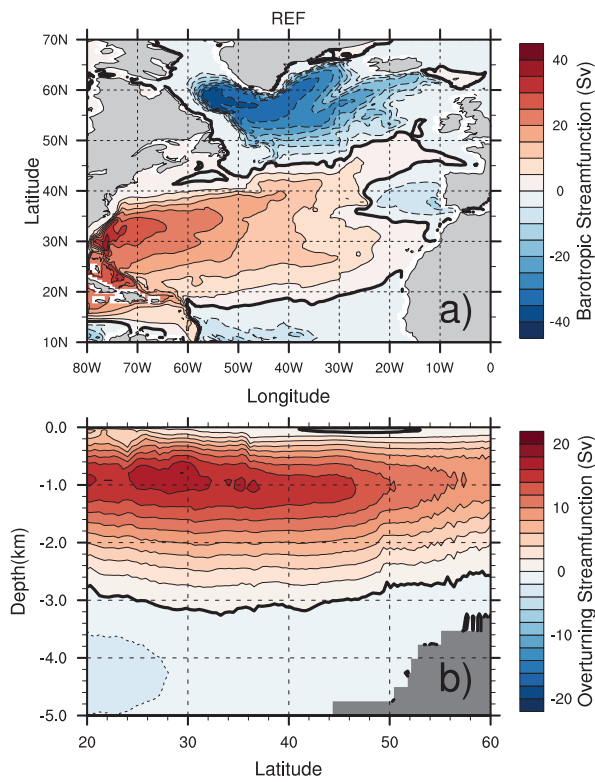
FIG. 3. Mean circulation in the REF experiment averaged over 45 years. a) Barotropic streamfunction (contour interval: 5 $Sv$). b) Meridional Overturning Streamfunction (contour interval: 2 $Sv$).
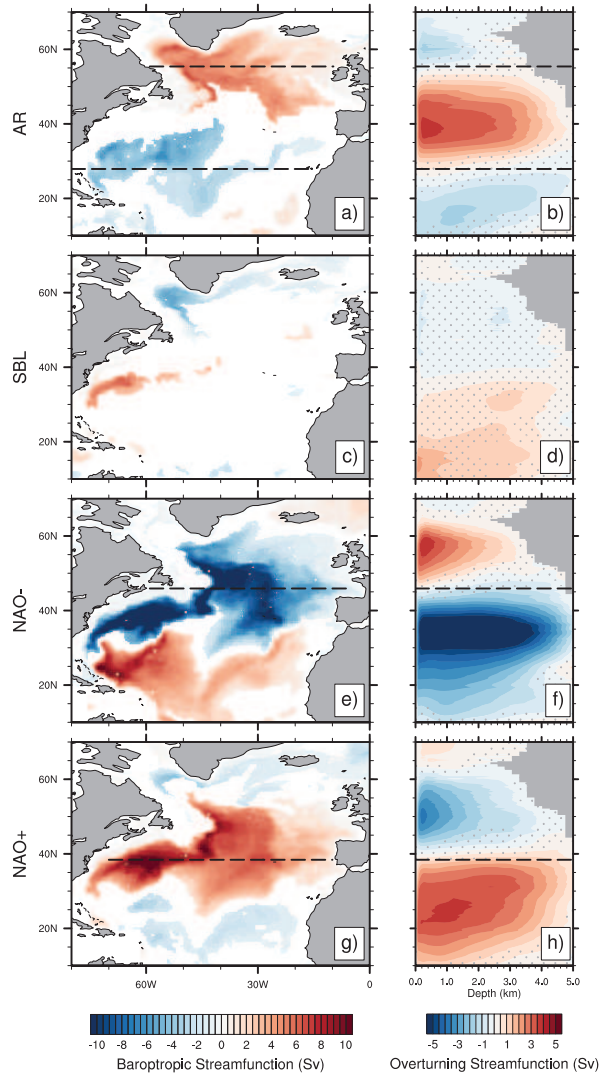
FIG. 4. Monthly composites of barotropic (a, c, e, g) and overturning (b, d, f, h) stream-function anomalies issued from REF (see text for details). Non-significant values ($t$-test at the 95% level of confidence) are omitted in the left panels and stippled in the right panels. Dashed black lines represent meridional Ekman transport anomalies convergence/divergence, determined from zonally averaged zonal winds.
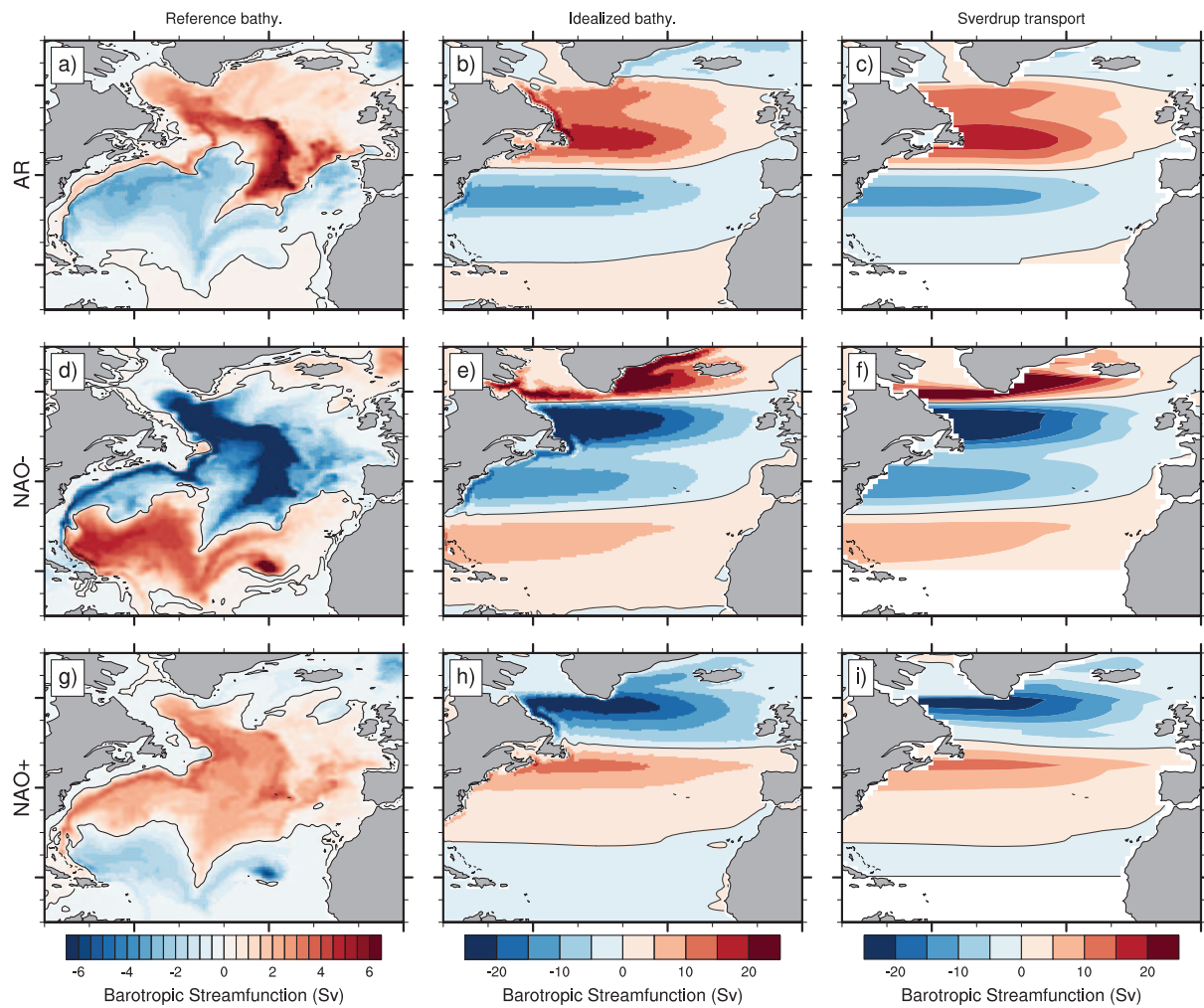
FIG. 5. Barotropic streamfunction averaged over the $4^{th}$ year of the idealized barotropic experiments (a, b, d, e, g, h). Left panel: reference bathymetry. Middle panel: idealized bathymetry (3000 $m$ everywhere). Right panel: classical Sverdrup theory.
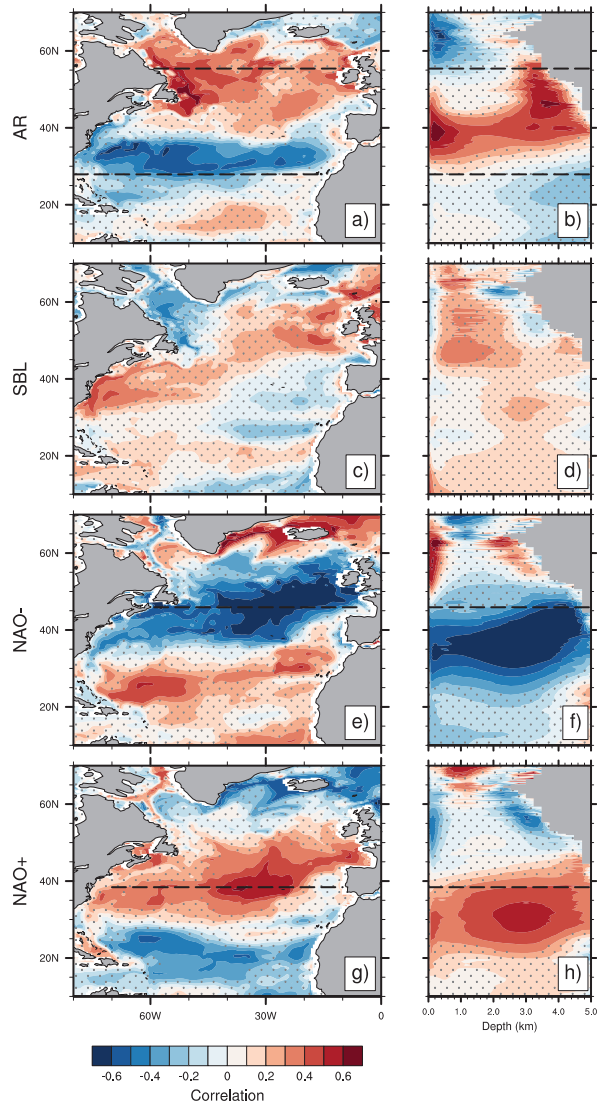
FIG. 6. 0-lag correlations between yearly averaged barotropic (a, c, e, g) and overturning (b, d, f, h) streamfunction anomalies issued from REF and the winter WRs occurrences. Non significant values (*t*-test at 95%) are stippled. Dashed black lines represent meridional Ekman transport anomalies convergence/divergence, determined from zonally averaged zonal winds.

44
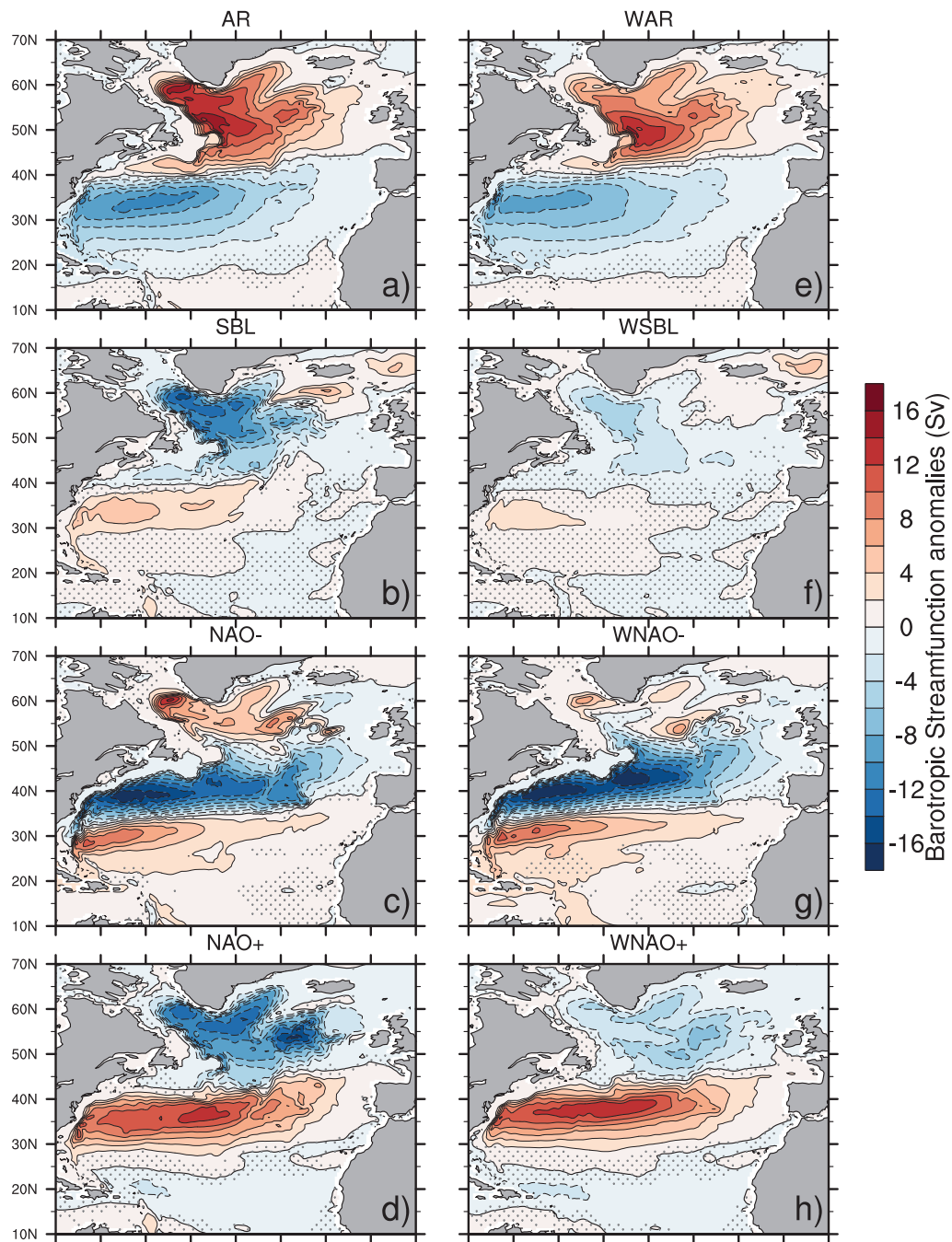
Fig. 7. Differences between the barotropic streamfunction of the idealized WR or WWR experiments averaged over the last 10 years and the barotropic streamfunction of their respective reference experiments (REF or WREF) averaged over 45 years. Thick black lines represent the 0-contour. Stippled contours are non-significant values based on $t-$ statistics at the 95% level.
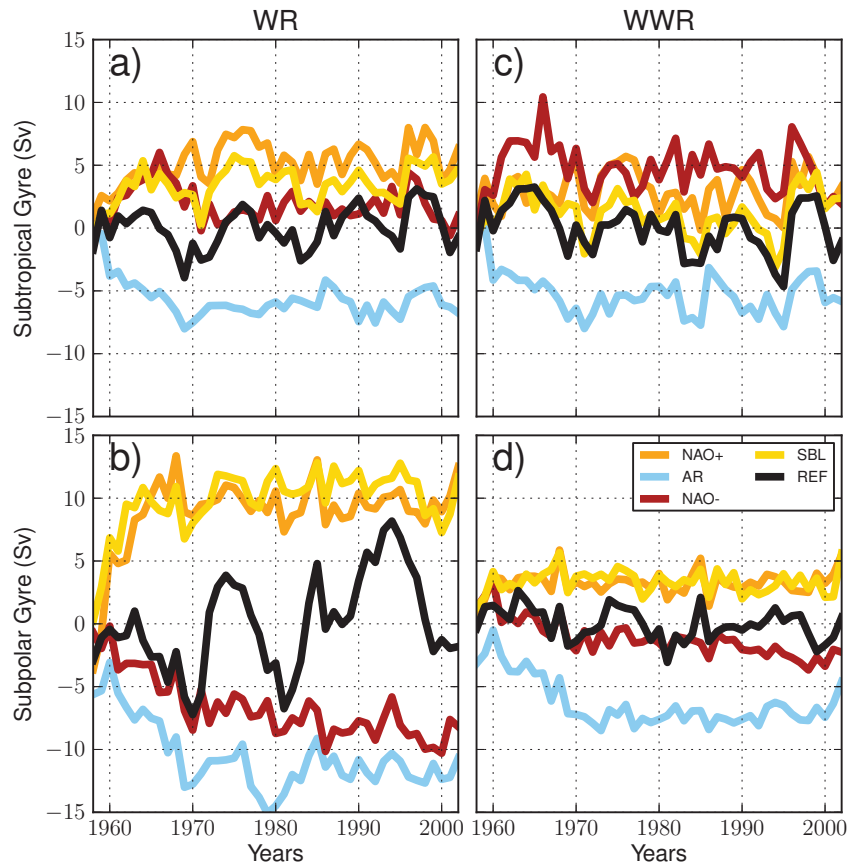
FIG. 8. Maximum strength of the subtropical (a, c) and subpolar (b, d) gyres in the sensitivity experiments (colored lines). In each panel, the means of the reference experiments (REF in the left columns, WREF in the right columns, black lines) have been removed.
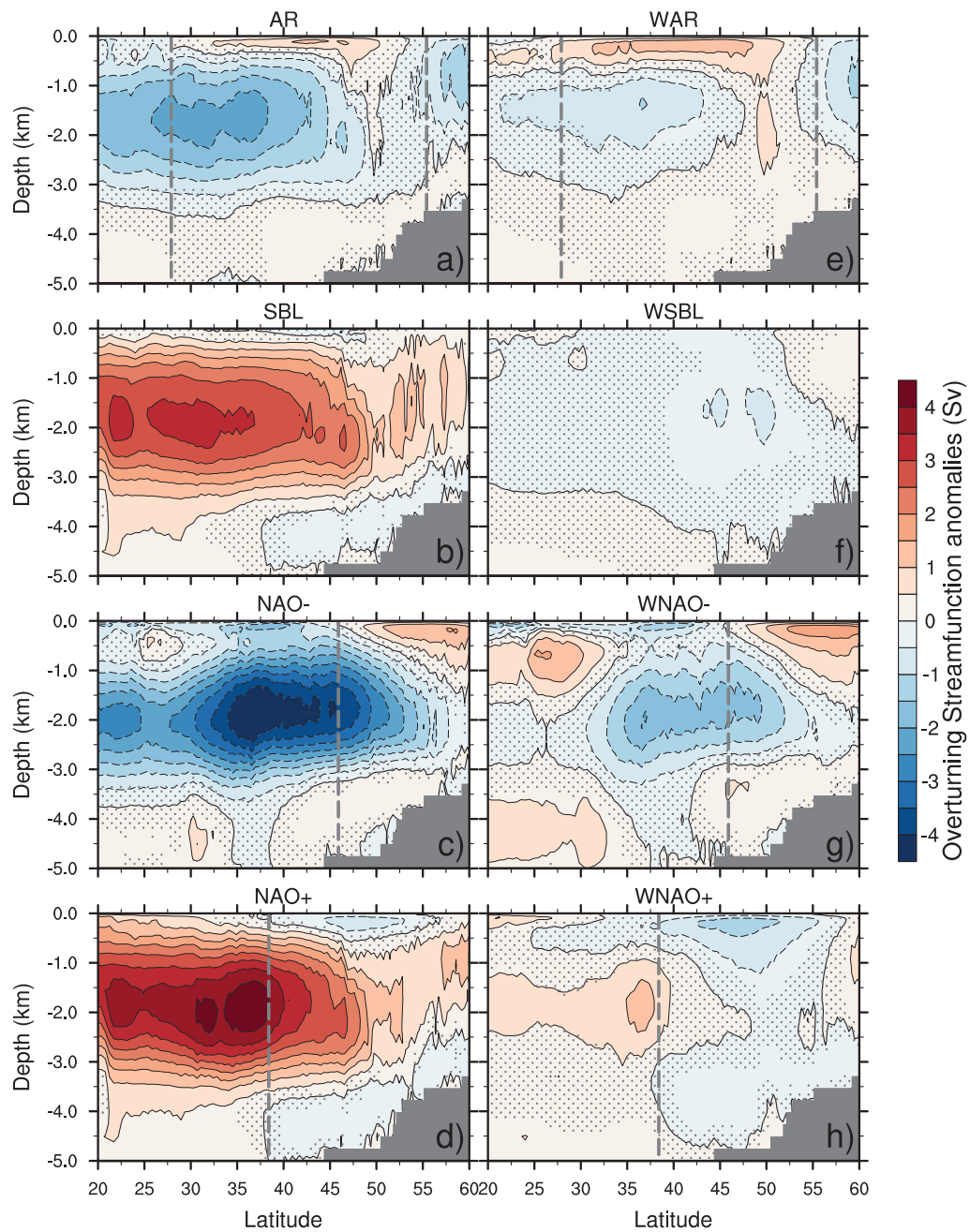
FIG. 9. Same as figure 7 but for the overturning streamfunction. Dashed gray lines represent meridional Ekman transport anomalies convergence/divergence, determined from zonally averaged zonal winds.
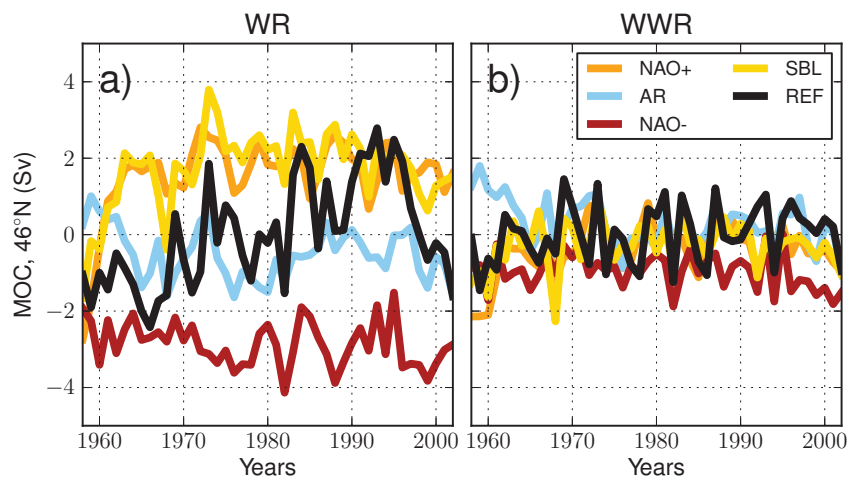
FIG. 10. Same as figure 8 but for the maximum overturning streamfunction at 46°N.
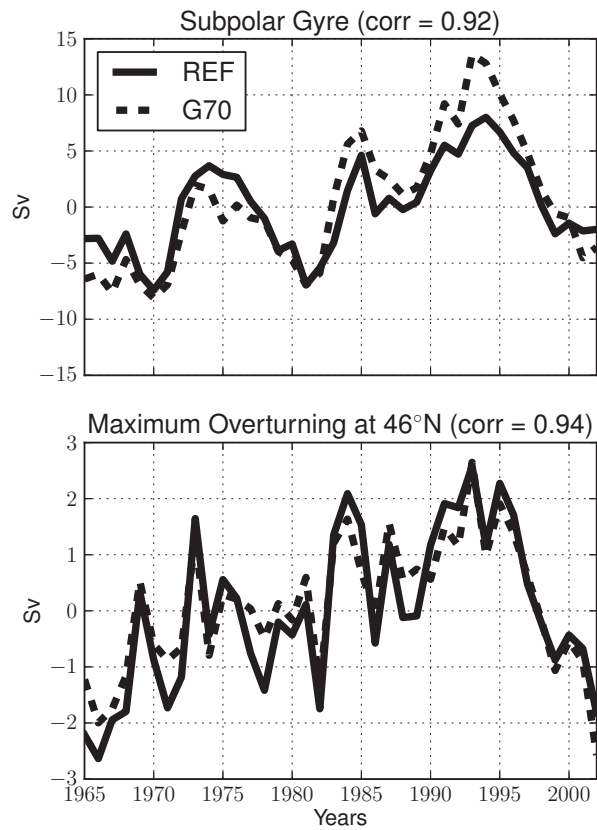
FIG. 11. Yearly averaged anomalies of subpolar gyre and overturning streamfunction strength for the regional model configuration used in this study (black lines) and the global NEMO simulation of Barnier et al. (2006). Correlations between the two models are indicated on top of the panels.
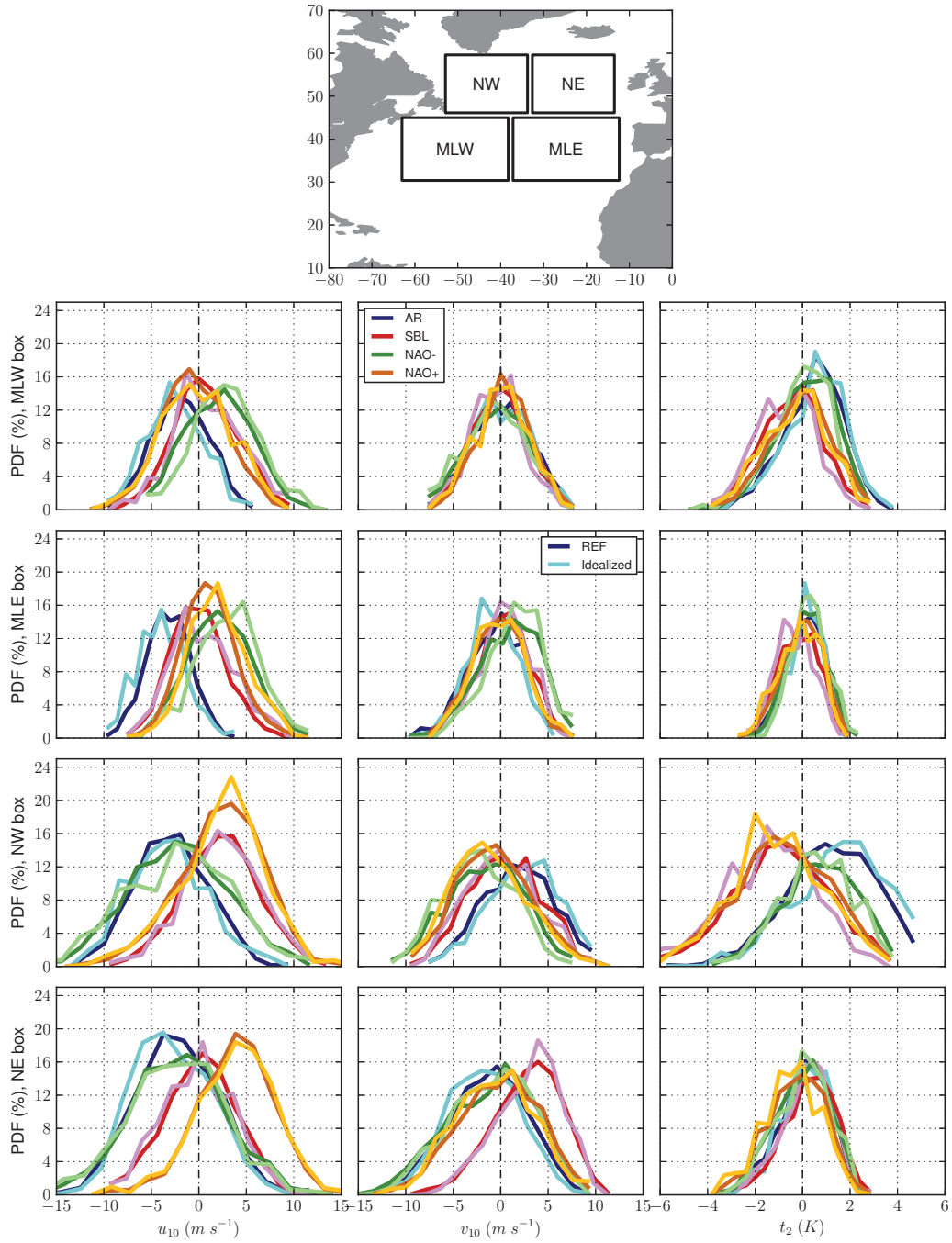
FIG. 12. Probability density function (in %) for $u_{10}$ (left column), $v_{10}$ (middle column) and $t_2$ (right column) in the midlatitude western (MLW), midlatitude eastern (MLE), northwestern (NW) and northeastern (NE) Atlantic boxes. Dark colors are the PDFs from the reference forcings while light colors are used for the idealized ones.

50
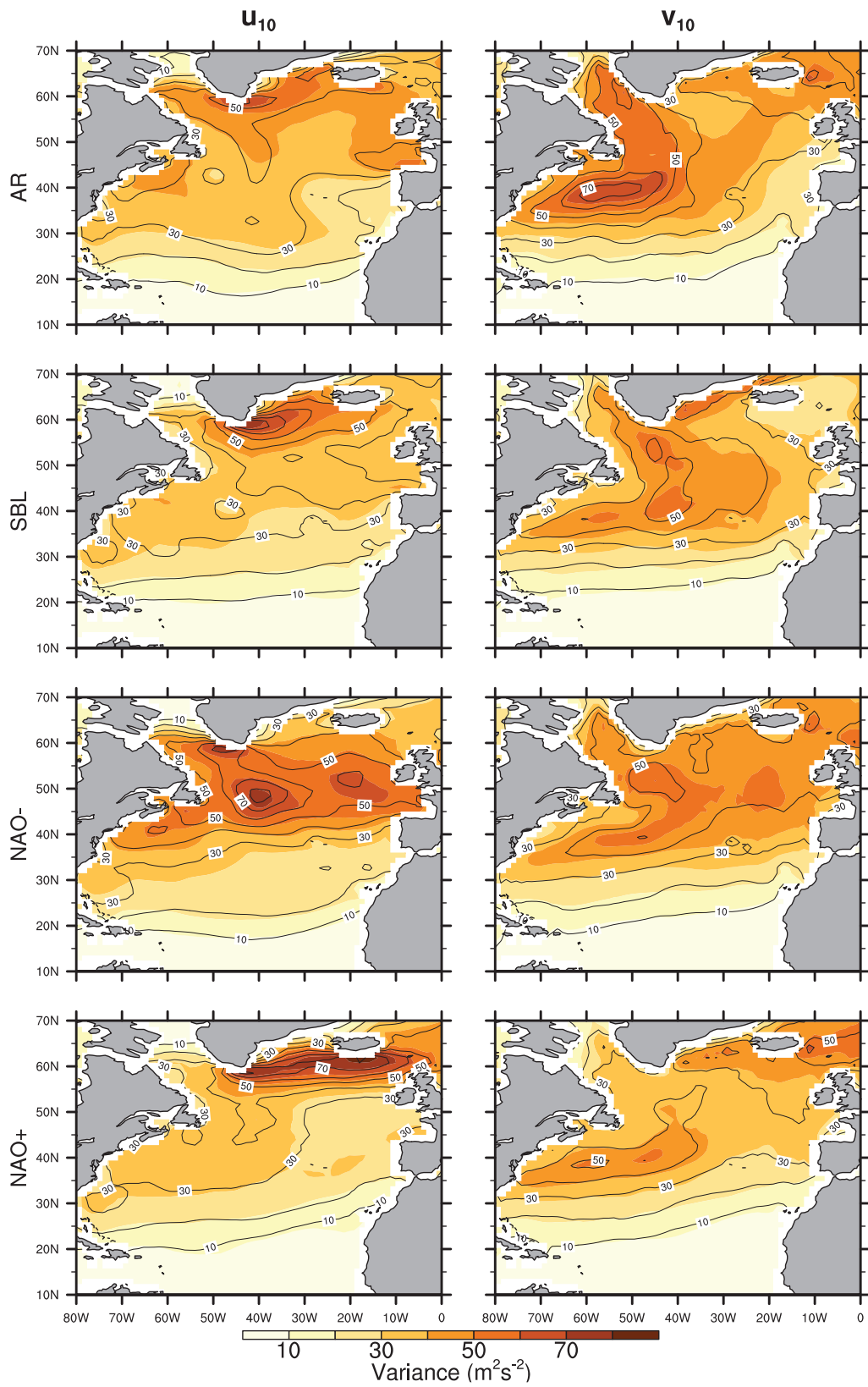
FIG. 13. Winter daily variance of observed (color shading) and reconstructed (black contours) wind components $u_{10}$ (left) and $v_{10}$ (right) within each regime.

## 4.4 Conclusion and discussions

In this chapter, a forced ocean only model of coarse resolution is used to analyse the response of North-Atlantic ocean circulation to weather regimes. Using statistical analysis on an historical simulation, the fast (monthly to interannual timescales) response of the ocean circulation to changes in the weather regimes has been addressed. Among the four regimes, only three (AR, NAO$^-$ and NAO$^+$) drive a fast wind-driven adjustment of the circulation. AR induces a reduction of the horizontal circulation, while NAO$^-$ and NAO$^+$ both drive an intergyre-gyre, cyclonic for NAO$^-$ and anticyclonic for NAO$^+$. Because of NAO asymmetry, this intergyre gyre is southward shifted for NAO$^+$. This fast response of the gyre circulation involves topographic Sverdrup balance, as confirmed by a barotropic configuration of the model. The influence of topography on the gyres is striking at monthly timescales but is less obvious at yearly timescales, when the barotropic mode has already been modified by the baroclinic modes. The meridional overturning circulation shows top-to-bottom anomalies that are the signature of a surface Ekman surface flow compensated at depth by a returned flow.

The slow adjustment (decadal timescales) of the ocean circulation to persistent regime conditions has also been investigated using sensitivity model experiments, in which the winter forcings of the historical simulation have been replaced by idealised forcings. These forcings have been constructed through an original method, based on the weather regimes, that successfully captures the forcings statistics. The major findings of these sensitivity experiments are summarised in table 4.1.

As emphasised in chapter 2, the use of the *k*-mean algorithm assumes that the number of clusters is a priori known. In this study, 4 weather regimes have been considered. When decomposing sea-level pressure anomalies into five regimes, these four regimes are returned in addition to a fifth one that resembles to AR, although with opposite signs and an eastward shifted pattern. This regime is defined as the "Atlantic Low" (AL hereafter). Wind-stress curl anomalies associated with AL are eastward shifted compared to AR ones (figure 4.5a), consistently with its eastward shifted center of action. AL is also associated with cold air-temperature anomalies at 50°N (figure 4.5b). These anomalies, however, are eastward shifted in comparison with AR and do not reach the Labrador Sea (figure 2.7).

A sensitivity experiment of the ocean circulation to AL-like buoyancy and wind forcing has been

|  | AR | BLK | NAO$^-$ | NAO$^+$ |
|---|---|---|---|---|
| STG | Wind-driven reduction | | Wind-driven inter-gyre gyre | Wind-driven intensification |
| SPG | Wind-driven reduction. Contribution of reduced heat loss to the atmosphere in the LS | Strengthening driven by enhanced heat loss in the LS | Wind-driven inter-gyre gyre. Weakening of the northern subpolar gyre due to reduced heat loss in the LS | Strengthening driven by enhanced heat loss in the LS |
| MOC | Weakening due to reduced heat loss in the LS. Contribution of wind-driven gyre changes | Strengthening due to enhanced heat loss in the LS. | Weakening due to reduced heat loss in the LS. Contribution of wind-driven gyre changes | Strengthening due to enhanced heat loss in the LS. Contribution of wind-driven gyre changes. |

*Table 4.1: Summary of the major findings of the idealized sensitivity experiments. Acronyms used are: STG=subtropical gyre, SPG=subpolar gyre, MOC=meridional overturning circulation, LS=Labrador Sea.*

performed in the same way as discussed in Barrier et al. (2013). Persistent AL conditions are associated with a strengthening of the gyre circulation (figure 4.5c) that is presumably wind-driven: the latitudinal position of the AL wind-stress curl anomalies is the same as for AR; hence, they also project fairly well onto the mean position of the gyres and are thus effective in impacting their strength. The MOC anomalies for persistent AL conditions mirror those for persistent AR conditions (figure 9a of Barrier et al. 2013), but with smaller amplitudes. This is presumably because eastward shifted pattern displaces the wind and air-temperature anomalies out of the Labrador Sea, hence preventing deep water formation to increase. As a consequence, MOC anomalies only reflect the contributions of Ekman transport anomalies and of the adiabatic spin-up of the gyres. Hence, in addition to the NAO$^+$/NAO$^-$ examples, the AL/AR comparison highlights the added value of the weather regime framework, since even small spatial asymmetries can lead to significantly different oceanic response.

The weather regimes, through their impacts on the ocean circulation and surface heat fluxes, could potentially impact ocean heat content variability. The full understanding of heat content variability is a major challenge for oceanographers, since in the context of global warming, the excess of heat will ultimately be stored by the ocean. Many studies aimed at understanding the changes in ocean heat content in response to changes in the large-scale atmospheric forcing. The warming of the subpolar gyre of 1995 has been especially scrutinised and has often been attributed to the abrupt change of the NAO in 1995 (Sarafanov et al. 2008). However, Hakkinen et al. (2011a) suggest that
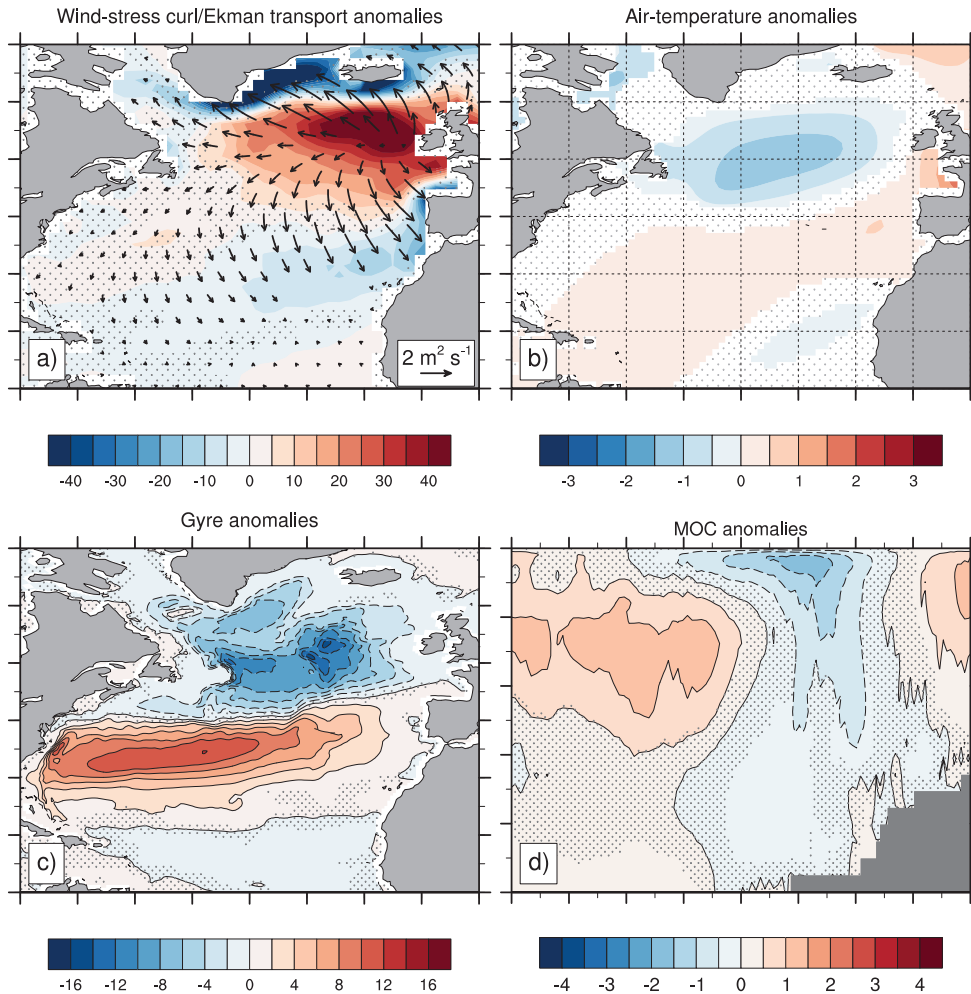
*Figure 4.5: (a) Wind-stress curl and Ekman transport anomalies. (b) Air-temperature anomalies (c and d) gyre and overturning anomalies averaged over the last 10 years of the AL-only experiment.*

this warming has been induced by stronger than normal EAP conditions. Hence, it remains unclear which large-scale atmospheric pattern (if any) has induced this warming.

The impacts of the weather regimes on ocean heat content has not been addressed in the present chapter for two main reasons:

- The model configuration has closed boundaries, at which the tracer fields (temperature and salinity) are restored to Levitus et al. (1998) climatology. Hence, the variability of ocean heat content is, in all likelihood, impacted by this specific model configuration.

- Ocean heat content variability strongly depends on the mean and variability of the ocean circulation. Both strongly depend on the model resolution (horizontal and vertical), parameterizations (like sea-surface salinity restoring) and on the forcing dataset. Hence, multi-model analysis is necessary to assess the robustness of the results against these parameters.

Accordingly, the next chapter is devoted to the understanding of the ocean heat content variability and its possible linkages with the atmospheric weather regimes. This is addressed through heat budget calculations in the subpolar gyre and the Nordic Seas, using a series of global hindcasts.

# Chapter 5

# Interannual to decadal heat budget in the subpolar North Atlantic and the Nordic Seas

## Contents

# 5.1 Introduction

The global increase of ocean heat content, as discussed in e.g. Levitus et al. (2001), Willis et al. (2004) and Levitus et al. (2009), is presumably attributed to the increase in anthropogenic greenhouse gases emission. The accumulation of heat by the ocean induces a thermosteric sea-level rise (Cabanes et al. 2001; Willis et al. 2004; Antonov et al. 2005) that may have disastrous societal impacts (Nicholls and Tol, 2006; Dasgupta et al., 2007; Nicholls et al., 2007). However, the consideration of global heat content may hide the regional disparities (Lozier et al. 2008; Levitus et al. 2012; Zhai and Sheldon 2012). This is especially true in the North-Atlantic Ocean, which has been shown to warm in the subtropics and to cool at subpolar latitudes between the 20 year periods 1950-1970 and 1980-2000 (Lozier et al. 2008). In order to determine whether these changes are indeed caused by climate change supposes a good knowledge of the drivers of heat content variability.

Many studies have been devoted to the understanding of ocean heat content variability in the North-Atlantic and its possible linkages with large-scale atmospheric variability. The two major contributors to changes in ocean heat content are surface heat flux and ocean heat convergence anomalies. Surface heat flux variability is closely related to the North-Atlantic Oscillation (NAO). Positive NAO conditions are associated with increased latend heat loss in the Labrador Sea and with reduced sensible heat loss in the subtropics (Cayan 1992b; Visbeck et al. 1998). A first aim of the present study is to determine whether the other modes of variability of the North-Atlantic region (EAP and SCAN, section 2.2) impact the variability of surface flux, and if so in which region.

Furthermore, changes in the large-scale atmospheric circulation have also been shown to impact the ocean circulation and, in turn, horizontal heat convergence. Using model experiments, Lozier et al. (2008) suggest that the heat content difference between 1950-1970 and 1980-2000 can be explained by the strong shift in the NAO index (mostly negative in the first period, mostly positive in the latter period). They suggest that the warming of the subtropical gyre is a consequence of wind-driven circulation change, while the cooling of the subpolar gyre is a consequence of buoyancy-driven circulation change. Additionally, the dramatic switch in the NAO index from highly positive in 1995 (1.04[1]) to highly negative in 1996 (-1.11), has been proposed as one of the triggers of the warming of the subpolar gyre that started in 1995. The change in the NAO index presumably induced a

---

[1]Source: `https://climatedataguide.ucar.edu/climate-data/hurrell-north-atlantic-oscillation-nao-index-pc-based`

reduction of the subpolar gyre and a concomitant westward shift of the subpolar front (Hátún et al. 2005), which facilitated the intrusion of warm and saline subtropical water (Bersch 2002, Bersch et al. 2007, Sarafanov et al. 2008, Lozier and Stewart 2008, Chaudhuri et al. 2011 among others). However, Hakkinen et al. (2011a,b) argue that the reduction in the strength of the subpolar gyre and the associated shift of the subpolar front was not due to the change in the NAO index but to the change in the East-Atlantic Pattern (EAP), the second mode of atmospheric variability in the North-Atlantic. Herbaut and Houssais (2009) suggest that positive NAO conditions induce a wind-driven anticyclonic intergyre-gyre (Marshall et al. 2001) that advects "fresh, cold water from the western to the eastern subpolar gyre" and "warm, saline subtropical water to the south of Newfoundland". They also suggest that the buoyancy driven spin-up of the subpolar gyre under persistent NAO$^+$ conditions "does not force the changes in the eastern North Atlantic". In other words, it does not change the proportion of subtropical water that enters into the eastern subpolar gyre, as proposed by Hátún et al. (2005).

Marsh et al. (2008), Grist et al. (2010) and Desbruyeres et al. (2013) have conducted midlatitude heat budget calculations within closed domains and concluded that the interannual to decadal variability in ocean heat content is primarily driven by changes in ocean heat convergence, while surface heat flux anomalies play only a minor damping role. However, their domains exclude the regions where the variance of surface heat fluxes is strong (figure 5.1), hence likely to impact ocean heat content variability. The domain considered by Grist et al. (2010) mixes two regions: the Labrador Sea, where the variance of surface heat fluxes is strong, and the eastern subpolar gyre, where it is negligible. As a consequence, the possible influence of surface heat fluxes might be blurred by the consideration of such a zonally extended region. A different domain decomposition might lead to different conclusions. In the western subpolar gyre and the Nordic Seas, where winter surface heat fluxes vary the most, they could be expected to significantly impact ocean heat content variability.
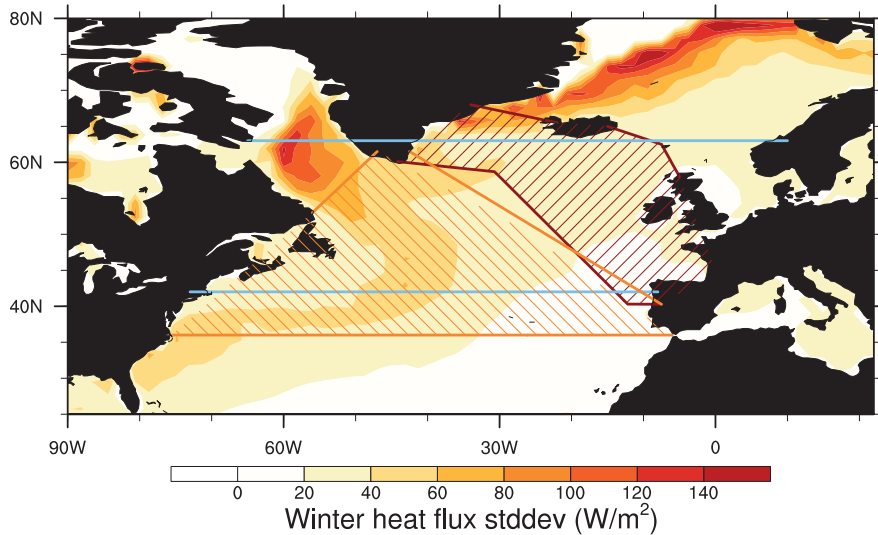
*Figure 5.1: Standard deviation of winter averaged downward heat flux anomalies (latent+sensible+longwave+shortwave) determined from NCEP/NCAR reanalysis (Kalnay et al. 1996). Brown and orange hatchings represent the domain considered in Desbruyeres et al. (2013) and Marsh et al. (2008), respectively. The domain considered by Grist et al. (2010) is confined between the two zonal sections depicted in blue.*

Hence, the full understanding of heat content variability in the North-Atlantic and its linkages with large-scale atmospheric variability remains unclear and needs further investigation, which is the aim of the present chapter. Using the weather regime framework, the following questions are addressed:

i) Are surface heat fluxes only related to NAO$^-$/NAO$^+$? Or are they also related to AR and/or BLK? If so, in which specific region?

ii) How do the weather regimes modify the heat convergence and heat transport? What are the impacts of the large-scale atmospheric variability (NAO and EAP) on the heat convergence into the subpolar gyre?

iii) Considering a different decomposition of the North-Atlantic, is the heat content variability dominated by anomalous heat convergence, as suggested by Marsh et al. (2008), Grist et al. (2010) and Desbruyeres et al. (2013)? Or do surface heat fluxes contribute significantly?

These questions are addressed using a series of global, ocean only numerical experiments sharing the same platform. Heat budget calculations are performed within closed domains in the North-Atlantic/Nordic Seas regions, using the "Physical Analysis of Gridded Ocean data" (hereafter,

PAGO) set of programs, described in Deshayes et al. (2012)[1]. The consideration of several models enables to determine whether the results are robust against the resolution (vertical and horizontal), the forcing dataset or the model parameterizations (restoring of the sea-surface salinity for instance), which all impact the mean state and the variability of the ocean circulation.

The chapter is organised as follows. In section 5.2, the four models used in this study are described, and the closed domains in which the heat budget calculations are performed are introduced. A brief description of PAGO is also provided. In section 5.3, the models are compared with observations. In section 5.4, the linkages between the weather regimes and the winter averaged surface heat fluxes, heat convergence and heat transport are assessed through correlation analysis. In section 5.5, the interannual to decadal variability of ocean heat content is analysed. Conclusions are given in section 6.6.

## 5.2 Methodology

### 5.2.1 Model description

The model experiments used in the present study are listed in table 5.1. They are issued from the Drakkar Project[2] and share the "Nucleus for European Modelling of the Ocean" (NEMO) modelling framework (Madec 2008).

| Name | Drakkar nomenclature | Period considered | Forcings | Horizontal resolution | Vertical levels | Salinity restoring | Reference |
|------|----------------------|-------------------|----------|----------------------|-----------------|--------------------|-----------|
| LR1 | ORCA025.L46-G70 | 1964-2004 | DFS3 | 1/4° | 46 | 0.167 | Treguier et al. (2007) |
| LR2 | ORCA025.L75-G85 | 1964-2007 | DFS4.3 | 1/4° | 75 | 0.027 | Lique and Steele (2013) |
| LR3 | ORCA025.L75-GRD88 | 1964-2010 | DFS4.4 | 1/4° | 75 | 0.167 | |
| HR | ORCA12.L46-MJM88 | 1964-2009 | DFS4.4 | 1/12° | 46 | 0.167 | Deshayes et al. (2013) |

*Table 5.1: List of model experiments used in this study. The horizontal resolution is valid at the equator and decreases with increasing latitude (same is true for the model used in chapter 4).*

The "Low-Resolution 1" experiment (LR1 hereafter) has for a long time been considered as Drakkar reference historical experiment. As such, it has been used in a large number of publications (Treguier et al. 2007; Lique et al. 2010; Desbruyeres et al. 2013 among others). It uses the DFS3 forcing set, introduced by Brodeau et al. (2010) and constructed from the ERA-40 reanalysis (Uppala et al. 2005).

---

[1]see also `http://www.whoi.edu/science/PO/pago/index.html`)
[2]`http://www.drakkar-ocean.eu/`

The "Low-Resolution 2" (LR2) experiment has been described in Lique and Steele (2013). The major differences between LR1 and LR2 are the vertical resolution (75 levels instead of 46), the forcing dataset (DFS4.3 instead of DFS3, Brodeau et al. 2010) and the salinity restoring (six times weaker in LR2 than in LR1).

The "Low-Resolution 3" (LR3) experiment is the same as LR2 save for salinity restoring (identical to LR1) and for atmospheric forcings. LR3 uses a blend of the DFS4.3 forcings (until 1988) and of the ERA-Interim (Dee et al., 2011) forcings after 1988.

The "High Resolution" (HR hereafter) experiment has the same vertical resolution as LR1 and uses the same forcings as LR3, but has a horizontal resolution of 1/12°. Details on the HR configuration can be found in Deshayes et al. (2013).

In the LR experiments, heat transports are computed using the monthly means of velocity and temperature. These monthly transports are then averaged over the year or over winter (December to March, hereafter DJFM). In the HR experiment, yearly and DJFM averages of heat transports are computed using the 5-day averages of heat transports, hence taking into-account more carefully the non-linearity of heat transport than in the LR runs.

## 5.2.2 Domains and sections definition

In this study, the North-Atlantic is divided into three closed domains (figure 5.2). The western subpolar gyre (hereafter west) is limited in the northwest by a section across the Hudson strait (HUD) and by a section across the Davis strait (BAF). Its western limit is defined by the Denmark Strait section (DSO) in the north, and by a section that goes from Iceland to 52.5°N-35.5°W (hereafter P) following the Reykjanes/Mid-Atlantic Ridge (MAR). The section that links P and Newfoundland (section 42W) closes the domain in the south. This domain encompasses the Labrador Sea and the Irminger Basin, where the variance of surface forcings is sufficiently strong to impact ocean heat content (figure 5.1).

The eastern subpolar gyre has a volume approximately 1.8 times smaller than the western subpolar gyre and is limited in the northeast by the Iceland-Faroe (IFO) and Faroe-Scotland (FSO) sections, in the west by the MAR section and in the south by a zonal section that goes from P to Ireland (section 42E). The southern limits of both subpolar domains (sections 42E and 42W) are somehow

arbitrary, as they do not rely on any physical criteria. However, these sections are located sufficiently north to avoid the recirculation of the subtropical gyre.

The last domain covers the Nordic Seas and has a volume approximately 1.4 times smaller than the western subpolar gyre. It is limited in the south-west by the DSO, IFO and FSO sections, in the south-east by a section extending across the North Sea (MDN), in the north by a section across Fram Strait (NON) and a section across the Barents Sea (BAR). This domain links the Arctic Ocean to the North-Atlantic.

For each model and in each domain, the volume is conserved, ensuring that the domains have been successfully closed (there are no water leakages). The sections are positively oriented in the direction of the warm Atlantic water, except for DSO and 42W that are oriented in the direction of the East-Greenland Current and of the Labrador Current, respectively.
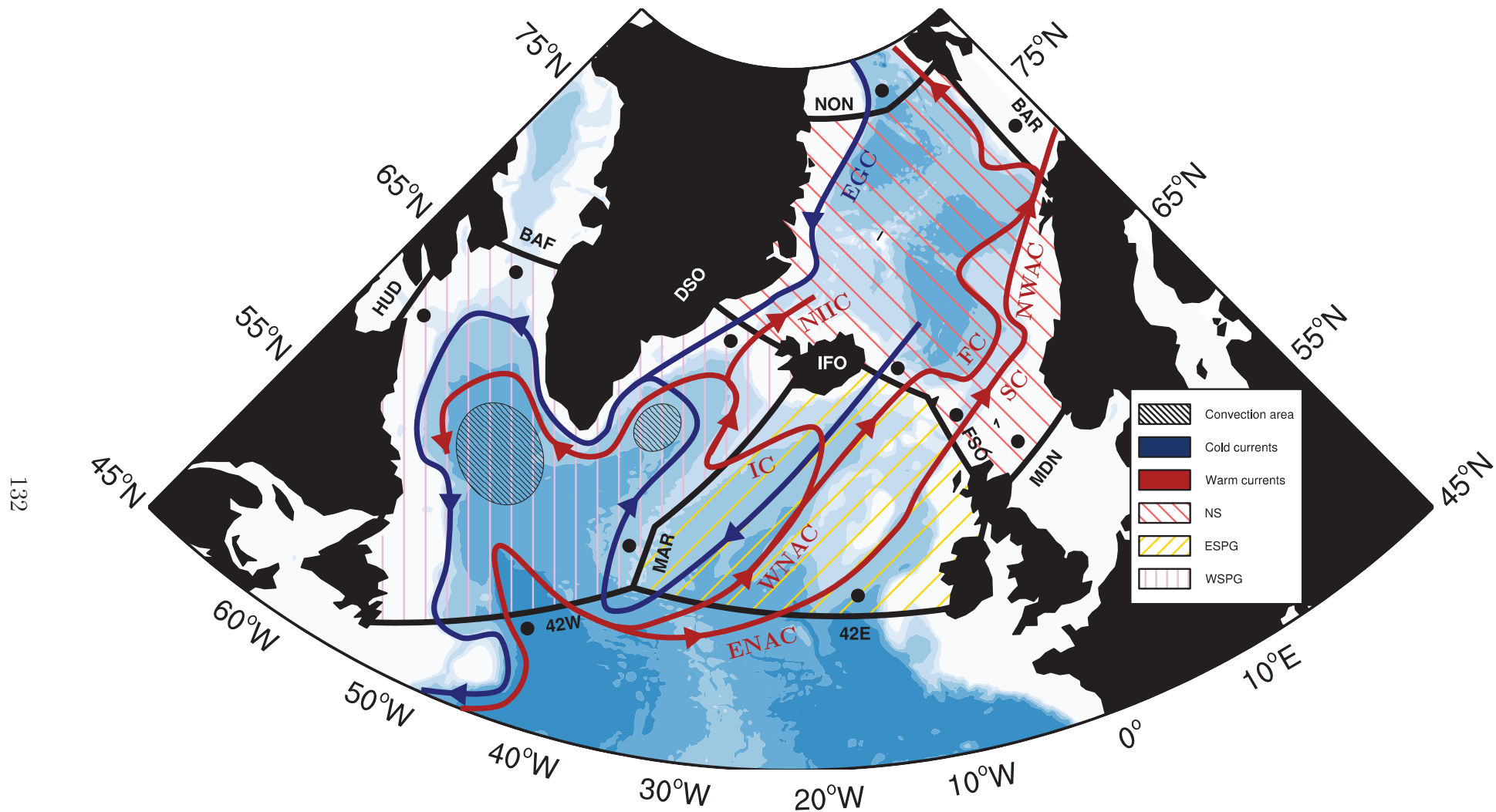
*Figure 5.2: Domains and sections discussed in the present study. Black points indicate the orientation of the sections (transport is counted positive toward the point). Map background shows the 0.5, 1, 2, 3, 4 and 5 km isobaths of the GEBCO bathymetry. NS=Nordic Seas, ESPG=Eastern Subpolar Gyre, WSPG=Western Subpolar Gyre, EGC=East Greenland Current, ENAC=Eastern North-Atlantic Current, WNAC=Western North-Atlantic Current, FC=Faroe Current, SC=Shetland Current, NWAC=Norwegian Atlantic Current, NIIC=North Irminger Icelandic Current, IC=Irminger Current. Adapted from Mercier et al. 2013 and Hansen and Østerhus 2000)*

### 5.2.3 Heat budgets using PAGO

Heat content variability in the three domains of figure 5.2 is investigated using the PAGO suite of programs of Deshayes et al. (2012). It permits inter-comparison of model outputs along predefined sections with limited interpolation. The functioning of PAGO for Arakawa C grids (i.e. tracer fields at the center of the cell, zonal speed at the left and right faces, meridional speed at the bottom and top faces) is depicted in figure 5.3. PAGO connects two section endpoints as a continuous sequence of grid faces, following a great circle pathway between the two points. This implies that speed along the section does not undergo any interpolation, contrary to tracer fields that are interpolated at the center of the grid faces using a second order centered scheme.
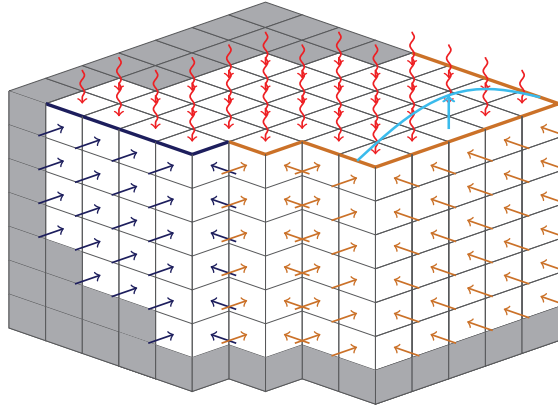


*Figure 5.3: Schematic describing the functioning of PAGO. Each cube represents a temperature grid point. Gray points represent land cells. Red arrows represent surface heat fluxes, centered on the cells. Sections (resp. transport across the sections) are represented by blue/orange lines (resp. blue/orange arrows). A cyan blue line symbolises the ocean free surface.*

Heat content ($h_c$) changes within the volume $V$ are given by:

$$\frac{\partial h_c}{\partial t} = \underbrace{\iint\limits_{S_a} Q_{net} \; dx \; dy}_{SF} + \underbrace{\rho_0 C_p \oiint\limits_{S_o} [UT_{int}] \; dl \; dz}_{OC} + \varepsilon \tag{5.1}$$

with $\rho_0$ and $C_p$ the reference density and heat capacity of sea-water, respectively, $S_a$ the surface of the ocean that is in contact with the atmosphere and $S_o$ the surface that closes the volume $V$. $x$ is the longitude, $y$ is the latitude, $z$ the depth and $l$ the length coordinate along the closed contour of $S_o$. $Q_{net}$ is the net (latent, sensible, shortwave and longwave) surface heat flux (at the center of the grid cells, red arrows in figure 2) and $[UT_{int}]$ represents the ocean heat transport (with $U$ the normal velocity and $T_{int}$ the temperature interpolated at the center of the grid face). The first term

on the right-hand side of equation 5.1 represents the contribution of surface fluxes (hereafter SF) to changes in ocean heat content, while the second term represents the contribution of ocean heat convergence (hereafter OC). The last term, $\varepsilon$, represents the residual.

When heat content is integrated from the surface to a fixed level (section 5.3.2), the residual includes vertical exchanges, which are especially strong in convective regions. When the heat content is integrated from the surface to the bottom (section 5.5), $\varepsilon$ is limited to the exchanges through diffusive isopycnal mixing across the opened boundaries of the domain. In the LR experiments, where heat transport is computed from monthly means, it might also contain numerical errors, although Desbruyeres et al. (2013) suggest that they do not contribute much to the residual.

The term on the left hand side of equation 5.1 can further be decomposed into:

$$\frac{\partial h_c}{\partial t} = \rho_0 C_p \frac{\partial}{\partial t} \left[ \iiint\limits_{V} T \, dx \, dy \, dz + \iint\limits_{S_a} SST \, \eta \, dx \, dy \right] \tag{5.2}$$

with $T$ the temperature at the center of the cells (i.e. not interpolated), $SST$ the sea-surface temperature and $\eta$ the sea-surface height.

We have verified that the residual term is weak in the LR experiment by applying the same methodology as Desbruyeres et al. (2013): heat content has been averaged over the December-January pairs of each year in order to determine the heat content change between January, $1^{st}$ and December, $31^{st}$ of each year. The time series of $\varepsilon$ is determined as the difference between this heat content change and the yearly averages of OC and SF.

The residual term is weak in comparison with OC and SF, and its standard deviation is much smaller (figure 5.4). Hence, this residual is not likely to dominate changes in ocean heat content. Accordingly, it will be neglected in the following and heat content changes will be assumed to be only influenced by surface heat fluxes SF and ocean convergence OC.
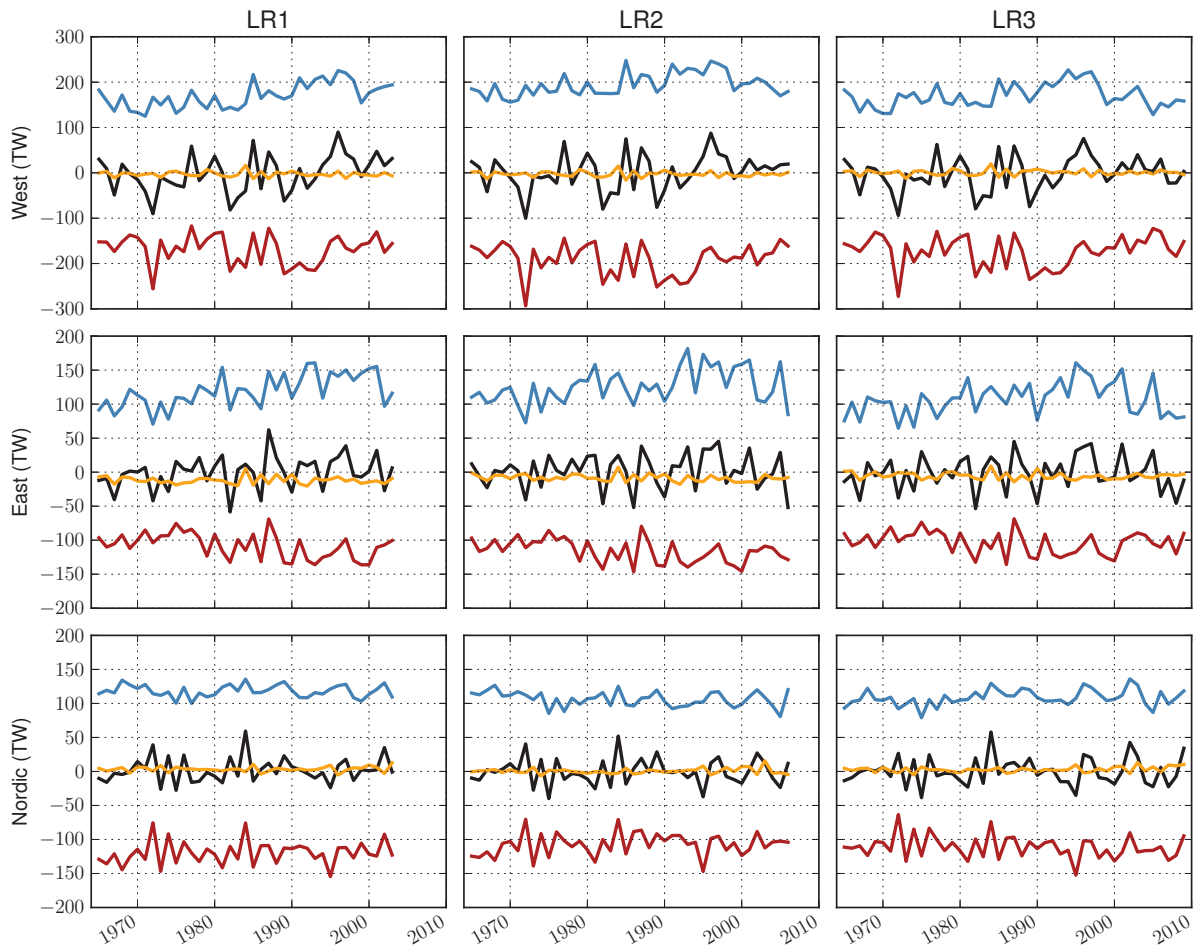
*Figure 5.4: Variations in heat content within a year (black line) and yearly averaged OC (blue), SF (brown) and residual (orange).*

## 5.3 Comparison with observations

In this section, modelled and observation-based estimates of heat transport and heat content are compared.

### 5.3.1 Heat transports

At 46°N, the LR models compares reasonably well with the observation-based (inverse calculation) estimates of Ganachaud and Wunsch 2003 (table 5.2). The HR experiment, on the other hand, has a heat transport that is more than 200 TW higher than observations. At 56°N and across the Greenland-Iceland-Scotland section, however, all the models compare well with the observed estimates of Lumpkin and Speer (2007).

135

| Section | Year(s) | LR1 | LR2 | LR3 | HR | Observations | Reference |
|---|---|---|---|---|---|---|---|
| Net, 46°N | 1993 | 648 | 673 | 617 | 853 | 600 | Ganachaud and Wunsch (2003) |
| Net, 56°N | 1992 | 533 | 512 | 497 | 571 | 540 | Lumpkin and Speer (2007) |
| Net, IFO+FSO+DSO | 1995 | 256 | 223 | 233 | 276 | 290 | Lumpkin and Speer (2007) |
| AW (S>35, $\theta$>5°C), FSO | 1999-2001 | 173 | 156 | 189 | 156 | 156 | Østerhus et al. (2005) |
| AW (S>35, $\theta$>5°C), IFO | 1999-2001 | 61 | 57 | 61 | 92 | 134 | Østerhus et al. (2005) |
| AW ($\theta$>1°C) through NON | 2001-2006 | 39 | 36 | 38 | 64 | $\approx 40$ | Schauer et al. (2008) |
| Net, BAR | 1997-2007 | 83 | 66 | 82 | 108 (58) | (50) | Smedsrud et al. (2010) |

*Table 5.2: Modelled and observed heat transports (units: TW=$10^{12}$W). The years at which the transports have been averaged is indicated. In the last line, values in brackets indicate the heat transport of AW as defined by Smedsrud et al. (2010). Section names refer to figure 5.2.*

The Atlantic Water (AW) inflow across IFO and FSO is defined following Aksenov et al. 2010 (S>35, $\theta$>5°C). AW heat transport across FSO compares well with observations in LR2 and HR but is overestimated in LR1 and LR3. In the LR experiments, heat transport across IFO is underestimated by approximately 80 TW, while in the HR experiment it is underestimated by only 40 TW. This is presumably due to a too zonal North-Atlantic Current in the LR experiments.

The mean heat transport of AW to the Arctic Ocean ($\theta$>1°C, Schauer et al. 2008) through Fram Strait (NON section) is close to observations in the LR runs, while it is overestimated in HR.

Smedsrud et al. (2010) define the AW that flows through BAR as water for which S>35 psu and $\theta$>3°C. Using this criteria, the heat transport of AW through BAR in the HR run compares well with observations. However, in the LR runs, the salinity at BAR is less than 35 psu; hence this criteria cannot be used and the net heat transport is presented instead in table 5.2. The reasons for this fresh bias in the LR experiments is beyond the scope of the present study.

## 5.3.2   0-700 m heat content anomalies

Modelled and observed heat content in the top 700 $m$ of the water column are compared in figure 5.5. Observation-based (objective analysis) estimates are extracted from the "World Ocean Atlas 2009" (WOA09, Locarnini et al. 2010), the EN3 dataset (Ingleby and Huddleston 2007) and from the "Analysis, Reconstruction, Indices of the Variability of the Ocean" (ARIVO, described in von Schuckmann et al. (2009) but extended to 2011).

In the western subpolar gyre, modelled heat content closely follows the WOA09 observations, except for the negative trend between 1966 to 1976 that is underestimated in HR, presumably reflecting an incomplete spin-up of the HR run. The strong warming of 1995 is especially well captured by all the simulations

In the eastern subpolar gyre, heat content variability apparently shows less low frequency variability than in the western part of the gyre. The increase of heat content in 1995, which occurs concomitantly in the western subpolar gyre, is well represented in all the models. The decrease of 2006 is stronger in the models than in the observations.

In the Nordic Seas, the agreement is not so good. Ocean heat content in the LR experiments shows a good agreement with the observations until the mid 90s, when the two time series start diverging. HR heat content variability only shows a good agreement with the observations between 1980 and 1995. Between 1997 and 2004, observed heat content shows a very strong increase which is not captured by the models. Between 2002 and 2004, heat content in WOA09 shows a strong warming ($+2\ ZJ$), which is not visible in the other observation datasets. Hence, this peak is, in all likelihood, spurious.
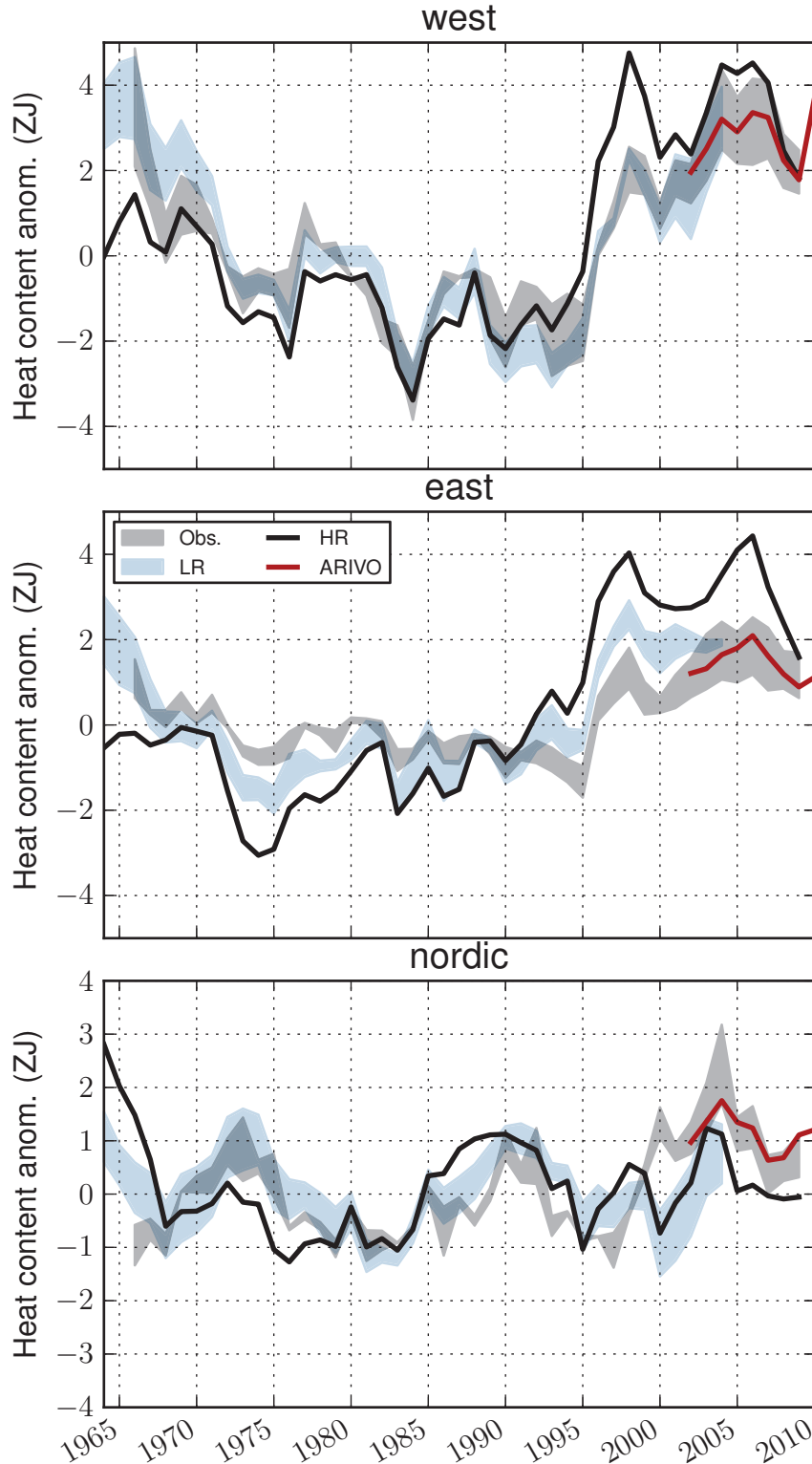
*Figure 5.5: Observed and modelled heat content anomalies over the first $0 - 700m$ of the water column. The gray shading represents the enveloppe between heat content anomalies of the EN3 and of the WOA09 datasets. The blue shading represents the enveloppe between the heat content anomalies of the LR experiments, while the black line represents the HR heat content anomalies. In all these time-series, the anomalies are computed by removing the 1966-2004 mean. The brown line represents the ARIVO heat content anomalies computed by removing the 2002-2009 average and by adding the 2002-2009 average of WOA09/EN3. ZJ=$10^{21}$ J*

# 5.4   Variability of winter heat transport and heat fluxes

In this section, the linkages between the weather regimes and the sources of heat into each domain are assessed through correlation analysis. The correlations are performed between winter (December through March, hereafter DJFM) regime occurrences and winter averaged SF, OC (defined in equation 5.1), net heat and mass transports across the individual sections. This methodology is retained because, as discussed in the introduction, wind-driven circulation changes have been proposed to explain changes in ocean heat content, and it is during winter that the variance of wind forcings is more likely to impact the ocean circulation. Moreover, the linkages between wind forcings and weather regimes are more robust in winter than in the other seasons (see Cassou et al. 2011; Minvielle et al. 2011)
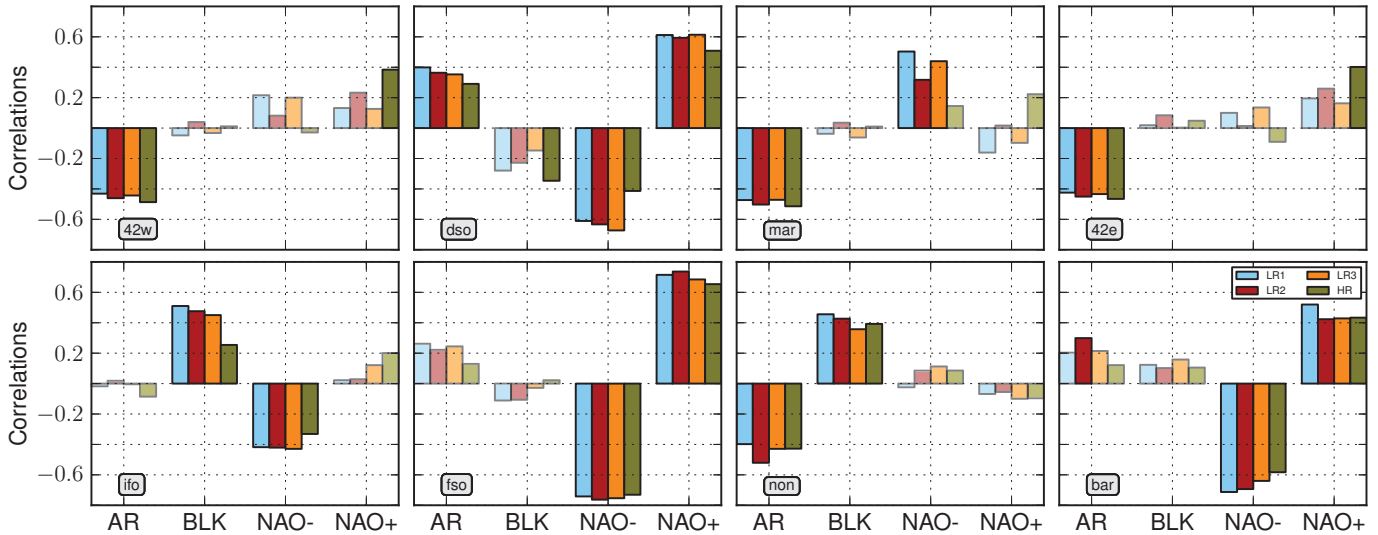


*Figure 5.6: 0-lag correlations between the winter regime occurrences and the winter averaged net volume transport across the individual sections. Non-significant correlations (t-test at 95%) are shadowed.*
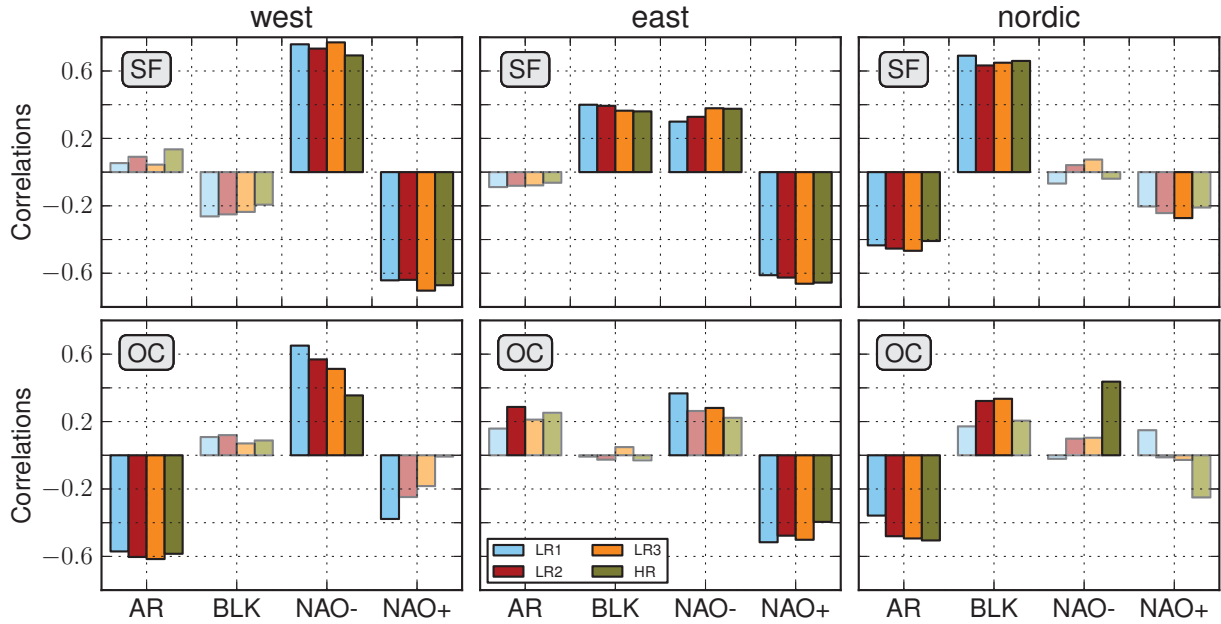
*Figure 5.7: 0-lag correlations between the winter regime occurrences and the winter averaged SF (top) or OC (bottom) in each domain. Non-significant correlations (t-test at 95%) are shadowed.*
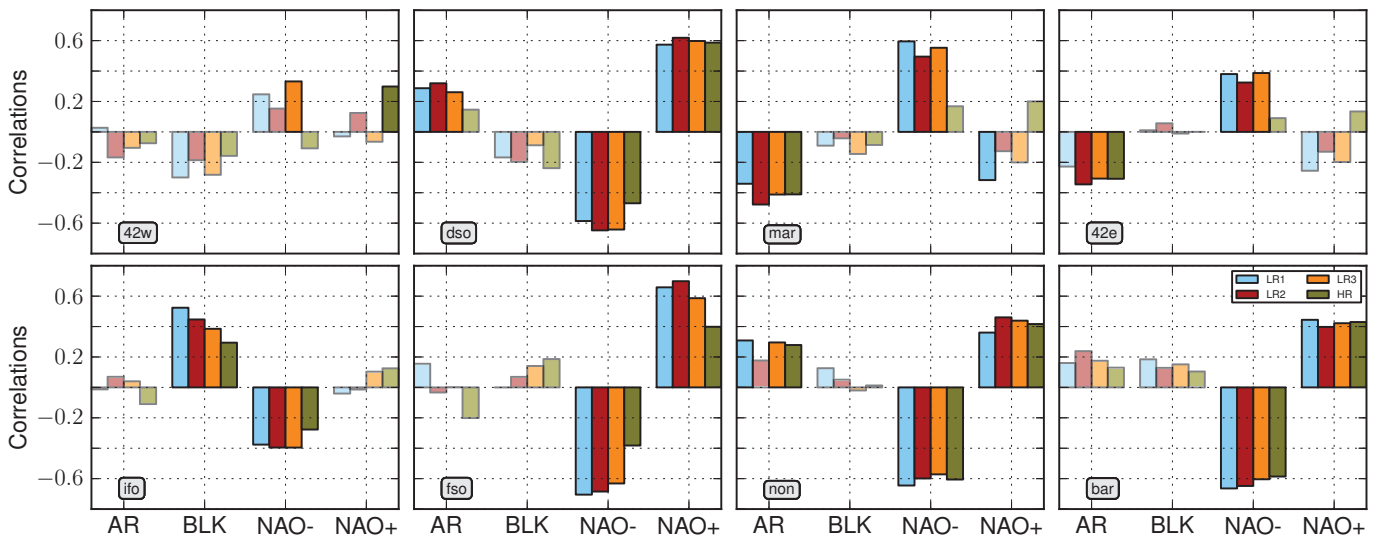


*Figure 5.8: Same as figure 5.8 but for net heat transport.*

## 5.4.1 Impacts of the AR regime

AR is characterised by warm air-temperature anomalies in the subpolar gyre and cold anomalies in the Nordic Seas (figure 2.7). AR is also associated with anticyclonic wind-anomalies off Europe, which have been shown to reduce the strength of the subtropical and subpolar gyres (Hakkinen et al., 2011a; Langehaug et al., 2012; Ruprich-Robert and Cassou, 2013; Barrier et al., 2012, 2013). According to

Hakkinen et al. (2011a), during the early 2000s, greater than average AR winter occurrences induced a reduction of the subpolar gyre, which was accompanied by a westward shift of the subpolar front (Hátún et al. 2005). As a consequence, a greater proportion of subtropical water invaded the subpolar gyre, causing a warming of the northern North-Atlantic.

Our results confirm the reduction of the subpolar gyre associated with AR (cf. the negative correlations between AR winter occurrences and the mass transport across 42E, MAR and 42W, figure 5.6). However, this reduction is not associated with an increased heat convergence in the subpolar gyre, as proposed by Hakkinen et al. (2011a), but with a decreased heat convergence in the western subpolar gyre (5.7). This contradiction likely indicates that the reduction of the subpolar gyre associated with AR does not facilitate the intrusion of subtropical water into the subpolar gyre.

The mass transport across 42W is negatively correlated with AR occurrences, but not the heat transport. This reflects the compensation between a decreased advection of temperature ($u'\overline{T}$, where primes indicate anomalies and bars indicate means) and the increased advection of temperature anomalies ($\overline{u}T'$).

AR winter occurrences are negatively correlated with SF and OC in the Nordic Seas figure 5.7). The negative correlation with OC, however, is hard to explain from the heat transports across the individual sections (IFO, FSO, DSO, NON or BAR, cf. figure 5.8). This highlights the non-linear character of correlation coefficients ($\mathrm{Corr}[X + Y, Z] \neq \mathrm{Corr}[X, Z] + \mathrm{Corr}[Y, Z]$).

## 5.4.2 Impacts of the BLK regime

BLK is characterised by anticyclonic anomalies over Europe, which prevent the midlatitude westerlies to penetrate inland. Instead, the winds are tilted northward toward the Nordic Seas. This specific wind-pattern has been shown to impact the exchanges between the Atlantic Ocean and the Nordic Seas. Using transport observations, Richter et al. (2012) suggest that the mass transport across IFO is driven by the meridional gradient of Sea-Surface Height (SSH) across the Greenland-Scotland-Ridge: negative SSH anomalies in the Nordic Seas induce an increased mass transport (see also Hansen et al. 2010). They also suggest that SSH anomalies in the Nordic-Seas are positively correlated with the variations of the Scandinavian Pattern (SCAN, of which BLK can be viewed as the positive phase). From their results, one would expect a negative correlation between the mass transport across IFO

and the SCAN index. They indeed find a negative correlation, but which is weak and therefore not significant (see the table 2 of Richter et al. 2012). Using a control run of the coupled Bergen Climate Model, Medhaug et al. (2011) argue that variations in the SCAN pattern (as defined in Richter et al. 2012) induce a two-time response (one fast and one slower) of water mass exchanges across the Greenland Scotland Ridge. First, across-ridge wind anomalies give rise to along ridge Ekman transport anomalies, inducing negative SSH anomalies in the western Nordic Seas and positive anomalies in the eastern Nordic Seas, causing a northward mass transport anomaly (figure 5.9). Second, consistently with Richter et al. (2012), they suggest that SCAN also induces an increased SSH in the Nordic Seas that leads, through barotropic adjustment, to a southward mass and heat transport anomaly across the Greenland-Scotland Ridge after one year (see the figure 14 of Medhaug et al. 2011). But using an ocean only model, Nilsen et al. (2003) came to an opposite conclusion. Regressing the net mass transport across IFO and the sea-level pressure anomalies, they obtain a pattern that is characterised by negative anomalies over Greenland and weakly positive anomalies over Europe (cf. their figure 4b). This pattern closely resembles the SCAN, hence associated with increased mass transport.
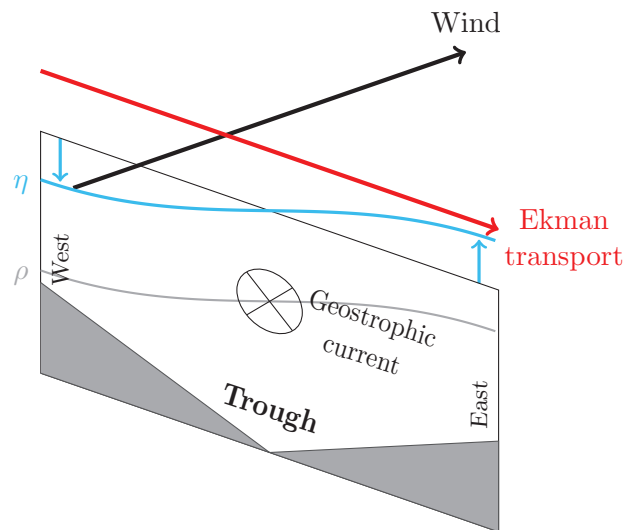


*Figure 5.9: Ekman driven response of the water mass exchange between the Atlantic and the Nordic Seas to BLK wind anomalies. The black arrow represents the wind anomalies associated with BLK and the red arrow the corresponding Ekman transport. The blue line represents the sea-surface height and the gray line an isopycnal. The geostrophic current is directed northward ($\otimes$ symbol).*

The correlations in tables 5.8 and 5.6 suggest that BLK is associated with increased northward heat and mass transport across IFO, consistent with Nilsen et al. (2003). This is, however, inconsis-

tent with the barotropic adjustment proposed by Richter et al. (2012) and Medhaug et al. (2011). It thus corroborates the hypothesis of the Ekman-driven mechanism depicted in figure 5.9. BLK winter occurrences are also positively correlated with the net volume transport across the NON section but not with the associated heat transport, for reasons that remain unexplained. From figures 5.6, 5.7 and 5.8, one can notice that BLK has rather a local impact, limited to the Nordic Seas.

Moreover, BLK is associated with positive SF in the Nordic Seas, and to a lesser extent, the eastern subpolar gyre (figure 5.7). No significant correlation is obtained between SF in the western subpolar gyre and BLK occurrences. This suggests that in the western subpolar gyre, SF variations are dominated by the NAO regimes, as already proposed by Cayan (1992b).

## 5.4.3 Impacts of the NAO⁻ regime

The NAO⁻ regime is characterised by a reduction of the prevailing midlatitude westerlies and Trade winds in the subtropics. The associated cyclonic wind-stress curl anomalies are located at the boundary between the subpolar and the subtropical gyres, which induce cyclonic horizontal circulation anomalies (the intergyre-gyre, Marshall et al. 2001; Barrier et al. 2013). According to Herbaut and Houssais (2009), this intergyre-gyre will advect warm/salty water northwestward in the east and cold/fresh water southeastward in the west (cf. figure 5.10).
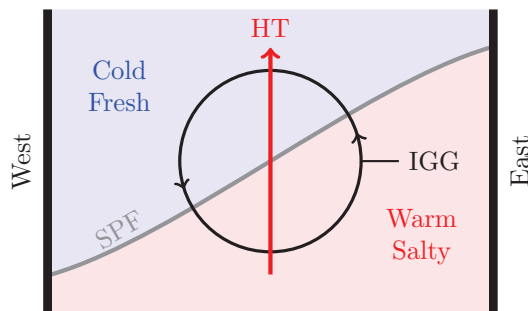


*Figure 5.10: Schematic of a cyclonic intergyre gyre (IGG) associated driven by NAO⁻ (black circle). The gray line represents the subpolar front (SPF). The thick red line represents the overall heat transport (HT).*

In all the model experiments, significant correlations between NAO⁻ occurrences and OC in the western subpolar gyre are obtained (figure 5.7). These correlations are mostly due to increased westward heat transport across MAR (figure 5.8), consistently with Herbaut and Houssais (2009). Note, however, that this correlation is not significant in the HR experiment. In 1996, HR heat

transport through MAR shows a strong negative anomaly, which is absent in the LR runs (figure 5.11). If year 1996 is removed prior to computing the correlations, the latter increase from 0.17 to 0.36 and become significant. This strong negative anomaly is compensated by a concomitant heat transport anomaly across 42W, hence having barely no effect on HC.

The increased heat transport across MAR associated with NAO⁻ is accompanied by an increased northward heat transport across DSO by the North-Icelandic Irminger Current (NIIC, figure 5.2). Indeed, the southward component of heat transport across DSO shows no correlations with NAO⁻ winter occurrences, contrary to its northward component which shows positive ones. On the contrary, the northward heat transport into the Nordic Seas (through IFO by the Faroe Current and FSO by the Shetland Current, figure 5.2) and out of the Nordic Seas (into the Barents Sea through BAR and into the Arctic Ocean through NON) is reduced (figure 5.8).

NAO⁻ is also associated with a reduced heat loss in the western subpolar gyre and, to a lesser extent, the eastern subpolar gyre (figure 5.7).
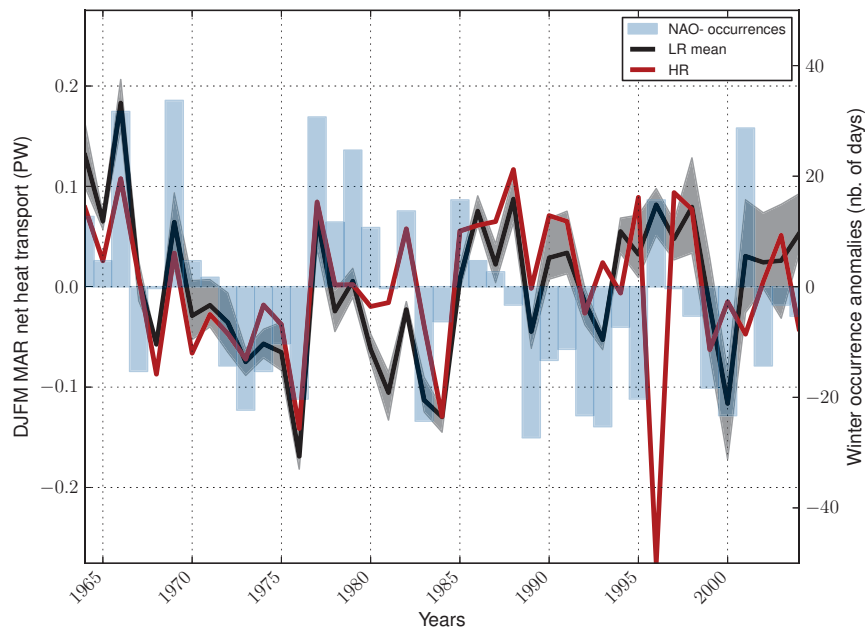


*Figure 5.11: DJFM averaged net heat transport across MAR. Gray shading encompasses the minimum and maximum values among the LR experiments. Blue bars show the NAO⁻ occurrences anomalies.*

## 5.4.4   Impacts of the NAO$^+$ regime

The atmospheric forcings associated with NAO$^+$ are, to first order, opposite to those associated with NAO$^-$ (figure 2.7). However, the midlatitude negative wind-stress curl anomalies are located further south than their NAO$^-$ counterpart. This asymmetry of wind-anomalies between the two NAO regimes has been shown to be paramount to understand the ocean response induced by the NAO (Barrier et al., 2013). This asymmetry is also important to understand the linkages between ice export through Fram Strait and the NAO (Hilmer and Jung 2000).

NAO$^+$ winter occurrences are associated with a decreased OC into the eastern subpolar gyre (figure 5.7), presumably due to increased heat export toward the Nordic Seas through FSO (figure 5.8). This is consistent with Flatau et al. (2003), who suggest that under NAO$^+$ conditions, the North-Atlantic Current has an eastward trajectory. This is also consistent with Blindheim et al. (2000) and Orvik et al. (2001), who used observations to infer that a larger proportion of NAC water enters the Nordic Seas during positive NAO conditions. Heat export out of the Nordic Seas across NON and BAR are also increased under NAO$^+$ conditions, presumably reflecting the close linkages between the heat transport through FSO and the heat transports through NON (correlations at 0 lag, ranging from 0.4 in HR to 0.8 in LR1) and, to a lesser extent, BAR (correlations at 0 lag, 0.4 in the LR experiments and 0.2 in HR). The volume transport across Fram Strait (section NON), however, shows no correlations: greater than normal NAO$^+$ winter occurrences lead to increased northward transport of warm water and increased southward transport of cold water, resulting in a small net volume transport but a northward heat transport anomaly.

NAO$^+$ is also associated with southward volume and heat transport anomalies across DSO, contrary to the NAO$^-$ that is associated with northward transport anomalies. With NAO$^+$, the anomalies are due to both a strengthening of the East-Greenland Current (EGC) and a reduction of the transport by the NIIC: indeed, the southward component shows positive correlation with the NAO$^+$ winter occurrences, while its northward component shows negative correlations, hence giving a net southward transport anomaly. This is slightly different from the response of heat and mass transport across this same section to changes in NAO$^-$ winter occurrences.

The winter occurrences of NAO$^+$ are also negatively correlated with SF in the western and eastern subpolar gyres. However, the correlations show similar amplitudes between the western and eastern

subpolar gyre (more than 0.6), contrary to the correlations with the NAO$^-$. Hence, SF associated with the NAO$^+$ extend further east than for NAO$^-$, as could have been inferred from air-temperature anomaly composites (figure 2.7).

## 5.4.5 Summary

The correlations discussed in the present section are summarised in figure 5.12. The major conclusions are:

- AR drives, as suggested by Hakkinen et al. (2011a) and Barrier et al. (2012, 2013), a reduction of the gyre circulation, which is associated with a reduction ocean heat convergence (OC) into the western subpolar gyre. This reduction is inconsistent with Hakkinen et al. (2011a). Increased OC into the western subpolar gyre is associated with greater than average NAO$^-$ winter occurrences and presumably reflects its associated cyclonic intergyre-gyre (Marshall et al. 2001; Barrier et al. 2013), consistently with Herbaut and Houssais (2009).

- Surface heat fluxes (SF) in the subpolar gyre are closely related to the NAO$^-$/NAO$^+$ regimes. However, in the Nordic Seas, SF variability is driven by changes in BLK winter occurrences and, to a lesser extent, AR ones.

- NAO$^+$ in the eastern subpolar gyre, NAO$^-$ in the western subpolar gyre and AR in the Nordic Seas are associated with OC and SF anomalies that share the same signs, hence both contributing in the same way to changes in ocean heat content.
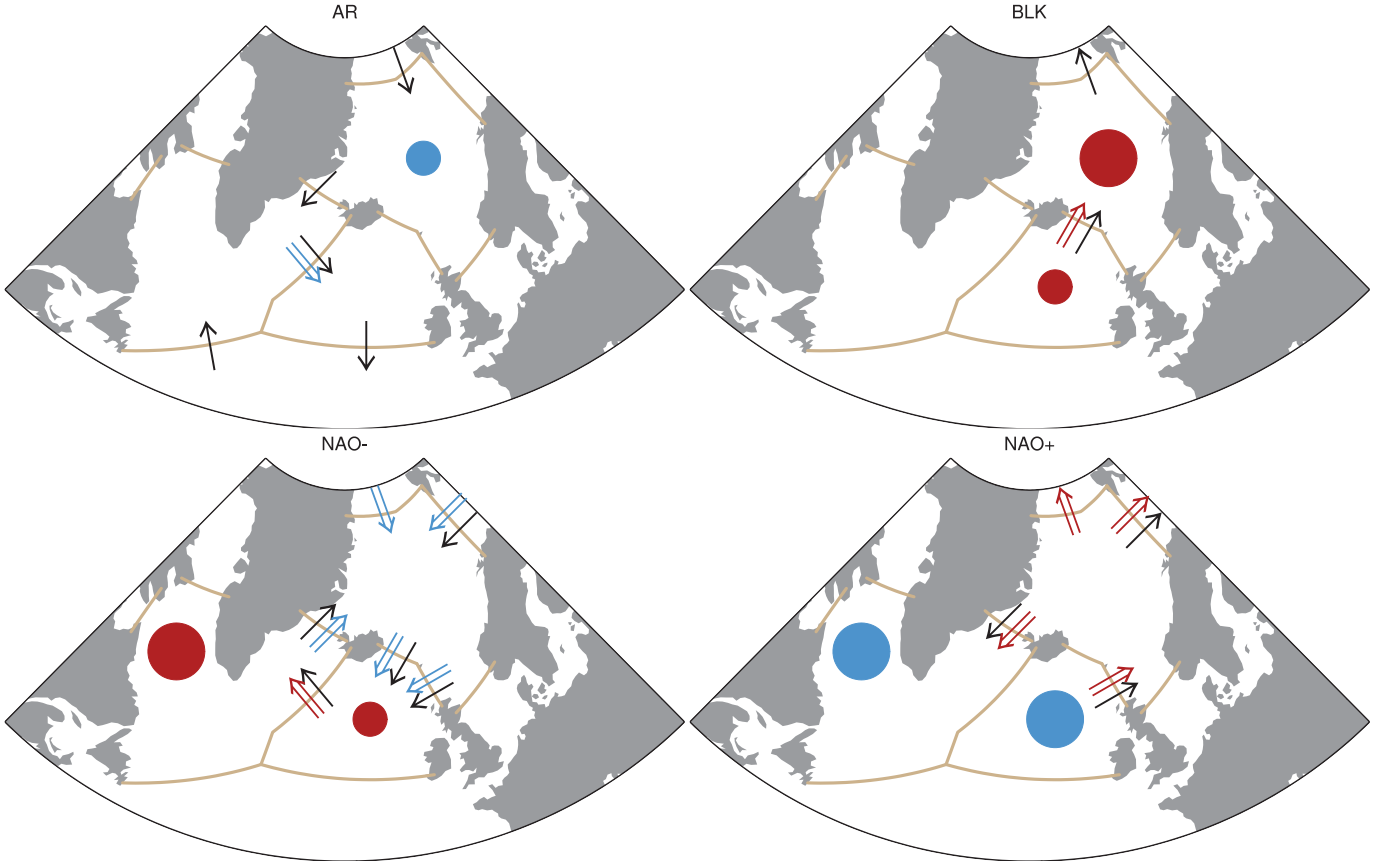
*Figure 5.12: Summary of the 0-lag correlations between winter regime occurrences, SF (filled circles), net heat (coloured arrows) and mass (black arrows) transports. Blue=negative correlations. Red=positive correlations.*

## 5.5 Heat content variability

This section is dedicated to the understanding of interannual to decadal variability of top-to-bottom ocean heat content in the three domains shown in figure 5.2 (contrary to section 5.3.2, in which heat content over the top 700 $m$ has been considered). The temporal integration of equation 5.1 between time $t$ and a reference time, $t_0$, gives:

$$\int_{t_0}^{t} \frac{\partial h_c}{\partial t} = h_c(t) - h_c(t_0) = \underbrace{\int_{t_0}^{t} SF(\lambda)\,d\lambda}_{TSF} + \underbrace{\int_{t_0}^{t} OC(\lambda)\,d\lambda}_{TOC} + \int_{t_0}^{t} \varepsilon(\lambda)d\lambda \tag{5.3}$$

As shown in section 5.2.3, the residual term has a weaker variance than the total heat input. Accordingly, it is expected to have less impact on ocean heat content variability. Hence, it is neglected

in the following and ocean heat content anomalies are approximated by:

$$h_{c_{approx}}(t) - h_{c_{approx}}(t_0) = TSF + TOC \tag{5.4}$$

where TOC stands for "Time-integrated Heat Convergence" and TSF for "Time-integrated surface flux". To lay emphasis on the interannual to decadal variability, yearly (January to December) averages of OC and SF are considered. In the following, heat content anomalies refer to $h_{c_{approx}}(t) - h_{c_{approx}}(t_0)$, where $t_0 = 1964$, which is the first available year in each model experiment (table 5.1).

## 5.5.1 Western subpolar gyre

Heat content anomalies in the western subpolar gyre are consistent among the four experiments (figure 5.13), although HR shows weaker anomalies than the LR experiments. TSF and THC, on the contrary, show strong differences between the LR experiments and HR, which are due to the linear trends in SF and OC as modelled by HR (the time-integration of a linear function returns a quadratic function). The removing of these trends before the time integration returns time series that compare well with the LR experiments (thin green line, figure 5.13), suggesting that the variability in HR, despite the trends, is consistent with the variability in the LR runs.
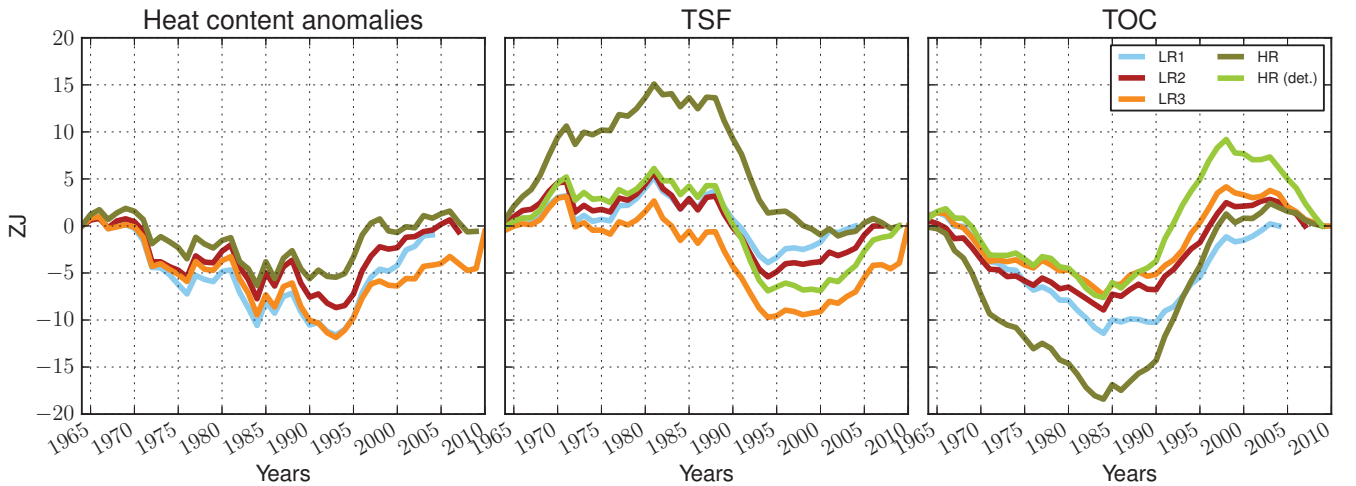


*Figure 5.13: Heat content anomalies, TSF and TOC in the western subpolar gyre. ZJ=Zetta Joule ($10^{21}$ J).*
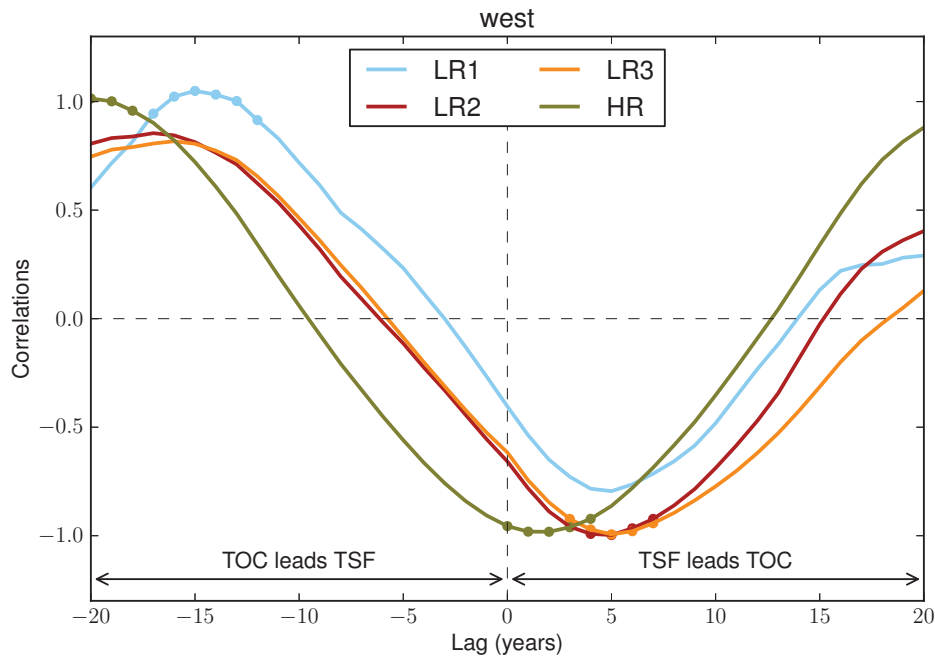
*Figure 5.14: Lead-lag correlations between TSF and TOC in the western subpolar gyre (TSF leads at positive lags).*

From 1964 to 1984, the negative trend in ocean heat content is dominated by the negative trend in TOC. However, in the early 70s and 80s, when convection was strong (Yashayaev 2007), the decrease in TSF contributed to cool the western subpolar gyre. From 1988 to 1994, the decrease in ocean heat content is dominated by the strong decrease of TSF (approximately 10 $ZJ$), that is due to anomalously strong deep convection in this period (Straneo 2006; Lazier et al. 2002; Pickart and Spall 2007). This period is characterised by very strong NAO[+]/BLK conditions that both favor convection in the Labrador Sea (Barrier et al. 2013). As suggested by Cuny et al. (2001) and Straneo (2006), TOC shows a positive trend from 1990 to 1998 (i.e. 3 to 5 years after the decrease of TSF, figure 5.14) in order to compensate this strong heat loss to the atmosphere. This positive trend originates from the MAR section, hence suggesting an increase heat transport by the Irminger Current consistent with Cuny et al. (2001) and Straneo (2006). Warm and salty water is advected by the cyclonic circulation of the subpolar gyre and reaches the East Greenland Current (EGC, figure 5.2). Eddy-induced lateral homogenisation and strong lateral exchange transports the properties of the boundary current toward the interior basin.
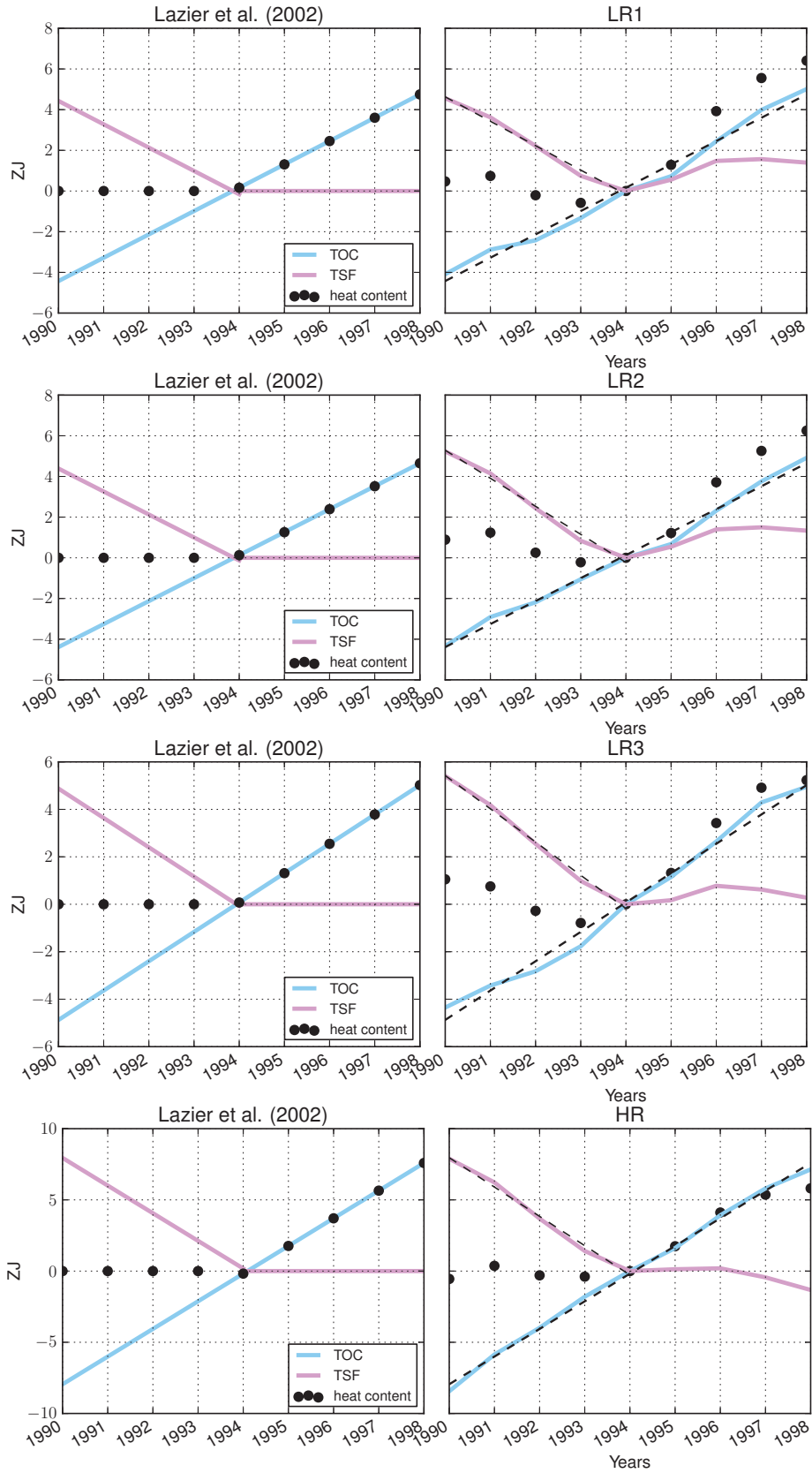
Figure 5.15: (Left) Time series that would be expected according to Lazier et al. (2002). (Right) Time series of figure 5.13 vertically centered around 1994. Dashed lines show the trends used on the left panel.

From 1990 to 1994, TSF and TOC compensate each other, stabilising the ocean heat content at its lowest value. But in 1994, when the strong convection in the Labrador Sea comes to an end, TSF no longer compensates THC, leading to an increase in ocean heat content. This is consistent with the results of Lazier et al. (2002), who used CTD data to assess the variability of the Labrador-Sea between 1990 and 2000. They suggest that the simplest model to explain the variability of mixed-layer temperature in the Labrador Sea in this period is to consider a constant and positive heat convergence in the Labrador Sea (hence a linear time-integrated heat convergence, figure 5.15, blue curve on the left panel). In the presence of deep convection, the positive heat convergence is balanced by heat loss to the atmosphere (purple curve in the left panel of figure 5.15). And when the convection ends, the heat loss to the atmosphere is zero and does not compensate heat convergence anymore, leading to an increased heat content.

Many authors argue that the warming of the subpolar gyre of 1995 was due to a change in large-scale atmospheric variability, and especially to the abrupt switch in the NAO from highly positive in 1995 to highly negative in 1996. They suggest that this sudden change in the NAO induced a wind-driven reduction of the subpolar gyre that facilitated the intrusion of warm and saline subtropical water into the subpolar gyre (Hátún et al. 2005; Bersch 2002; Bersch et al. 2007; Sarafanov et al. 2008; Lozier et al. 2008; Chaudhuri et al. 2011 among others). However, between 1964 and 1980, negative NAO conditions prevail while positive NAO conditions dominate the atmospheric variability afterward. Hence, one would expect an increase in TOC and in ocean heat content in the former period, and a decrease afterward, which is contradictory with figures 5.5 and 5.13.

To understand this apparent contradiction, one must remember that, as suggested in section 5.4, it is SF and OC that are modulated by changes in large-scale atmospheric circulation. But heat content anomalies are the results of their time-integration. Accordingly, to highlight the linkages between heat content anomalies and large scale atmospheric conditions, one need to temporally integrate the atmospheric signal. Using the weather regime framework, this is achieved as follows. Let $x$ be the winter occurrences of one weather regime, for example NAO$^+$. The winter occurrence anomalies are defined as:

$$m = x - \overline{x} \tag{5.5}$$

The temporal integration is then achieved by a cumulated sum of $m$ over the entire period:

$$wi(t) = \sum_{p=1}^{t} m(p) \tag{5.6}$$

where $wi$ is the integrated NAO$^+$ occurrences and $t$ the time in years. $m$ and $wi$ are depicted in figure 5.16 for each regime.
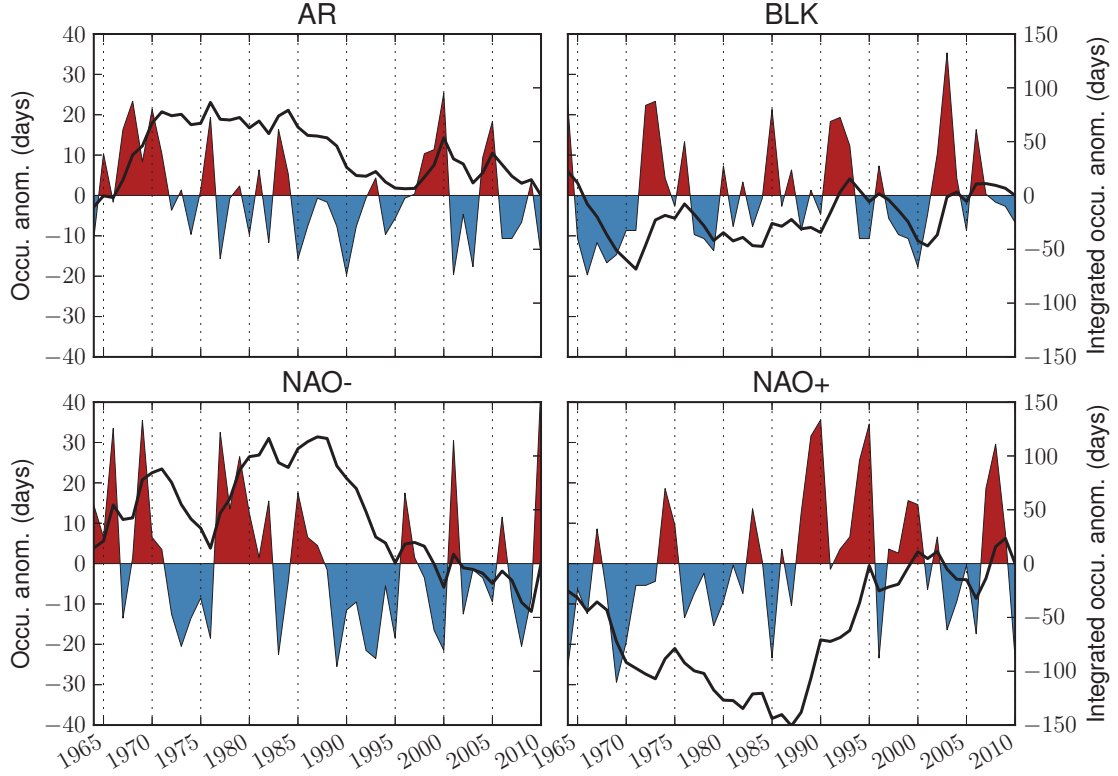


*Figure 5.16: Winter occurrences anomalies (m, filled plot) and time-integrated winter occurrences (wi, thick black line) for the period 1964-2010*

The time-integrated BLK and AR occurrences show less amplitude than their NAO$^+$/NAO$^-$ counterpart. This highlights the decadal variability of the NAO during the study period, with mostly negative NAO$^-$ in the first half, and mostly NAO$^+$ in the second half of the period.

The integrated NAO$^+$ occurrence (thick line of bottom right panel in figure 5.16) is now compared with heat content anomalies in the western subpolar gyre (figure 5.17). Heat content anomalies closely follow the integrated NAO$^+$ with a 6-year lag (figure 5.17), which is presumably due to the different timescales of response of TSF and TOC to changes in the integrated NAO$^+$ occurrences. TSF is negatively correlated with this index at lag 0, while TOC is positively correlated at lag 3 years (NAO$^+$ dominates).
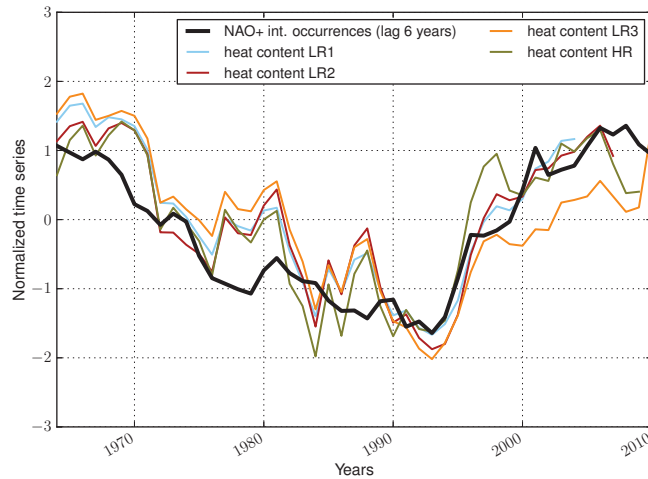
*Figure 5.17: Normalised cumulated sum of NAO+ winter occurrence anomalies (black lines) and modelled heat content anomalies (coloured lines). The lag of the occurrence time series is indicated in the legend.*

### 5.5.2 Eastern subpolar gyre

Heat content anomalies in the eastern subpolar gyre shows twice as less amplitude than TSF and THC (-4/4 ZJ versus -8/8 ZJ, figure 5.18). In all the model experiments, TSF increases from 1964 to 1980 and decreases afterward. TOC shows a similar behaviour, save for reversed signs.
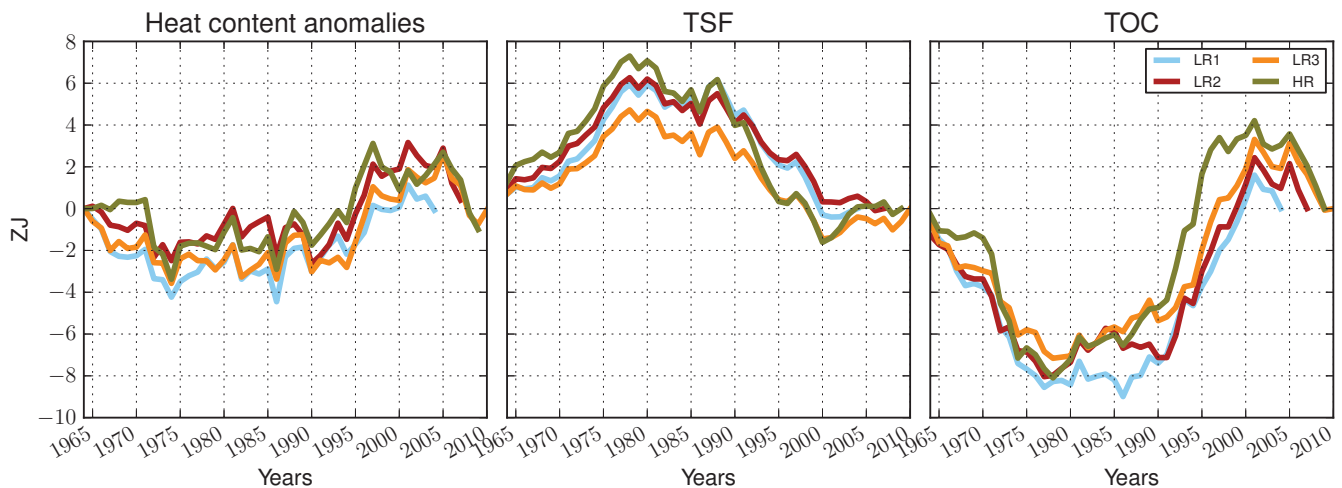


*Figure 5.18: Heat content anomalies, TSF and TOC in the eastern subpolar gyre. ZJ=Zetta Joule $(10^{21}$ J).*

Lead-lag correlations between TSF and TOC are significant at lags −3 to 1 (TSF dominates at positive lag, figure 5.19). Hence, consistent with Desbruyeres et al. (2013), TSF acts as a damper of the TOC contribution to heat content anomalies.

Two dramatic changes in ocean heat content are visible in figure 5.18 (left panel). Between 1994
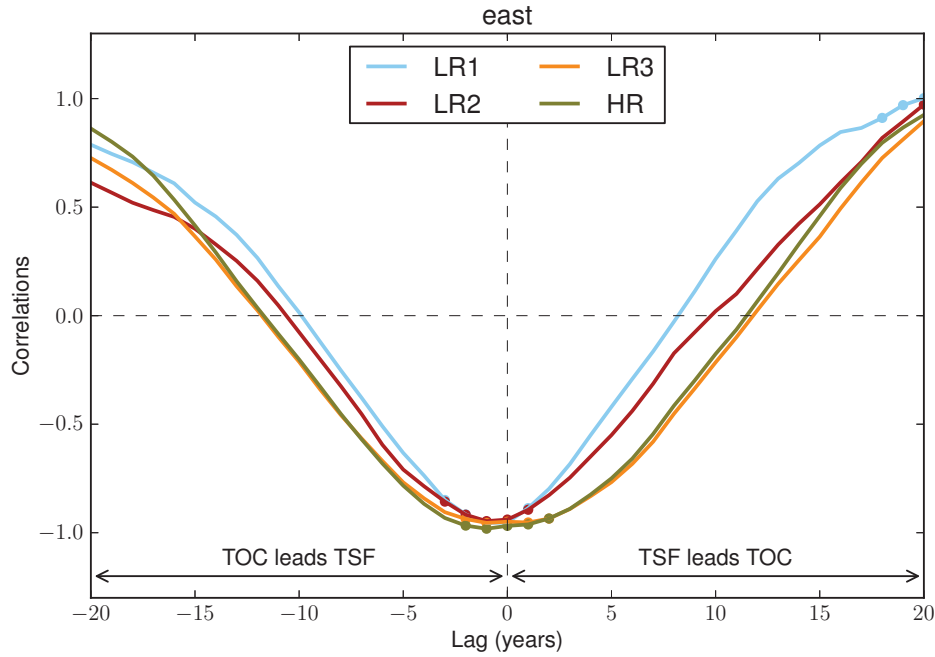
*Figure 5.19: Lead-lag correlations between TSF and TOC in the eastern subpolar gyre (TSF leads at positive lags).*

and 1997, ocean heat content increases by 4 $ZJ$ in LR2, LR3, HR and 2 $ZJ$ in LR1. Then, ocean heat content anomalies stabilise at higher means, before suddenly decreasing in 2005. The longest experiment, LR3, suggests that this cooling ends in 2009.

To determine the causes of the 1994 increase, the variations of OC and SF (equation 5.1) are analysed. Between 1994 and 1995, OC shows a dramatic increase (50 to 65 TW approximately, figure 5.20), causing a similar increase in the net heat input. Between 1995 and 1997, heat convergence either shows a slight (in the LR runs) or a sharp (in HR) decrease, which is however compensated by an increase in SF of similar amplitude. Hence, the total heat input remains high in this period.

The decomposition of heat convergence in the eastern subpolar gyre suggests that the increase in OC is mostly due to an increase in the net heat transport across 42E (40 to 50 TW, figure 5.21). In LR2 and LR3, less heat is exported through MAR, while in the HR run, less heat is exported through FSO (20 TW). These contributions to the change in heat convergence are significant, although dominated by the heat import through 42E.

As discussed above, the strong warming of subpolar gyre of 1994 has often been linked to the change in the NAO conditions, from positive in 1995 to negative in 1996 (figure 5.22). This is consistent with the negative correlations between OC in the eastern subpolar gyre and NAO[+] occurrences
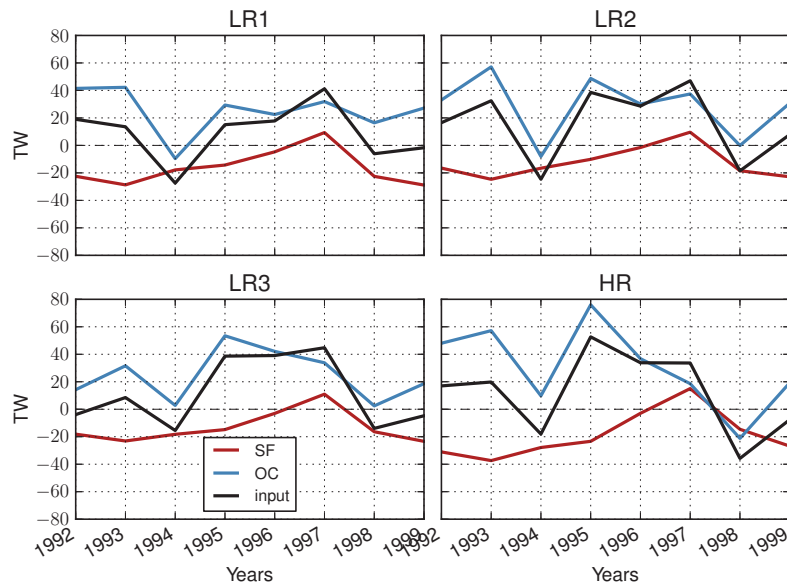
*Figure 5.20: Time series of surface heat flux, ocean heat convergence and heat input anomalies (TW) in the Eastern subpolar gyre*
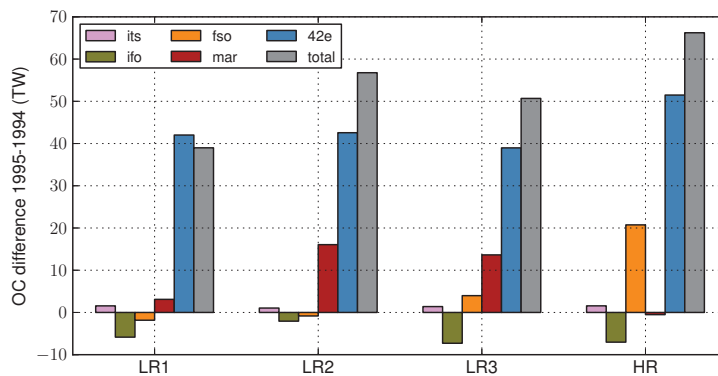


*Figure 5.21: Yearly net heat transport difference (1995 minus 1994). Positive values contribute to warm the eastern subpolar gyre.*

(figure 5.7) and with the positive correlations between heat transport across 42E and NAO$^-$ occurrences (only for the LR experiments, however, figure 5.8). But the abrupt change in OC precedes the change of NAO by one year. This mismatch is due to the averaging of HC from January to December, while winter occurrences are summed over DJFM. The strongest increase in HC occur in November and December 1995, thus contributing to the yearly increase of 1995. But the change in monthly NAO$^+$ occurrences of December 1995 contributed to the change in winter NAO$^+$ occurrences of 1996, accounting for the apparent one year lag between the two.

As suggested in section 5.5.1, the increase in heat convergence of 1995 might also be a delayed response of the strong NAO$^+$/BLK events of 1988-1995. To test this hypothesis, correlations between the heat content anomalies computed over the entire western subpolare gyre (figure 5.13, left panel),
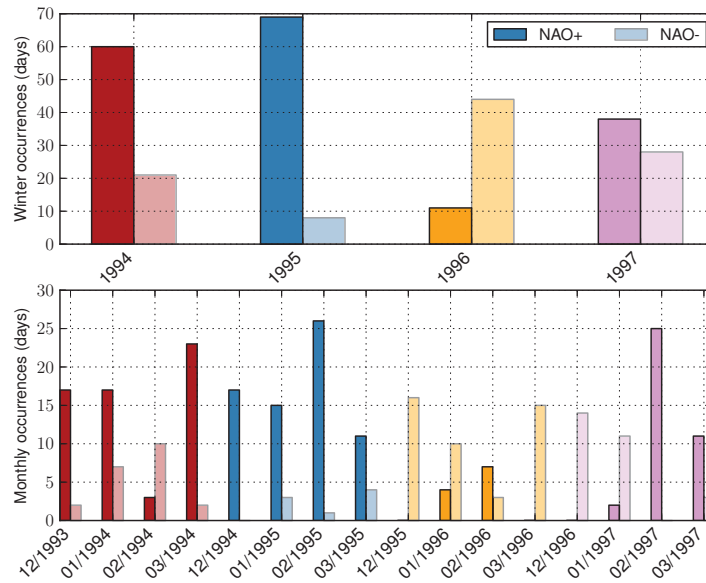
*Figure 5.22: Winter (top) and monthly (bottom) occurrences of $NAO^+$ and $NAO^-$.*
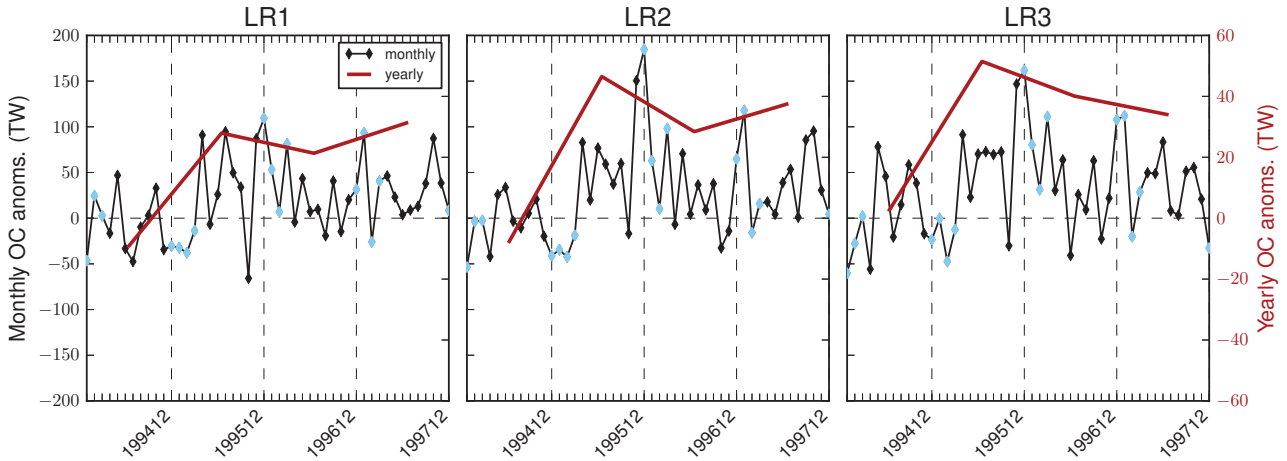


*Figure 5.23: Monthly (black, seasonal cycle removed) and yearly (brown) ocean heat convergence anomalies in the Eastern subpolar gyre. Blue points highlight DJFM months in the monthly time-series.*

which has been shown to be a delayed response to the integrated NAO, and heat content at each grid point, have been computed (figure 5.24). The strong correlations ($>0.8$) are limited to the western subpolar gyre in all the models, although it is less clear in the HR experiment. Hence, the 1995 warming of the eastern subpolar gyre might not be due to the delayed response to the time-integration of $NAO^+$ forcings but more likely is a consequence of the abrupt changes in $NAO^+$ forcings.
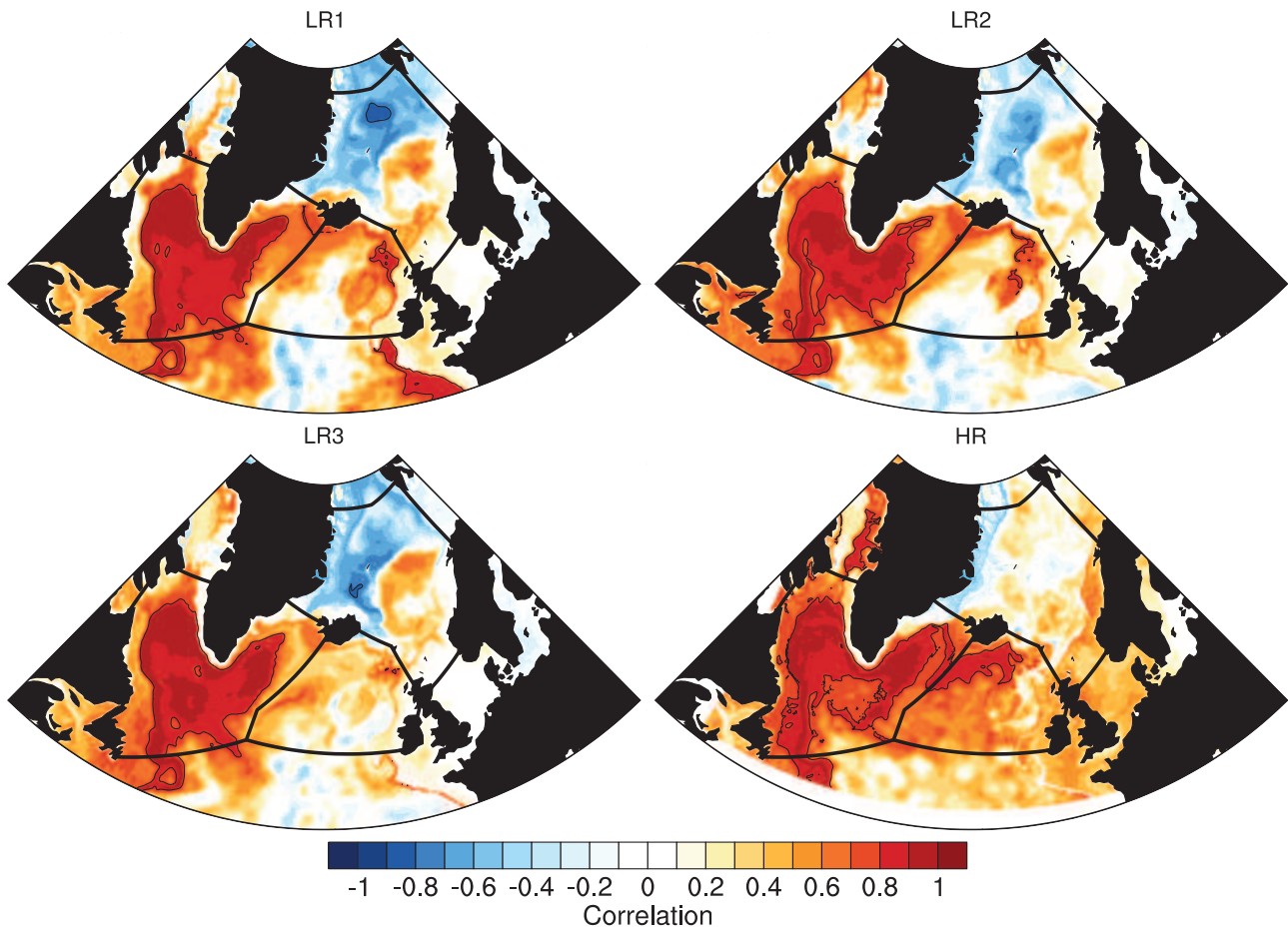
*Figure 5.24: Correlation map between heat content anomalies at each grid point and heat content anomalies in the western subpolar gyre (figure 5.13, left panel). Black contour lines represent the −0.8/ + 0.8 contours.*

### 5.5.3 Nordic Seas

In the Nordic Seas, heat content anomalies among the model experiments share some common features (figure 5.25). However, the time series of TSF and TOC are not the least comparable among the different experiments. The warming of 1983-1989, which is reproduced in all the experiments, is mostly due to TOC in HR, while in LR2 it is mostly due to TSF. In LR2 and LR3, both components contribute to this warming. The only conclusion that can be drawn from figure 5.25 is that the interannual variability of ocean heat content is dominated by TSF, while THC modulates this variability at longer time-scales. However, the strong discrepancies in THC among the different model runs prevent to draw any conclusion on the reasons for HC variability. This highlights the difficulty to correctly model the Nordic Seas (Drange et al. 2005).
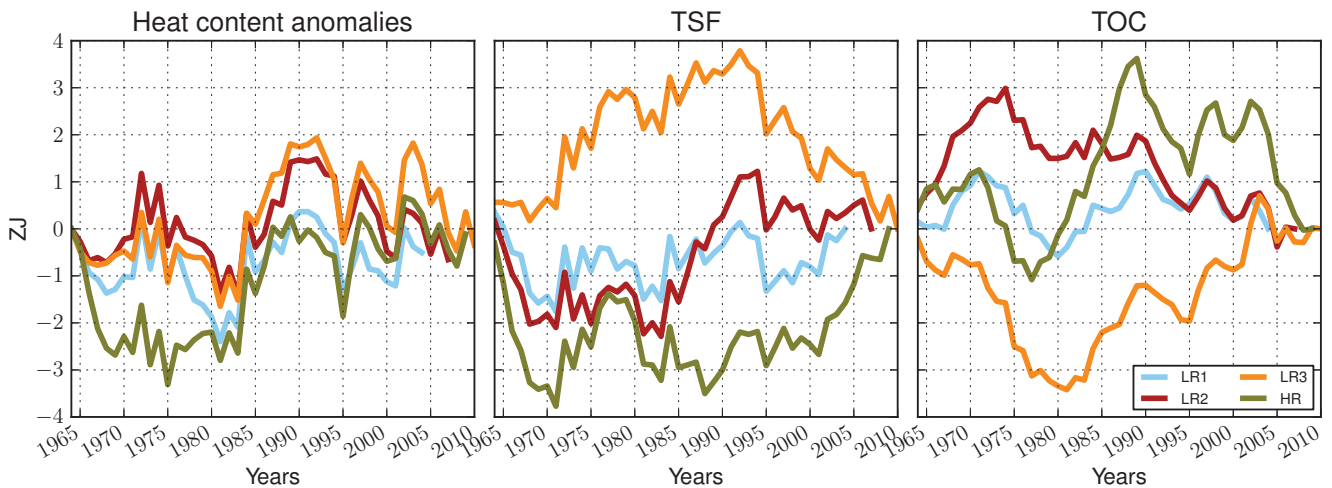


*Figure 5.25: Heat content anomalies and anomalous heat input, heat fluxes and heat convergence in the Nordic Seas.*

## 5.6 Conclusion

In the present chapter, heat budget calculations in the subpolar gyre and the Nordic Seas have been performed using four global ocean only models. The variability of winter averaged sources of heat (surface heat flux, heat convergence and heat transport) has been first linked to the variability of winter regime occurrences through correlation analysis. Consistent with Cayan (1992a), heat flux variability in the subpolar gyre is related to variations in NAO$^-$ and NAO$^+$ occurrences. As a signature of NAO asymmetry, the eastern subpolar is more impacted by NAO$^+$ than by NAO$^-$.

Heat flux variability in the Nordic Seas is dominated by changes in BLK occurrences and, to a lesser extent, AR occurrences.

Our results suggest that NAO$^-$ is associated with increased heat convergence in the western subpolar gyre, driven due to an increased westward heat transport across the Mid-Atlantic Ridge by the intergyre-gyre (Marshall et al. 2001; Barrier et al. 2013), as suggested by Herbaut and Houssais (2009). Similarly with Hakkinen et al. (2011a), AR is associated with a weakened subpolar gyre. However, this reduction induces a reduced heat convergence into the western subpolar gyre. Hence, the reduction of the subpolar gyre associated with AR unlikely facilitates the intrusion of subtropical water into the subpolar gyre, as proposed by Hakkinen et al. (2011a).

Yearly average ocean heat convergence and surface heat flux in each domain have then been temporally integrated, in order to analyse the variability in ocean heat content. The western and eastern subpolar gyres significantly warmed in 1995. This warming has often been attributed to an abrupt change in the NAO index between 1995 and 1996. We propose that this might be true in the eastern subpolar gyre. However, using a time-series of time-integrated NAO$^+$ occurrences, we suggest that the concomitant warming of the western subpolar gyre might be the delayed response (by approximately 6 years) to the integrated NAO$^+$ forcings. In the Nordic-Seas, the strong discrepancies among the model experiments prevent to draw any affirmative conclusions. However, the interannual variability of ocean heat content seems dominated by surface heat fluxes, while ocean heat convergence seems to modulate heat content anomalies at lower frequencies.
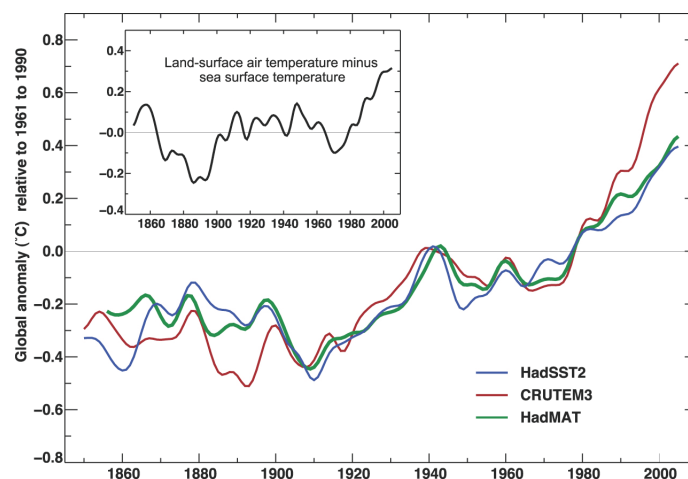


*Figure 5.26: Annual anomalies of global averaged SST (blue curve) and land-surface air-temperature (red curve). Source: Trenberth et al. (2007)*

Global average sea-surface temperature and land-surface temperature observations show sharp

upward trend in the 1979-2005 period (figure 5.26). To determine this global warming trend has some impact on the heat budget calculations performed here, the trends in the surface heat fluxes have been computed in each domain and for each model experiment. In each model, the surface heat flux in the western subpolar gyre shows positive trend. However, this trend is robust only in the LR3 run. In the two other domains, the trends are never significant. Furthermore, the signs are inconsistent: in the eastern subpolar gyre, the trends are negative in LR1 and LR2 but positive in LR3 and HR. In the Nordic Seas, the trends are positive in LR1 and HR but negative in LR2 and LR3. Hence, we suggest that in the second half of the 20th century (from 1979 onward), the sharp increase in global warming (figure 5.26) is unlikely to impact much the surface heat flux in any of the regions studied here.

| Modele | West | East | Nordic |
|--------|------|------|--------|
| LR1 | 0.38 | -0.24 | 0.13 |
| LR2 | 0.86 | -0.01 | -0.21 |
| LR3 | **1.72** | 0.35 | -0.32 |
| HR | 0.02 | 0.43 | 0.57 |

*Table 5.3: Trend in yearly surface heat flux (TW/year) computed from 1979 onward. Significant trend at the 95% level of confidence are shown in bold.*

# Chapter 6

# Conclusion and discussions

## Contents

## 6.1   Summary

The literature concerning the impacts of the atmospheric forcings on the variability of the ocean circulation in the North-Atlantic, which is a key region for the Earth climate system, is abundant. In most of these studies, the concept of modes of variability (Barnston and Livezey 1987) is used in order to reduce the atmospheric variability to a finite number of spatial patterns (fixed over time), to which are associated a specific time series. These modes of variability are traditionally determined by decomposing sea-level pressure anomalies into "Empirical Orthogonal Functions" (EOFs), which assume the orthogonality and the symmetry of these modes. The latter assumption, however, has been shown to be partly inadequate for the first mode of variability in the North-Atlantic/European domain, the North-Atlantic Oscillation (NAO, Hurrell 1995).

     The aim of the PhD was to use an alternative concept that allows to circumvent these limitations, the so-called weather regimes, in order to analyse the variability of the ocean circulation forced by

the atmosphere. The weather regimes are large-scale, recurrent and quasi-stationary atmospheric patterns, which have been shown to successfully capture the variability of surface forcing to the ocean (wind and air-temperature anomalies, Cassou et al. 2011; Minvielle et al. 2011). Since the variance of atmospheric forcing is greater in winter (December to January) than in the other seasons, hence the most likely to impact the ocean circulation, only the winter weather regimes are considered. These regimes are the Atlantic-Ridge (AR), the Scandinavian Blocking (BLK) and the two phases of the NAO (NAO$^+$ and NAO$^-$). AR is characterised by anticyclonic wind anomalies off Europe, warm air-temperature anomalies in the subpolar gyre and cold anomalies in the Nordic Seas. BLK is characterised by anticyclonic conditions over Europe that prevent the midlatitude westerlies from penetrating inland by tilting them northward toward the Nordic Seas. BLK is also associated with cold temperature anomalies in the Labrador Sea and warm anomalies in the Nordic Seas. NAO$^+$ is characterised by reinforced midlatitude westerlies and trade winds, cold temperature anomalies in the Labrador Sea and warm anomalies in the subtropics and the Nordic Seas (Cayan 1992b). NAO$^-$ surface forcing anomalies are, to first order, opposite to those associated with the NAO$^+$. However, wind stress curl anomalies associated with the NAO$^-$ are located 5°N further north than the anomalies associated with the NAO$^+$ and the air-temperature anomalies in the Labrador Sea extend further east with the NAO$^+$ than with the NAO$^-$.

The weather regime framework has been used to approximate the atmospheric variability in order to analyse the changes in ocean circulation in the North Atlantic driven by the atmosphere. The major findings are summarised hereafter.

### 6.1.1 Subtropical sea-surface height variability

As a first step, the variability of the subtropical gyre, assessed through observations of subtropical sea-surface height (SSH) anomalies (altimetry and tide-gauge data), has been linked to changes in weather regimes conditions. SSH anomalies are negatively correlated with AR winter occurrences, hence suggesting that AR drives a reduction of the subtropical gyre. Especially, the negative SSH anomalies of 1970 are likely due to the numerous AR days during this period. This contradicts the results of Ezer (1999) who attributed these negative anomalies to changes in the NAO. In our study, neither simultaneous nor lagged significant correlation has been found with the winter occurrences

of NAO$^+$ or NAO$^-$.

The use of a planetary geostrophic model confirms that the variability of subtropical SSH anomalies is mostly wind-driven, as suggested by Ezer (1999); Hong et al. (2000); Cabanes et al. (2006). Hence, the negative SSH anomalies under strong AR conditions are wind-driven and consistent with the gyre-mode of Hakkinen et al. (2011a), the sea-level pressure anomaly pattern of which projects fairly well onto the AR centroid.

Furthermore, sensitivity experiments confirm that most of the wind-driven interannual variability of the subtropical gyre is due to the winter wind-forcing, while the summer wind forcing only plays a minor role. This justifies the choice to only consider the winter weather regimes. These results are summarised in Barrier et al. (2012), published in *Climate Dynamics.*

## 6.1.2 Gyre circulation and overturning circulation

Using an ocean general circulation model forced by atmospheric reanalysis, the response of the gyres (subtropical and subpolar) and of the meridional overturning circulation to changes in regime conditions has been assessed. The fast (monthly to interannual timescales) response has been inferred using statistical analysis on a realistic model experiment and by using a simplified barotropic configuration of the model. At these timescales, AR induces a reduction of the gyres, consistent with Hakkinen et al. (2011a). NAO$^-$ drives a cyclonic gyre circulation anomaly centerred at 45°N, which resembles the intergyre-gyre of Marshall et al. (2001). NAO$^+$ gyre anomalies mirror those of NAO$^-$ but are southward shifted (centered at 40°N). The mechanism at stake is topographic Sverdrup balance. No fast adjustment of the gyres is obtained for the BLK regime. As for the gyres, only AR, NAO$^-$ and NAO$^+$ impact the overturning circulation at monthly to interannual time-scales via Ekman-driven surface flow compensated at depth by a return flow.

To analyse the slow (decadal timescales) adjustment of the circulation to persistent regime conditions, the model has been forced with idealised forcing conditions that are representative of one and only one regime. In these idealised experiments, the mechanical influence of wind forcing (in the momentum equation) has been separated from their influence on turbulent fluxes. The results of these idealised experiments suggest that AR induces a slackening of the gyres through baroclinic adjustment to wind-stress curl anomalies. Persistent BLK conditions are associated with a strength-

ening of the subpolar gyre, due to baroclinic adjustment of the gyre to increased heat loss in the Labrador Sea. During persistent NAO$^-$ conditions, gyre circulation shows cyclonic anomalies at 40°N, similar to the intergyre-gyre of Marshall et al. (2001). The northern subpolar gyre shows a weaker circulation due to reduced deep convection in the Labrador Sea. Moreover, a greater inflow of warm water of subtropical origin into the subpolar gyre provides a positive feedback for the slackening of the subpolar gyre. Under persistent NAO$^+$ conditions, the subtropical gyre is strengthened via baroclinic adjustment to wind-stress curl, while the subpolar gyre is strengthened via baroclinic adjustment to increased heat loss in the Labrador Sea. Persistent NAO$^-$ and AR conditions are also associated with a reduction of the large-scale overturning circulation, due to a reduction of deep water formation in the Labrador Sea. Opposite results are obtained for persistent NAO$^+$ and BLK conditions. These results are detailed in the *Journal of Physical Oceanography* (Barrier et al. 2013, in press).

### 6.1.3 Heat budget in the subpolar gyre and the Nordic Seas

Finally, heat budgets have been computed in the subpolar gyre and the Nordic Seas, following the same methodology as Marsh et al. (2008), Grist et al. (2010), Desbruyeres et al. (2013) or Lique and Steele (2013). A novelty, however, is that the Mid-Atlantic Ridge has been used as a separation border between the western and eastern subpolar gyres. Moreover, four numerical models have been considered, in order to assess the uncertainty of the results.

Linkages between the winter averaged sources of heat in each domain (surface heat flux and ocean heat convergence) and the weather regimes have been sought for using correlation analysis. Surface heat flux in the western and eastern parts of the subpolar gyre are strongly correlated with the winter occurrences of NAO$^+$ (negative correlations) and NAO$^-$ (positive correlations), consistent with Cayan (1992b). However, in the eastern subpolar gyre, the correlation is stronger with NAO$^+$ because of the eastward extension of air-temperature anomalies. Surface heat flux in the Nordic Seas shows strong positive correlation with BLK winter occurrences and significant positive correlations with the AR ones.

Contrary to the suggestion of Hakkinen et al. (2011a,b), winter averaged ocean heat convergence in the western subpolar gyre is negatively correlated with AR winter occurrences. Hence, the re-

duction of the gyre circulation associated with AR is unlikely to facilitate the intrusion of warm and salty subtropical water (as hypothesised by Hátún et al. 2005). Ocean heat convergence in the western subpolar gyre is positively correlated with NAO$^-$ occurrences: during NAO$^-$ conditions, the cyclonic intergyre-gyre transports warm water of subtropical origin northwestward toward the western subpolar gyre, consistently with Herbaut and Houssais (2009). Heat convergence in the eastern subpolar gyre is negatively correlated with NAO$^+$ occurrences, which reflects a greater heat export into the Nordic Seas through the Faroe-Shetland passage.

The variability of ocean heat content anomalies, issued from the integration over time of surface heat flux and ocean heat convergence anomalies, have been analysed for each domain. In the western subpolar gyre, ocean heat content decreases from 1964 to 1994 and increases afterward. The time-series of heat content anomalies in this domain closely resembles the time-integrated NAO$^+$ winter occurrences with a lag of approximately 6 years. Hence, the low frequency variability of heat content in the western subpolar gyre is likely reflecting the delayed response to the time-integrated NAO forcing. Especially, the warming of 1995 is presumably due to the strong NAO$^+$/BLK conditions of 1988-1995, during which dramatic heat loss to the atmosphere occurs, hence cooling the subpolar gyre. This increased heat loss is compensated after a 3 year lag by increased heat convergence, stabilising the heat content at its lower values. In 1994, when deep convection stops and the heat loss to the atmosphere is reduced, the western subpolar gyre starts to warm, consistent with the results of Lazier et al. (2002).

Correlation maps between heat content anomalies in the western subpolar gyre and heat content anomalies at each grid point suggests that the above statement only holds for the western subpolar gyre. Hence, the concomitant warming of the eastern subpolar gyre in 1995 might only be due to the strong shift in the NAO that occurred between 1995 and 1996, as suggested by Sarafanov et al. (2008). In the eastern subpolar gyre, the contributions of time-integrated surface heat flux and ocean heat convergence compensate each other.

While the results in the western and eastern subpolar gyres are fairly robust among the model experiments, it is not the case in the Nordic Seas. Especially, the respective contributions of surface heat flux and ocean heat convergence to heat content anomalies show clear discrepancies among the four model experiments.

## 6.2 Perspectives

Besides what has been done in the PhD, there are a few subjects that could be revisited using the weather regime framework in the North Atlantic, in light of their impact on the ocean circulation as highlighted here. We introduce these subjects below, briefly review the corresponding literature, and eventually describe ongoing activities to address the related questions.

### 6.2.1 Impact of the summer season

During the PhD, the emphasis was laid on the impacts of the winter weather regimes on the ocean circulation, since the variance of atmospheric forcing is greater in winter than in the other seasons, hence the most likely to impact the ocean circulation. However, the consideration of the summer season might be important. For instance, Msadek and Frankignoul (2009) and Ruprich-Robert and Cassou (2013) suggest that the reduction of the AMOC after a positive wintertime EAP index leads to a SST anomaly pattern that resembles the opposite of the Atlantic Multidecadal Variability (AMV). This SST pattern favours the negative phase of the summertime EAP, hence providing a weak positive feedback. Accordingly, the ocean could potentially force the summer weather regimes.

Furthermore, the consideration of the summer season could be important when investigating heat content variations. Indeed, during summer, the variance of surface heat fluxes in the western and eastern subpolar gyre is weaker than the variance of heat convergence. Hence, the variability of summer heat content in these regions is dominated by heat convergence. It would be interesting to analyse how the heat provided or extracted by winter surface heat fluxes is transported out of the domain in summer by the ocean. This has been done by Straneo (2006), who suggests that after wintertime convection in the Labrador Sea, strong lateral exchanges take place in order to bring back the properties to the boundary current values. This restratification occurs from May to December. One could ask whether the weather regimes during this period (described in Cassou et al. 2011) could potentially impact this restratification mechanism.

## 6.2.2  Biogeochemistry and small-scale processes

All along the PhD, the emphasis was laid on the impacts of the large-scale atmospheric variability on the ocean circulation. Yet, large-scale atmospheric variability has also been shown to impact the marine biogeochemistry. Keller et al. (2012) used the pre-industrial control runs of six coupled climate models to analyse the linkages between the North-Atlantic Oscillation and the carbon cycle. They suggest that the changes in key carbon-related parameters (e.g. dissolved organic carbon, alkalinity) all shows an instantaneous (timescales shorter than 3 months) dipole pattern with negative anomalies in the subtropical gyre and positive anomalies in the subpolar gyre under positive NAO, which is mainly driven by vertical mixing between the surface and the thermocline. They also highlight the asymmetric nature of the NAO observed in all the models. Patara et al. (2011), using a coupled climate model, suggest that the impacts of the NAO on the chlorophyll depends on the time-scales. The direct response (0-year lag) to positive NAO reflects changes in the vertical mixing that leads to a deepening of the mixed layer in the subpolar gyre accompanied by an increase in the chlorophyll, and conversely in the subtropical gyre. The advection by the North-Atlantic Current of subsurface nutrient reservoirs lead, after a one year lag, to an increase of the chlorophyll at midlatitudes. At decadal timescales, the spin-up of the gyre circulation and the changes in local mixing and sea-ice fraction lead to a redistribution of the biogeochemical properties and in turn to changes in chlorophyll. Since these studies use the classical NAO index, it would be interesting to perform similar analysis using the weather regime framework, in order to assess the impacts of the NAO asymmetry. Furthermore, since the AR has been shown to reduce the strength of both gyres, one could anticipate significant impacts of the AR on the chlorophyll.

Large-scale atmospheric variability has also been shown to impact the small-scale processes. Chaudhuri et al. (2009) suggest that changes in the NAO index are positively correlated with the annual rates of Gulf-Stream warm core rings (WCRs). They suggest that strengthened winds under positive NAO$^+$ conditions lead to increase eddy-kinetic energy (EKE) in the Gulf-Stream, hence favouring the baroclinic instability in the Gulf-Stream front and the occurrences of WCRs. They suggest that the NAO-related meridional displacements of the Gulf-Stream (after a one year lag) and the resulting interactions with the New England Seamounts are unlikely to contribute to the changes in the WCRs occurrences. Penduff et al. (2004) suggest that strong variability in the

NAO, as observed in 1993, leads to a meridional redistribution of the EKE after a 4-12 months lag, presumably due to the wind-driven input of potential vorticity anomalies that would impact the large-scale circulation. Volkov (2005) used satellite altimetry to analyse the interannual variability of EKE variability. They suggest that the meridional shifts of the Gulf-Stream are correlated with changes in the NAO after a 2 year lag, while in the Iceland Basin and the Irminger Basin, EKE anomalies reflect the NAO-related zonal displacements of the subpolar front. Again, the use of the weather regime framework might be promising to understand the impacts of the large-scale atmospheric variability on the variability of the EKE. Especially, since the gyre anomalies are five degrees further north for the NAO$^-$ than for the NAO$^+$ (Barrier et al. 2013), one could suspect that these two regimes would have different impacts on the EKE generation.

### 6.2.3 Salinity budget

The role of salinity is of considerable importance for the future state of the Atlantic Meridional Overturning Circulation (AMOC). In the context of climate change, a stronger hydrological cycle and an increase in Greenland ice melting would lead to a fresher/lighter water in the North-Atlantic and in turn to a weaker AMOC. If the AMOC exports freshwater southward (i.e. imports salt northward), as suggested by Deshayes et al. (2012) using high-resolution ocean models, the reduction of the AMOC will lead to a reduced transport of salinity, hence providing a positive feedback to the AMOC slackening (the so-called "salt-advection feedback"). The presence of this positive feedback is a necessary condition for a bistable AMOC, with both a strong and a weak state.

Bojariu and Reverdin (2002) used canonical correlation analysis on NCEP/NCAR reanalysis to link the variability of freshwater fluxes (evaporation minus precipitation) to the large-scale modes of variability. They suggest that the first mode of variability of precipitations and freshwater fluxes is driven by the NAO, while their second mode of variability is driven by the EAP. Treguer et al. 2013 (in preparation for the *Journal of Marine System*), using the weather regime framework and the GPCP precipitation dataset[1] between 1979-2012, obtained precipitation anomalies associated with the weather regimes that compare well with the patterns of Bojariu and Reverdin (2002). At the local scale, they suggest that the precipitations recorded at the Guipavas meteorological station (Brittany,

---

[1]`http://www.gewex.org/gpcp.html`

France) are reduced under EAP/AR conditions. Using a climate model, Mignot and Frankignoul (2004) suggest, however, that the sea-surface salinity (SSS) variations in response to the NAO/EAP are mostly driven by anomalous Ekman advection of mean SSS, the impacts of the freshwater fluxes being significant only at decadal timescales.

Msadek and Frankignoul (2009) and Ruprich-Robert and Cassou (2013) suggest, using coupled climate models, that the decadal variability of the EAP impacts the decadal variability of the AMOC: positive EAP conditions induce a reduction of the subpolar gyre, hence a reduced northward advection of warm and salty water. The resulting negative density anomalies will reduce the deep convection in the Nordic Seas and in turn lead to a reduction in the strength of the AMOC. On the other hand, Frankignoul et al. (2009) used an ocean only model to analyse salinity variations in the eastern subpolar gyre. They suggest that these variations are dominated by the NAO through increased precipitations (consistent with Bojariu and Reverdin 2002 and Treguer et al. 2013), reduced northward salt transport due to the anticyclonic intergyre-gyre (consistent with Herbaut and Houssais 2009) and increased southward freshwater transport across the Greenland-Scotland-Ridge. They also suggest that the NAO induces a spin-up of the AMOC hence an increased northward salt transport that is counterbalanced by the eastward shift of the subpolar front induced by the strengthening of the subpolar gyre, which limit the northward transport of salt by the North-Atlantic Current. As a consequence, the impacts on the salinity in the northeastern subpolar gyre are almost zero, as opposed to Msadek and Frankignoul (2009) and Ruprich-Robert and Cassou (2013).

A better understanding of freshwater content variability in the subpolar gyre and the Nordic Seas could be gained by the computation of salt budgets similar to those described in section 5 for heat content.

### 6.2.4   Climate change studies

All along this study, the focus was on the past variability (1949-2010). However, global warming is expected to significantly warm the ocean at the surface, leading to a more stratified ocean. Hence, the question that arises is whether the results discussed are robust with respect to the mean state, i.e. whether similar results would be obtained in the context of climate change. To answer such a question, the following methodology, based on the coupled climate models used in the IPCC, has

been thought of and started using the CNRM-CM5 climate model. As a first step, the surface ocean forcings of the control experiment, in which the external forcings are fixed to their 1850 estimated pre-industrial values, are used to force the ocean component of the climate model, initialised by the oceanic component of the coupled climate model. The comparison between the forced and the coupled runs will allow to determine whether the variability of the ocean circulation is reproduced in the forced mode.

The daily anomalies of surface atmospheric forcing issued from this "pre-industrial control" experiment are then extracted by removing the mean seasonal cycle. These forcing anomalies are added to the mean seasonal cycle of the surface forcings issued from the climate change scenario RCP8.5. Hence, this new forcing could be considered as an artificial combination of intrinsic variability issued from the "pre-industrial control" experiment and the mean state of a climate change scenario. A forced run is then performed using these new forcings but initialised from the oceanic state of the climate change scenario. These two forced experiments, the "forced control" and the "forced climate change scenario", share the same variability but not the mean states. As a consequence, the comparison of these two experiments might provide the answer as to the impact of the mean state on the ocean response to atmospheric variability.

However, sea-ice contributes to the variability of winter averaged air-temperature and specific humidity, especially in the Nordic Seas, where most of the winter averaged sea-ice variability occurs. As a consequence, the air-temperature and specific humidity anomalies issued from "pre-industrial control" have been corrected from these effects because the sea-ice has melted in the climate change scenario.

The runs are currently being performed and 17 years of the "forced control" experiments have been subjected to a cursory analysis. The variability of the Atlantic Meridional Overturning Circulation in the forced run is consistent with the variability in the coupled run. The variability of the subtropical and subpolar gyres is also consistent among these two runs, with weaker amplitudes in the forced run however. The next step is to run the "forced climate change scenario" in order to assess whether the impacts of the large-scale atmospheric variability, assessed by using the weather regime framework, on the ocean circulation are the same as in the "forced control" run.

# Bibliography

Aksenov, Y., Bacon, S., Coward, A. C., and Nurser, A. (2010). The north atlantic inflow to the arctic ocean: High-resolution model study. *Journal of Marine Systems*, 79(1):1–22.

Antonov, J., Levitus, S., and Boyer, T. (2005). Thermosteric sea level rise, 1955-2003. *Geophysical Research Letters*, 32(12).

Barnston, A. and Livezey, R. (1987). Classification, seasonality and persistence of low-frequency atmospheric circulation patterns. *Monthly Weather Review*, 115(6):1083–1126.

Barrier, N., Treguier, A., Cassou, C., and Deshayes, J. (2013). Response of north-atlantic ocean circulation to atmospheric weather regimes. *Journal of Physical Oceanography*, in press:in press.

Barrier, N., Treguier, A.-M., Cassou, C., and Deshayes, J. (2012). Impact of the winter north-atlantic weather regimes on subtropical sea-surface height variability. *Climate Dynamics*, pages 1–13.

Bellucci, A., Gualdi, S., Scoccimarro, E., and Navarra, A. (2008). NAO-ocean circulation interactions in a coupled general circulation model. *Climate Dynamics*, 31(7-8):759–777.

Bellucci, A. and Richards, K. (2006). Effects of NAO variability on the north Atlantic ocean circulation. *Geophysical Research Letters*, 33(2).

Bersch, M. (2002). North Atlantic Oscillation-induced changes of the upper layer circulation in the northern North Atlantic Ocean. *Journal of Geophysical Research-Oceans*, 107(C10).

Bersch, M., Yashayaev, I., and Koltermann, K. P. (2007). Recent changes of the thermohaline circulation in the subpolar North Atlantic. *Ocean Dynamics*, 57(3):223–235.

Bindoff, N., Willebrand, J., Artale, V., A, C., Gregory, J., Gulev, S., Hanawa, K., Quéré, C. L., Levitus, S., Nojiri, Y., Shum, C., Talley, L., and Unnikrishnan, A. (2007). Observations: Oceanic Climate Change and Sea Level. *Climate Change 2007: The Physical Science Basis. Contribution of Working Group I to the Fourth Assessment Report of the Intergovernmental Panel on Climate Change*.

Blindheim, J., Borovkov, V., Hansen, B., Malmberg, S.-A., Turrell, W., and Østerhus, S. (2000). Upper layer cooling and freshening in the norwegian sea in relation to atmospheric forcing. *Deep Sea Research Part I: Oceanographic Research Papers*, 47(4):655–680.

Bojariu, R. and Reverdin, G. (2002). Large-scale variability modes of freshwater flux and precipitation over the atlantic. *Climate Dynamics*, 18(5):369–381.

Brayshaw, D. J., Hoskins, B., and Blackburn, M. (2011). The basic ingredients of the north atlantic storm track. part ii: Sea surface temperatures. *Journal of the Atmospheric Sciences*, 68(8):1784–1805.

Brodeau, L., Barnier, B., Treguier, A.-M., Penduff, T., and Gulev, S. (2010). An ERA40-based atmospheric forcing for global ocean circulation models. *Ocean Modelling*, 31(3-4):88–104.

Cabanes, C., Cazenave, A., and Le Provost, C. (2001). Sea level rise during past 40 years determined from satellite and in situ observations. *Science*, 294(5543):840–842.

Cabanes, C., Huck, T., and De Verdiere, A. C. (2006). Contributions of wind forcing and surface heating to interannual sea level variations in the Atlantic Ocean. *Journal of Physical Oceanography*, 36(9):1739–1750.

Cassou, C., Minvielle, M., Terray, L., and Perigaud, C. (2011). A statistical-dynamical scheme for reconstructing ocean forcing in the Atlantic. Part I: weather regimes as predictors for ocean surface variables. *Climate Dynamics*, 36(1-2):19–39.

Cassou, C., Terray, L., Hurrell, J., and Deser, C. (2004). North Atlantic winter climate regimes: Spatial asymmetry, stationarity with time, and oceanic forcing. *Journal of Climate*, 17(5):1055–1068.

Cayan, D. (1992a). Latent and sensible heat-fluxes anomalies over the Northern Oceans - Driving the Sea-Surface Temperature. *Journal of Climate*, 5(4):354–369.

Cayan, D. R. (1992b). Latent and sensible heat flux anomalies over the northern oceans: The connection to monthly atmospheric circulation. *Journal of Climate*, 5(4):354–369.

Cazenave, A. and Llovel, W. (2010). Contemporary sea level rise. *Annual Review of Marine Science*, 2:145–173.

Chaudhuri, A. H., Gangopadhyay, A., and Bisagni, J. J. (2009). Interannual variability of Gulf Stream warm-core rings in response to the North Atlantic Oscillation. *Continental Shelf Research*, 29(7):856–869.

Chaudhuri, A. H., Gangopadhyay, A., and Bisagni, J. J. (2011). Contrasting Response of the Eastern and Western North Atlantic Circulation to an Episodic Climate Event. *Journal of Physical Oceanography*, 41(9):1630–1638.

Cuny, J., Rhines, P., Niiler, P., and Bacon, S. (2001). Labrador sea boundary currents and the fate of the Irminger Sea Water. *Journal of Physical Oceanography*, 32(2):627–647.

Curry, R. and McCartney, M. (2001). Ocean gyre circulation changes associated with the North Atlantic Oscillation. *Journal of Physical Oceanography*, 31(12):3374–3400.

Dasgupta, S., Laplante, B., Meisner, C., Wheeler, D., and Jianping Yan, D. (2007). The impact of sea level rise on developing countries: a comparative analysis. *World Bank policy research working paper*, (4136).

Dee, D., Uppala, S., Simmons, A., Berrisford, P., Poli, P., Kobayashi, S., Andrae, U., Balmaseda, M., Balsamo, G., Bauer, P., et al. (2011). The era-interim reanalysis: Configuration and performance of the data assimilation system. *Quarterly Journal of the Royal Meteorological Society*, 137(656):553–597.

Delecluse, P. (2011). Caractéristiques de la variabilité climatique. In *Le Climat à découvert*. CNRS Éditions.

Desbruyeres, D., Mercier, H., and Thierry, V. (2013). On the mechanisms behind decadal heat content changes in the eastern subpolar gyre. *Progress in Oceanography*, submitted:submitted.

Deshayes, J., Curry, R., and Msadek, R. (2012). Cmip5 model inter-comparison of freshwater budget and circulation in the north atlantic. *Journal of Climate*, submitted:submitted.

Deshayes, J. and Frankignoul, C. (2008). Simulated variability of the circulation in the North Atlantic from 1953 to 2003. *Journal of Climate*, 21(19):4919–4933.

Deshayes, J., Tréguier, A.-M., Barnier, B., Lecointre, A., Sommer, J. L., Molines, J.-M., Penduff, T., Bourdallé-Badie, R., Drillet, Y., Garric, G., et al. (2013). Oceanic hindcast simulations at high resolution suggest that the atlantic moc is bistable. *Geophysical Research Letters*.

Drange, H., Dokken, T., Furevik, T., Gerdes, R., Berger, W., Nesje, A., Orvik, K. A., Skagseth, Ø., Skjelvan, I., and Østerhus, S. (2005). The nordic seas: An overview. In *The Nordic Seas: An Integrated Perspective*, volume 158. American Geophysical Union.

Eden, C. and Willebrand, J. (2001). Mechanism of interannual to decadal variability of the North Atlantic circulation. *Journal of Climate*, 14(10):2266–2280.

Ezer, T. (1999). Decadal variabilities of the upper layers of the subtropical North Atlantic: An ocean model study. *Journal of Physical Oceanography*, 29(12):3111–3124.

Fasullo, J. T. and Trenberth, K. E. (2008). The annual cycle of the energy budget. Part II: Meridional structures and poleward transports. *Journal of Climate*, 21(10):2313–2325.

Flatau, M., Talley, L., and Niiler, P. (2003). The North Atlantic Oscillation, surface current velocities, and SST changes in the subpolar North Atlantic. *Journal of Climate*, 16(14):2355–2369.

Foucault, A. (2009). *Climatologie et paléoclimatologie*. Dunod.

Frankignoul, C., Deshayes, J., and Curry, R. (2009). The role of salinity in the decadal variability of the north atlantic meridional overturning circulation. *Climate dynamics*, 33(6):777–793.

Ganachaud, A. and Wunsch, C. (2003). Large-scale ocean heat and freshwater transports during the world ocean circulation experiment. *Journal of Climate*, 16(4):696–705.

Grist, J. P., Josey, S. A., Marsh, R., Good, S. A., Coward, A. C., de Cuevas, B. A., Alderson, S. G., New, A. L., and Madec, G. (2010). The roles of surface heat flux and ocean heat transport convergence in determining Atlantic Ocean temperature variability. *Ocean Dynamics*, 60(4):771–790.

Grossmann, I. and Klotzbach, P. J. (2009). A review of North Atlantic modes of natural variability and their driving mechanisms. *Journal of Geophysical Research-Atmospheres*, 114.

Hakkinen, S., Rhines, P. B., and Worthen, D. L. (2011a). Atmospheric Blocking and Atlantic Multidecadal Ocean Variability. *Science*, 334(6056):655–659.

Hakkinen, S., Rhines, P. B., and Worthen, D. L. (2011b). Warm and saline events embedded in the meridional circulation of the northern North Atlantic. *Journal of Geophysical Research-Oceans*, 116.

Hansen, B., Hátún, H., Kristiansen, R., Olsen, S., and Østerhus, S. (2010). Stability and forcing of the iceland-faroe inflow of water, heat, and salt to the arctic. *Ocean Science Discussions*, 7(4):1245–1287.

Hansen, B. and Østerhus, S. (2000). North atlantic–nordic seas exchanges. *Progress in Oceanography*, 45(2):109–208.

Hátún, H., Sandø, A. B., Drange, H., Hansen, B., and Valdimarsson, H. (2005). Influence of the atlantic subpolar gyre on the thermohaline circulation. *Science*, 309(5742):1841–1844.

Herbaut, C. and Houssais, M. (2009). Response of the eastern North Atlantic subpolar gyre to the North Atlantic Oscillation. *Geophysical Research Letters*, 36.

Hilmer, M. and Jung, T. (2000). Evidence for a recent change in the link between the north atlantic oscillation and arctic sea ice export. *Geophysical Research Letters*, 27(7):989–992.

Hong, B., Sturges, W., and Clarke, A. (2000). Sea level on the US East Coast: Decadal variability caused by open ocean wind-curl forcing. *Journal of Physical Oceanogaphy*, 30(8):2088–2098.

Houghton, J., Meira Filho, L., Callander, B., Harris, N., Kattenberg, A., and Maskell, K. (1996). *Climate change 1995: The Science of Climate Change*. Cambridge University Press.

Hurrell, J. (1995). Decadal Trends in the North-Atlantic Oscillation - Regional temperatures and precipitations. *Science*, 269(5224):676–679.

Ingleby, B. and Huddleston, M. (2007). Quality control of ocean temperature and salinity profiles—historical and real-time data. *Journal of Marine Systems*, 65(1):158–175.

Kalnay, E., Kanamitsu, M., Kistler, R., Collins, W., Deaven, D., Gandin, L., Iredell, M., Saha, S., White, G., Woollen, J., Zhu, Y., Chelliah, M., Ebisuzaki, W., Higgins, W., Janowiak, J., Mo, K., Ropelewski, C., Wang, J., Leetmaa, A., Reynolds, R., Jenne, R., and Joseph, D. (1996). The NCEP/NCAR 40-year reanalysis project. *Bulletin of the American Meteorological Society*, 77(3):437–471.

Keller, K. M., Joos, F., Raible, C. C., Cocco, V., Frölicher, T. L., Dunne, J. P., Gehlen, M., Bopp, L., Orr, J. C., Tjiputra, J., et al. (2012). Variability of the ocean carbon cycle in response to the north atlantic oscillation. *Tellus B*, 64.

Langehaug, H. R., Medhaug, I., Eldevik, T., and Ottera, O. H. (2012). Arctic/Atlantic Exchanges via the Subpolar Gyre. *Journal of Climate*, 25(7):2421–2439.

Lazier, J., Hendry, R., Clarke, A., Yashayaev, I., and Rhines, P. (2002). Convection and restratification in the Labrador Sea, 1990-2000. *Deep-Sea Research Part I-Oceanographic Research Papers*, 49(10):1819–1835.

Levitus, S., Antonov, J., Boyer, T., Baranova, O., Garcia, H., Locarnini, R., Mishonov, A., Reagan, J., Seidov, D., Yarosh, E., et al. (2012). World ocean heat content and thermosteric sea level change (0–2000 m), 1955-2010. *Geophysical Research Letters*, 39(10).

Levitus, S., Antonov, J., Wang, J., Delworth, T., Dixon, K., and Broccoli, A. (2001). Anthropogenic warming of Earth's climate system. *Science*, 292(5515):267–270.

Levitus, S., Antonov, J. I., Boyer, T. P., Locarnini, R. A., Garcia, H. E., and Mishonov, A. V. (2009). Global ocean heat content 1955-2008 in light of recently revealed instrumentation problems. *Geophysical Research Letters*, 36.

Levitus, S., Boyer, T., Conkright, M., O'Brien, T. Antonov, J., Stephens, C., L., S., D., J., and Gelfeld, R. (1998). NOAA Atlas NESDIS 18 and World Ocean Database 1998. *NOAA Atlas NESDIS 18 and World Ocean Database 1998*.

Lique, C. and Steele, M. (2013). Seasonal to decadal variability of arctic ocean heat content: A model-based analysis and implications for autonomous observing systems. *Journal of Geophysical Research-Oceans.*

Lique, C., Treguier, A.-M., Blanke, B., and Grima, N. (2010). On the origins of water masses exported along both sides of greenland: A lagrangian model analysis. *Journal of Geophysical Research-Oceans*, 115(C5).

Locarnini, R., Mishonov, A.V.and Antonov, J., Boyer, T., and Garcia, H. (2006). World Ocean Atlas 2005, Volume 1: Temperature. *NOAA Atlas NESDIS 61.*

Locarnini, R., Mishonov, A.V.and Antonov, J., Boyer, T., and Garcia, H. (2010). World Ocean Atlas 2009, Volume 1: Temperature. *NOAA Atlas NESDIS 68.*

Lohmann, K., Drange, H., and Bentsen, M. (2009). Response of the North Atlantic subpolar gyre to persistent North Atlantic oscillation like forcing. *Climate Dynamics*, 32(2-3):273–285.

Lozier, M. S., Leadbetter, S., Williams, R. G., Roussenov, V., Reed, M. S., and Moore, N. J. (2008). The spatial pattern and mechanisms of heat-content change in the north atlantic. *Science*, 319(5864):800–803.

Lozier, M. S. and Stewart, N. M. (2008). On the temporally varying northward penetration of Mediterranean Overflow Water and eastward penetration of Labrador Sea water. *Journal of Physical Oceanography*, 38(9):2097–2103.

Lumpkin, R. and Speer, K. (2007). Global ocean meridional overturning. *Journal of Physical Oceanography*, 37(10):2550–2562.

Madec, G. (2008). *NEMO ocean engine.*

Mallet, P.-E., Claud, C., Cassou, C., Noer, G., and Kodera, K. (2013). Polar lows over the nordic and labrador seas: Synoptic circulation patterns and associations with north atlantic-europe wintertime weather regimes. *Journal of Geophysical Research-Atmospheres.*

Marsh, R., Josey, S. A., de Cuevas, B. A., Redbourn, L. J., and Quartly, G. D. (2008). Mechanisms for recent warming of the North Atlantic: Insights gained with an eddy-permitting model. *Journal of Geophysical Research-Oceans*, 113(C4).

Marshall, J., Johnson, H., and Goodman, J. (2001). A study of the interaction of the North Atlantic oscillation with ocean circulation. *Journal of Climate*, 14(7):1399–1421.

Maurage, P., Heeren, A., and Pesenti, M. (2013). Does Chocolate Consumption Really Boost Nobel Award Chances? The Peril of Over-Interpreting Correlations in Health Studies. *Journal of Nutrition*, 143(6):931–933.

McMichael, A., Woodruff, R., and Hales, S. (2006). Climate change and human health: present and future risks. *Lancet*, 367(9513):859–869.

Medhaug, I., Langehaug, H., Eldevik, T., and Furevik, T. (2011). Mechanisms for multidecadal variability in a simulated Atlantic Meridional Overturning Circulation. *Climate Dynamics*.

Meehl, G., Stocker, T., Collins, W., Friedlingstein, P., Gaye, A., Gregory, J., Kitoh, A., Knutti, R., Murphy, J., Noda, A., Raper, S., Watterson, I., Weaver, A., and Zhao, Z.-C. (2007). Global climate projections. *Climate Change 2007: The Physical Science Basis. Contribution of Working Group I to the Fourth Assessment Report of the Intergovernmental Panel on Climate Change.*

Mercier, H., Lherminier, P., Sarafanov, F., Gaillard, F., Desbruyères, D., Falina, A., Ferron, B., Huck, T., and Thierry, V. (2013). Variability of the meridional overturning circulation at the greenland-portugal ovide section from 1993 to 2010. *Progress in Oceanography.*

Messerli, F. H. (2012). Chocolate Consumption, Cognitive Function, and Nobel Laureates. *New England Journal of Medicine*, 367(16):1562–1564.

Michelangi, P., Vautard, R., and Legras, B. (1995). Weather Regimes - Recurrence and quasi-stationarity. *Journal of Atmospheric Sciences*, 52(8):1237–1256.

Mignot, J. and Frankignoul, C. (2004). Interannual to interdecadal variability of sea surface salinity in the Atlantic and its link to the atmosphere in a coupled model. *Journal of Geophysical Research-Oceans*, 109(C4).

Minvielle, M. (2009). Méthode de désaggrégation statistico-dynamique adaptée aux forçages atmosphériques pour la modélisation de l'océan Atlantique: développement, validation et application au climat présent. PhD Thesis.

Minvielle, M., Cassou, C., Bourdalle-Badie, R., Terray, L., and Najac, J. (2011). A statistical-dynamical scheme for reconstructing ocean forcing in the Atlantic. Part II: methodology, validation and application to high-resolution ocean models. *Climate Dynamics*, 36(3-4):401–417.

Msadek, R. and Frankignoul, C. (2009). Atlantic multidecadal oceanic variability and its influence on the atmosphere in a climate model. *Climate Dynamics*, 33(1):45–62.

Nicholls, R. J. and Tol, R. S. (2006). Impacts and responses to sea-level rise: a global analysis of the sres scenarios over the twenty-first century. *Philosophical Transactions of the Royal Society A: Mathematical, Physical and Engineering Sciences*, 364(1841):1073–1095.

Nicholls, R. J., Wong, P. P., Burkett, V., Codignotto, J., Hay, J., McLean, R., Ragoonaden, S., Woodroffe, C. D., Abuodha, P., Arblaster, J., et al. (2007). Coastal systems and low-lying areas.

Nilsen, J., Gao, Y., Drange, H., Furevik, T., and Bentsen, M. (2003). Simulated north atlantic-nordic seas water mass exchanges in an isopycnic coordinate ogcm. *Geophysical Research Letters*, 30(10).

Orvik, K. A., Skagseth, Ø., and Mork, M. (2001). Atlantic inflow to the nordic seas: Current structure and volume fluxes from moored current meters, vm-adcp and seasoar-ctd observations, 1995–1999. *Deep Sea Research Part I: Oceanographic Research Papers*, 48(4):937–957.

Østerhus, S., Turrell, W. R., Jónsson, S., and Hansen, B. (2005). Measured volume, heat, and salt fluxes from the atlantic to the arctic mediterranean. *Geophysical Research Letters*, 32(7).

Patara, L., Visbeck, M., Masina, S., Krahmann, G., and Vichi, M. (2011). Marine biogeochemical responses to the north atlantic oscillation in a coupled climate model. *Journal of Geophysical Research-Oceans*, 116(C7):C07023.

Penduff, T., Barnier, B., Dewar, W., and O'Brien, J. (2004). Dynamical response of the oceanic eddy field to the North Atlantic Oscillation: A model-data comparison. *Journal of Physical Oceanography*, 34(12):2615–2629.

Penduff, T., Juza, M., Barnier, B., Zika, J., Dewar, W. K., Treguier, A.-M., Molines, J.-M., and Audiffren, N. (2011). Sea level expression of intrinsic and forced ocean variabilities at interannual time scales. *Journal of Climate*, 24(21):5652–5670.

Pickart, R. S. and Spall, M. A. (2007). Impact of Labrador Sea convection on the north Atlantic meridional overturning circulation. *Journal of Physical Oceanography*, 37(9):2207–2227.

Plaut, G. and Simonnet, E. (2001). Large-scale circulation classification, weather regimes, and local climate over France, the Alps and Western Europe. *Climate Research*, 17:303–324.

Rex, D. (1950). Blocking action in the middle troposphere and its effect upon regional climate. part i: An aerological study of blocking action. *Tellus*, 2:196–211.

Richman, M. B. (1986). Rotation of principal components. *Journal of Climatology*, 6(3):293–335.

Richter, K., Segtnan, O., and Furevik, T. (2012). Variability of the atlantic inflow to the nordic seas and its causes inferred from observations of sea surface height. *Journal of Geophysical Research-Oceans*, 117(C4).

Robertson, A. W. and Ghil, M. (1999). Large-scale weather regimes and local climate over the western united states. *Journal of Climate*, 12(6):1796–1813.

Ruprich-Robert, Y. and Cassou, C. (2013). Combined influences of seasonal east atlantic pattern and north atlantic oscillation to excite atlantic multidecadal variability in a climate model. *Climate Dynamics*, submitted:submitted.

Sarafanov, A., Falina, A., Sokov, A., and Demidov, A. (2008). Intense warming and salinification of intermediate waters of southern origin in the eastern subpolar North Atlantic in the 1990s to mid-2000s. *Journal of Geophysical Research-Oceans*, 113(C12).

Schauer, U., Beszczynska-Möller, A., Walczowski, W., Fahrbach, E., Piechura, J., and Hansen, E. (2008). Variation of measured heat flow through the fram strait between 1997 and 2006. In *Arctic–Subarctic Ocean Fluxes*, pages 65–85. Springer.

Smedsrud, L. H., Ingvaldsen, R., Nilsen, J., and Skagseth, Ø. (2010). Heat in the barents sea: Transport, storage, and surface fluxes. *Ocean Science*, 6(1):219–234.

Straneo, F. (2006). Heat and freshwater transport through the central Labrador Sea. *Journal of Physical Oceanography*, 36(4):606–628.

Sturges, W. and Hong, B. (1995). Wind forcing of the Atlantic Thermocline along 32 degrees N at low frequencies. *Journal of Physical Oceanography*, 25(7):1706–1715.

Sturges, W., Hong, B., and Clarke, A. (1998). Decadal wind forcing of the North Atlantic subtropical gyre. *Journal of Physical Oceanography*, 28(4):659–668.

Treguer, P., Goberville, E., Barrier, N., L'Helguen, S., Morin, P., Rimelin-Maury, P., Czamanski, M., Grosstefan, E., and T., C. (2013). Interannual variability of physical and chemical parameters of coastal waters of western europe during winter in relation with river inputs and climate variability. *Journal of Marine Systems*, in prep:in prep.

Treguier, A. M., England, M. H., Rintoul, S. R., Madec, G., Le Sommer, J., and Molines, J. M. (2007). Southern Ocean overturning across streamlines in an eddying simulation of the Antarctic Circumpolar Current. *Ocean Science*, 3(4):491–507.

Trenberth, K., Jones, P., Ambenje, P., Bojariu, R., Easterling, D., Klein, T., Renwick, J., et al. (2007). Observations: surface and atmospheric climate change. *Climate Change 2007: The Physical Science Basis. Contribution of Working Group I to the Fourth Assessment Report of the Intergovernmental Panel on Climate Change.*

Trenberth, K. and Solomon, A. (1994). The Global Heat-Balance - Heat Transports in the Atmosphere and Ocean. *Climate Dynamics*, 10(3):107–134.

Uppala, S., Kallberg, P., Simmons, A., Andrae, U., Bechtold, V., Fiorino, M., Gibson, J., Haseler, J., Hernandez, A., Kelly, G., Li, X., Onogi, K., Saarinen, S., Sokka, N., Allan, R., Andersson, E., Arpe, K., Balmaseda, M., Beljaars, A., Van De Berg, L., Bidlot, J., Bormann, N., Caires, S., Chevallier, F., Dethof, A., Dragosavac, M., Fisher, M., Fuentes, M., Hagemann, S., Holm, E., Hoskins, B., Isaksen, L., Janssen, P., Jenne, R., McNally, A., Mahfouf, J., Morcrette, J., Rayner, N., Saunders, R., Simon, P., Sterl, A., Trenberth, K., Untch, A., Vasiljevic, D., Viterbo, P., and Woollen, J. (2005). The ERA-40 re-analysis. *Quaterly Journal of the Royal Meteorological Society*, 131(612, Part b):2961–3012.

Vautard, R. (1990). Multiple weather regimes over the North-Atlantic. Analysis of precursors and successors. *Monthly Weather Review*, 118(10):2056–2081.

Vautard, R. and Legras, B. (1988). On the source of midlatitude low-frequency variability. Part 2: Non-linear equilibration of Weather Regimes. *Journal of Atmospheric Sciences*, 45(20):2845–2867.

Visbeck, M., Cullen, H., Krahmann, G., and Naik, N. (1998). An ocean model's response to North Atlantic Oscillation-like wind forcing. *Geophysical Research Letters*, 25(24):4521–4524.

Volkov, D. (2005). Interannual variability of the altimetry-derived eddy field and surface circulation in the extratropical North Atlantic Ocean in 1993-2001. *Journal of Physical Oceanography*, 35(4):405–426.

von Schuckmann, K., Gaillard, F., and Le Traon, P. Y. (2009). Global hydrographic variability patterns during 2003-2008. *Journal of Geophysical Research-Oceans*, 114.

Wang, Y. H., Magnusdottir, G., Stern, H., Tian, X., and Yu, Y. (2012). Decadal variability of the NAO: Introducing an augmented NAO index. *Geophysical Research Letters*, 39.

Willis, J., Roemmich, D., and Cornuelle, B. (2004). Interannual variability in upper ocean heat content, temperature, and thermosteric expansion on global scales. *Journal of Geophysical Research-Oceans*, 109(C12).

Winters, J. R. and Roberts, S. G. (2012). Chocolate Consumption, Traffic Accidents and Serial Killers.

Yashayaev, I. (2007). Hydrographic changes in the labrador sea, 1960–2005. *Progress in Oceanography*, 73(3):242–276.

Yiou, P. and Nogaj, M. (2004). Extreme climatic events and weather regimes over the north atlantic: When and where? *Geophysical Research Letters*, 31(7).

Zhai, X. and Sheldon, L. (2012). On the North Atlantic Ocean Heat Content Change between 1955-70 and 1980-95. *Journal of Climate*, 25(10):3619–3628.

Zhu, J. and Demirov, E. (2011). On the mechanism of interannual variability of the Irminger Water in the Labrador Sea. *Journal of Geophysical Research-Oceans*, 116.